Turbomachinery Analysis and Design for Hybrid SOFC-GT Systems Optimized Performance

THESIS

submitted in partial fulfillment of the requirements

for the degree of Doctor of Philosophy in Mechanical Engineering

of the Department of Mechanical Engineering

University of Thessaly

BY

DIAMANTIS P. BAKALIS

Dipl. Mechanical Engineer

University of Thessaly

Volos, October 2014

Institutional Repository - Library & Information Centre - University of Thessaly
02/06/2024 00:35:58 EEST - 18.226.159.139

Institutional Repository - Library & Information Centre - University of Thessaly
02/06/2024 00:35:58 EEST - 18.226.159.139

© 2014 Diamantis Bakalis

The approvement of the Thesis by the Department of Mechanical Engineering of the Engineering School of the University of Thessaly, do not implies acceptance of the author's beliefs (N. 5343/32 αρ. 202 παρ. 2).

Institutional Repository - Library & Information Centre - University of Thessaly
02/06/2024 00:35:58 EEST - 18.226.159.139

Approved by:

Dr. Anastassios Stamatis, Supervisor
Associate Professor, Dept. of Mechanical Engineering, University of Thessaly

Dr. Anastassios Stamatelos, Advisor Committee
Professor, Dept. of Mechanical Engineering, University of Thessaly

Dr. Herricos Stapountzis, Advisor Committee
Associate Professor, Dept. of Mechanical Engineering, University of Thessaly

Dr. Panagiotis Tsiakaras, Final examination Committee
Professor, Dept. of Mechanical Engineering, University of Thessaly

Dr. Nikolaos Andritsos, Final examination Committee
Professor, Dept. of Mechanical Engineering, University of Thessaly

Dr. Nikolaos Aretakis, Final examination Committee
Lecturer, Dept. of Mechanical Engineering, National Technical University of Athens

Dr. Vassilios Pachidis, Final examination Committee
Senior Lecturer, Energy and Power Division, School of Engineering, Cranfield University

Institutional Repository - Library & Information Centre - University of Thessaly
02/06/2024 00:35:58 EEST - 18.226.159.139

Ανάλυση και σχεδιασμός στροβιλομηχανών για βέλτιστη λειτουργία υβριδικών συστημάτων τύπου SOFC-GT

Turbomachinery Analysis and Design for Hybrid SOFC-GT Systems Optimized Performance

Επιβλέπων καθηγητής: Δρ. Αναστάσιος Σταμάτης, Αναπληρωτής καθηγητής

Περίληψη

Μεγάλη προσπάθεια γίνεται τα τελευταία χρόνια για την ανάπτυξη αποδοτικών μηχανών μετατροπής ενέργειας. Τα κίνητρα για αυτή την προσπάθεια είναι κυρίως η ολοένα αυξανόμενη ζήτηση για ηλεκτρική ενέργεια, η εξάντληση των κοιτασμάτων ορυκτών καυσίμων καθώς και η μόλυνση του περιβάλλοντος από εκπομπές αέριων ρύπων. Μια τεχνολογία που φαίνεται ότι θα συμβάλει σημαντικά στην διαμόρφωση του ενεργειακού τομέα στο μέλλον, είναι οι μικροστρόβιλοι. Οι μικροστρόβιλοι λόγω των πλεονεκτημάτων που παρουσιάζουν μπορούν να χρησιμοποιηθούν σε εφαρμογές κατανεμημένης παραγωγής ηλεκτρικής ενέργειας, smart grids, υβριδικά συστήματα και συστήματα συμπαραγωγής.

Αντικείμενο της παρούσας διατριβής είναι η μελέτη εφαρμογών μικροστροβίλων, τόσο υπολογιστικά όσο και πειραματικά. Οι υπολογιστικές δραστηριότητες περιλαμβάνουν κυρίως την μελέτη υβριδικών συστημάτων τύπου SOFC-GT (Solid Oxide Fuel Cell – Gas Turbine). Στα συστήματα αυτά γίνεται συνδυασμός ενός μικροστροβίλου και μιας γεννήτριας τύπου SOFC, η οποία λειτουργεί σε συνθήκες υπερπίεσης (υπετροφοδοτείται). Το καύσιμο αντιδρά ηλεκτροχημικά στις κυψέλες καυσίμου SOFC (που υποκαθιστούν το θάλαμο καύσης του μικροστροβίλου) και παράγει ηλεκτρική ενέργεια μαζί με θερμότητα. Η θερμότητα χρησιμοποιείται από το μικροστρόβιλο για την παραγωγή επιπλέον ηλεκτρικής ενέργειας. Τα συστήματα αυτά έχουν υψηλούς βαθμούς απόδοσης και θεωρούνται ως μια εναλλακτική επιλογή των συμβατικών συστημάτων ηλεκτροπαραγωγής.

Για την μοντελοποίηση των υβριδικών συστημάτων χρησιμοποιήθηκε ένα λογισμικό γενικής χρήσης (AspenPlus). Ξεκινώντας με μια προτεινόμενη μέθοδο από την διαθέσιμη βιβλιογραφία, έγιναν προσθήκες νέων στοιχείων με σκοπό την δημιουργία ενός βελτιωμένου μοντέλου. Επιπλέον, αναπτύχθηκαν μοντέλα για την προσομοίωση των στροβιλομηχανών στο λογισμικό γενικής χρήσης, ιδιαίτερα σε μερικό φορτίο, για πρώτη φορά σε αυτό το περιβάλλον.

Στην παρούσα διατριβή εξετάζονται σχεδιασμοί υβριδικών συστημάτων βασιζόμενοι σε εμπορικά διαθέσιμους μικροστροβίλους και σε μια επιτυχημένη γεννήτρια τύπου SOFC η οποία δοκιμάστηκε σε αρκετά πιλοτικά προγράμματα διεθνώς. Αναπτύχθηκαν μοντέλα και βαθμονομήθηκαν με βάση πειραματικά δεδομένα από την βιβλιογραφία. Μελετήθηκε η συμπεριφορά σε συνθήκες πλήρους και μερικού φορτίου καθώς και η επίδραση σημαντικών λειτουργικών παραμέτρων στις επιδόσεις των υβριδικών συστημάτων. Τα αποτελέσματα έδειξαν ότι τα συστήματα αυτά μπορεί να οδηγήσουν σε υψηλούς βαθμούς απόδοσης, εφόσον γίνει κατάλληλη βελτιστοποίηση στο σχεδιασμό του συστήματος καθώς και στο μέγεθος του μικροστροβίλου.

Institutional Repository - Library & Information Centre - University of Thessaly
02/06/2024 00:35:58 EEST - 18.226.159.139

Η προηγούμενη εμπειρία που αποκτήθηκε οδήγησε σε μια μεθοδολογία για την βελτιστοποίηση των στροβιλομηχανών σε υβριδικά συστήματα SOFC-GT. Η μεθοδολογία περιλαμβάνει δυο βήματα. Στο πρώτο γίνεται μια παραμετρική ανάλυση για να αποτιμηθεί το λειτουργικό πεδίο του συστήματος και στο δεύτερο, λαμβάνοντας υπόψη τις πληροφορίες του πρώτου βήματος, υπολογίζονται οι βέλτιστες γεωμετρίες για τον συμπιεστή και τον στρόβιλο χρησιμοποιώντας in-house κώδικες που αναπτύχθηκαν για αυτό τον σκοπό. Τα αποτελέσματα έδειξαν σημαντική βελτίωση των επιδόσεων του συστήματος σε όλο το εύρος λειτουργίας του. Η υποδομή που δημιουργήθηκε επιτρέπει τη μελέτη επιπλέον σχεδιαστικών επιλογών, με χωριστή επιλογή συμπιεστή και στροβίλου, διαφορετικού τύπου συμπιεστή κτλ, όπως και διαφορετικών επιλογών στο σύστημα ελέγχου.

Οι πειραματικές δραστηριότητες που έγιναν στα πλαίσια αυτής της διατριβής, αφορούν ένα μικροστρόβιλο τύπου turbojet. Παρουσιάζεται η εμπειρία που αποκτήθηκε από την ανάπτυξη ενός μοντέλου για την προσομοίωση της συμπεριφοράς του σε μόνιμες συνθήκες λειτουργίας. Τα αποτελέσματα έδειξαν ότι κάποιες μετρήσεις που λαμβάνονται από την λειτουργία της μηχανής δεν είναι αντιπροσωπευτικές της μέσης τιμής που επικρατεί σε κάθε διατομή. Ωστόσο η απόκλιση είναι συστηματική και επαναλήψιμη με αποτέλεσμα να μπορούν να υιοθετηθούν διαδικασίες διόρθωσης των μετρήσεων. Εκτός από την μελέτη σε μόνιμες συνθήκες λειτουργίας, μελετήθηκε και η μεταβατική λειτουργίας της μηχανής μέσω ενός μοντέλου που αναπτύχθηκε για αυτό το σκοπό. Τα αποτελέσματα των προσομοιώσεων είναι σε αρκετά καλή συμφωνία με τα πειραματικά δεδομένα. Η εμπειρία που αποκτήθηκε από το μεταβατικό μοντέλο λειτουργίας αναμένεται να αξιοποιηθεί για την ανάπτυξη μεταβατικού μοντέλου λειτουργίας για τα συστήματα SOFC-GT, προκειμένου να μελετηθεί καλύτερα το σύστημα ελέγχου για προστασία της συστοιχίας SOFC από αιχμές πίεσης, surge, αποσυσμπίεση κτλ.

Institutional Repository - Library & Information Centre - University of Thessaly
02/06/2024 00:35:58 EEST - 18.226.159.139

Abstract

Nowadays, great effort is made by the research community to develop efficient energy conversion engines. The motivation for this effort derives from the growing demand for electricity, the exhaustion of fossil fuels reserves and the environmental pollution caused by the exhaust emissions from engines. A technology that seems to play an important role in the development of energy sector is the microturbines. The microturbines have many advantages over the conventional reciprocating engines, which make them suitable for distributed generation applications, smart grids, hybrid and cogeneration systems.

In this thesis, applications of microturbines are studied, both numerically and experimentally. The numerical works include the study of hybrid SOFC-GT (Solid Oxide Fuel Cell – Gas Turbine) systems. These systems combine a microturbine with a SOFC generator that operates at elevated pressure conditions. The fuel reacts electrochemically within the fuel cell stack (which substitutes the combustion chamber of the microturbine) and produces electric power and heat. The heat is utilized from the microturbine to produce additional electric power. The hybrid SOFC-GT systems have high efficiency and are considered as an alternative to conventional electric plants.

For the modeling of the hybrid systems a general purposes software (AspenPlus) was used. Starting from a method published in the literature for the modeling of a SOFC generator, changes were made in order to develop an improved model. Moreover, simulation models for the part-load performance of turbomachines were developed for the first time using this general software.

In the present thesis, hybrid systems were examined which are based on commercially available microturbines and a successful SOFC generator, which have been tested in various research programs. Models were developed and validated against experimental data from the available bibliography. The models were used to study the behavior of hybrid systems under full and part-load operating conditions. Also, the influence of important performance parameters, such as the SOFC stack temperature, was investigated. The results showed that these systems can achieve high efficiency values with a proper choice of the design parameters as well as of the size of the microturbine.

The previous experience was used to develop a method for the optimization of the compressor and turbine components in hybrid SOFC-GT systems. The method consists of two steps. In the first step a parametric study is conducted in order to assess the operating range of the hybrid system and, in the second, the compressor and turbine geometric parameters are calculated using in-house turbomachinery design codes and an optimization procedure. Based on the new turbomachines the hybrid system has shown a clear efficiency advantage over the whole operating range. The developed optimization tools allow the study of further design options, such as a separate compressor and turbine selection or a different compressor type.

Institutional Repository - Library & Information Centre - University of Thessaly
02/06/2024 00:35:58 EEST - 18.226.159.139

The experimental activities conducted in this thesis concern a small turbojet engine. The experience gained during the development of a simulation model for the steady state operation is presented. Data analysis showed that some measurements were not thermodynamically consistent and representative of the average value of the thermodynamic parameter in the engine station. However, there were systematic deviations which were repetitive. This led to adoption of data correction procedures in order to correct the non-representative measurements and make them compatible with the others. Apart from the steady state model, a transient model was developed. The model was validated by comparing model predictions with experimental data. The gained experience will be used for the development of a transient model for SOFC-GT applications, in order to study control methods that ensure protection against pressure spikes, surge, overpressure etc.

Institutional Repository - Library & Information Centre - University of Thessaly
02/06/2024 00:35:58 EEST - 18.226.159.139

Acknowledgments

The completion of this thesis constitutes a significant milestone in my professional career. I hold a deep gratitude to the people who have contributed to the conduction of this research work. I would like to express my special thanks to the following people for their overall support and assistance:

My supervisor Dr. Anastassios Stamatis for his guidance and support throughout the years of my studies. It would have been impossible to complete this work, without his tireless encouragement or his priceless advices.

Dr. Anastassios Stamatelos and Dr. Errikos Stapountzis, members of the advisor committee, for their helpful discussions and advices under the frame of this thesis and beyond.

Dr. Panagiotis Tsiakaras, Dr. Nikolaos Andritsos, Dr. Nikolaos Aretakis and Dr. Vassilios Pachidis, members of the final examination committee, for their useful comments on improving this thesis.

Mr. Apostolos Goudas for his willing and helpful cooperation on my experimental activities in the laboratory

Last but not least, I would like to thank my family for their continuous encouragement and support during the difficult time of the research.

Institutional Repository - Library & Information Centre - University of Thessaly
02/06/2024 00:35:58 EEST - 18.226.159.139

Institutional Repository - Library & Information Centre - University of Thessaly
02/06/2024 00:35:58 EEST - 18.226.159.139

Table of Contents

Institutional Repository - Library & Information Centre - University of Thessaly
02/06/2024 00:35:58 EEST - 18.226.159.139

Institutional Repository - Library & Information Centre - University of Thessaly
02/06/2024 00:35:58 EEST - 18.226.159.139

Institutional Repository - Library & Information Centre - University of Thessaly
02/06/2024 00:35:58 EEST - 18.226.159.139

Institutional Repository - Library & Information Centre - University of Thessaly
02/06/2024 00:35:58 EEST - 18.226.159.139

List of figures

Institutional Repository - Library & Information Centre - University of Thessaly
02/06/2024 00:35:58 EEST - 18.226.159.139

Institutional Repository - Library & Information Centre - University of Thessaly
02/06/2024 00:35:58 EEST - 18.226.159.139

Institutional Repository - Library & Information Centre - University of Thessaly
02/06/2024 00:35:58 EEST - 18.226.159.139

Institutional Repository - Library & Information Centre - University of Thessaly
02/06/2024 00:35:58 EEST - 18.226.159.139

Nomenclature

A	area
A_s	effective surface area
b	blade height
C_p	specific heat
D	diffusion coefficient, diameter
D_m	cell mean diameter
E	activation energy
$\dot{E}$	exergy flow
e	specific exergy
F	Faraday constant, thrust
G	Gibbs free energy
H	enthalpy
h	enthalpy
i	current density
I	electric current
i_o	exchange current density
k	thermal conductivity, pre-exponential factor
L	length
M	molecular weight, Mach number
$\dot{m}$	mass flow
N	rotational speed
$\dot{n}$	molar flow
n_e	number of electrons
Nu	Nusselt number
P	power
p	pressure
$p_{()}$	partial pressure of component ()
Pr	Prandtl number
PR	pressure ratio
$\dot{Q}$	heat transfer rate
R	gas constant, resistance
r	average pore radius
R_m	universal gas constant
S	entropy
s	specific entropy
SE	efficiency deviation
S_f	skin friction coefficient
SP	pressure ratio deviation
SW	mass flow parameter deviation
t	thickness
T	temperature

Institutional Repository - Library & Information Centre - University of Thessaly
02/06/2024 00:35:58 EEST - 18.226.159.139

U	overall heat transfer coefficient (W/m^2.K)
u	blade speed
U_f	fuel utilization factor
V	Velocity, voltafe
v	Fuller diffusion coeficience
W	work
w	specific work, relative velocity
Z	number of blades or vanes
Δh	enthalpy losses

Greek symbols

β	electronic transfer coefficient, relative flow angle
γ	ratio of specific heats, pre-exponential coefficient
δ	ratio of inlet total pressure to standard atmospheric pressure
ε	porosity, emissivity, function of γ used in relating parameters to those using air inlet conditions at standard sea level conditions
η	efficiency
θ	ratio of inlet total temperature to standard atmospheric temperature
θ_{cr}	squared ratio of critical velocity at turbine inlet to critical velocity at standard atmospheric temperature
ν	Fuller diffusion coefficient, kinematic viscocity
ξ	tortuosity
ρ	resistivity, density
σ	Stefan-Boltzman constant
φ	angle

Subscripts

A	anode
Act	activation
b	blade
bl	blade loading
c	compressor, cold
C	cathode
Conc	concentration
cor	corrected
df	diffusion
E	electrolyte
eff	effective
el	electrons
ex	exergetic
f	fuel, full blades
GEN	generator
h	hot
h	hub
id	ideal
inc	incidence
Int	interconnection

Institutional Repository - Library & Information Centre - University of Thessaly
02/06/2024 00:35:58 EEST - 18.226.159.139

is	isentropic
K	Knudsen
m	mechanical
mix	mixture
N	Nernst
o	reference
Ohm	ohmic
r	rotor, component in meridional direction
rc	recirculation
ref	reference
rel	relative
rev	reversible
s	stator
sp	split blades
t	turbine, total, tip
u	component in tangential direction
v	vane
vd	vaned diffuser
vld	vaneless diffuser

Superscripts

ch	chemical
I	inlet
k	kinetic
p	potential
ph	physical
r	reaction
eff	effective

Abbreviations

AC	alternating current
CCHP	combined cooling , heat and power
CHP	combined heat and power
COP	coefficient of performance
DC	direct current
GT	gas turbine
HS	hybrid systm
SCR	steam to carbon ratio
SOFC	Solid Oxide Fuel Cell
LHV	lower heating value

Institutional Repository - Library & Information Centre - University of Thessaly
02/06/2024 00:35:58 EEST - 18.226.159.139

Institutional Repository - Library & Information Centre - University of Thessaly
02/06/2024 00:35:58 EEST - 18.226.159.139

Chapter 1

Introduction

In this chapter, the reasons and motivations for undertaking this thesis are presented. A brief introduction about the trends in energy market is done and the role of the main systems studied in this thesis is discussed.

1.1 Background

Demand for energy is increasing steadily since the beginning of the industrial revolution. The energy sector is vital for the industry, services, transporting the people and goods, protecting against weather conditions etc. Most of the energy comes from the fossil fuels (see Figure 1-1). The fossil fuels have two major drawbacks: firstly, their reservoirs are finite, which is one of the main reasons that the prices are high, and secondly, the large amounts of greenhouse gas emissions. Because of these two drawbacks, the fossil fuels should be used efficiently and with technologies that contribute to lower CO_2 emissions.

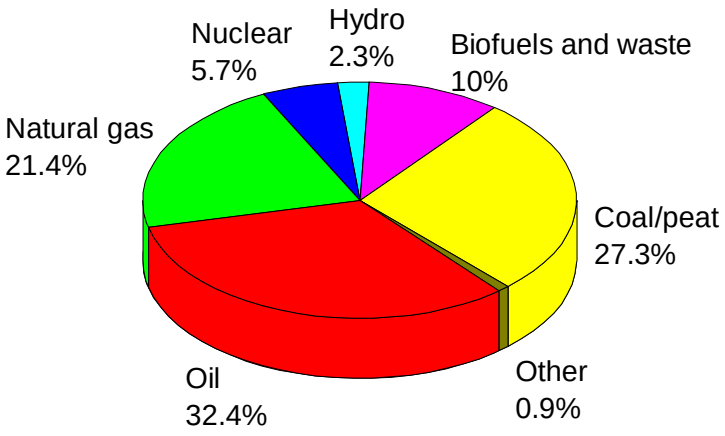

Figure 1-1 World total primary energy supply for 2010,[1].

The worldwide trends in the energy policy can be classified into three groups:

- Energy savings: This group includes socio-political actions to sensitize the society, through informative campaigns, to a more rational use of the available energy. This does not necessarily imply the decline in standards of living but the adoption of actions that contribute to energy savings. There are many ways to save energy, such as turning of the

Institutional Repository - Library & Information Centre - University of Thessaly
02/06/2024 00:35:58 EEST - 18.226.159.139

lights when it is not necessary, regular maintenance and proper setting of heating/cooling equipment, use of public transport, green buildings, distributed generation systems etc.
These actions not only produce individual economic benefits, but also make a positive impact on the society and the economy of a country, since they contribute to a reduction of dependence on oil rich countries and on price variations.

- Environmental protection: This group includes actions to switch to more environmentally friendly technologies, with low greenhouse gas emissions. This goal can be met effectively by the renewable energy sources (such as solar, wind, hydropower, tidal and geothermal power) which have zero CO_2 emissions. However, there are renewable energy sources such as biogas, biodiesel and biomass with emissions, but nevertheless remain eco-friendly. A disadvantage of the renewable sources is the low availability since it is high susceptible to environmental conditions (adverse weather, day/night cycle etc.). To overcome this problem, several ways have been proposed in the literature to store excess energy and release it when needed.
  Apart from the renewable energy technologies, considerable effort has been made on CO_2 capture and separation technologies. There are many options available including absorption, low temperature distillation and membrane separation.
- Conversion efficiency: There is a big effort to develop and use efficient energy conversion devices such as high energy efficiency class appliances, hybrid cars and efficient electric power plants. Towards this direction is the use of fuel cells, which convert the chemical energy of the fuel directly and efficiently to electric energy.
  Various energy systems have been proposed for the simultaneous production of more than one useful form of energy, e.g. cogeneration of heat and electric power or trigeneration systems. These systems present high total efficiencies, since they utilize a larger amount of the primary fuel (energy). Moreover, in recent years the popularity of hybrid energy systems increases steadily. These systems combine different type of energy supply devices and achieve very high efficiencies.

From the previous analysis, it is clear that there is a need for efficient and environmentally friendly techniques to produce electric power. In the available literature, there are many proposed systems that fulfill the criteria described previously. Among them, the microturbines have a leading role in the energy market. Their advantages make them an ideal solution for numerous applications. The microturbines have a prominent role in the hybrid systems, and especially in the systems that combine fuel cells with microturbines.

In this research activity, applications of the microturbines in hybrid fuel cell gas turbine systems are mainly studied. In the following sections, the characteristics of the main systems that this thesis deals with i.e. microturbines and fuel cells are presented and discussed.

1.2 The role of the microturbines

The microturbines are miniatures of larger gas turbines (GT) engines, either turbojet or turboshaft type. The small turbojet engines are mainly used for the propulsion of Unmanned Aerial Vehicles (UAVs) or from airplane modelers. The small turboshaft engines are suitable for distributed generation applications, because of their advantages such as high specific power, multi-fuel operation, low maintenance costs, ability to provide reliable and stable power, parallel connection to serve larger loads and low pollutant emissions [2].

Institutional Repository - Library & Information Centre - University of Thessaly
02/06/2024 00:35:58 EEST - 18.226.159.139

Typical applications of microturbines are:

- Stand-alone applications
- CHP and CCHP
- Backup/standby power
- Peak shaving and base load power

Microturbines can be used in public buildings such as universities, hospitals etc., in small or large commercial applications (e.g. hotels, industries), in apartment buildings covering totally or partially, the electricity and/or thermal needs. They can provide electricity in remote areas that are out of the electricity grid or for telecommunications and military purposes, such as the operation of transmitters, radars etc.

The use of the microturbines is expected to increase in the near future. A major reason is the ability to utilize the rejected thermal energy for cogeneration and trigeneration purposes, with very high efficiency (80-90%). Another reason is the avoidance of the transmission and distribution losses since the electric power is produced close to the consumption points; and moreover, the development of natural gas distribution networks expands the geographical area in which microturbines can be installed.

1.3 The role of the fuel cells

The fuel cells are electrochemical devices that convert the chemical energy of the fuel directly and efficiently to electricity. A typical fuel cell consists of an ion-conducting electrolyte in contact with a fuel electrode (anode) on the one side and an oxidant electrode (cathode) on the other side. It is a promising technology since it offers very high energy conversion efficiencies and low environmental impact.

There is a plurality of fuel cells that are classified according to the electrolyte and fuel type, which in turn determine the electrochemical reactions that take place inside the cells [3]. As the power produced by a single fuel cell is very low, it is necessary to stack many cells together to obtain a reasonable power output. The fuel cells are constructed in several geometries, each having its pros and cons, broadly classified as either tubular or planar.

Of the available fuel cell technologies, the Solid Oxide Fuel Cells (SOFCs) show the most promising results for stationary applications. The main characteristics of the SOFCs are the high efficiency and the high operating temperature that make them an ideal choice for distributed generation applications. The high temperature of the exhaust gases from the SOFC stack is able to power a gas turbine without additional fuel supply, leading to electric efficiency values over 60%.

1.4 Thesis aims and objectives

The coupling of microturbines and fuel cells is not a simple process. There is a plethora of different combinations that can be made. Each combination has its pros and cons. Moreover, during their operation critical phenomena can appear such as carbon deposition, high temperatures, compressor surge etc. In order to avoid these dangerous conditions a careful selection of key operating parameters should be done and a suitable control strategy should be applied.

Institutional Repository - Library & Information Centre - University of Thessaly
02/06/2024 00:35:58 EEST - 18.226.159.139

This thesis is targeted at the analysis of hybrid SOFC–GT systems. It is intended to help understand better the processes take place in a hybrid SOFC–GT system and give recommendations for improving its performance. The main objectives of this research are:

- Study the interaction of the microturbine and the SOFC generator in a hybrid SOFC-GT system. More practical applications are covered due to the absence of relative bibliography.
- Development of a detailed and accurate computational model for a SOFC generator.
- Gain knowledge on the part load performance of the hybrid systems.
- Study the irreversibilities in a hybrid SOFC–GT system.
- Optimization of a hybrid system as there is no effort by the research community to suggest a practical method to optimize the performance over the whole operating engine.
- Experimental study of microturbines and development of a transient model which in the future will be helpful for the development of a transient SOFC–GT model.

1.5 Thesis contribution

The work carried out in this thesis has made significant contributions to the field of hybrid SOFC – GT systems and on the gas turbine field, inter alia:

- Improvements were done in a simulation methodology for a SOFC generator.
- A methodology was proposed for improving the hybrid SOFC-GT systems performance through turbomachinery design.
- A complete approach for the modeling of hybrid SOFC-GT systems in AspenPlus simulation environment was developed.
- The non-representativeness of some measurements in a turbojet engine was studied and a correction procedure was proposed.

A list of papers published in international journals and conferences are enlisted here:

1. Bakalis, D. P.; Stamatis, A. G., Optimization methodology of turbomachines for hybrid SOFC-GT applications. *Energy* 2014, 70, 86-94.
2. Bakalis, D. P.; Stamatis, A. G., Improving hybrid SOFC-GT systems performance through turbomachinery design. *International Journal of Energy Research* 2014.
3. Bakalis, D. P.; Stamatis, A. G., Incorporating available micro gas turbines and fuel cell: Matching considerations and performance evaluation. *Applied Energy* 2013, 103 (0), 607-617.
4. Bakalis, D. P.; Stamatis, A. G., Full and part load exergetic analysis of a hybrid micro gas turbine fuel cell system based on existing components. *Energy Conversion and Management* 2012, 64 (0), 213-221.
5. Bakalis, D.; Stamatis, A., Exergy Analysis of a Hybrid Micro Gas Turbine Fuel Cell System Based on Existing Components. ASME Conference Proceedings 2012, ASME Paper No. GT2012-69258.
6. Bakalis, D. P.; Stamatis, A. G., Data analysis and performance model calibration of a small turbojet engine. *Proceedings of the Institution of Mechanical Engineers, Part G: Journal of Aerospace Engineering* 2011, 226 (12), 1523-1533.
7. Bakalis, D.P., Stamatis, A.G. Performance simulation of a hybrid micro gas turbine fuel cell system based on existing components , ASME Conference Proceedings 2011, ASME Paper No. GT2011-45834.

Institutional Repository - Library & Information Centre - University of Thessaly
02/06/2024 00:35:58 EEST - 18.226.159.139

1.6 Thesis outline

This thesis is organized in 10 chapters. Following this introduction the technology background is given in Chapter 2. The characteristics of the main components are described and the design challenges of the hybrid SOFC – GT systems are discussed. In Chapter 3 the operating principles of the system components are presented. Chapter 4 presents the model developed for the hybrid SOFC-GT system. In Chapter 5 a hybrid system based on existing devices is analyzed and an exergetic analysis is performed. Chapter 6 discusses the matching consideration of a SOFC generator with four different microturbines. In Chapter 7 a methodology to improve the performance of a hybrid SOFC-GT system for the whole operating range is proposed. In Chapter 8 the experience gained during the development of a microturbine simulation model is presented. Chapter 9 presents a transient model developed for a microturbine, and finally, Chapter 10 concludes this research and makes recommendations for future work.

Institutional Repository - Library & Information Centre - University of Thessaly
02/06/2024 00:35:58 EEST - 18.226.159.139

Institutional Repository - Library & Information Centre - University of Thessaly
02/06/2024 00:35:58 EEST - 18.226.159.139

Chapter 2

Technology background

In this chapter the characteristics of the main components and the auxiliary equipment are described. The basic hybrid system layouts and their basic auxiliary equipment are presented. The SOFC generator developed by Siemens-Westinghouse is presented and the design challenges of hybrid systems are discussed.

2.1 Microturbines

The microturbines are small gas turbine engines, either turbojet or turboshaft type. The turboshaft type microturbines operate similarly to the conventional, larger gas turbine engines [4]. Their operation is usually based on the recuperated Brayton thermodynamic cycle in the case of the distributed generation applications. A schematic diagram of this type of microturbines is shown in Figure 2-1. Atmospheric air enters the compressor and exits at an elevated pressure. Then, the compressed air passes through a heat exchanger where it is heated by extracting heat from the hot exhaust gas. The compressed and heated air is guided into the combustor where it is mixed with the fuel and the gaseous mixture burns. The hot gas expands in the turbine and generates power to drive both the compressor and the generator. The hot exhaust gas is directed into the recuperator, where it provides heat for the compressed air before it enters into the combustor.

The ideal thermodynamic diagram of the recuperated Brayton cycle is shown in Figure 2-2.

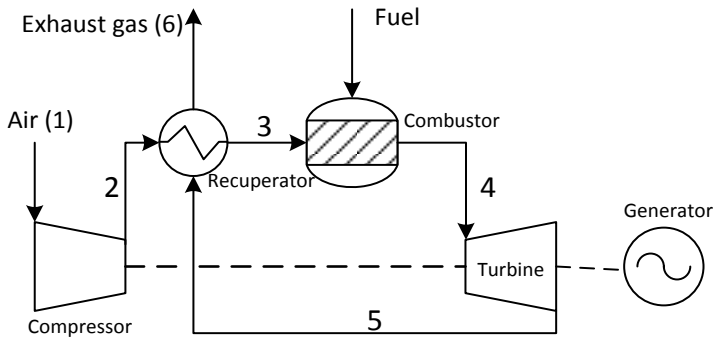

Figure 2-1 Schematic diagram of a microturbine

Institutional Repository - Library & Information Centre - University of Thessaly
02/06/2024 00:35:58 EEST - 18.226.159.139

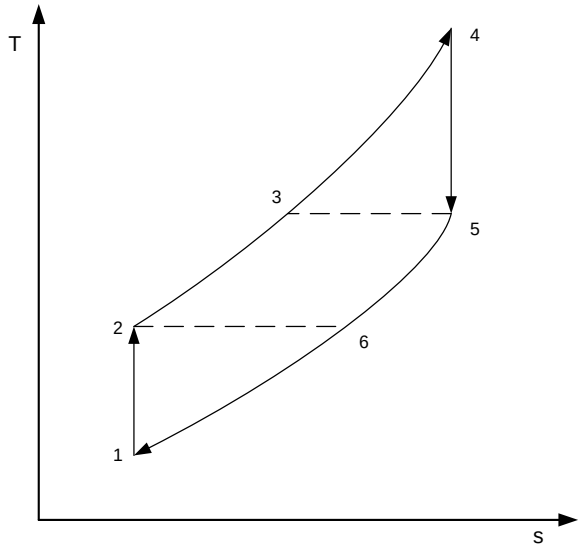

Figure 2-2 T-s diagram of the ideal recuperated Brayton cycle

The turbojet type microturbines are simpler than the turboshaft type, since they do not utilize the recuperator component. The air is compressed in a centrifugal compressor, is burned in an annular type or reverse flow combustor and is partially expanded in an axial type turbine to produce power for the compressor. The hot and pressurized gases that exit the turbine are expanded to atmosphere though a convergent nozzle and produce thrust.

Microturbines operate at very high rotational speeds. The turboshaft type can have either a single shaft or a dual shaft configuration. In the single shaft configuration (Figure 2-1) the turbine generates power to drive the compressor and the generator which are mounted on the same shaft. In this design, the produced electric power has a very high frequency, which is variable as the generator speed varies during the part load operation. The output power of the generator is adjusted to the desired voltage and frequency values with an AC/DC/AC power controller.

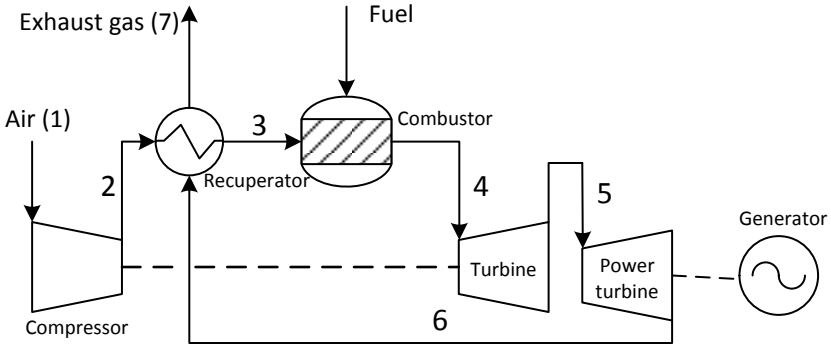

Figure 2-3 Dual shaft microturbine

On the other hand, in the dual shaft configuration the hot gases exit from the combustor expand partially on the high pressure turbine and produce power for the compressor. Thereinafter, the gases exit from the high pressure turbine and fully expand on the low pressure turbine (power turbine) and produce power for the generator. In this configuration the rotating speed of the power turbine remains constant. Some designs incorporate a gear box to reduce the shaft speed and to

Institutional Repository - Library & Information Centre - University of Thessaly
02/06/2024 00:35:58 EEST - 18.226.159.139

transmit the power to the generator. The generator produces the desired frequency without the use of a power converter. In Table 2-1 the two types of microturbines are compared.

Table 2-1 Comparison of single shaft and dual shaft microturbines, [4]

Difference item	Single shaft	Dual shaft
Speed of rotation (rpm)	50000 - 120000	3000 or 3600
Alternator frequency (Hz)	1500 - 4000	50 or 60
Coupling	Turbine and alternator are directly coupled	Gear box is used to couple turbine shaft with alternator shaft
Power electronics	Power electronics section is needed to convert the high frequency AC output voltage into DC and then into AC with frequency of 50Hz or 60Hz	No need for power electronics
Alternator type	Usually permanent magnet synchronous generator	Usually induction generator
Maintenance	Less maintenance	Higher maintenance because of additional moving parts.
Cost	Usually higher cost because of the power electronics section and type of generator used.	Lower cost
Chances of failure	Higher chances	Lower chances as gearbox is more robust than complex power electronics section.
Dimensions and weight	Lower	Higher because of gear box and the lubricating system

As the microturbines operate, they reject heat to the environment, like all thermal engines. The superiority of the microturbines, over the diesel and spark ignition engines, is that the rejected heat is mainly available in the exhaust gases. The hot exhaust gases can be used for space heating purposes, for hot water production, for cooling, by a bottoming cycle etc. There are a lot of research works that study applications of microturbines. Colombo et al. [5] studied experimentally the performance of a cogeneration plant based on a 100 kW microturbine. In high electrical load the systems' efficiency remained nearly constant, while it reduced as the power dropped below 60 kW. Also, the SO_2 and CO emissions increased significantly at part load conditions. Gomes et al. [6] studied experimentally the performance (full and part load) of microturbines fuelled with natural gas and diesel. The results showed that the efficiency is higher at full load and decreases significantly as the power decreases below 50% of the full load. The microturbines had very low emissions which make them appropriate for residential applications. The economic analysis results showed that the cogeneration is the most economically effective application of microturbines since a short payback period is achieved because of the high energy savings. Tassou et al. [7] studied the application of a trigenetation system in a supermarket and compared the results with a conventional system. The trigeneration system was based on a microturbine with an efficiency of 28% at maximum electrical power of 80 kW. The microturbine was coupled with an ammonia-water absorption chiller of cooling capacity 12 kW. They concluded that the economic viability of the system is sensitive to the prices of electricity and natural gas. The COP of the absorption refrigeration system affects the environmental

Institutional Repository - Library & Information Centre - University of Thessaly
02/06/2024 00:35:58 EEST - 18.226.159.139

benefits of trigeneration over conventional systems. Huicochea et al. [8] based on experimental data for a microturbine studied numerically the performance of a trigeneration system, that consisted from the microturbine, a double effect absorption chiller and a heat exchanger.

The microturbines can operate either in stand-alone or in grid-connected applications [9]. For the latter case, it is required a connection with the electricity distribution network for account of any shortage or surplus results from changes in energy demand. Also, the microturbines can be connected in parallel to meet higher power demands. These modular systems have a lot of benefits such as easier maintenance, higher availability, easy replacement of a single faulty engine and high energy conversion efficiencies.

A major benefit of microturbines is the ability to operate with various fuels. Gomes et al. [6] studied the performance of two Capstone C30 microturbines, fuelled with natural gas or diesel. Krishna [10] tasted the same engine with different soy-based biodiesel blends. The results showed no significant changes in efficiency. The addition of biodiesel contributed to a reduction of CO, NO_x as well as SO_2 emissions. Habib et al. [11] used a small turbojet engine to study the effect on the performance and the emissions of pure biofuels and their blends with Jet A aviation fuel. The addition of biofuel had a positive impact on the thermal efficiency, however it hadn't a distinct static thrust advantage since the results with the biodiesel was comparable with those of the reference fuel (Jet A). The CO and the NO emissions decreased significantly when biodiesel was used; on the other hand, the turbine inlet and exhaust temperatures did not change notably. Park et al. [12] fed with biogas a microturbine. The raw biogas, from waste water treatment process, was further treated to remove the harmful contaminants (moisture, H_2S, NH_3, siloxane etc.) before it was burned in the microturbine. The experiment showed that engine operation was unstable when the CH_4 was below 32%. The NO_x emissions were not affected from the N_2 concentration in biogas or the engine power level. On the other hand, the CO concentration increased at part load conditions.

Microturbines can be combined with one or more generation sources [4]. The resulted systems are called hybrid systems and their main advantage is the higher efficiencies compared to single sources. These microturbines can be effectively combined with renewable energy sources such as a photovoltaic system and a wind turbine and mitigate the effect of randomness of these sources, or can be combined with high temperature fuel cells (MCFC and SOFC) and supply electric power with very high efficiency. More details about the latter group of hybrid systems can be found in section 2.3.

The main pollutants resulting from the operation of the microturbines are CO, NO_x, unburned hydrocarbons and negligible amounts of SO_x [13]. They are designed to produce low specific emissions at full load; however, at part load conditions the emissions are higher compared to full load. CO and unburned hydrocarbons are due to the incomplete combustion process. Various reasons contribute to incomplete combustion such as the bad fuel-air mixing, the low residence time and the bad maintenance. The NO_x emissions in microturbines are mainly depended on the high flame temperature and the residence time.

2.2 Fuel cells

Fuel cells are electrochemical devices that convert the chemical energy of a fuel into electricity with high efficiency and low environmental impact [3]. There are many types of fuel cells, which are commonly classified by the type of the electrolyte [3, 14] (see Table 2-2). Moreover, fuel cells can

Institutional Repository - Library & Information Centre - University of Thessaly
02/06/2024 00:35:58 EEST - 18.226.159.139

be classified according to the operating temperature (high, low or medium), the operating pressure (atmospheric or pressurized) or the cell geometry (planar, tubular etc.). Among the various types of fuel cell, in this study only the Solid Oxide Fuel Cells (SOFCs) are examined.

All the fuel cells consist of an electrolyte layer, in contact with two electrodes (anode and cathode) on each side. A schematic representation of a SOFC type unit cell is presented in Figure 2-4. The oxidant, pure oxygen or oxygen from the atmospheric air, are inserted in the cathode side of the fuel cell. The porous material of the cathode allows the adsorption of oxygen molecules and the catalytic dissociation of them into atoms. The atoms are reduced by electrons to oxide ions according to the reaction (2-1). The oxygen ions are conducted through the electrolyte to the anode side of the fuel cell while the depleted oxidant exits the cell.

$$\tfrac{1}{2}O_2 + 2e^- \rightarrow O^{2-} \tag{2-1}$$

In the anode side, the oxide ions react with the fuel (e.g. hydrogen) and release electrons which travel through an external circuit to the cathode side of the fuel cell as shown in Figure 2-4. The reaction that takes place in the anode side is described from the relation (2-2).

$$H_2 + O^{2-} \rightarrow H_2O + 2e^- \tag{2-2}$$

The overall reaction is:

$$H_2 + \tfrac{1}{2}O_2 \rightarrow H_2O \tag{2-3}$$

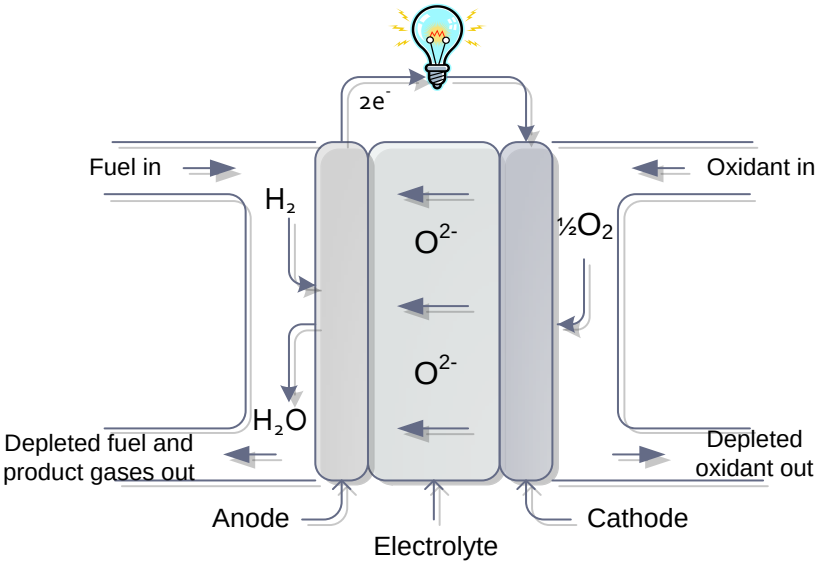

Figure 2-4 Operating principle of SOFC

Institutional Repository - Library & Information Centre - University of Thessaly
02/06/2024 00:35:58 EEST - 18.226.159.139

Table 2-2 Fuel cell types

Fuel Cell Type	Polymer Electrolyte Membrane (PEM)	Alkaline Fuel Cell (AFC)	Phosphoric Acid Fuel Cell (PAFC)	Molten Carbonate Fuel Cell (MCFC)	Solid Oxide Fuel Cell (SOFC)
Electrolyte	Hydrated Polymeric Ion Exchange Membranes	Mobilized or Immobilized Potassium Hydroxide in asbestos matrix	Immobilized Liquid Phosphoric Acid in SiC	Immobilized Liquid Molten Carbonate in $LiAlO_2$	Perovskites (Ceramics)
Operating Temperature	50-100 °C	90-100 °C	150-200 °C	600-700 °C	700-1000 °C
Charge Carrier	H^+	OH^-	H^+	CO_3^{2-}	O^{2-}
Typical Stack Size	<1 – 100 kW	10 – 100 kW	100 – 400 kW	300 kW – 3 MW	1 kW – 2 MW
Efficiency	60% transportation 35% stationary	60%	40%	45-50%	60%
Applications	▪ Backup power ▪ Portable power ▪ Distributed generation ▪ Transportation ▪ Specialty vehicles	▪ Military ▪ Space	▪ Distributed generation	▪ Electric utility ▪ Distributed generation	▪ Auxiliary power ▪ Electric utility ▪ Distributed generation
Advantages	▪ Reduced corrosion & electrolyte management problems ▪ Low temperature ▪ Quick start-up	▪ Cathode reaction faster in alkaline electrolyte leads to high performance ▪ Low cost components	▪ Higher temperature enables CHP ▪ Increased tolerance to fuel impurities	▪ High efficiency ▪ Fuel flexibility ▪ Can use a variety of catalysts ▪ Suitable for CHP	▪ High efficiency ▪ Fuel flexibility ▪ Can use a variety of catalysts ▪ Suitable for CHP & CCHP ▪ Hybrid/GT cycle
Disadvantages	▪ Expensive catalysts ▪ Sensitive to fuel impurities ▪ Low temperature waste heat	▪ Sensitive to CO_2 in fuel and air ▪ Electrolyte management	▪ Pt catalyst ▪ Long start up time ▪ Low current and power	▪ High temperature corrosion and breakdown of cell components ▪ Long startup time ▪ Low power density	▪ High temperature corrosion and breakdown of cell components ▪ High temperature operation requires long start up time and limits

Institutional Repository - Library & Information Centre - University of Thessaly
02/06/2024 00:35:58 EEST - 18.226.159.139

The fuel cells are considered as a very promising alternative to traditional power generation systems, since they offer higher electric efficiencies and lower emissions [15]. Beside the high efficiency, the fuel cells do not utilize moving parts, except the balance of plant equipment. This contributes to low vibration operation, with low noise level, which make them appropriate for installation in urban areas and even in dwellings. Moreover, the absence of moving parts enhances the reliability and reduces the maintenance cost. Furthermore, the SOFC type generators can operate with a variety of fuels [16, 17] which make them suitable for various applications . Finally, the size of a SOFC stack is flexible since can be easily modified by adding or removing cells, allowing it to be constructed for use in any power range.

Ideal operation

The fuel cell converts the chemical energy of a fuel into electric work. The maximum electrical work is obtained when the fuel cell operates ideally. At constant operating temperature and pressure, the ideal work is equal to the Gibbs free energy of the reaction [18].

$$w_{rev} = \Delta^r G = \Delta^r H - T_{SOFC}\Delta^r S \tag{2-4}$$

Taking into account the reaction (2-2) the molar flow of the electrons is:

$$\dot{n}_{el} = 2\dot{n}_{H_2} \tag{2-5}$$

The electric current is defined as the flow rate of the electric charge in an electric field, usually an electrical circuit. For the case of a fuel cell the electric current can be estimated by multiplying the mole flow of the electrons by the charge of a single mole, i.e. the Faraday constant.

$$I = -\dot{n}_{el}F = -2\dot{n}_{H_2}F \tag{2-6}$$

The minus sign is for negative charge of the electrons.

The reversible power is the product of the electric current by the reversible operating voltage, or taking into account the Eq. (2-4) is written as

$$P_{rev} = V_{rev}I = \dot{n}_{H_2}w_{rev} = \dot{n}_{H_2}\Delta^r G \tag{2-7}$$

By combining the relations (2-5)-(2-7) the reversible voltage can be estimated from the following equation

$$V_{rev} = \frac{-\Delta^r G}{2F} \tag{2-8}$$

The Gibbs free energy change for the total reaction (2-3) can be expressed as:

$$\Delta^r G(T,p) = \Delta^r G(T,p^0) + R_m T \ln\left(\frac{p_{H_2O}}{p_{H_2}p_{O_2}^{1/2}}\right) \tag{2-9}$$

where the p^o is the standard pressure (100 kPa).

The standard Gibbs free energy of formation is given from the following relation

$$\Delta^r G(T,p^0) = G(T,p^0)_{H_2O} - G(T,p^0)_{H_2} - \frac{1}{2}G(T,p^0)_{O_2} \tag{2-10}$$

By combining the Eq.(2-9) and Eq. (2-8) the reversible voltage is:

Institutional Repository - Library & Information Centre - University of Thessaly
02/06/2024 00:35:58 EEST - 18.226.159.139

$$V_{rev} = \frac{-\Delta^r G(T, p^0)}{2F} + \frac{R_m T}{2F} \ln\left(\frac{p_{H_2} p_{O_2}^{1/2}}{p_{H_2O}}\right) \quad (2\text{-}11)$$

which is the well-known Nernst equation. The reversible (or Nernst) voltage is the maximum voltage value that can be achieved at given operating conditions.

Voltage losses

During the actual operation of a fuel cell, the voltage is different from the reversible voltage due to voltage losses. The voltage loses are dependent from the operating conditions and the characteristics of the fuel cell. The main voltage losses in an actual fuel cell are [19]:

- Activation losses are due to the sluggish electrode kinetics. There is an energy barrier that must be overcome to transfer the electrons to or from electrodes.
- Ohmic losses are due to the resistance of the components along the current path. They are depended from material properties and the geometric characteristics of the conductive components.
- Concentration losses are due to the diffusion phenomena taking place between the bulk flow and the place where the electrochemical reactions occur.

The voltage losses can be easy distinguished in the V-I diagram (Figure 2-5) of a fuel cell [3]. In the V-I diagram the cell voltage is plotted against the current density. The current density is a typical parameter to describe a fuel cell performance. It is defined as the current per unit area. Usually, it is given in A/m^2.

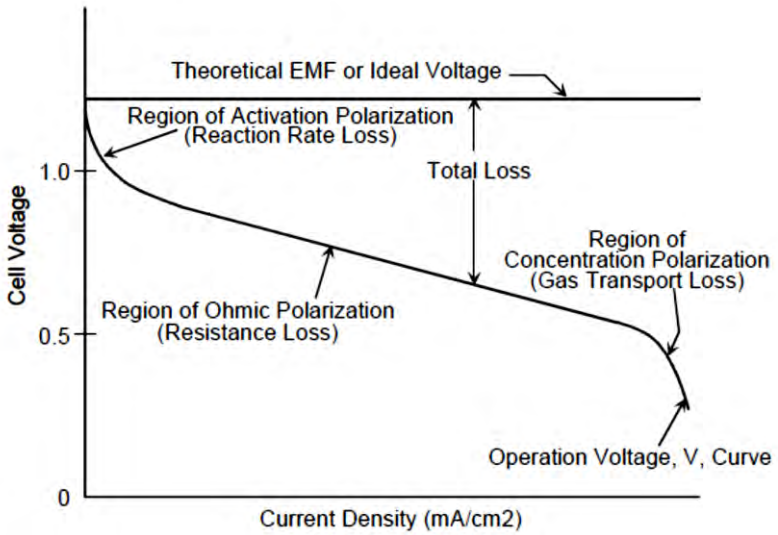

Figure 2-5 V-I diagram

Fuel utilization factor

Another parameter that describes the fuel cell operation is the fuel utilization factor. It is a measure of the amount of fuel consumed to produce electric current. It is defined as the ratio of the hydrogen amount consumed and the equivalent hydrogen amount supplied to the fuel cell.

Institutional Repository - Library & Information Centre - University of Thessaly
02/06/2024 00:35:58 EEST - 18.226.159.139

$$U_f = \frac{\dot{n}_{H_2,consumed}}{\dot{n}_{H_2,equivalent}} \quad (2\text{-}12)$$

The equivalent hydrogen (Eq.2-13) flow is calculated for the inlet fuel composition assuming that all hydrocarbons are fully reformed to hydrogen and carbon monoxide, and moreover, the carbon monoxide is completely shifted to hydrogen.

$$\dot{n}_{H_2,equivalent} = \dot{n}_{fresh\ fuel} \cdot \left(y_{H_2} + y_{CO} + 4 \times y_{CH_4} + 7 \times y_{C_2H_6} + \cdots \right) \quad (2\text{-}13)$$

Fuel - Reforming process

The most common fuel for the SOFC type fuel cells is the hydrogen or hydrogen rich fuel mixtures. The reasons are the high reactivity for the reactions that take place in the anode side of the fuel cell, and also it can be produced from a wide range of available fuels (fossils or renewables) [3]. Although, the fuel cells theoretically can operate with various fuels, in practical applications, the direct use of any fuel is difficult to be realized since it contributes to carbon formation on the anode side [20, 21].

The carbon formation on the anode side is a serious problem since it can deactivate the cells. Two mechanisms are known to exist for carbon deposition at high temperatures [22]. The first is the carbon formation, as a result of the reactions taking place over the catalyst, the deposition onto the metal surface, the dissolution into the bulk of the metal and finally precipitation of the carbon as fiber at some surface of the metal particle. The second is the formation of carbonaceous compounds in the absence of a catalyst via free-radical, gas-phase condensation reactions. The problem is severe when high hydrocarbons (e.g. butane) are present in the fuel [21, 23].

In order to prevent the carbon deposition, the hydrocarbon fuel, together with water steam is catalytically converted to hydrogen, carbon monoxide and some carbon dioxide within the fuel cell stack (internal reforming) according to the following reactions.

$$C_nH_m + nH_2O \leftrightarrow (m/2 + n)H_2 + nCO \quad (2\text{-}14)$$

$$CO + H_2O \leftrightarrow CO_2 + H_2 \quad (2\text{-}15)$$

The internal reforming process of the fuel can be achieved, either directly on the anode side of the fuel cell or indirectly by using a separate catalyst within the fuel cell stack or by combining direct and indirect internal reforming [24]. The advantages of internal reforming include the simple system layout and the increased overall system efficiency since the rejected heat from the electrochemical reactions is utilized. Nevertheless, the problem with carbon deposition still remains with the higher than methane hydrocarbons. In order to overcome this problem, a pre-reformer stage is installed upstream the internal reformer so as to reform the higher hydrocarbons. The pre-reformer operates at lower temperatures to preclude the carbon deposition. Moreover, as the reforming reactions are endothermic, the pre-reforming process prevents the generation of cold spots on the fuel cell stack or on the internal reformer, which can be catastrophic for these devices.

Steam to carbon ratio

In steam reforming reaction excess steam is needed in order to inhibit the soot formation and force the reactions to completion [3]. A parameter to describe the amount of water in the hydrocarbon

Institutional Repository - Library & Information Centre - University of Thessaly
02/06/2024 00:35:58 EEST - 18.226.159.139

fuel is the steam to carbon ratio. It is defined as the ratio of the steam moles to the number of moles of carbon in the fuel (Eq. 2-16), and usually takes values in the neighborhood of 2.5.

$$SCR = \frac{\text{number of } H_2O \text{ moles}}{\text{number of fuel C moles}} \quad (2\text{-}16)$$

2.3 Hybrid systems

A hybrid energy system is a synergetic combination of two or more energy conversion technologies which supply the same type of useful output. Usually, the hybrid systems achieve higher efficiency greater than either technology is capable independently.

The microturbines are an attractive choice for hybrid systems. In the literature there are many examples where the microturbines are coupled with different types of energy systems. Kalantar and Mousavi [25] proposed a hybrid system consisting of a wind turbine, a solar array, a microturbine and a lead acid battery pack for a stand-alone application. The microturbine and the batteries are used as a backup to meet the power demand under all weather conditions. The authors chose a microturbine instead of a diesel engine because of the significant advantages of the former. Mohamed and Koivo [26] presented a method to optimize the operation of a micro-grid unit consisting of a microturbine, a wind turbine, a fuel cell, a diesel generator, a photovoltaic array and a battery storage with respect to the operating cost and emissions. Verda and Sciacovelli [27] studied and optimize the performance of a hybrid system obtained by integrating a microturbine and molten carbonate fuel cell. The system was fuelled with biogas and produces electric power and heat for the anaerobic digester. The digester treated the organic waste collected from a small town and used bacteria to break down the biodegradable material in an oxygen free environment. One of the products of the anaerobic digestion is the biogas which was used to fuel the hybrid system. The exhaust gas of the hybrid system was used to supply heat for the digestion process.

One of the most effective combinations is the microturbines and the SOFC type fuel cells (SOFC-GT). In hybrid SOFC- GT system the high temperature exhaust of the fuel cell generator is used to drive a gas turbine which produces supplementary power and supplies the fuel cell generator with compressed air. This integration contributes to very high efficiency values of about 60%. Integrating a fuel cell and a gas turbine is by no means trivial and a significant system-level effort has been made to understand hybrid system integration and thermodynamics. The most important concern is the smooth matching of a SOFC module with a gas turbine [28, 29].

A plethora of studies can be found in the literature dealing with hybrid SOFC-GT systems [30-36]. These systems are based on micro-turbines, a sufficiently mature technology, which has been developed significantly in the last decades [37, 38]. Microturbines present some unique characteristics compared with the larger gas turbine engines such as the high rotational speeds, the ability to burn various fuels and the radial turbomachines. Various integration strategies have been proposed, for example see [15, 39]. When a SOFC generator is coupled directly to a Brayton cycle, two basic arrangements can be recognized [15]: (a) the SOFC stack operates under pressure and substitutes (totally or partially) the burner of the gas turbine cycle and (b) the SOFC is placed at the exit of the turbine and operates close to atmospheric pressure.

In the case of the pressurized SOFC systems high efficiency values are achieved. These hybrid systems show high specific power values which contributes to small equipment sizes. The

Institutional Repository - Library & Information Centre - University of Thessaly
02/06/2024 00:35:58 EEST - 18.226.159.139

disadvantage in this arrangement is the demanding design of the pressure vessel for the SOFC generator, which leads to an increased manufacturing cost. In the non-pressurized configuration, the SOFC generator is placed at the exit of the turbine component. These systems have lower efficiency values than the pressurized ones. Due to the gas expansion in the turbine, the inlet air for the SOFC generator may not have the required temperature value, if the operating temperature of the fuel cell is too high. This fact makes the non-pressurized configuration suitable for intermediate-temperature SOFC applications. Furthermore, the exhaust gases in the non-pressurized systems have higher temperature, which contribute to less effective waste heat recovery.

The simplified layouts of the two basic arrangements are shown in Figure 2-6. This work deals only with pressurized SOFC-GT systems.

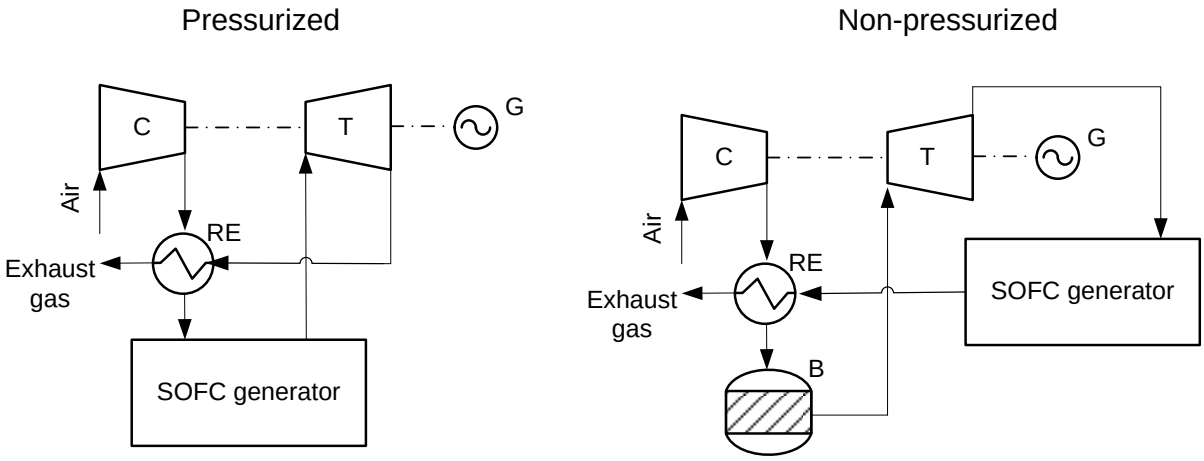

Figure 2-6 The two basic layouts of hybrid SOFC-GT systems (C: Compressor, T: Turbine, B: Burner, G: Generator, RE: Recuperator)

2.4 Balance of plant equipment

A practical fuel cell system installation, apart from the fuel cell stack, requires several auxiliary items for its operation. This auxiliary equipment is usually referred as balance of plant (BoP) and includes the fuel processing system, the air processing system, the power conditioning and the control unit, the valves etc. In the following paragraphs the basic BoP equipment is presented and discussed.

2.4.1 Desulfurizer

The fossil fuels contain sulfur compounds that have to be removed before they are used by the fuel cell. The sulfur contents can deactivate the reforming process as well as the anode catalysts , even if in low concentrations [19]. A usual desulfurization process involves the conversion of any organic sulfur-containing compounds into hydrogen sulfide (H_2S), over a supported cobalt-molybdenum or nickel-molybdenum catalyst, by reaction with hydrogen (hydrogenolysis) and subsequently the absorption of H_2S onto a bed of zinc oxide. Unfortunately, the previous process cannot be easily implemented for an internal reforming SOFC system, since it requires hydrogen for the hydrogenolysis reaction. To overcome this limitation an absorbent such as activated carbon can be used to remove sulfur from feed gases.

2.4.2 Ejector/Jet pump

The ejector is a simple pump without moving parts. In SOFC systems it is used to recirculate part of the anode exhaust gases. The recycled gases contain hot steam which is necessary for the

Institutional Repository - Library & Information Centre - University of Thessaly
02/06/2024 00:35:58 EEST - 18.226.159.139

endothermic reforming process. The operating principle of the ejector is based on the momentum transfer between two streams (Figure 2-7). The high pressure actuating fluid (fresh fuel) expands through a nozzle and enters the mixing chamber with high velocity. The high velocity of the actuating flow lowers the pressure and creates a suction effect which draws the induced fluid (recycled fuel) into the suction chamber. The fresh and recycled fuels are mixed in the mixing chamber and slow-down in the diffuser to recover static pressure. The ejector outlet pressure is greater than the inlet pressure of the recycled fuel to overcome the pressure loses in the fuel path.

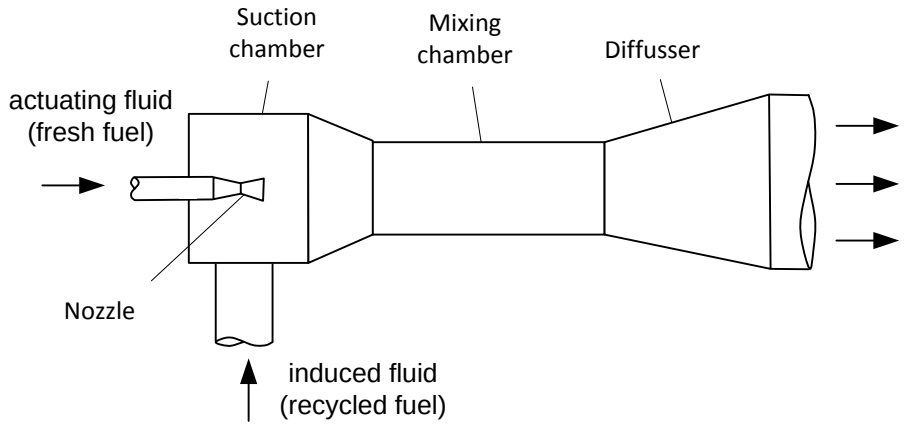

Figure 2-7 Ejector scheme

2.4.3 Fuel pre-reformer

In the pre-reformer, the higher hydrocarbons with the steam contained in the recycled fuel are converted into methane, hydrogen and carbon oxides [3]. As the process is endothermic, it utilizes the heat of the recycled fuel. At the operating conditions (low temperature < 500 °C) of pre-reformer carbon formation does not occur. The reformed fuel that exits the pre-reformed is routed to the SOFC stack where internal reforming is achieved.

2.4.4 Internal reforming

The internal reforming process can be achieved either indirectly or directly or by a combination of direct and indirect reforming approach. The indirect internal reforming (IIR) utilizes a separate catalyst to reform the supplied fuel. The catalyst is placed upstream the anode and utilizes the generated heat from the fuel cell stack for the endothermic reforming process. In the direct internal reforming the reforming reactions take place on the anode. Although, this is a simpler, cheaper and more efficient solution, it contributes to large temperature gradients in the cell between inlet and outlet which can result in cracking of the fuel cell materials.

2.4.5 Power conditioning unit

In a hybrid SOFC-GT system a power conditioning sub-system is necessary to convert the electric power supplied from generator and SOFC stack to the desired voltage and frequency. The generator is mounted on the shaft of the microturbine, so it rotates with very high rotational speed which varies at part load conditions. Consequently, the delivered alternating current (AC) has to be converted (to 50 or 60 Hz) for general use. The power condition process involves rectifying the high-frequency AC to DC, and then inverting the DC to the desired AC [9]. The SOFC stack produces DC

Institutional Repository - Library & Information Centre - University of Thessaly
02/06/2024 00:35:58 EEST - 18.226.159.139

output voltage that is unregulated since it varies with the operating conditions (pressure, temperature etc.). A DC-DC converter is connected to the output of the SOFC stack to convert the unregulated voltage to the desired voltage level. The regulated DC voltage is then fed to an inverter to convert to the desired AC output [19].

It is a usual practice in hybrid SOFC-GT systems to utilize a common DC-AC converter for the gas turbine and the SOFC outputs [3]. This choice can reduce significantly the cost of the power conditioning system.

2.5 Solid Oxide Fuel Cells

Several fuel cell designs have been proposed over the years. Generally, the proposed designs are divided into two groups, the first is the planar and the second is the tubular design. The planar fuel cells are composed from planar layers of the anode, cathode, electrolyte and interconnection which are connected in electrical series. The main advantages of this design are the high power densities and the easy fabrication [40], but their major drawbacks are the mechanical loads and the sealing at high operating temperatures. The seals are necessary for a planar SOFC stack in order to block the mixing of the oxidant and fuel gases. A typical planar fuel cell is shown in Figure 2-8. During the operation the fuel and the oxidant guided from the flow channels formed by the bipolar separator to the anode and cathode sides of the fuel cells, respectively. In a planar fuel cell, the fuel and oxidant flows can be arranged in different flow configurations (Figure 2-9). The flow configuration plays a major role in the temperature and current distribution in a fuel cell stack.

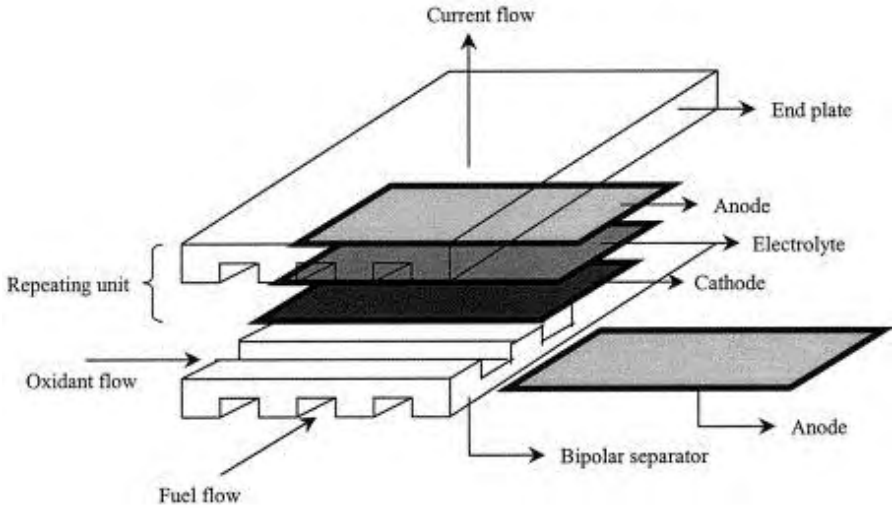

Figure 2-8 Typical planar SOFC, [41].

Institutional Repository - Library & Information Centre - University of Thessaly
02/06/2024 00:35:58 EEST - 18.226.159.139

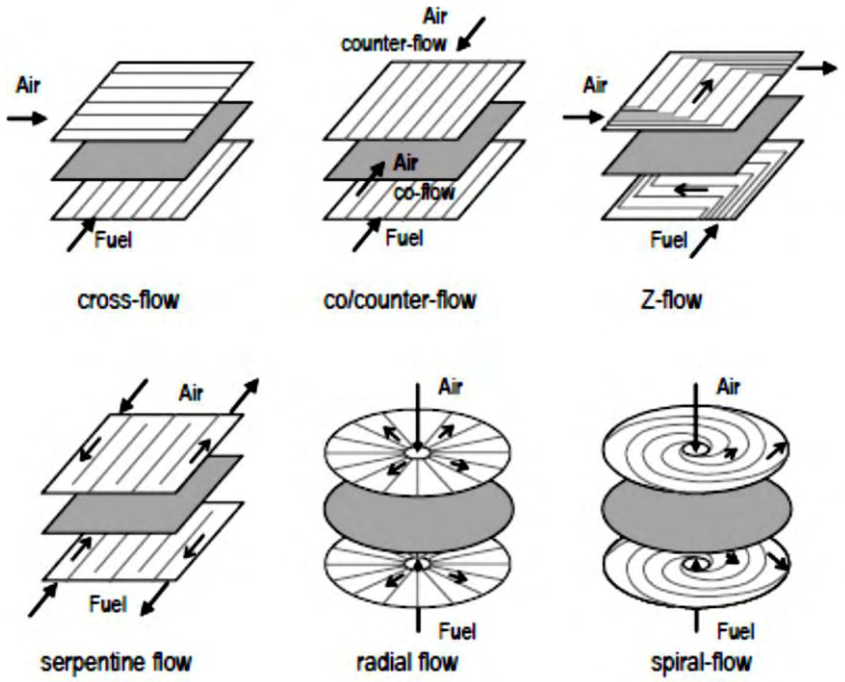

Figure 2-9 Flow configurations of a planar SOFC, [42].

A cross section of a tubular SOFC design is shown in Figure 2-10. This design solved the sealing problems existing for the planar fuel cells and, moreover, has a very good mechanical integrity [40]. In contrast to the planar design, the tubular SOFCs have lower power densities. This is due to higher ohmic – resistance, resulting from the longer current path along the circumference of the circular cross section.

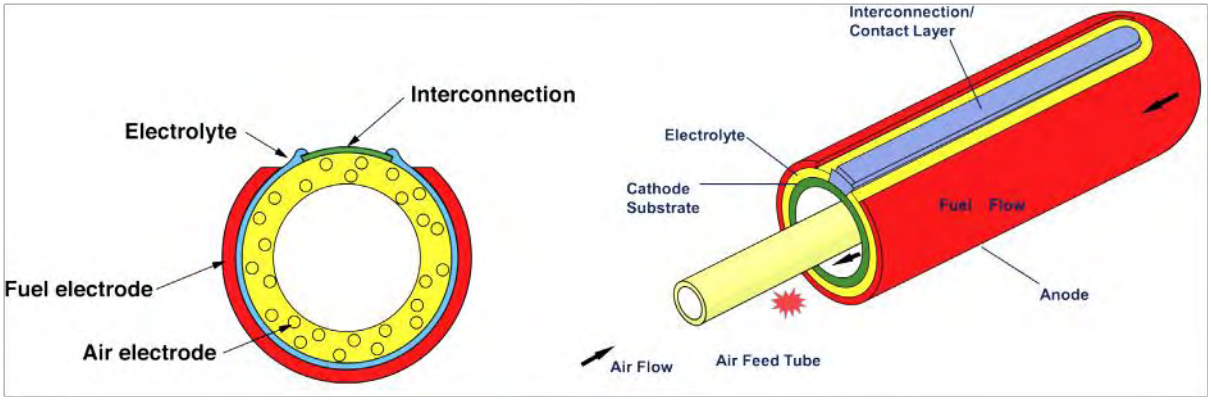

Figure 2-10 A schematic of tubular SOFC, [43].

To eliminate the problem of low power densities alternative designs have been developed by Siemens-Westinghouse (Figure 2-11). In these flattened tubular fuel cells the current pathway is shorter. The ribs inside the cell, as well as the wavy shape reduce the current path; they work like a bridge for the electrons, and reduce the internal resistance [40, 43]. The formed cavities (cathode) are used for the oxidant supply.

Institutional Repository - Library & Information Centre - University of Thessaly
02/06/2024 00:35:58 EEST - 18.226.159.139

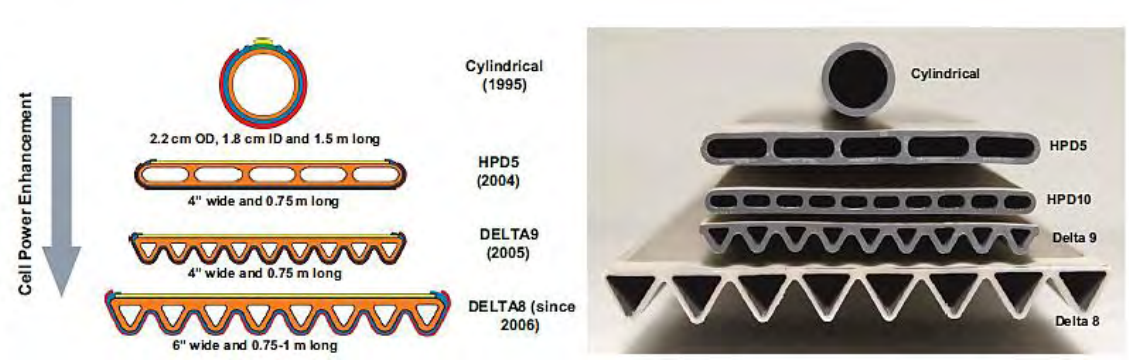

Figure 2-11 Schematic (left) and actual image (right) fuel cell developed by Siemens-Westinghouse [43]

2.5.1 Siemens – Westinghouse tubular design

Siemens – Westinghouse is a pioneer in tubular SOFCs. This company, in 1997, presented a 100 kWe atmospheric pressure SOFC-CHP system. The system was able to produce 105 – 110 kWe net AC power with an electrical efficiency of 46% [43, 44]. It was the first demonstration that utilizes the commercial prototype cathode supported cells and in stack reformers. The system accumulated ~16600 testing hours, becoming the longest-running fuel cell in the world [41].

The geometric data of the tubular SOFC are presented in Table 2-3, [45, 46]. Each fuel cell has 834 cm^2 effective area. The system consists of 1152 fuel cells. The cells are arranged in bundles of 24 units, which are organized in three series of eight cells. Four bundles are connected in series to form a bundle row of 96 cells. Twelve bundle rows are placed side-by-side to form the SOFC stack of the 100 kWe system (Figure 2-12).

Table 2-3 Geometric data of tubular SOFC

Cell length, (m)	1.5
Cell diameter, (m)	0.022
Anode thickness, (m)	0.0001
Cathode thickness, (m)	0.0022
Electrolyte thickness, (m)	0.00004
Interconnection thickness, (m)	0.000085
Interconnection width, (m)	0.009

Institutional Repository - Library & Information Centre - University of Thessaly
02/06/2024 00:35:58 EEST - 18.226.159.139

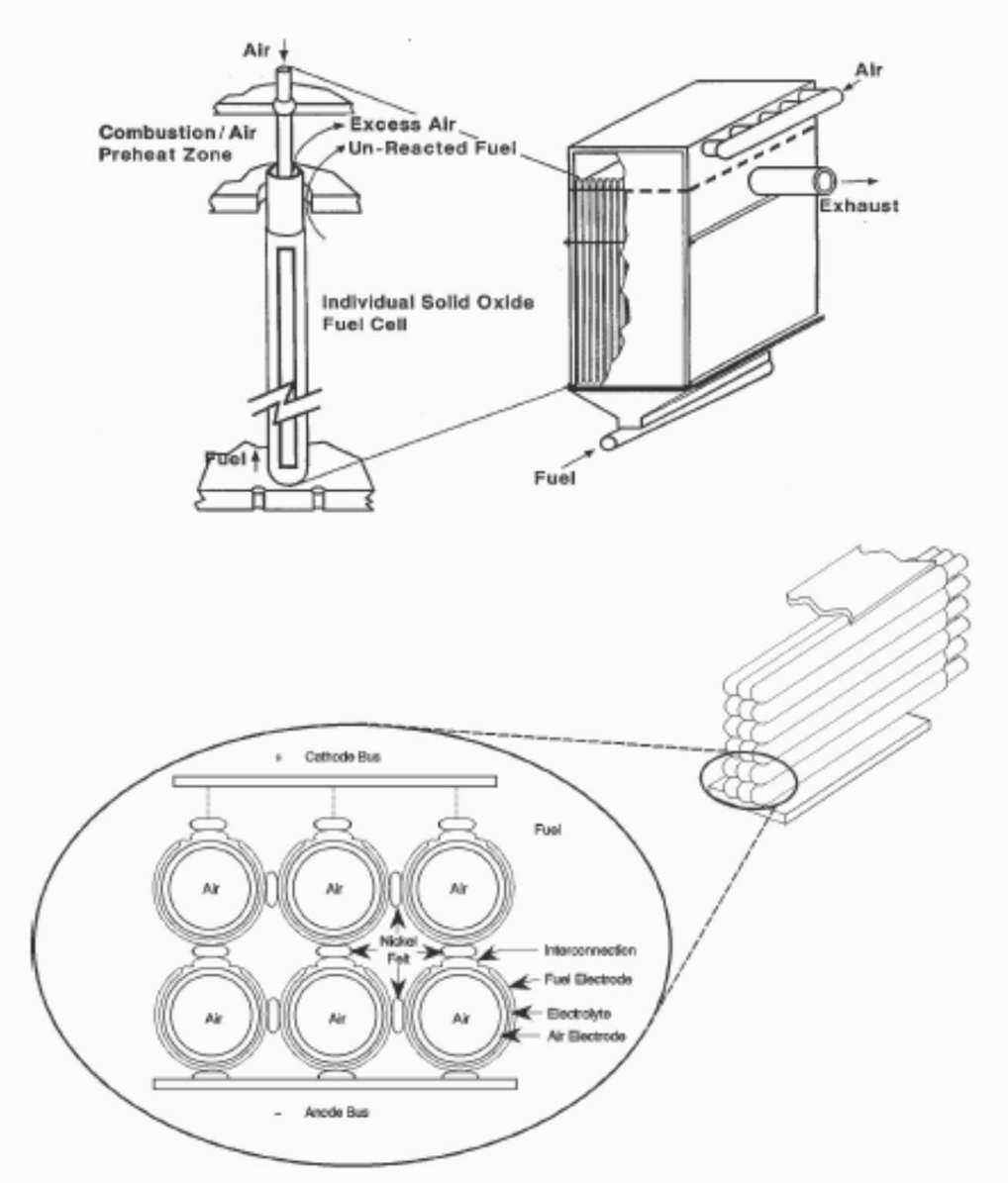

Figure 2-12 Siemens – Westinghouse SOFC stack, [3].

A schematic layout of the Siemens – Westinghouse SOFC generator is shown in Figure 2-13. Desulfurized fuel, in high pressure passes through the ejector and is mixed with the anode exhaust gases (depleted fuel). The mixture is fed into the adiabatic pre-reformer in order to reform the higher hydrocarbons and then is guided to the top of the IIR, where is further reformed as it flows downward through a catalytically active space to the fuel distribution plenum [44]. The IIR is heated by the hot fuel cells. The completely reformed fuel flows through the exterior of the tubular fuel cells where electrochemically reacts to produce electric power and heat. Thereinafter, the depleted fuel flows into the recirculation plenum where partially recirculates and the rest flows into the combustion plenum. The air enters into the air plenum and is guided to the bottom of the internal side of the fuel cells by the air feed tube. The air exits the feed tube and moves upward in the annular space formed by the air feed tube and the fuel cell where it reacts electrochemically. The depleted air exits the fuel cells and reacts with the depleted fuel in the combustion plenum to supply heat for the incoming air passes through the air feed tubes. After the heat exchange process the exhaust gasses are guided out of the SOFC generator.

Institutional Repository - Library & Information Centre - University of Thessaly
02/06/2024 00:35:58 EEST - 18.226.159.139

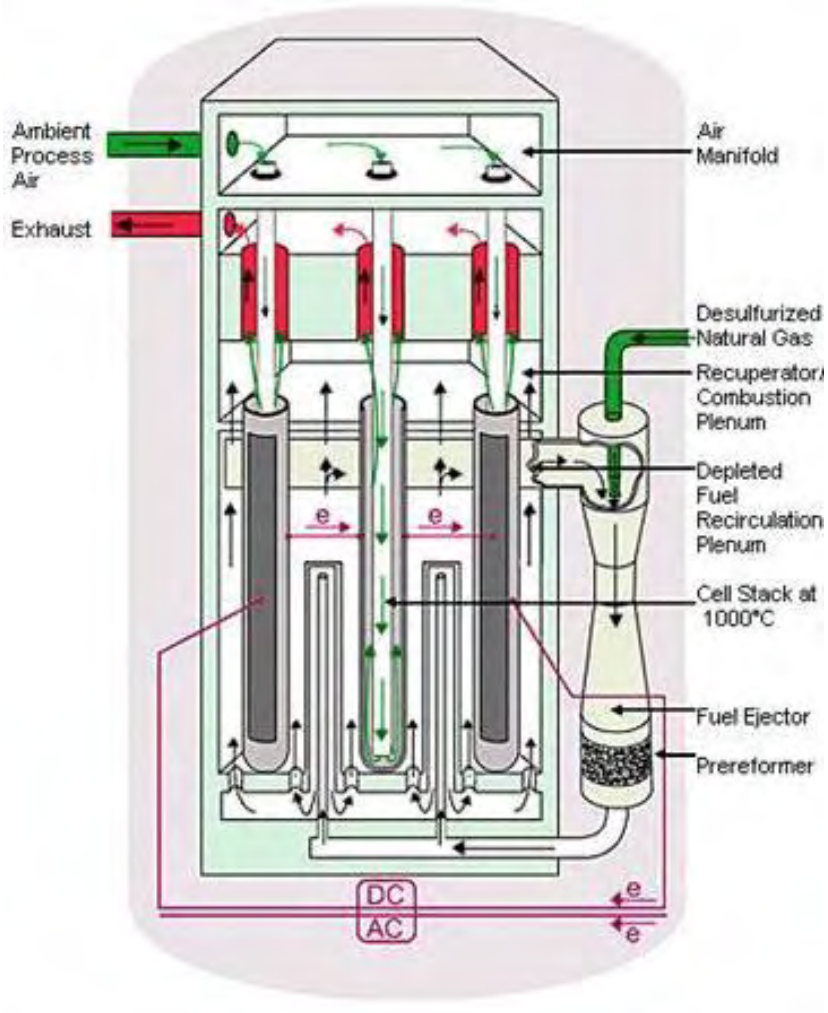

Figure 2-13 Siemens – Westinghouse SOFC generator, [42].

The previously described SOFC generator was matched with a microturbine to form a hybrid system (Figure 2-14). The system operated at an elevated pressure (about 3 atm) and it was able to produce 220 kWe net AC power, 176 kW from the SOFC generator and 47 kW from the gas turbine (minus 3 kW for auxiliary loads). The system was fueled with natural gas and achieved a net electrical efficiency value of 57% [44].

The system operated for about 3400 hours from June 2001 to April 2002. It was the world's first SOFC-GT hybrid system [47]. The operation showed that coupling of a SOFC system with a microturbine is technically feasible but it requires further investigation regarding the microturbine design and integration.

Institutional Repository - Library & Information Centre - University of Thessaly
02/06/2024 00:35:58 EEST - 18.226.159.139

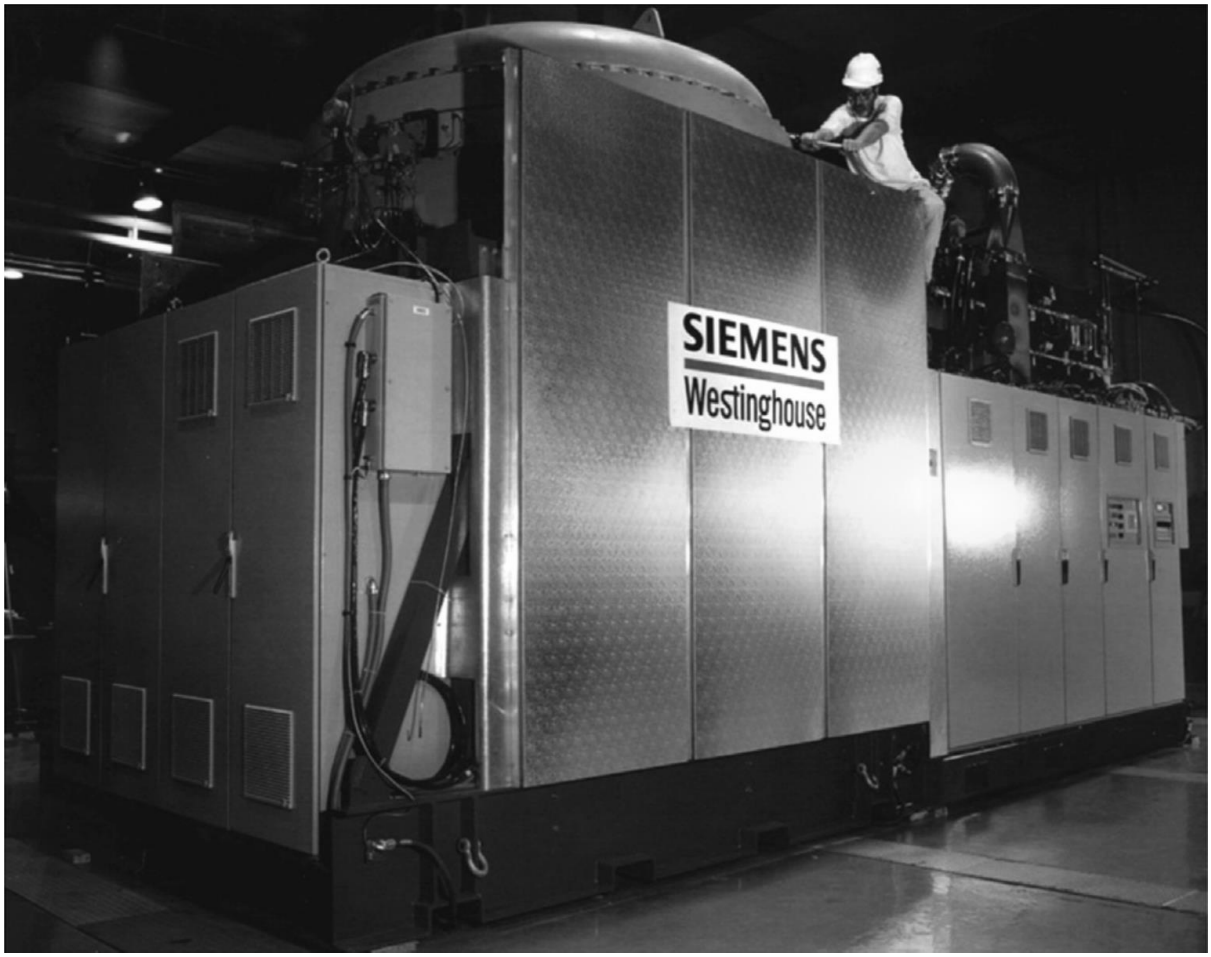

Figure 2-14 The hybrid SOFC – GT system developed from Siemens – Westinghouse, [43].

2.5.2 Other hybrid SOFC-GT system

Except from the Siemens-Westinghouse, several companies including Rolls-Royce and Mitsubishi Heavy Industries have developed hybrid SOFC-GT systems. The Rolls-Royce utilize a planar SOFC technology based on the "multi-cell membrane electrode assembly" (MEA)[48], which is characterized by thin fuel cells stacked in series as shown in Figure 2-15.

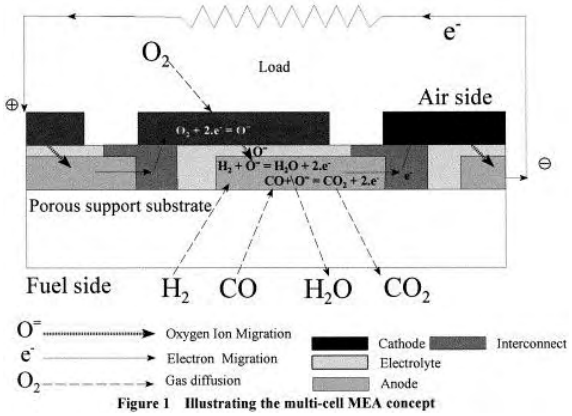

Figure 2-15 Multi-cell MEA concept, [48].

Rolls-Royce developed small hybrid systems (250 kW) which were successfully demonstrated between 2008 and 2010. Rolls-Royce has also been developing a hybrid SOFC-GT system on the

Institutional Repository - Library & Information Centre - University of Thessaly
02/06/2024 00:35:58 EEST - 18.226.159.139

order of 1 MW fueled by natural gas. The system consists of a 200kW gas turbine and a 800kW SOFC generator [49].

Mitsubishi Heavy Industries developed of a SOFC-GT hybrid system rated at 200 kW, combing a SOFC module and a modified gas turbine [50]. The system was reported to operate successfully with an efficiency of 52%.

2.6 Design challenges

As previously mentioned, the hybrid SOFC-GT systems are a very effective energy conversion technology. The coupling of a gas turbine with a SOFC generator has two advantages: a) the hot exhaust gases from the SOFC generator are used to produce additional electrical power and b) the gas turbine supplies the SOFC stack with the required air for the electrochemical reactions and the rejection of the produced heat.

An important concern in SOFC-GT systems is the smooth matching of the SOFC generator and the gas turbine [51-53] since the systems operating parameters must match both in design point and in part load conditions. The purpose of the good matching is twofold, to ensure: a) the good performance in the whole operating range and b) the safe operation since the key process variables (e.g. SOFC operating temperature) must be kept within certain bounds.

For the design of a new hybrid system there are three alternative solutions:

1. Design a totally new hybrid system, optimized for the desired range of power output. This solution is time consuming and costly, since it requires the development of new devices which have to be studied and tested to ensure their safe and efficient operation.
2. Starting with an existing SOFC generator and choosing the characteristics of the microturbine or finding an appropriate microturbine package.
3. And finally, starting with an existing microturbine package and choosing the characteristics of the SOFC generator.

The last two cases are the more economical solutions because they are based on existing devices which are incorporated on the developed hybrid system. Attention must be paid in critical operating conditions such as the SOFC stack operating temperature, turbine inlet and outlet temperatures, air mass flow and compressor surge margin.

The integration of a SOFC generator into the Brayton cycle can affect the operating points of the turmbomachines, because, the SOFC generator components affect the pressure difference between the compressor and turbine. This cause a rematching of the turbomachines which may have a negative impact on the system performance since it can affect their efficiencies. A major concern is the reduction of the surge margin. This situation should be avoided since it can drive the compressor to unstable operation which is characterized by rapid air flow and pressure fluctuations. The surge events are harmful not only for the microturbine, but also for the SOFC stack since they can lead to overheating as the air mass flow varies and additionally, the pressure waves formed at the surge event can travel along the gas path and affect its mechanical integrity.

The SOFC fuel flow is greater than for the coupled microturbine. This fact slightly increases the mass flow through the turbine and consequently the power production [54]. Also, the higher amount of water vapor in the exhaust gases has impact on the heat transfer processes that takes place on the hot side of the recuperator.

Institutional Repository - Library & Information Centre - University of Thessaly
02/06/2024 00:35:58 EEST - 18.226.159.139

The microturbine can affect the temperature difference in the cathode compartment of the fuel cell [55]. As the larger microturbines operate with higher air mass flow, the inserted air to the SOFC may not sufficiently be preheated in the recuperator. This contributes to low temperature at cathode inlet and consequently larger temperature gradients which results in higher thermal stresses.

The temperature of exhaust gases from the SOFC stack is crucial for the turbine operation. It contributes to high turbine inlet and exit temperatures which can affect the mechanical integrity of the turbine and recuperator respectively.

In order to avoid the overheating of the devices of a hybrid system, a well-designed control system is necessary. The system should collect data during the system operation and do the appropriate settings to avoid dangerous conditions. Also, it should be capable to start up and shut down the system with safety and track the load demand by keeping the operating parameters within a prescribed region bounded by system and process constraints.

Institutional Repository - Library & Information Centre - University of Thessaly
02/06/2024 00:35:58 EEST - 18.226.159.139

Chapter 3

Modeling of SOFC-GT system

In this section the operating principles of the main components of the hybrid SOFC-GT system are presented and discussed.

3.1 Gas turbine components modeling

The gas turbine systems are a mature technology and a lot of work has been done for their modeling. In the available literature there are many methodologies to model gas turbines such as ~~CFD modeling~~, neural networks, Kalman filters and zero -dimensional methods.

The most common approach to simulate a gas turbine engine is the zero-dimensional models since they are able to reproduce the overall engine performance with low computational cost and adequate accuracy. Those methods are mainly used is design and off-design simulations as well as during the preliminary design phase where the design parameters are under discussion and it essential to estimate the engine performance under various operating conditions.

With the zero-dimensional models the averaged working media characteristics (e.g. temperature and pressure) are estimated at discrete positions along the flow path. Generally, the discrete positions are the inlets and outlets of subsystems of the engine such as compressor, turbine, combustion chamber and exhaust nozzle. These models do not require a detailed geometric description of the engine.

3.1.1 Turbomachinery models

According to Stamatis [56] the turbomachinery components (compressor, turbine) are modeled with three groups of equations:

Definition equations: These are the pressure ratio and isentropic efficiency relations for the compressor (Eq.3-1) and turbine(Eq. 3-2) components.

$$\left\{ PR_c = \frac{p_{out}}{p_{in}}, \eta_{is,c} = \frac{h_{out,is} - h_{in}}{h_{out} - h_{in}} \right\} \quad (3\text{-}1)$$

$$\left\{ PR_t = \frac{p_{in}}{p_{out}}, \eta_{is,t} = \frac{h_{in} - h_{out}}{h_{in} - h_{out,is}} \right\} \quad (3\text{-}2)$$

Conservation equations: In general form are:

$$\dot{m}_{out} - \dot{m}_{in} = 0 \qquad \text{(mass balance)} \quad (3\text{-}3)$$

Institutional Repository - Library & Information Centre - University of Thessaly
02/06/2024 00:35:58 EEST - 18.226.159.139

$$\dot{Q} - P = h_{out}\dot{m}_{out} - h_{in}\dot{m}_{in} \quad \text{(energy balance)} \tag{3-4}$$

Usually, the compressor and turbine devices are considered adiabatic, so the heat transfer rate $\dot{Q}$ is equal to zero. Also, the power output *P* is negative in case of the compressor and positive in case of the turbine.

Relations of characteristic parameters: Usually, they are referred as performance characteristics or performance maps and used to describe the off design performance of compressor and turbine components. They are given in table form. The tables contain the pressure ratio, the mass flow parameter and the isentropic efficiency for different speed values.

The values in performance maps are in quasi-dimensionless form [57]. Moreover, the map parameters are referred to a reference working media (e.g. dry air). For this reason, corrections should be applied to consider the changes in working media composition.

The corrected parameters for the map interpolation are [58]:

- Compressor

$$\left(\frac{N}{\sqrt{\theta}}\right)_{ref} = \left(\frac{N}{\sqrt{\theta}}\right)_{mix} \sqrt{\frac{\gamma_{ref} R_{ref}}{\gamma_{mix} R_{mix}}} \tag{3-5}$$

$$\left(\frac{\dot{m}\sqrt{\theta}}{\delta}\right)_{ref} = \left(\frac{\dot{m}\sqrt{\theta}}{\delta}\right)_{mix} \sqrt{\frac{\gamma_{ref} R_{mix}}{\gamma_{mix} R_{ref}}} \tag{3-6}$$

$$PR_{ref} = \left[\left(PR_{mix}^{\frac{\gamma_{mix}-1}{\gamma_{mix}}} - 1\right)\frac{R_{ref}\gamma_{ref} Cp_{mix}}{R_{mix}\gamma_{mix} Cp_{ref}} + 1\right]^{\frac{\gamma_{ref}}{\gamma_{ref}-1}} \tag{3-7}$$

There is not a general equation for the isentropic efficiency variation due to changes in working media composition [58]. Therefore, it is common practice to assume that efficiency does not change with fluid properties.

- Turbine

$$\left(\frac{N}{\sqrt{\theta}}\right)_{ref} = \left(\frac{N}{\sqrt{\theta}}\right)_{mix} \sqrt{\frac{R_{ref}}{R_{mix}} \frac{\gamma_{ref}}{\gamma_{ref}+1} \frac{\gamma_{mix}+1}{\gamma_{mix}}} \tag{3-8}$$

$$\left(\frac{\dot{m}\sqrt{\theta}}{\delta}\right)_{ref} = \left(\frac{\dot{m}\sqrt{\theta}}{\delta}\right)_{mix} \sqrt{\frac{\gamma_{ref} R_{mix}}{\gamma_{mix} R_{ref}}} \left(\frac{2}{\gamma_{ref}+1}\right)^{\frac{\gamma_{ref}+1}{2(\gamma_{ref}-1)}} \left(\frac{\gamma_{mix}+1}{2}\right)^{\frac{\gamma_{mix}+1}{2(\gamma_{mix}-1)}} \tag{3-9}$$

$$PR_{ref} = \left[1 - \left(1 - PR_{mix}^{-\frac{\gamma_{mix}-1}{\gamma_{mix}}}\right)\frac{R_{ref}}{R_{mix}} \frac{\gamma_{ref}}{\gamma_{ref}+1} \frac{\gamma_{mix}+1}{\gamma_{mix}} \frac{Cp_{mix}}{Cp_{ref}}\right]^{-\frac{\gamma_{ref}}{\gamma_{ref}-1}} \tag{3-10}$$

The isentropic efficiency variation with the working media composition was not taken into account as in compressor's case.

Institutional Repository - Library & Information Centre - University of Thessaly
02/06/2024 00:35:58 EEST - 18.226.159.139

Typical performance maps for the compressor and turbine components are presented in Figure 3-1. The constant speed lines are shown with solid lines and the efficiency contours with dashed lines.

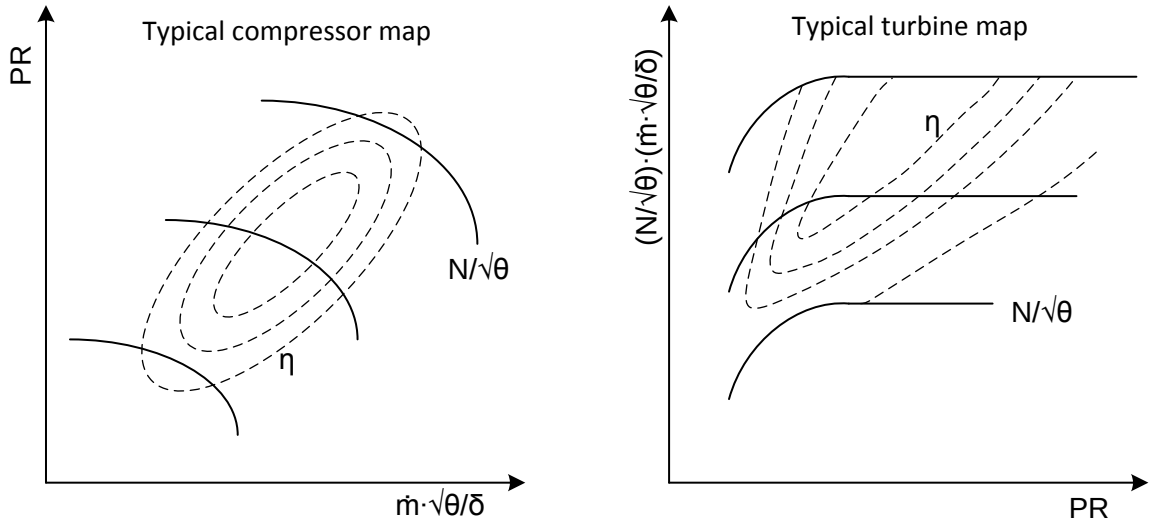

Figure 3-1 Typical form of turbomachinery maps

In simulation models, maps from similar engines are utilized which are scaled according to the following scaling factors in order to correspond to the engine.

$$f_m = \frac{\dot{m}_{c,engine}^{design}}{\dot{m}_{c,map}^{design}} \tag{3-11}$$

$$f_{PR} = \frac{PR_{engine}^{design} - 1}{PR_{map}^{design} - 1} \tag{3-12}$$

$$f_\eta = \frac{\eta_{engine}^{design}}{\eta_{map}^{design}} \tag{3-13}$$

3.1.2 Burner model

The role of the burner is to mix the air with the fuel and burn the mixture to produce thermal energy for use elsewhere in the system. Usually, for simplification purposes, the combustion process is considered complete and the burner adiabatic. In common applications, the supplied fuel is a mixture of hydrocarbons which reacts with the oxygen of the supplied air according to the following reaction:

$$C_a H_b + \left(a + \frac{b}{4}\right) O_2 \rightarrow a CO_2 + \frac{b}{2} H_2 O \tag{3-14}$$

When the burner is fed with syngas consisting primarily of hydrogen and carbon monoxide, the following reactions take place:

$$H_2 + \frac{1}{2} O_2 \rightarrow H_2 O \tag{3-15}$$

Institutional Repository - Library & Information Centre - University of Thessaly
02/06/2024 00:35:58 EEST - 18.226.159.139

$$CO + \frac{1}{2}O_2 \rightarrow CO_2 \tag{3-16}$$

As the combustion process is complete, the fluid composition can be easily estimated [59]. Taking an energy and mass balance on the burner control volume, it is possible to estimate the temperature and the enthalpy at the exit.

3.1.3 Recuperator

The recuperator is a heat exchanger which is used to recover heat from the hot exhaust gases. The heat is supplied to the compressed air before it enters into the combustion chamber (or into the SOFC generator in case of hybrid SOFC-GT systems) contributing to lower fuel consumption.

A common method to model the steady state operation of a heat exchanger is the log mean temperature difference (LMTD) [60]. In Figure 3-2 is shown schematically a counter flow heat exchanger.

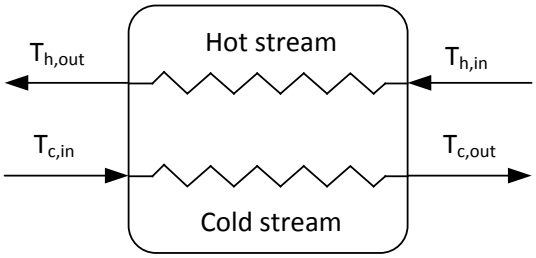

Figure 3-2 Counter flow heat exchanger

For a counter flow heat exchanger the heat transfer between the two fluid is given from the following equation (Eq. 3-17).

$$\dot{Q} = UA_s \left(\frac{\left(T_{h,in} - T_{c,out}\right) - \left(T_{h,out} - T_{c,in}\right)}{\ln\left(\frac{T_{h,in} - T_{c,out}}{T_{h,out} - T_{c,in}}\right)} \right) \tag{3-17}$$

The overall heat exchanger thermal conductance (UA_s) varies at off-design conditions according to the power low expression of Eq. (3-18), where the reference values are for the design point of heat exchanger.

$$U = U_{ref} \left(\frac{\dot{m}}{\dot{m}_{ref}} \right)^b \tag{3-18}$$

The outlet conditions can be estimated by taking energy and mass balances, according to the following relations.

$$\dot{m}_{c,in} = \dot{m}_{c,out} \tag{3-19}$$

$$\dot{m}_{h,in} = \dot{m}_{h,out} \tag{3-20}$$

$$\dot{Q} = \dot{m}_c C_{pc} \left(T_{c,out} - T_{c,in}\right) = \dot{m}_h C_{ph} \left(T_{h,in} - T_{h,out}\right) \tag{3-21}$$

Institutional Repository - Library & Information Centre - University of Thessaly
02/06/2024 00:35:58 EEST - 18.226.159.139

3.1.4 Power produced & thermal efficiency

The total power produced from a microturbine is given from the following relation. Where the η_m is the mechanical efficiency.

$$P_{GT} = \eta_m P_t - P_c \tag{3-22}$$

The thermal efficiency of the microturbine is given from the equation (3-23).

$$\eta_{GT} = \frac{P_{GT}}{\dot{m}_f LHV} \tag{3-23}$$

3.2 Literature review of SOFC modeling

The SOFC systems are complicated devices and consequently, advanced models are required in order to study their operation. A combination of complex phenomena, such as heat transfer mechanisms, chemical reactions, diffusion processes and conduction of electric charges should be considered. The developed models in the available bibliography vary from lumped models, which are mainly used for the simulation of thermal plants, to more detailed, for the study of the reactions at the interface between electrolyte and electrode. These models are characterized by different length scales. The following modeling levels can be distinguished [61-63]:

- **System level (m-scale)**: These models are used mainly to investigate the interaction of SOFC system with the balance of plant equipment in an energy production plant. They can be used for steady state or transient performance prediction. Moreover, are useful for defining values of critical operating parameters, operational bounds, optimization of the overall systems and for controlling purposes.
- **Stack level (cm-scale)**: Stack level models serve in the investigation of the complex interactions between thermal, fluid dynamic, chemical and electrochemical phenomena in the elements of a fuel cell stack. For example, they can be used to investigate the distributions of chemical species, thermal stresses, temperature, pressure and current density. Besides, are useful for the optimization of stack architecture, gas duct design etc.
- **Cell level (mm-scale)**: These models simulate the performance of a single cell. Indicative outputs are the polarization curve, the heat production in the cell and the temperature distribution. Typical design characteristics such as cell length or channel width as well as flow configurations are studied with these models.
- **Electrode level (μm-scale)**: Electrode level models offer a more detailed description of the performance of the fuel cell electrodes. They are used for the investigation of mass and charge transfer phenomena, Knudsen diffusion phenomena, voltage loss mechanisms and to define structural and geometrical details of the fuel cells.
- **Molecular level (nm-scale)**: Typical applications of these models are to investigate the reaction kinetics, ageing of materials, crack formation and propagation, oxygen ion diffusion phenomena.

The models in this thesis belong to the first category (system level). This type of modes is suitable to evaluate the matching of the SOFC generator with a gas turbine. The model provides realistic performance data, which are useful to analyze the global system. Moreover, they have low computational costs and they are useful for the preliminary design phase where a sufficient number of cases need to be examined.

Institutional Repository - Library & Information Centre - University of Thessaly
02/06/2024 00:35:58 EEST - 18.226.159.139

Examples of such models are copious in the available literature. Campanari [64] developed a simple thermodynamic model for a tubular SOFC stack. The system operated under atmospheric pressure running with natural gas. For the fuel cell voltage calculation, an experimental *V-i* curve was used for specific operating conditions and semi-empirical equations were incorporated to account the effects of pressure, temperature and air and fuel composition. The same methodology was used by Zhang et al. [65] and implemented in AspenPlus software. Akkaya [66] used a more detailed, zero-dimensional, modeling approach, which utilizes Butler –Volmer equation, Fick's law and Ohm's law to determine the voltage losses. The model was able to provide information for a tubular SOFC and it was used to study the effect of operating and design parameters on the fuel cell performance. Song et al. [67] developed a quasi-two dimensional mode for an internal reforming SOFC system to predict temperature and current density distributions along the longitudinal direction of tubular fuel cells, as well as temperature distributions along the internal reformer wall. The model was used to study a hybrid SOFC-GT system with different system arrangements. Zhang et al. [68] studied the electrical characteristics in both planar and tubular SOFCs by a three dimensional model. The simulations were performed using the Fluent CFD simulation software.

In this work an advanced software tool is used for the modeling of the SOFC generator. The model is based on the methodology developed by Zhang et al. [65] which is upgraded in order to approach more accurately the examined SOFC system. The modifications are related with the voltage calculations, the reforming process and the recycling of the depleted fuel.

3.2.1 SOFC modeling simplifications

An accurate numerical model for a SOFC system requires the solution of large systems of equations that describe the complex transport phenomena within. One of the main disadvantages of this type of models is the high computational time. Several reasonable simplifications can be made in order to reduce their complexity and simultaneously to establish a suitable level of modeling accuracy and detail. The following assumptions and considerations are applied to the SOFC stack model.

1. The calculations are done for steady state conditions.
2. The current density distribution along the tubular SOFC is uniform.
3. Only the voltage of a single cell is estimated. The stack voltage is computed by taking into account the number of the cell and the relative connection configuration.
4. The temperature and composition distribution of the gases (fuel and oxidant) entering the SOFC stack are uniform.
5. Isothermal fuel cell. The elements of the fuel cell structure (anode, cathode, electrolyte) have the same temperature (lumped temperature).Moreover, there is a uniform temperature distribution along the tubular cell.
6. The species compositions are taken as the average values of the cathode and anode inlet and outlet streams.
7. Only the H_2 reacts electrochemically, the CO it is assumed that shifted to H_2 according to the reaction (2-15).
8. There are not gas leakages.
9. All reactions reach equilibrium.
10. Fuel cell operates with 100% current efficiency.

Institutional Repository - Library & Information Centre - University of Thessaly
02/06/2024 00:35:58 EEST - 18.226.159.139

3.2.2 Voltage calculations

The operating voltage of a fuel cell is equal to the open circuit voltage minus the voltage losses (Eq.3-24). These losses are due to ohmic, activation and diffusion phenomena.

$$V = V_N - (V_{Ohm} + V_{Act} + V_{Conc}) \tag{3-24}$$

The open circuit voltage is calculated using the Nernst equation (Eq. 2-11), which takes into account the partial pressures of the components participating in electrochemical reactions.

The ohmic losses represent the voltage losses due to the resistance of the components along the current path. They are depended from material properties and the geometric characteristics of the conductive components. The ohmic losses are calculated using the equations presented by Song et al. [67] which takes into account realistic electron/ion paths. The total ohmic losses for the fuel cell are the sum of the following quantities:

$$V_{Ohm}^{Anode} = \frac{i\rho_A (A\pi D_m)^2}{8t_A} \tag{3-25}$$

$$V_{Ohm}^{Cathode} = \frac{i\rho_C (\pi D_m)^2}{8t_C} A[A + 2(1 - A - B)] \tag{3-26}$$

$$V_{Ohm}^{Electrolyte} = i\rho_E t_E \tag{3-27}$$

$$V_{Ohm}^{Int} = i\rho_{Int} (\pi D_m) \frac{t_{Int}}{w_{Int}} \tag{3-28}$$

The activation losses are owing to the sluggish electrode kinetics. Activation losses are calculated through the Butler-Volmer relation [45, 66].

$$i = i_o \left\{ \exp\left(\beta \frac{n_e F V_{Act}}{RT} \right) - \exp\left[-(1-\beta) \frac{n_e F V_{Act}}{RT} \right] \right\} \tag{3-29}$$

where the exchange current density i_o is different for the anode and cathode components and it is given from the following relationships respectively:

$$i_{o,A} = \gamma_A \left(\frac{p_{H_2}}{p_{ref}} \right) \left(\frac{p_{H_2O}}{p_{ref}} \right) \exp\left(-\frac{E_A}{RT} \right) \tag{3-30}$$

$$i_{o,C} = \gamma_C \left(\frac{p_{O_2}}{p_{ref}} \right)^{0.25} \exp\left(-\frac{E_C}{RT} \right) \tag{3-31}$$

The concentration losses are due to the diffusion phenomena taking place between the bulk flow and the place where the electrochemical reactions occur. The equations (Eqs 3-32 and 3-33) developed by Chan and Xia [69] are used to calculate the concentration losses. The developed equations take into account the ordinary and Knudsen diffusion phenomena.

$$V_{Conc}^{Anode} = -\frac{RT}{2F} \ln\left[\left(1 - \frac{RT}{2F} \frac{t_A}{D_A^{eff} p_{H_2}} i \right) \Big/ \left(1 + \frac{RT}{2F} \frac{t_A}{D_A^{eff} p_{H_2O}} i \right) \right] \tag{3-32}$$

Institutional Repository - Library & Information Centre - University of Thessaly
02/06/2024 00:35:58 EEST - 18.226.159.139

$$V_{Conc}^{Cathode} = -\frac{RT}{4F}\ln\left\{\left[\frac{p}{\delta_{O_2}} - \left(\frac{p}{\delta_{O_2}} - p_{O_2}\right)\exp\left(\frac{RT}{4F}\frac{\delta_{O_2} t_C}{D_C^{eff} p}\right) i\right] \Big/ p_{O_2}\right\} \quad (3\text{-}33)$$

The diffusion coefficients for the anode and cathode compartments are functions of the effective diffusion coefficients of the components participating in electrochemical reactions.

$$D_A^{eff} = \left(\frac{p_{H_2O}}{p}\right) D_{H_2}^{eff} + \left(\frac{p_{H_2}}{p}\right) D_{H_2O}^{eff} \quad (3\text{-}34)$$

$$D_C^{eff} = D_{O_2}^{eff} \quad (3\text{-}35)$$

$$\delta_{O_2} = \frac{D_{K,O_2}^{eff}}{D_{K,O_2}^{eff} + D_{O_2-N_2}^{eff}} \quad (3\text{-}36)$$

The effective diffusion coefficients for each component are calculated taking into account the ordinary and Knudsen diffusion phenomena as follows.

$$\frac{1}{D_x^{eff}} = \frac{\varepsilon}{\xi}\left(\frac{1}{D_{x-y}} + \frac{1}{D_{K,x}}\right) \quad (3\text{-}37)$$

where the subscripts *x* and *y* represent the gaseous components. The ordinary diffusion coefficients for both anode and cathode compartments are given from the following equation.

$$D_{x-y} = \frac{1\times 10^{-7} T^{1.75} (1/M_x + M_y)^{1/2}}{p\left(v_x^{1/3} + v_y^{1/3}\right)^2} \quad (3\text{-}38)$$

The calculations are done for the H_2-H_2O and O_2-N_2 binary gas mixtures. The Fuller diffusion volumes are given in Table 3-1.

Table 3-1 Fuller diffusion volumes

Element	Fuller diffusion volume
H_2	7.07
H_2O	12.7
O_2	16.6
N_2	17.9

Further details about the calculations and Fuller diffusion volumes can be found in references [46, 70]. Knudsen diffusion occurs when the mean free path of the molecules is long compared with the pore size of the porous media. The following equation is used in order to estimate the Knudsen diffusion coefficients for the anode and cathode gases.

$$D_{K,x} = 97r\sqrt{\frac{T}{M_x}} \quad (3\text{-}39)$$

Institutional Repository - Library & Information Centre - University of Thessaly
02/06/2024 00:35:58 EEST - 18.226.159.139

Chapter 4

Hybrid SOFC-GT model description

This chapter presents an overview of the approach for the modeling of a hybrid SOFC – GT system. The developed models of subsystems are presented and discussed. Finally, model validation for the SOFC generator is done with data from the available bibliography.

4.1 Introduction

The hybrid SOFC-GT system model was developed using the commercially available process simulator AspenPlus [71]. This software has a large number of databanks and permits the evaluation of the thermodynamic properties required for the modeling purposes. The model is based on both built in blocks and user models. The user models are developed in FORTRAN programming language and are incorporated into AspenPlus. The blocks are interconnected with material, power and heat streams to form a complete flowsheet.

AspenPlus is a widely accepted software for studying the performance of energy plants. Vidal et al.[72] used the AspenPlus in order to develop a simulation model for a microturbine. The system was simulated for high ambient temperatures. These results were useful since the microturbine was coupled with thermally activated cooling devices at hot climate conditions. Zheng and Furimsky [73] used it to simulate a combined cogeneration plant with a gas turbine of 43.6 MW output and a steam turbine rated at 28.6 MW. The results were in good agreement with the measurements. Barelli et el. [74] studied the energetic and exergetic performance between two CHP systems based on PEM and SOFC respectively. The models were developed in AspenPlus simulation environment. The authors conclude the most efficient system is the PEM based CHP system when it operates at low temperature and atmospheric pressure. Fryda et al. [32] used the AspenPlus software to simulate the combination of an air blown fluidized bed biomass gasifier with a SOFC and/or microturbine for cogeneration purposes. The system based on the microturbine was more efficient than the system based on the atmospheric SOFC. But, both of the previous systems were less efficient than the integrated system that combines the SOFC generator with the microturbine.

In the present work, it is the first time that AspenPlus simulation tool is used to simulate the part load performance of hybrid SOFC-GT system. The model incorporates performance maps for the turbomachinery components in order to estimate the off-design performance. The part load operation is determined by the external power demand. As the power demand changes, the SOFC operating temperature, the fuel utilization and the air flow have to be regulated to ensure safe

Institutional Repository - Library & Information Centre - University of Thessaly
02/06/2024 00:35:58 EEST - 18.226.159.139

system operation. The controlled parameters are the fuel flow, the SOFC current and the generator power.

4.2 Hybrid system layout

Figure 4-1 presents the hybrid system's layout. The ambient air is compressed and heated during the transit through the recuperator. Then, the air enters the SOFC generator, where after the heat exchanging with the leaving hot exhaust gases in the air feed tube (the process is simulated with a heat exchanger named pre-heater), is fed to the cathode side of the fuel cells in order to react electrochemically with the fuel. In the ejector, the fresh fuel is mixed with the recycled fuel from the anode outlet, before entering the pre-reformer (PR). In the pre-reformer, the mixed fuel is partially reformed, and then is fed into the indirect internal reformer (IIR) where is totally reformed. The IIR is heated radiatively by the fuel cells. The fully reformed fuel is directed into the anode compartment of fuel cell stack where it is electrochemically reacted. The depleted fuel and air from the SOFC stack are burned into the afterburner and supply heat for the air preheating process. After that, the exhaust gases expand in the turbine to produce the necessary power for the compressor and the generator. Thereinafter, the gasses pass through the recuperator to heat the compressed air.

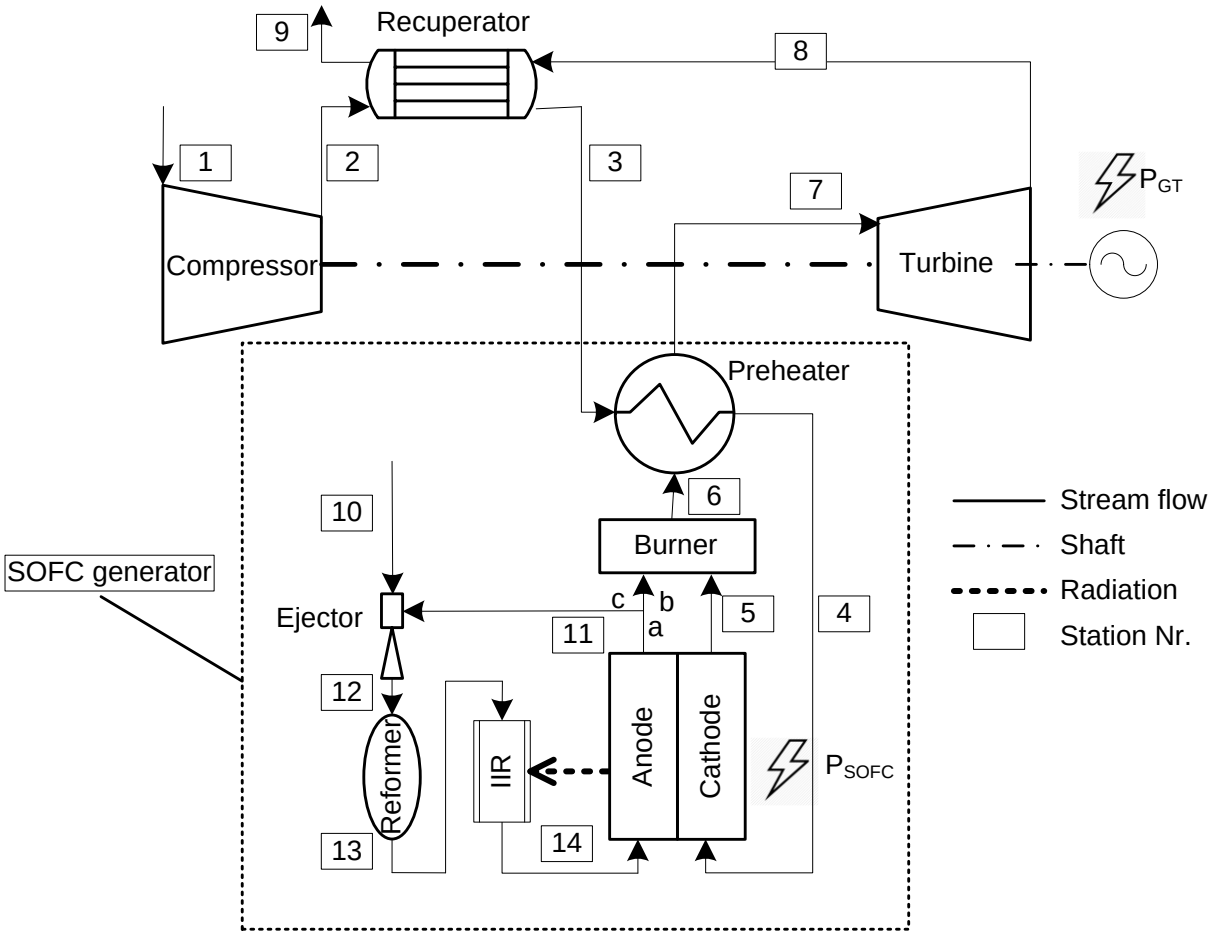

Figure 4-1 Hybrid SOFC-GT system layout

Institutional Repository - Library & Information Centre - University of Thessaly
02/06/2024 00:35:58 EEST - 18.226.159.139

The power output of the hybrid system is estimated as:

$$P_{HS} = P_{SOFC} + P_{GT} \tag{4-1}$$

The power generation efficiency is defined as:

$$\eta_{HS} = \frac{P_{HS}}{\dot{m}_f LHV} \tag{4-2}$$

The following assumptions are made to simplify the hybrid system analysis:

- Steady state operation is considered.
- There are no gas leakages from the system.
- The operating cell voltage in each fuel cell is constant.
- The distributions of temperature, pressure and gas compositions are neglected.
- The fuel is desulfurized.
- The fuel compression work is not taken into account.
- SOFC and afterburner thermal losses = 2 %
- Mechanical efficiency = 0.97, generator efficiency = 0.95, power condition systems efficiency = 0.96.

4.3 Compressor model

The compressor is simulated in AspenPlus using the COMPR block. This block simulates the compression process, by specifying the efficiency and the outlet specifications such as pressure ratio or discharged pressure. The block can be fed directly with performance curves or indirectly, through a user subroutine written in Fortran programming language. The AspenPlus provides a template subroutine which can be used as a driver for the performance curve interpolations. The map is provided in table form through a text file. For the interpolation procedures, in-house subroutines where incorporated into the external code.

4.4 Turbine model

The COMPR block can also be used for the turbine simulation. But, in this case, it cannot handle performance curves [71]. So, it was decided to develop an external subroutine for the expansion process. The USER2 block was used to interface the external subroutine developed in Fortran programming language with the AspenPlus. The AspenPlus incorporates a specific template for the external subroutine.

The inputs to the turbine model are:

- The inlet stream data (mass flow, composition, pressure etc.)
- The outlet pressure
- The rotational speed
- The performance curves (map)

The model based on the input data fills in the outlet material stream and the work stream.

Apart from the calculations presented in section 3.1.1, the turbine model performs interpolations on the supplied performance map to state the operating point of the turbine. An operating point is

Institutional Repository - Library & Information Centre - University of Thessaly
02/06/2024 00:35:58 EEST - 18.226.159.139

specified when two of the four parameters of the performance curves are given. In the specific case the given parameters are the speed and pressure ratio, and the resulted parameters are the corrected mass flow and isentropic efficiency. Another way to locate the operating point on the performance map is the well-known beta line grid method [75].In this method the operating point is determined by the speed and the arbitrary beta value. It is used in performance computer programs since it offer a stable method for interpolations on performance maps. In this model it was not used since there were not arisen interpolation problems during the determination of the operating point.

4.5 Afterburner model

The afterburner is simulated with two AspenPlus blocks, the RSTOIC "AFTERBUR" and the HEATER "HEATER2" (Figure 4-2). The RSTOIC block is used when the reaction stoichiometry and extent of conversion are known. The user must define the reactions that take place. The heat generated by the oxidation reactions (Eqs 3-15 and 3-16) is calculated by the "AFTERBUR" block and is put into the stream "2". The heating process of the exhaust gases is simulated by the "HEATER2" block. The block is fed with the heat stream "2" and calculates the burner exit temperature after taking into account the heat losses "QLOSS"

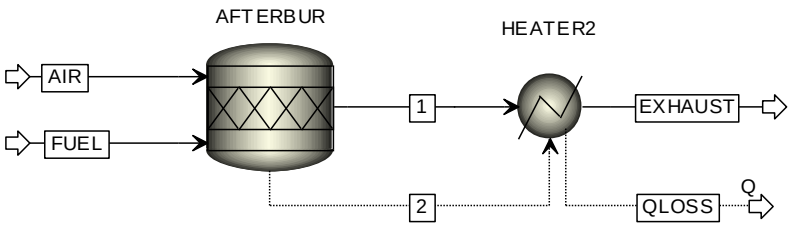

Figure 4-2 Afterburner model in AspenPlus

A Design-Spec block is used to specify the amount of heat loss (equal to a percent of heat stream "2") by changing the temperature increment in the "HEATER2" block.

Comments

With the methodology used in this work, the combustion and the heat transfer processes take place in the combustion plenum are simulated independently. This fact contributes to quite high afterburner outlet temperatures as the afterburner model simulates only the combustion process, namely the reaction of air and fuel and the head addition to the exhaust gases. Then the hot exhaust gases enter into the preheater and exchange thermal energy with the fresh air that enters the SOFC generator. In the actual system, the reactions and the heat exchange process take place simultaneously, and thereupon the exhaust gases exits the combustion plenum at lower temperature.

This methodology is acceptable from the researchers study hybrid SOFC-GT system, when it is not needed to simulate with accuracy the processes that take place in the combustion and air plenums, but the total performance of the SOFC generator.

4.6 Recuperator-Preheater

The heat exchange process in the recuperator and preheater (air plenum) is simulated with a HEATX block. The shortcut calculation method was used since the heat exchanger's configuration and

Institutional Repository - Library & Information Centre - University of Thessaly
02/06/2024 00:35:58 EEST - 18.226.159.139

geometry were unknown. For the design point, as the inlet data are known, the desired temperatures at outlets and the overall heat transfer coefficient need to be specified. Then, the block estimates the heat exchanger area. This area value is used for off-design calculations for the determination of the outlet temperatures according to the relations of section 3.1.3. The heat exchangers are adiabatic.

The pressure drop values or the pressure drop correlation parameter have to be specified for the pressure drop calculations according to equation:

$$\Delta p = k_p \dot{m} \frac{\left(1/\rho_{in} + 1/\rho_{out}\right)}{2} \tag{4-3}$$

4.7 Ejector

Usually, in SOFC models, the ejector performance is represented by the ratio of the recycling fuel to fresh fuel determined either by a specified SCR value [30, 65, 76] or by a constant recycle ratio [77]. More complicated methodologies based on momentum and mass balances [78, 79], have been also utilized [64, 80, 81]. The ejector model adopted in this work is based on the methodology of Leucht et al. [82]. It utilizes a polynomial relation (Eq. 4-4) which relates the recycled fuel and fresh fuel enters to the system.

$$\dot{n}_{rec} = \left[A\left(\frac{p_{fuel} - p_{anode}}{p_{fuel}}\right)^2 + B\left(\frac{p_{fuel} - p_{anode}}{p_{fuel}}\right) + C \right] \cdot \dot{n}_{fuel} \tag{4-4}$$

with A,B, C constants

An AspenPlus CALCULATOR was used for the calculation of the recycled fuel. The model despite its simplicity it is able to predict the off-design performance of ejector, as it calculates the molar flow ratio between the recirculated depleted fuel and fresh fuel based on the fresh fuel and anode gas pressures.

The fuel flow at the anode side exit is divided in two streams, the first one is guided in the afterburner and the second one is recycled. This process is simulated with the FSPLIT “SPLIT” block. As the recycled fuel is determined from the ejector model the remaining depleted fuel guided to the afterburner is calculated to satisfy the flow continuity. The recycled fuel is mixed in the MIXER “EJECTOR” block.

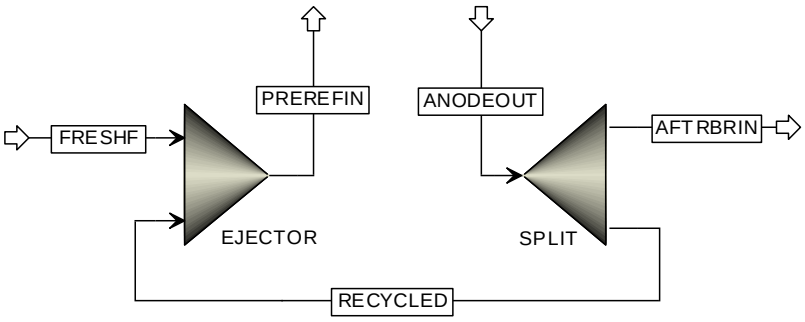

Figure 4-3 Ejector model in AspenPlus

Institutional Repository - Library & Information Centre - University of Thessaly
02/06/2024 00:35:58 EEST - 18.226.159.139

4.8 Pre-reformer

The pre-reforming process is simulated with a combination of two AspenPlus blocks, an equilibrium reactor block RGIBBS “PRE-REF” and a HEATER “COOLER1” block. The RGIBBS reactor is used to simulate the reactions taking place into the pre-reformer while the HEATER is used to simulate the temperature decrease due to the overall endothermic reaction. The temperature of stream at the “COOLER1” exit represents the temperature of the fuel at the pre-reformer exit equal with the operating temperature of the “PRE-REF” block. The heat stream “Q1” represents the thermal energy consumed from the reactions, while the heat stream (Q2) is used to ensure that the pre-reformer component is adiabatic. This is done using a Design-Spec block in AspenPlus, which varies the temperature of COOLER1 until the net heat duty (Q2) of the PRE-REF equals zero.

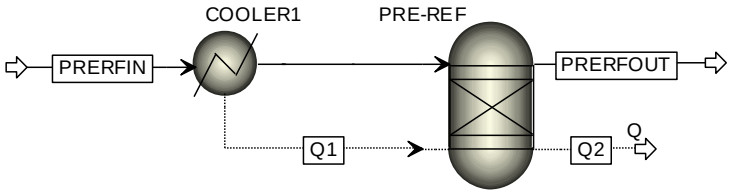

Figure 4-4 Pre reformer model in AspenPlus

4.9 Indirect internal reformer

The indirect internal reformer is modeled with the Gibbs reactor model (RGIBBS), an equilibrium reactor that calculates the equilibrium composition by minimizing the Gibbs free energy. The indirect internal reformer components are placed between the fuel cells and are heated radiantly (“RAD” heat stream) from” the fuel cells in order to support the endothermic reforming reaction [81].

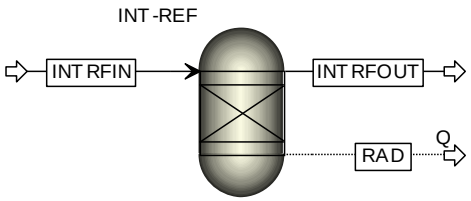

Figure 4-5 Indirect internal reformer in AspenPlus

4.10 Cathode

The cathode side phenomena are simulated with two AspenPlus blocks (Figure 4-6). A SEP “CATHODE” block has been selected to simulate the oxygen ion diffusion in the cathode side. The SEP block extracts the required oxygen amount for the electrochemical process. The steam “13” simulates the oxygen ions moves to the anode side of the fuel cell. The block HEATER “HEATER” simulates the heat addition to the cold air during the pass from the cathode side of the fuel cell. The heat amount “14” is determined by specifying that the temperature of the depleted air (“CATHOUT”) equals to the anode outlet temperature (see next session).

Institutional Repository - Library & Information Centre - University of Thessaly
02/06/2024 00:35:58 EEST - 18.226.159.139

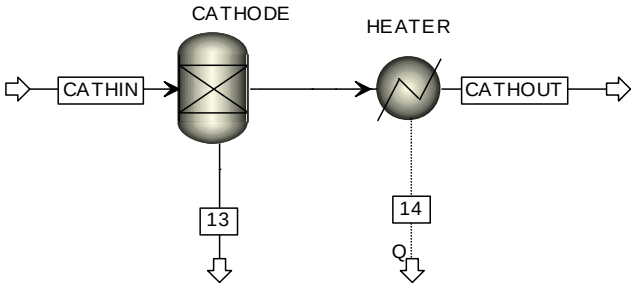

Figure 4-6 Cathode model in AspenPlus

An AspenPlus CALCULATOR was used to calculate the molar flow rate of the stream "13" ($\dot{n}_{O_2,required}$) based on the fuel utilization factor and the equivalent hydrogen flow (Eq. 2-13).

$$\dot{n}_{O_2,required} = 0.5 \cdot U_f \cdot \dot{n}_{H_2,equivalent} \tag{4-5}$$

4.11 Anode

The reformed fuel and the oxygen amount from the cathode are inserted into the RGIBBS "ANODE" block. The "ANODE" block calculates the anode outlet composition by minimizing the Gibbs free energy. The reactions that take place are exothermic and the produced heat is used to heat up the indirect internal reformer ("RAD") and the depleted air of the cathode ("Q3").

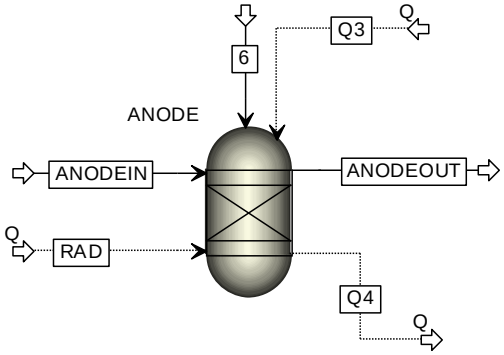

Figure 4-7 Anode model in AspenPlus

The "Q4" heat stream represents the net energy production from the fuel cell stack. By assuming a certain amount of heat losses from the stack we can write:

$$\dot{Q}_4 - \dot{Q}_{loss} - P_{DC} = 0 \tag{4-6}$$

The electric power P_{DC} is estimated from the following relation

$$P_{DC} = iAV \tag{4-7}$$

The fuel cell voltage (V) estimation was described in section 3.2.2. The calculations were implemented in a CALCULATOR block.

Institutional Repository - Library & Information Centre - University of Thessaly
02/06/2024 00:35:58 EEST - 18.226.159.139

4.12 SOFC model

By combining the previous models for the sub-systems, the model for the whole SOFC generator arises. Figure 4-8 presents the SOFC generator model as it was implemented in AspenPlus.

The operating point of the SOFC generator is determined by defining the fuel utilization factor (U_f), fuel cell operating temperature (T_{SOFC}) and current density (i). Two AspenPlus Design-Spec blocks were used to determine the fuel and air inputs to the generator

i. The first Design-Spec is used to determine the fuel flow by satisfying the Eq. 4-6.
ii. The second Design-Spec is used to achieve the desired current density value by varying the air mass flow.

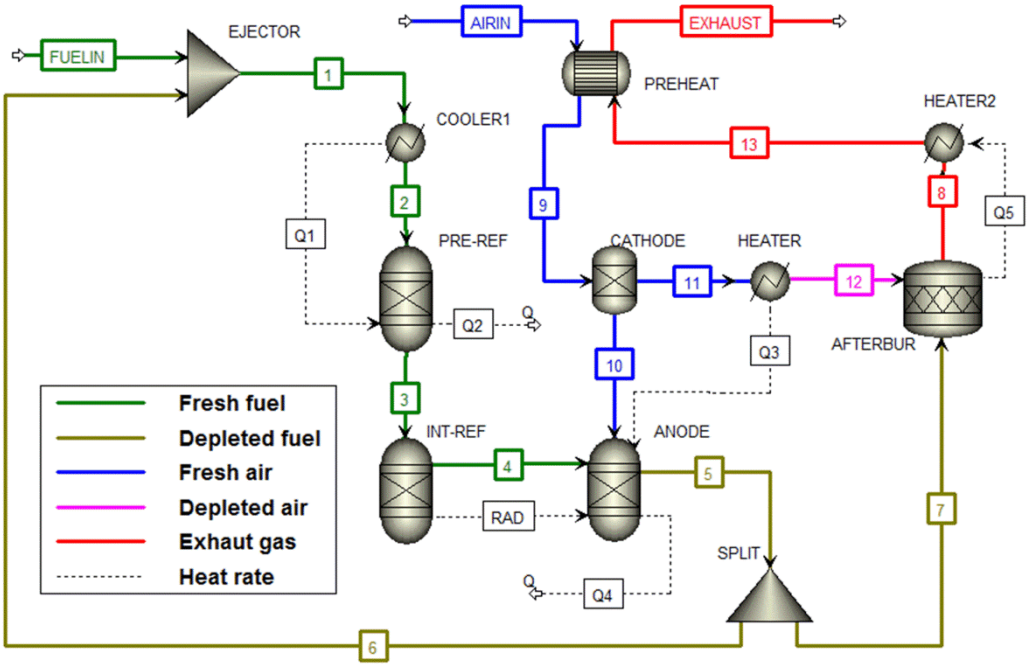

Figure 4-8 AspenPlus flowsheet of SOFC model

4.13 SOFC model validation

The developed model for the SOFC generator that was described in the previous sections requires information for the material properties in order to perform the voltage calculations. The data used for the simulations are presented in Table 4-1.

The voltage calculations require the geometric data of the fuel cell as shown in Table 2-3. Moreover, a fuel utilization factor of 0.85 was considered. Typical values for that parameter are in the range of 0.7 to 0.9 [83]. The lower values can lead to deterioration of the fuel cell performance, while the higher values can cause permanent damage due to fuel starvation.

Institutional Repository - Library & Information Centre - University of Thessaly
02/06/2024 00:35:58 EEST - 18.226.159.139

Table 4-1 SOFC model parameters

Material properties, [46, 66]	
Anode resistivity, (Ω m)	$2.98\times10^{-5}\exp(-1392/T)$
Cathode resistivity, (Ω m)	$8.114\times10^{-5}\exp(600/T)$
Electrolyte resistivity, (Ω m)	$2.94\times10^{-5}\exp(10350/T)$
Interconnection resistivity, (Ω m)	$0.012\exp(4690/T)$
Ohmic losses, [46, 67]	
Coefficients A / B	0.804 / 0.13
Activation losses[a]	
Anode activation energy, (kJ/mol)	115
Cathode activation energy, (kJ/mol)	129
Anode pre-exponential coefficient, (A m^{-2})	2.13×10^{10}
Cathode pre-exponential coefficient, (A m^{-2})	1.49×10^{8}

[a] The specific values were calculated through model calibration

The SOFC model was validated with experimental data from the available literature [84] ,and the results are presented in Table 4-2. The model shows good agreement with the experimental data. The error in the simulated operating points is below 1% for all operating parameters. Compared with the date in Table 3 of reference [84] it has been attained better fitting than the model presented by the specific authors. This is probably due to the more detailed equations for the ohmic and the concentration losses that are adopted in this work.

Table 4-2 SOFC model validation

	Experiment	Model	Error (%)
T_{SOFC} = 1264 K, i = 1800 A/m^2			
Fuel flow rate (kg/h)	19.9	19.91	0.04
DC power (kW)	118	117.30	-0.59
Cell voltage (V)	0.682	0.678	-0.55
T_{SOFC} = 1254 K, i = 2000 A/m^2			
Fuel flow rate (kg/h)	22.24	22.12	-0.54
DC power (kW)	127.4	127.47	0.05
Cell voltage (V)	0.661	0.663	0.36
T_{SOFC} = 1241 K, i = 2350 A/m^2			
Fuel flow rate (kg/h)	26	25.99	-0.03
DC power (kW)	144.3	143.99	-0.21
Cell voltage (V)	0.639	0.638	-0.19

Institutional Repository - Library & Information Centre - University of Thessaly
02/06/2024 00:35:58 EEST - 18.226.159.139

4.14 Gas turbine model

Figure 4-9 presents the gas turbine model as it was implemented in AspenPlus. It incorporates the compressor, turbine and recuperator models presented previously. The burner was modeled using an RSTOIC "BURNER" block. The RSTOIC block was set adiabatic (Heat duty=0 W). Thus, the heat generated from the combustion process is totally given to the exhaust gases (stream "4"). The control variables of the model are the rotational speed and the turbine inlet (or outlet) temperature. For the engine state estimation two AspenPlus Design-Spec blocks are used.

i. The first determines the fuel flow, so as to achieve the desired turbine inlet (or outlet) temperature.
ii. The second varies the air mass flow (stream "1") until to satisfy the mass balance ($\dot{m}_{air}+\dot{m}_{fuel}=\dot{m}_{exhaust}$) of the gas turbine

The net electric power of the gas turbine is estimated from the following relation

$$P=(P_t\cdot\eta_{mech}-P_c)\cdot\eta_{gen}\cdot\eta_{inv} \quad (4\text{-}8)$$

Where

η_{mech} :mechanical efficiency

η_{gen} : generator efficiency

η_{inv} : power conditioning system efficiency

Validation of gas turbine model is done for each case study presented in the following chapters.

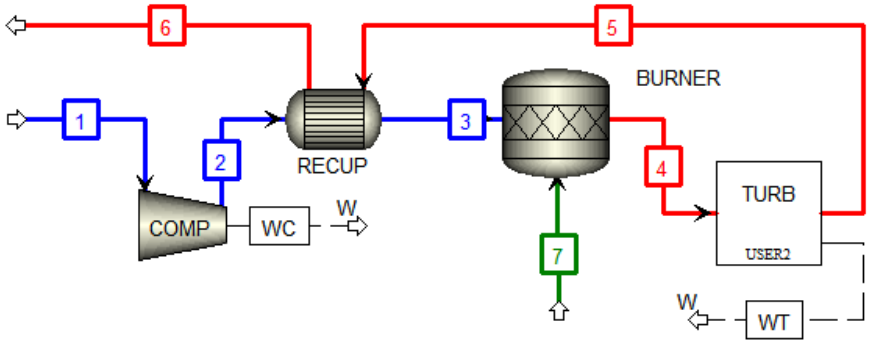

Figure 4-9 AspenPlus flowsheet of gas turbine model

4.15 Overall hybrid system model

The two independent models for the gas turbine and the SOFC generator were merged into a single one in order to investigate the performance of the integrated hybrid system. Figure 4-10 presents the hybrid system model as it was implemented in AspenPlus software. It utilizes the compressor model "COMP", the recuperator model "RECUP" and the turbine model "TURB" which were developed for the gas turbine. The burner model of the gas turbine was replaced with the model developed for the SOFC generator "FC". The SOFC generator model (Figure 4-8) was imported into a HIERARCHY block in order to simplify the model flowsheet. The HIERARCHY block offers the ability to

Institutional Repository - Library & Information Centre - University of Thessaly
02/06/2024 00:35:58 EEST - 18.226.159.139

group complex parts of a simulation code in order to simplify its presentation. In the specific case the “AIRIN” and “EXHAUST” streams of the SOFC generator, shown in Figure 4-8, are connected with the streams “3” and “4” respectively, in Figure 4-10. Similarly the “FUELIN” stream is connected with stream “7”.

In order to simulate the performance of the hybrid system at part load conditions, the rotational speed of the gas turbine is given as input to the model in order to adjust the produced power. Also, the SOFC operating temperature and the fuel utilization factor are determined.

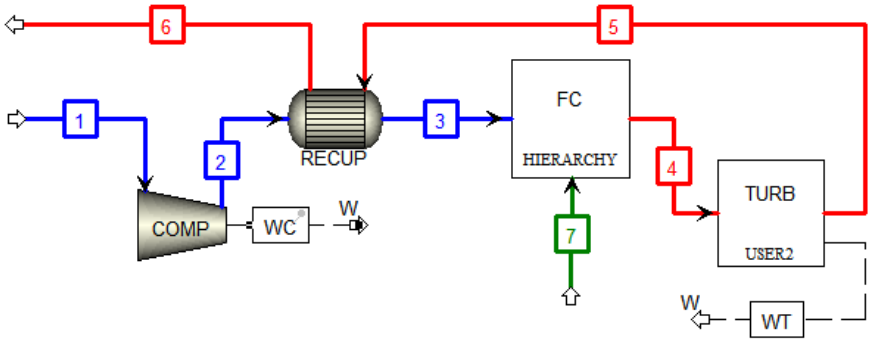

Figure 4-10 AspenPlus flowsheet of hybrid SOFC-GT model

An AspenPlus Design-Spec block is used to determine the required fuel flow in the SOFC stack as in section 4.12 and another one is used to determine the air fuel flow as in section 4.14.

Institutional Repository - Library & Information Centre - University of Thessaly
02/06/2024 00:35:58 EEST - 18.226.159.139

Institutional Repository - Library & Information Centre - University of Thessaly
02/06/2024 00:35:58 EEST - 18.226.159.139

Chapter 5

Analysis of a hybrid micro gas turbine fuel cell system based on existing components

Based on the methodology in Chapter 4, a hybrid SOFC-GT model was developed based on existing devices. It can be seen from a literature review that only few papers are dealing with existing integrated systems or potential cooperation of existing subsystems. In this chapter the performance of a hybrid system consisting of existing microturbine and fuel cell subsystems using appropriate models is studied. Such an effort has its own value as it is based on validated technologies and the models could be verified against real data for both subsystems. A model for the commercial available Capstone C30 recuperated gas turbine has been developed and compared against published performance data. The gas turbine model and the SOFC model developed in the previous chapter are merged into a single one in order to investigate the integrated hybrid system.

The irreversibilities and thermodynamic inefficiencies of the system are evaluated after examining the full and partial load exergetic performance and estimating the amount of exergy destruction and the efficiency of each hybrid system component. Furthermore, the effects of the various performance parameters such as fuel cell stack temperature and fuel utilization factor are assessed.

5.1 Model development

The selected gas turbine was the commercially available C30 micro turbine manufactured from Capstone. This recuperated gas turbine produces 30 kW of electrical power with 26% ± 2% (LHV) efficiency at ISO conditions. It consists of a centrifugal compressor, a recuperator, a combustion chamber, a radial turbine and a generator [72]. All the rotating components are mounted on a single shaft which rotates at high rotational speed. Owing to the high rotational speed of the generator this system requires an inverter – power conditioner system in order to reduce the high frequency AC output to the desirable value.

Table 5-1 summarizes the assumptions of the developed model for the micro turbine. The data presented are compiled from the available literature.

The model was validated using data available from the manufacturer. Table 5-2 presents the design point operating parameters as predicted from the developed model and compared with manufacturer's data.

Institutional Repository - Library & Information Centre - University of Thessaly
02/06/2024 00:35:58 EEST - 18.226.159.139

Table 5-1 Capstone design point assumptions at design point

Pressure ratio	3.6
Turbine inlet temperature	1117 K
Recuperator ΔP/P air/gas side	2%/5%
Combustion chamber ΔP/P	4%
Combustion chamber thermal losses	2%
Compressor isentropic efficiency	83%
Turbine isentropic efficiency	84%
Power condition system	96%
Mechanical efficiency	97%
Generator efficiency	95%

Table 5-2 Calibration results at 96000 rpm

	Capstone	AspenPlus	Error [%]
Power,(kW)	30	30.7	2.22
Fuel energy,(kW)	115.36	119.2	3.30
Air flow, (kg/s)	0.31	0.307	-0.99
EGT, (K)	549	546	-0.59
Net efficiency, (%)	26±2	25.7	-

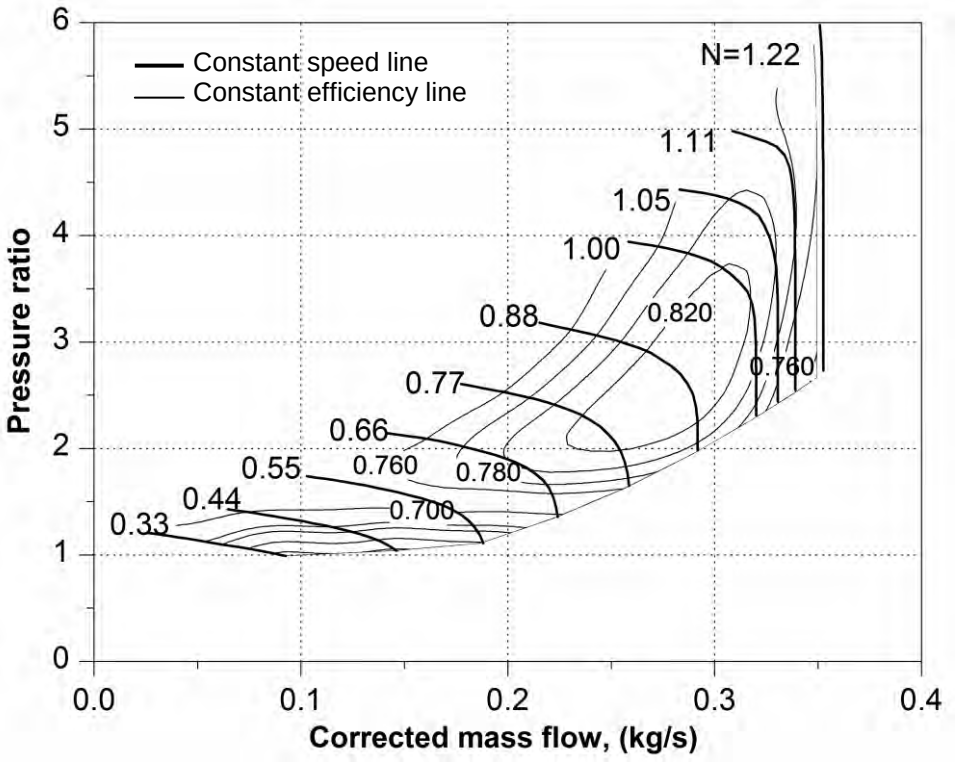

Figure 5-1 Compressor map

Institutional Repository - Library & Information Centre - University of Thessaly
02/06/2024 00:35:58 EEST - 18.226.159.139

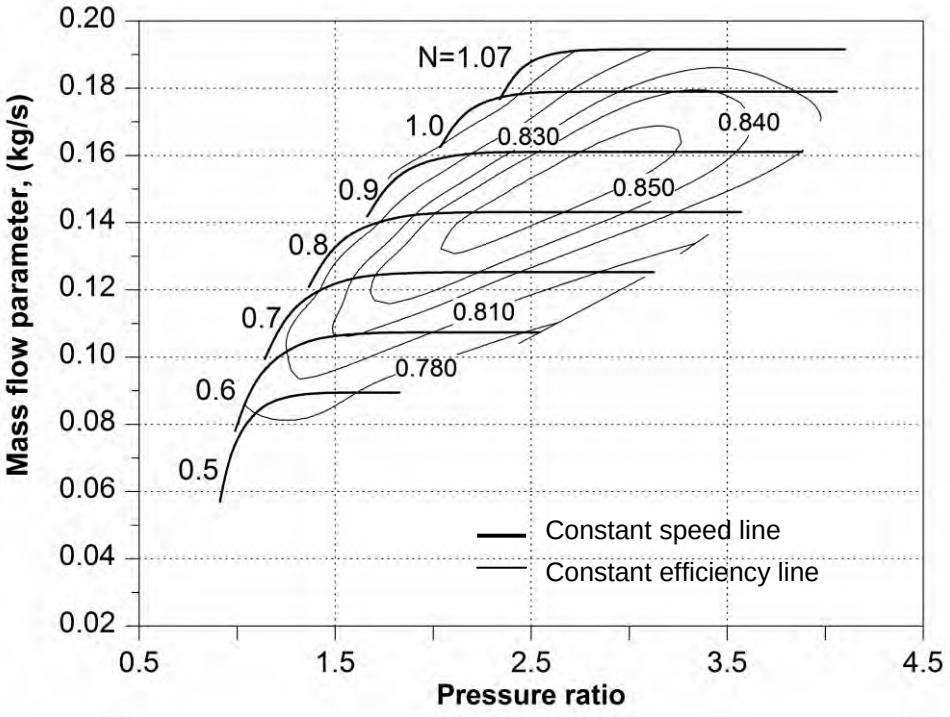

Figure 5-2 Turbine map

For the part load operations of the engine, the model is supplied with performance maps for the compressor (Figure 5-1) and the turbine (Figure 5-2). The resulted model predicts the part load operation of the engine with satisfactory accuracy as shown in Figure 5-3.

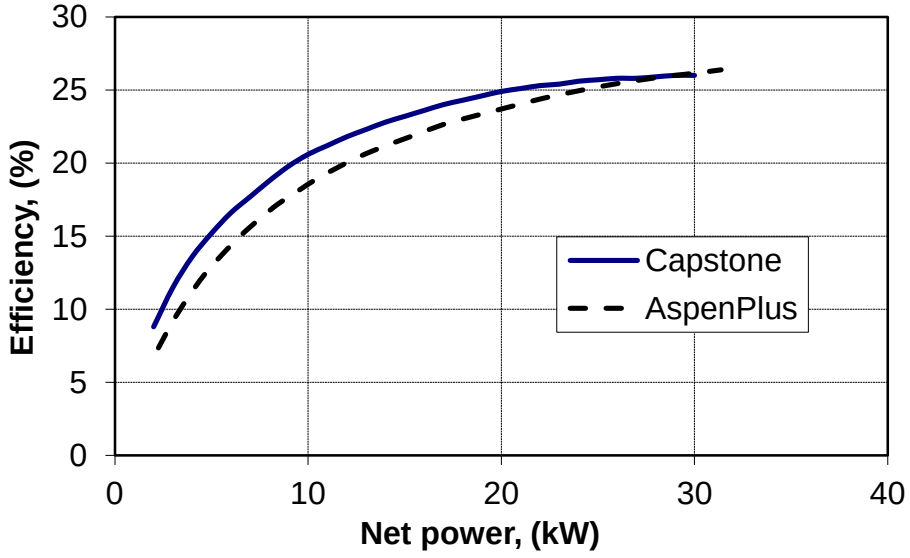

Figure 5-3 Part load performance of microturbine

In Table 5-3 are summarized the assumptions done for the fuel cell model. Validation of the SOFC model was done with the available literature data in Chapter 4 .

The two independent models developed for the gas turbine and the SOFC stack are merged into a single one in order to investigate the integrated hybrid system.

Institutional Repository - Library & Information Centre - University of Thessaly
02/06/2024 00:35:58 EEST - 18.226.159.139

Table 5-3 Assumptions for the fuel cell model

Active area (1152 cells)	96.1 m^2
Afterburner efficiency	100%
DC to AC inverter efficiency	96%
Overall fuel utilization factor	0.85
SOFC thermal losses	2%
Total SOFC stack pressure losses	4%
Cell operating temperature	1183 K

In Table 5-4 are presented the predicted design point data of the hybrid system. They are describing the performance of the hybrid system at full load and at standard conditions for temperature and pressure (288.15 K, 1.013 bar).

Table 5-4 Hybrid system design point data

Total power	175.7 kW
SOFC power	146.5 kW
GT power	29.2 kW
Fuel consumption	7.2 g/s
Air flow	0.315 kg/s
Exhaust gas temperature	549 K
Efficiency	63.8 %
Fuel cell efficiency	53.2 %

5.2 Part load performance

For the part load operation of the hybrid system the rotational speed, the SOFC operating temperature and the fuel utilization factor are given as inputs to the model in order to determine the operating point. The power output is adjusted by changing the rotational speed.

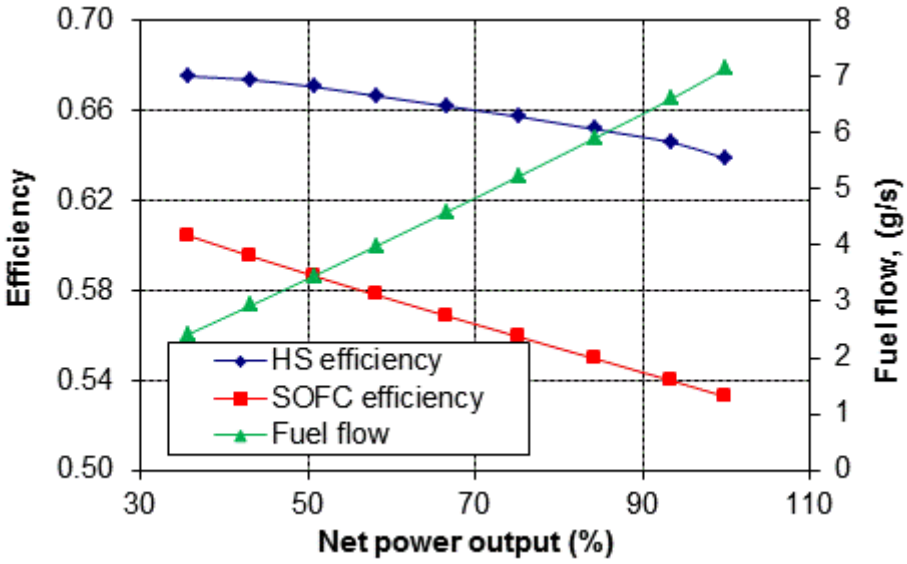

Figure 5-4 Part load performance of hybrid system

Institutional Repository - Library & Information Centre - University of Thessaly
02/06/2024 00:35:58 EEST - 18.226.159.139

Figure 5-4 presents the efficiency of the hybrid system under part load conditions, when the fuel cell operating temperature and the fuel utilization factor are kept constant at their design values. It is obvious that the system efficiency increases as the produced power decreases. This was expected since the system operates with variable rotational speed [85] . At part load conditions both the ingested air and the supplied fuel are reduced. In this case the fuel cell voltage increases (Figure 5-5) due to the influence of both the lower current density as the SOFC power decreases and the high cell operating temperature. As a result the SOFC efficiency as well as the total system efficiency are higher at part load conditions.

The calculated polarization curve (cell voltage versus current density) is shown in Figure 5-5. The reduction of fuel flow causes the fuel cell to operate with lower current density values (Eq. 2-6) which results in lower polarization losses and higher cell voltage values.

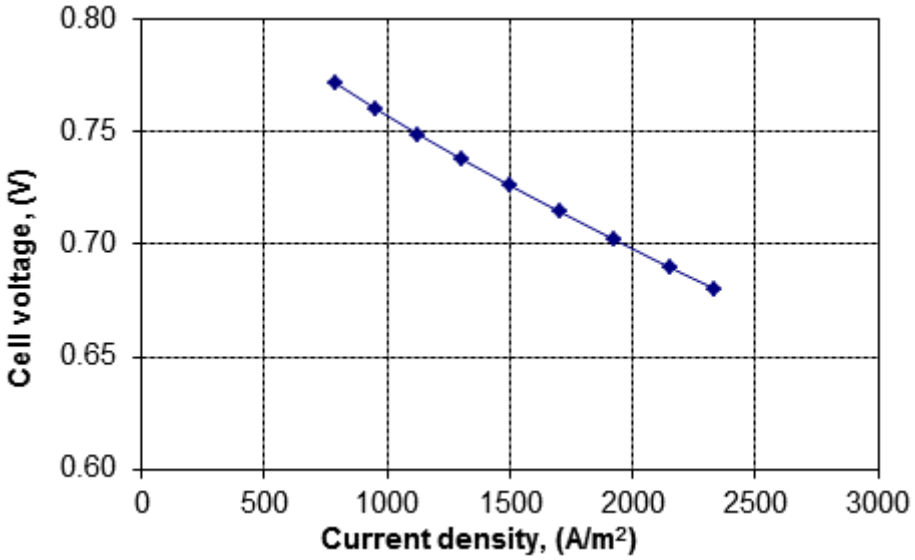

Figure 5-5 Polarization curve

Figure 5-6 presents the compressors' running line. It is obvious that at part load conditions the compressor operates with lower efficiencies. Moreover, the pressure ratio value is reduced. This fact has negative effect on the gas turbine performance. Nevertheless, this is not sufficient to reduce the total system efficiency. This is better explained in Figure 5-7.

Institutional Repository - Library & Information Centre - University of Thessaly
02/06/2024 00:35:58 EEST - 18.226.159.139

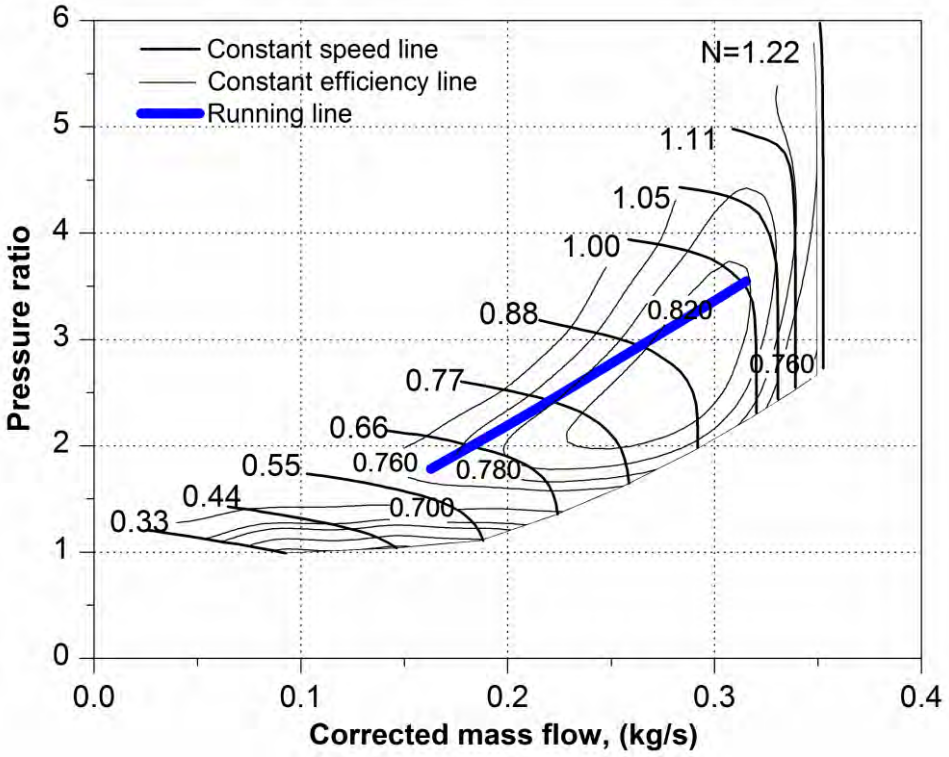

Figure 5-6 Compressor running line

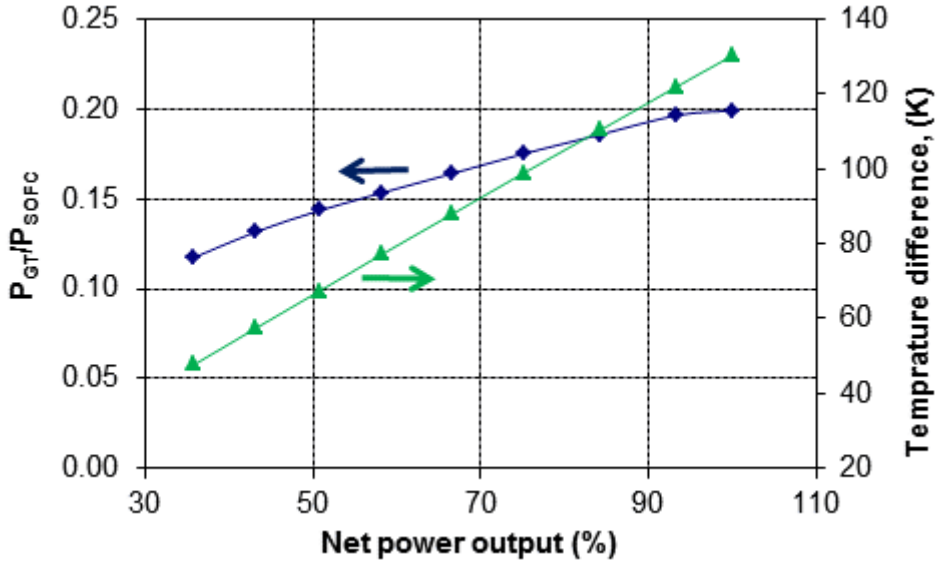

Figure 5-7 Gas turbine to SOFC power output and fuel cell cathode temperature rise at part load conditions

When the hybrid system operates at part load conditions the contribution of the gas turbine to the total system output decreases (Figure 5-7). This occurs since the gas turbine performance deteriorates sensibly (Figure 5-3) at part load conditions and on the other hand the SOFC stack operates more efficiently.

Institutional Repository - Library & Information Centre - University of Thessaly
02/06/2024 00:35:58 EEST - 18.226.159.139

In order to verify that the two independent systems (namely the C30 microturbine and the Siemens-Westinghouse SOFC generator) are combined safely, the fuel cell cathode temperature difference is checked. Tarroja et al. [86] suggest that this temperature difference must remain under 200 K in order to avoid high thermal stresses within fuel cells and possible failure. Figure 5-7 indicates that the temperature rise in the fuel cell cathode side (i.e. the temperature difference between the inlet and outlet of the stack) remains below that limit.

5.3 Effect of operating parameters

5.3.1 SOFC operating temperature

The SOFC temperature is one of the most important operating parameters for the fuel cell generators and hybrid systems since it has significant effects in power and efficiency. Figure 5-8 shows the part load performance of the hybrid system for various values of SOFC operating temperature. The system works more efficiently for the higher values of SOFC temperature. The effect of this operating parameter is stronger at higher rotational speeds since it affects considerably both the produced power and the system efficiency.

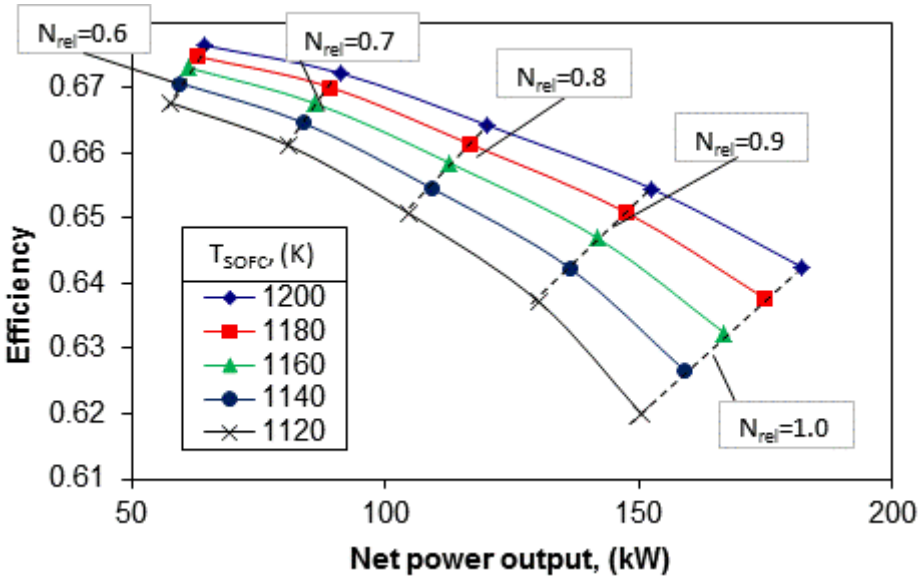

Figure 5-8 Effect of SOFC operating temperature in part load performance

The resulted values of the turbine inlet temperature are presented in Figure 5-9. As it was expected the higher values of turbine inlet temperature have arisen for the higher SOFC operating temperatures. The temperatures tend to constant values at low rotational speeds. Moreover, the turbine inlet temperature values are lower than the design value (1117 K) of Capstone C30 microturbine. The different turbine inlet temperatures can affect the matching of the turbomachinery components resulting in changes of the air flow and pressure ratio of the compressor. This fact has an impact on the surge margin of the compressor. The operating points of the compressor are presented in Figure 5-10. From the results it is apparent that the increment of SOFC operating temperature moves the operating line of the compressor towards to the surge area.

Institutional Repository - Library & Information Centre - University of Thessaly
02/06/2024 00:35:58 EEST - 18.226.159.139

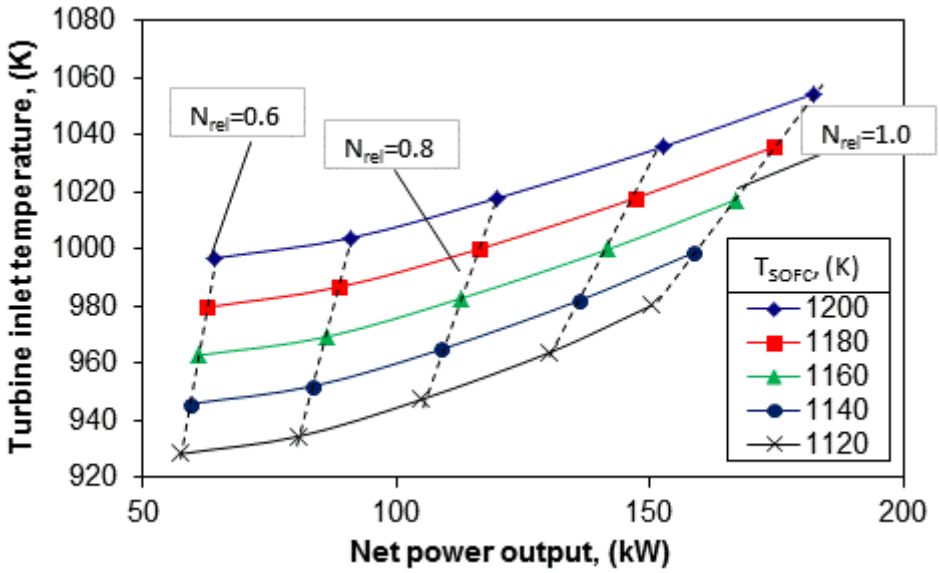

Figure 5-9 Turbine inlet temperature for different values of SOFC temperature

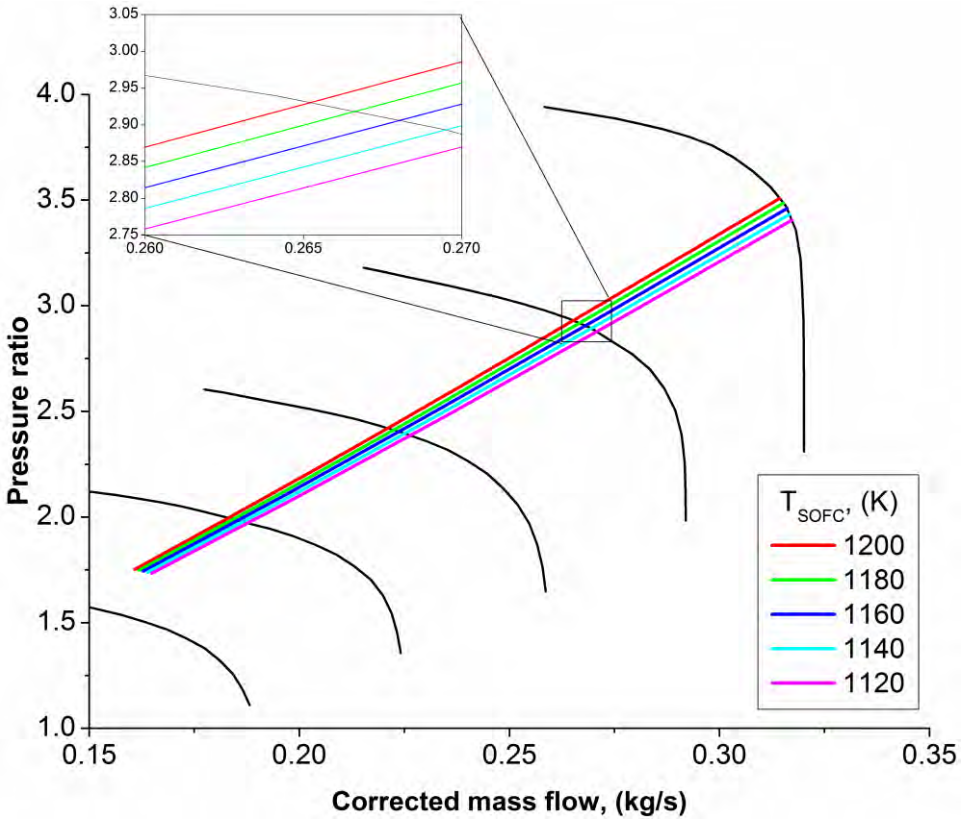

Figure 5-10 Compressor operating lines

5.3.2 Fuel utilization factor

Another important parameter that affects significantly the performance of the SOFC generator and consequently the performance of a hybrid system is the fuel utilization factor. It describes the amount of fuel that reacts electrochemically within the fuel cell stack. In practical applications a certain fuel amount does not react and escapes out of the fuel cells. This is done for two reasons [87]:

Institutional Repository - Library & Information Centre - University of Thessaly
02/06/2024 00:35:58 EEST - 18.226.159.139

- As the fuel mixture passes through the anode compartment of the fuel cell, the hydrogen concentration falls. If fuel utilization is large, the domain close to the outlet suffers from fuel starvation. In this situation the fuel cell voltage is lowered and can lead to permanent damage of the cell.
- Besides the unreacted fuel is burned in order to provide energy for the fresh air entering the stack or for a heat engine

Figure 5-11 presents the effect of fuel utilization factor on the part load performance of the hybrid system. The system operates more efficiently by increasing the value of fuel utilization factor. This occurs because more power is produced from the SOFC generator (Figure 5-12). The SOFC generator is a more efficient device than the gas turbine, and this fact contributes to higher efficiency values for the whole system.

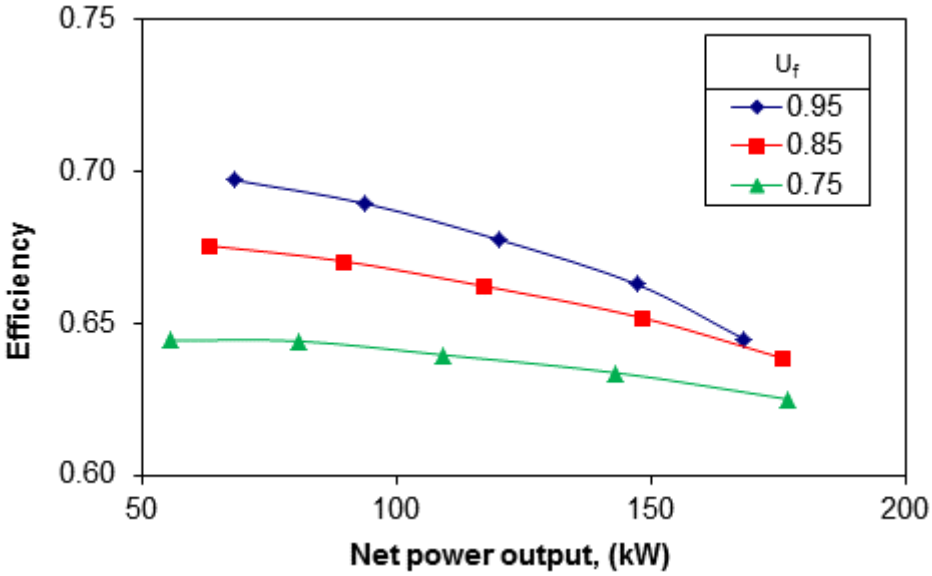

Figure 5-11 Effect of fuel utilization factor in part load performance

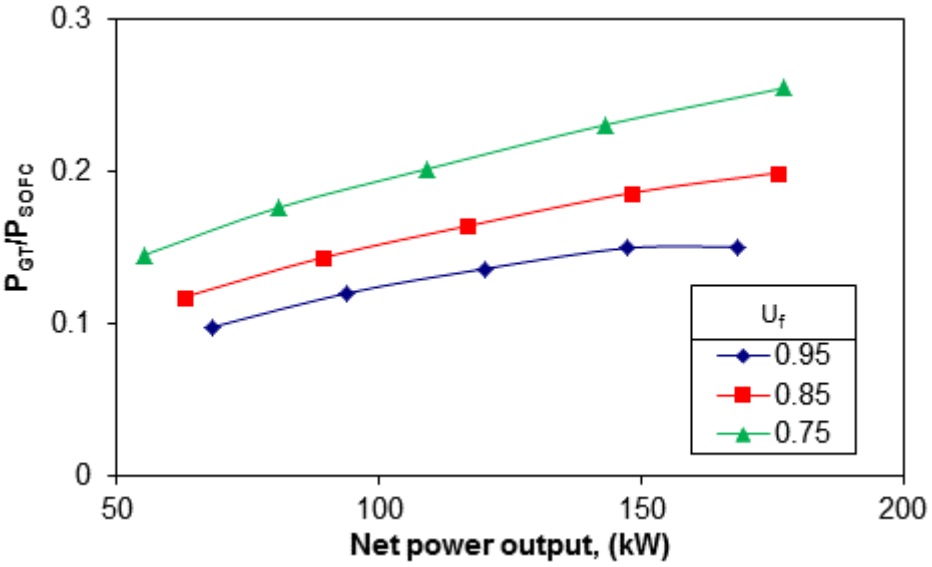

Figure 5-12 Gas turbine to SOFC power output for different values of fuel utilization factor

Institutional Repository - Library & Information Centre - University of Thessaly
02/06/2024 00:35:58 EEST - 18.226.159.139

The variation of the turbine inlet temperature is shown in Figure 5-13. The turbine inlet temperature increases with the decrement of the fuel utilization factor. This is done because larger amount of fuel escaped from the SOFC stack and is burned in the combustor, which produces energy for the incoming fresh air and the turbine.

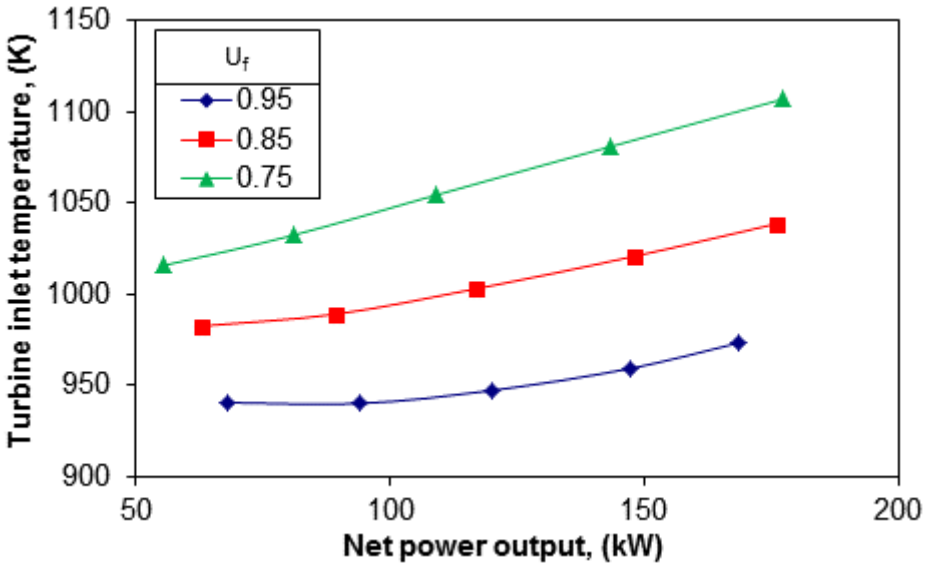

Figure 5-13 Turbine inlet temperature for different values of fuel utilization factor

5.3.3 Sensitivity analysis

Figure 5-14 presents the effect of SOFC operating temperature and fuel utilization factor of various operating parameters. The results have arisen by varying either T_{SOFC} or U_f by 1% and calculating the deviation of the performance parameters from their values at the reference case.

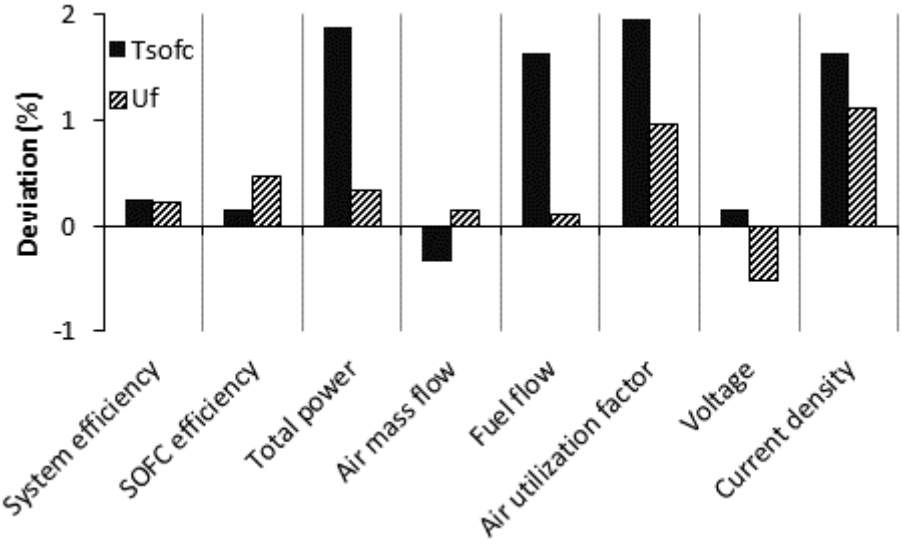

Figure 5-14 Effect of SOFC temperature and fuel utilization factor on various parameters

From the results it is obvious that the higher cell temperature contributes to higher fuel consumption which increases the total power production. The air mass flow slightly decreases with the increment of SOFC temperature since higher turbine inlet temperatures arise (see section 5.3.1).

Institutional Repository - Library & Information Centre - University of Thessaly
02/06/2024 00:35:58 EEST - 18.226.159.139

This fact contributes to higher oxygen utilization factors. The current density increases because of the higher amount of fuel flow. There is also an increment in the cell voltage since there are lower voltage losses. Finally, as it can be seen the increment of SOFC temperature leads to more efficient operation in both SOFC generator and whole system.

The effect of fuel utilization factor on various operating parameters is shown in Figure 5-14, too. The hybrid system responds similarly as in the case of varying the SOFC temperature. The differences are in air mass flow and in the fuel cell voltage.

By comparing the effect of those two parameters is obvious that the SOFC operating temperature affects significantly the power output of the system. The efficiency advantage is not very high when increase either the T_{SOFC} or U_f.

5.4 Exergetic analysis

The research work in the area of hybrid SOFC-GT system usually deals with the energy analysis of such a system [28, 30, 39, 88]. In the past few years there is a growing interest for the study of the exergetic performance of those systems. Calise et al. [89] simulated and studied a hybrid SOFC–GT system at design and part load conditions. Although different part load strategies were investigated, one of the main part load handles (variable speed control) was not considered. Their system presented an electrical efficiency of 65.4% at full load operation. It was also concluded that the best part load strategy corresponds to a constant value of fuel to air ratio. Granovskii et al. [39] compared two combined SOFC–GT systems with different configurations for supplying the required steam to methane ratio, on the basis of energetic and exergetic performance criteria. Haseli et al. [90] examined the exergetic performance of a hybrid SOFC–GT system as well as the effect of operating parameters such as the turbine inlet temperature and compression ratio. Their results were compared with a traditional gas turbine cycle and a significantly better performance of the SOFC–GT plant has demonstrated.

The exergy analysis is able to detect the position, the type and the magnitude of irreversibilities-losses on a thermal system [91]. This information is useful either in designing or upgrading existing (energy) systems, since it can help to improve the performance by making the appropriate modifications leading to reduction of irreversibilities.

5.4.1 Exergy

According to Kotas [92]: “Exergy of a system is the amount of work obtainable when the system is brought to a state of unrestricted equilibrium (that is, thermal, mechanical, and chemical) with the environment by means of reversible processes involving thermal and chemical interaction only with the environment”.

There are three ways that the energy is transferred: with work, with heat and with mass flow. The exergy of a flow is the sum of four quantities ($e = e^k + e^p + e^{ph} + e^{ch}$). Usually the components of the kinetic and potential exergy are considered negligible and are not taken into account. The specific physical exergy at a given state is given from Eq. 5-1.

$$e^{ph} = (h - h_o) - T_o(s - s_o) \tag{5-1}$$

Institutional Repository - Library & Information Centre - University of Thessaly
02/06/2024 00:35:58 EEST - 18.226.159.139

The specific chemical exergy of a gas mixture at a given state is defined as:

$$e^{ch} = \sum_j x_j e_j^{ch,0} + R_g T_o \sum_j x_j \ln x_j \tag{5-2}$$

where $e_j^{ch,0}$ is the standard chemical exergy of species [93].

The overall exergy of a stream flow is calculated from the following relation:

$$\dot{E} = \dot{n}\left(e^{ph} + e^{ch}\right) \tag{5-3}$$

The exergy destruction rate in a control volume at steady state conditions can be calculated from the difference between the inlet and exit exergy flows.

$$\dot{E}_{des} = \sum_j \left(1 - \frac{T_o}{T_j}\right)\dot{Q}_j + \dot{W}_{cv} + \sum_i \dot{E}_i - \sum_e \dot{E}_e \tag{5-4}$$

The exergy balances and exergetic efficiencies for the basic components can be found in references [90, 94]. Apart from the burner and SOFC stack, all other components are treated as adiabatic (Table 5-5).

Table 5-5 Exergy destruction rates and exergy efficiencies

Compressor	$\dot{E}_{des,c}$	$\dot{W}_c + \dot{E}_1 - \dot{E}_2$
	$\eta_{ex,c}$	$(\dot{E}_2 - \dot{E}_1)/\dot{W}_c$
Recuperator	$\dot{E}_{des,rec}$	$\dot{E}_2 + \dot{E}_8 - \dot{E}_3 - \dot{E}_9$
	$\eta_{ex,rec}$	$(\dot{E}_3 - \dot{E}_2)/(\dot{E}_8 - \dot{E}_9)$
Preheater	$\dot{E}_{des,pre}$	$\dot{E}_3 + \dot{E}_6 - \dot{E}_4 - \dot{E}_7$
	$\eta_{ex,pre}$	$(\dot{E}_4 - \dot{E}_3)/(\dot{E}_6 - \dot{E}_7)$
Burner	$\dot{E}_{des,b}$	$\dot{E}_5 + \dot{E}_{11b} - \dot{E}_6$
	$\eta_{ex,b}$	$1 - \dot{E}_{des,b}/(\dot{E}_5 + \dot{E}_{11b})$
SOFC stack	$\dot{E}_{des,SOFC}$	$\dot{E}_4 + \dot{E}_{14} - \dot{E}_5 - \dot{E}_{11a} - \dot{W}_{SOFC,DC} - (1 - T_o/T_{SOFC})\dot{Q}_{rad}$
	$\eta_{ex,SOFC}$	$1 - \dot{E}_{des,SOFC}/(\dot{E}_4 + \dot{E}_{14})$
Turbine	$\dot{E}_{des,t}$	$\dot{E}_7 - \dot{E}_8 - \dot{W}_t$
	$\eta_{ex,t}$	$\dot{W}_t/(\dot{E}_7 - \dot{E}_8)$
Ejector	$\dot{E}_{des,ej}$	$\dot{E}_{10} + \dot{E}_{11c} - \dot{E}_{12}$
	$\eta_{ex,ej}$	$1 - \dot{E}_{des,ej}/\dot{n}_{10}(e_{10} - e_{12})$
Reformer	$\dot{E}_{des,r}$	$\dot{E}_{12} - \dot{E}_{13}$
	$\eta_{ex,r}$	$\dot{E}_{13}/\dot{E}_{12}$
IIR	$\dot{E}_{des,IIR}$	$\dot{E}_{13} - \dot{E}_{14} + \left(1 - T_o/T_{SOFC}\right)\dot{Q}_{rad}$
	$\eta_{ex,IIR}$	$1 - \dot{E}_{des,IIR}\left[\dot{E}_{13} + \left(1 - T_o/T_{SOFC}\right)\dot{Q}_{rad}\right]$

Institutional Repository - Library & Information Centre - University of Thessaly
02/06/2024 00:35:58 EEST - 18.226.159.139

The overall exergy balance of the system is written as (see Figure 5-15):

$$\dot{E}_{des,sys} = \dot{E}_1 + \dot{E}_{10} - \dot{E}_9 - \dot{W}_{SOFC,AC} - \dot{W}_{MGT} - \sum_j \left(1 - \frac{T_o}{T_j}\right)\dot{Q}_j \quad (5\text{-}5)$$

The total exergetic efficiency is expressed by Eq. 5-6. It is the ratio of the net power output to the exergy supplied to the system.

$$\eta_{ex,sys} = \frac{P_{SOFC,AC} + P_{MGT}}{\dot{E}_{10}} \quad (5\text{-}6)$$

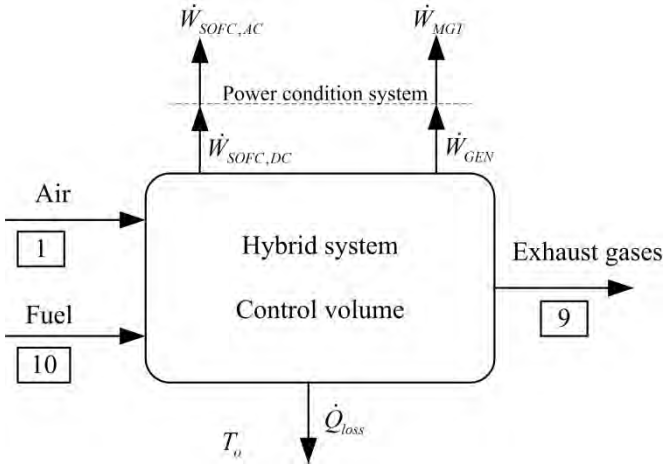

Figure 5-15 Control volume for the overall exergy balance

5.4.2 Exergy analysis results

The analysis described in the previous paragraphs is applied to the developed hybrid SOFC-GT system in order to locate the main exergy destructions and identify inefficiencies. The basic thermodynamic properties of each station of the system are presented in Table 5-6.

Table 5-6 Thermodynamic properties at each station

Station	$\dot{m}$ (kg/s)	T (K)	P (bar)	$\dot{E}$ (kW)
1	0.315	298	1.013	1.40
2	0.315	452	3.596	45.37
3	0.315	744	3.502	92.67
4	0.315	1053	3.493	165.48
5	0.297	1183	3.480	189.54
6	0.322	1314	3.480	256.99
7	0.322	1039	3.466	175.24
8	0.322	818	1.064	85.08
9	0.322	549	1.013	29.29
10	0.007	423	8.696	286.10
11a	0.097	1183	3.493	310.60
11b	0.026	1183	3.493	83.25
11c	0.071	1183	3.493	227.35
12	0.078	1072	3.493	509.62
13	0.078	882	3.493	507.71
14	0.078	1183	3.493	577.10

Institutional Repository - Library & Information Centre - University of Thessaly
02/06/2024 00:35:58 EEST - 18.226.159.139

Figure 5-16 presents the exergy destruction rate of each component of the hybrid system. It is obvious that the SOFC stack (anode-cathode) and the burner contribute the most to the irreversibility of the system. This is due to the chemical and electrochemical reactions as well as the mixing processes taking place in these devices.

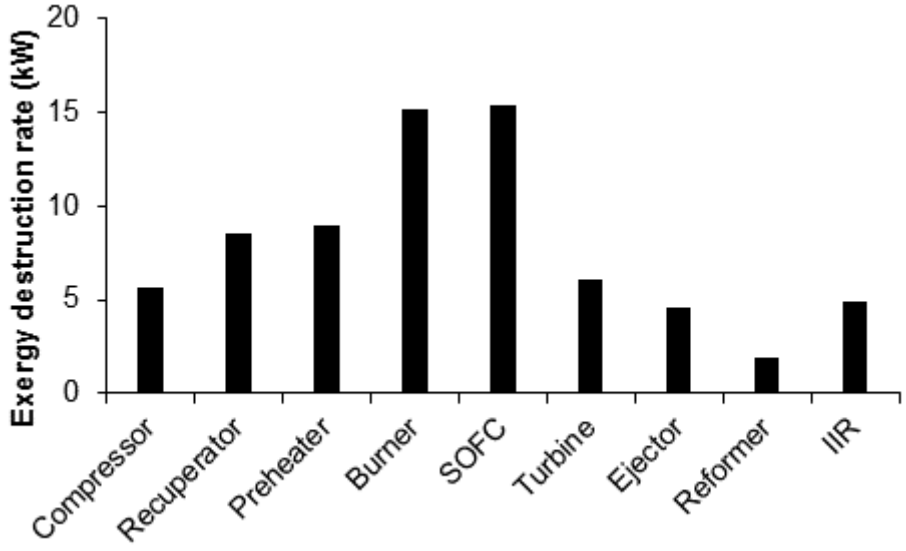

Figure 5-16 Exergy destruction rate of main devices at design point

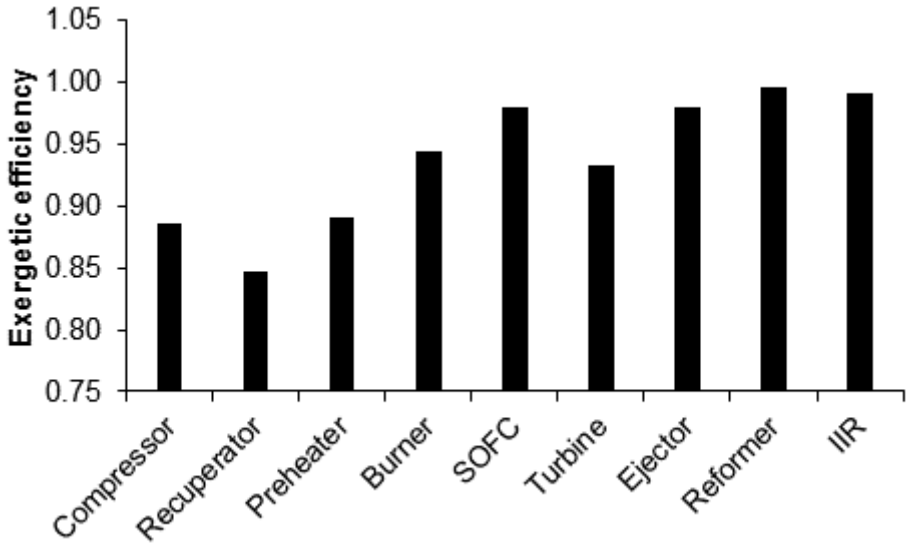

Figure 5-17 Exergetic efficiencies of main devices at design point

The exergetic efficiencies of the main components, i.e. the ratio of the exergy recovered to the supplied exergy, are presented in Figure 5-17. The lower exergetic efficiency value is for the recuperator. This is due to the high temperature differences between the fluids and the pressure losses. The SOFC stack exergetic efficiency is very high despite the high amount of exergy destruction rate.

Institutional Repository - Library & Information Centre - University of Thessaly
02/06/2024 00:35:58 EEST - 18.226.159.139

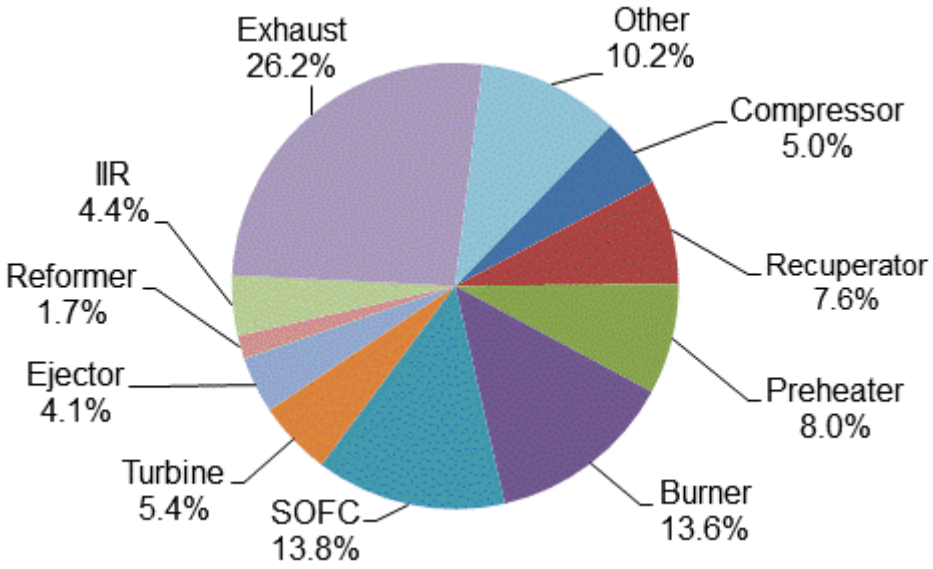

Figure 5-18 Exergy destruction in percentage of total exergy destructed

Figure 5-18 illustrates the exergy loss and destruction balance for the whole system. There is a large amount of exergy loss to the environment; about 26% of the total exergy destruction, larger than the amount of exergy destructed in SOFC stack. This high quality energy can be used further for useful energy production such as a bottoming cycle, space heating or cooling etc.

The exergy destruction rates at part-load conditions of the main components are shown in Figure 5-19. As the power output of the system decreases, the exergy destruction rates decrease too. The variation is larger for the SOFC stack and the burner because of the reduction of reaction rates. At very low loads the exergy destruction is larger for the recuperator. This is due to the lower mass flow rates and excess area of recuperator which enhances the exchange of thermal energy. That fact contributes to larger variation of the temperatures in the two streams, and consequently to larger irreversibilities and exergy destruction rates.

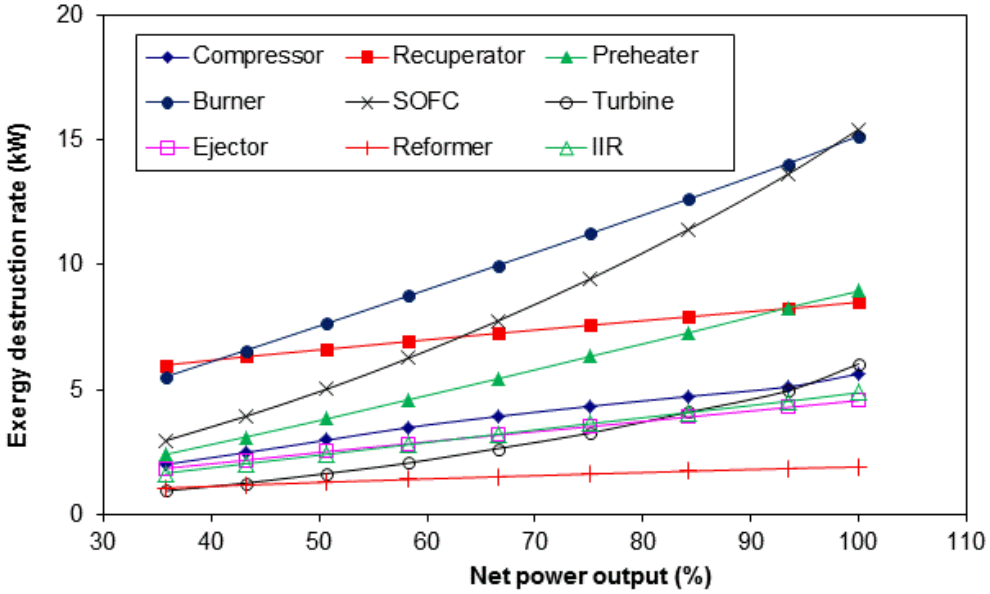

Figure 5-19 Exergy destruction rate at part-load operation

Institutional Repository - Library & Information Centre - University of Thessaly
02/06/2024 00:35:58 EEST - 18.226.159.139

Figure 5-20 illustrates the thermal and exergetic efficiency as well as the total exergy destruction rate at part load conditions. A nearly constant difference between the thermal and the exergetic efficiencies can be observed all over the range of operation. The system works more efficiently at part load conditions due to the smaller irreversibilities (see Figure 5-19).

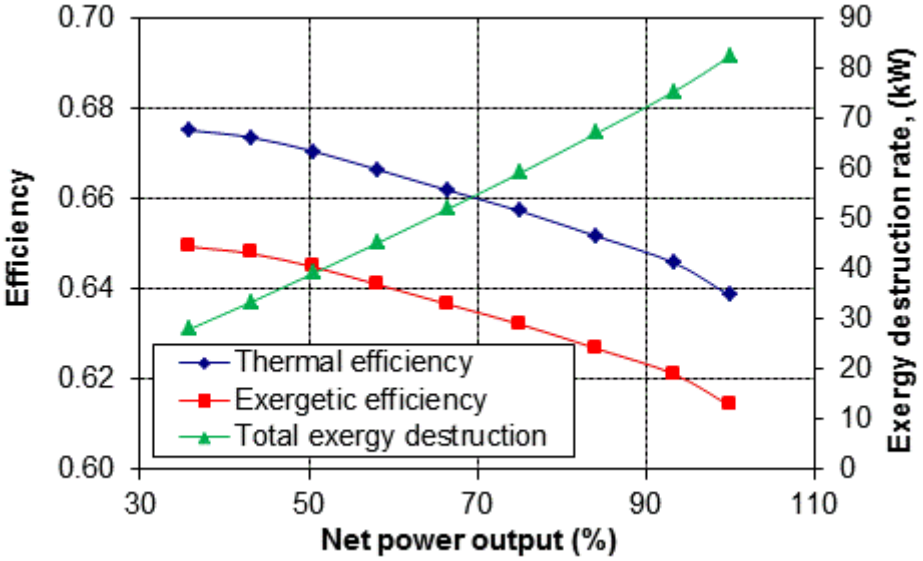

Figure 5-20 Efficiencies and total exergy destruction rate at part load conditions

The SOFC stack temperature is an important parameter in hybrid SOFC/GT system. This parameter affects significantly the exergetic efficiency of the system (Figure 5-21). As the SOFC temperature increases the exergy destruction increases due to the larger temperature differences in the system and the higher fuel consumption rates which contribute to higher values of current density and larger polarization losses. Nevertheless, the total exergetic efficiency increases since more net electrical power is produced. It is obvious that there is an upper bound in the exergetic efficiency increase. This is an interesting result which shows that very high values of fuel cell temperatures are not effective.

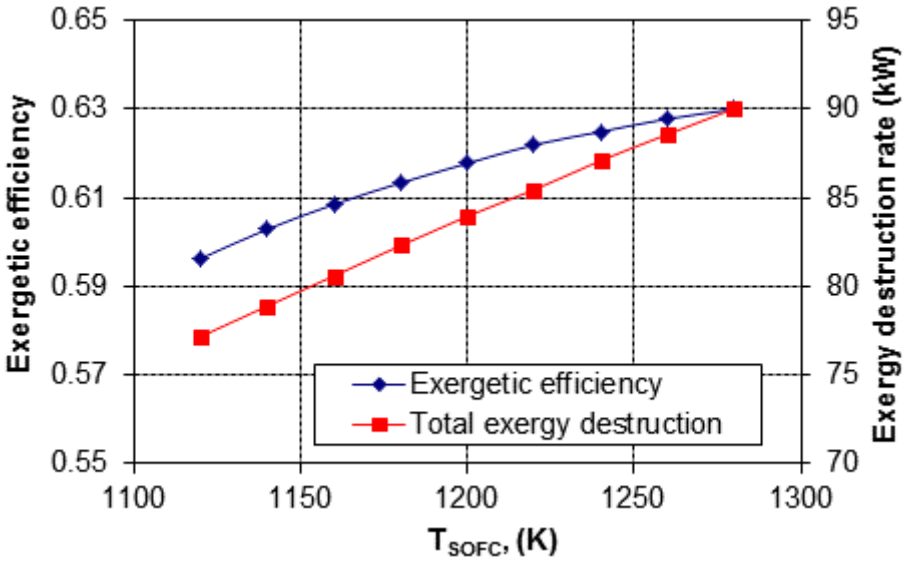

Figure 5-21 Effect of T_{SOFC} on exergetic efficiency and exergy destruction rate

Institutional Repository - Library & Information Centre - University of Thessaly
02/06/2024 00:35:58 EEST - 18.226.159.139

Figure 5-22 illustrates the effect of fuel utilization factor on the system exergetic performance. The variation in exergetic efficiency as well as in total exergy destruction rate is smaller compared with the variation caused from the SOFC stack temperature change. An increase in fuel utilization factor causes more fuel to react electrochemically within the fuel cell. Thus, the fuel amount reacting in the combustion chamber is reduced, causing a decrease in exergy destruction rate in this device. The total exergy destruction rate is reduced with the increment of fuel utilization factor. This is due to the lower amount of fuel introduced into the fuel cell according to Eq. 5-7 [46].

$$\dot{n}_{H_2,in} = \frac{i}{2FU_f} \tag{5-7}$$

This contributes to lower irreversibities, due to the restriction of mixing processes and chemical reactions. The exergetic efficiency of the system increases since the chemical exergy of the fuel is utilized more efficiently.

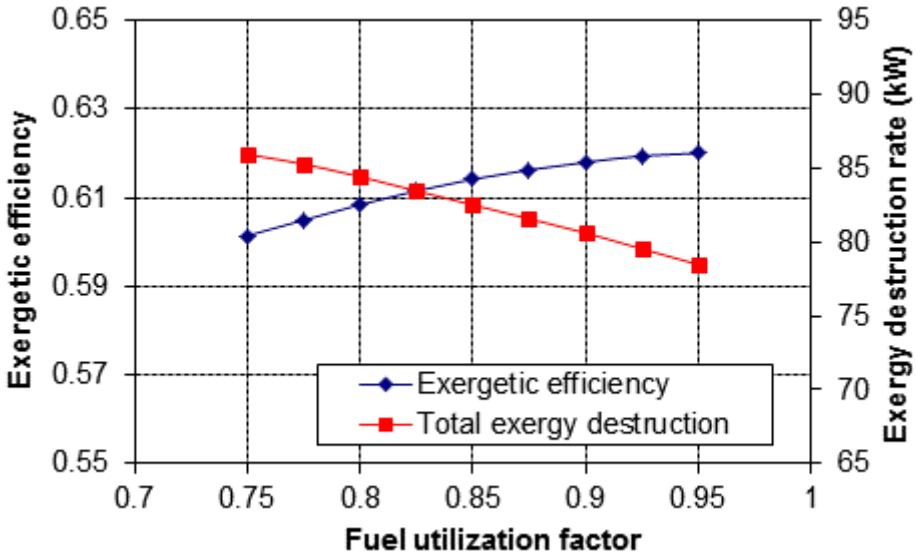

Figure 5-22 Effect of fuel utilization on exergetic efficiency and exergy destruction rate

Figure 5-23 illustrates the effect of the previous parameters on the exergy destruction rate of the components. The results are obtained by varying (increasing) each operating parameter by 1% and calculating the deviation of the exergy destruction rate of each component from the corresponding value at the design case. The increase of SOFC stack temperature has negative impact in most of the devices. The major impact is on the fuel processing system (ejector-reformer-IIR). This is due to two reasons: a) the hotter recycled fuel that enters the ejector and b) the higher fresh fuel flowrate. The SOFC stack irreversibilities tend to decrease since this device works more efficiently [95].

An increase of the of fuel utilization factor has a considerable positive impact on the burner in terms of irreversibility since less fuel reacts into the device. The exergy destruction rate increases only in the SOFC stack as well as in the reformers. The reason for the increase in fuel cell stack is the larger fuel amount reacting electrochemicaly.

Institutional Repository - Library & Information Centre - University of Thessaly
02/06/2024 00:35:58 EEST - 18.226.159.139

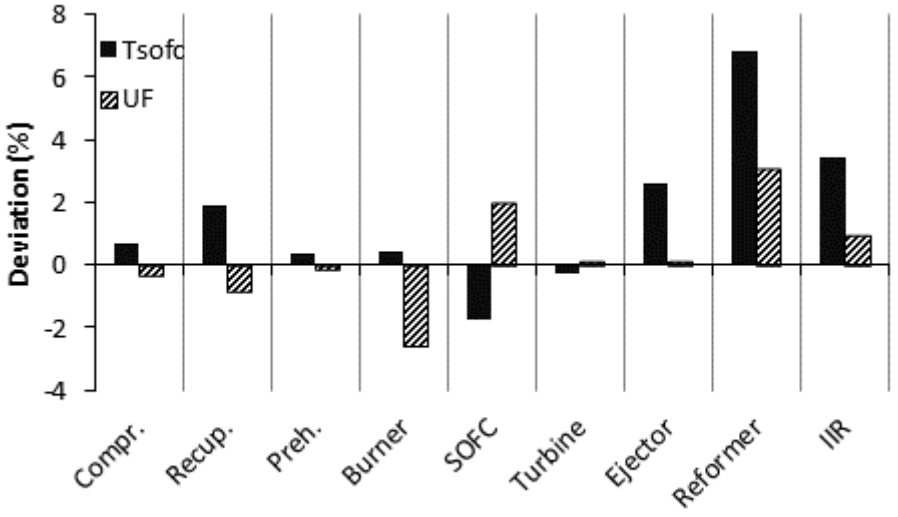

Figure 5-23 Sensitivity analysis of operating parameters in exergy destruction rate

Taking into account the previous results, certain improvements may be suggested in order to reduce the system exergy destruction. A possible improvement refers to the utilization of the exhaust gas heat carrying a high exergy amount which can be used further for useful energy production. This could be done with the use of a heat recovery steam generator or/and an absorption chiller, a bottoming cycle etc.

Another improvement would be the operation at higher fuel utilization factor as it results in reduced irreversibilities at the system or a different control strategy in which the SOFC temperature and fuel utilization factor will be regulated simultaneously in order to achieve the optimal performance. Finally, as large amounts of exergy are destructed in the heat exchangers, an optimization concerning the matching of the temperature levels on these devices could probably reduce irreversibilities.

Further investigation has been performed in order to compare the exergetic performance as well as the greenhouse gas emissions of the hybrid SOFC/GT system against a similar conventional GT system. Both systems rated at nearly the same electric power output. The conventional GT system was based on the commercially available Capstone C200 micro-turbine generator. Design parameters for the calculation of the thermodynamic cycle of the engine were taken from [96] (see Table 5-7).

Table 5-7 Capstone C200 design parameters

Electrical power (kW)	200
Mass flow (kg/s)	1.3
Pressure ratio	4.3
Turbine inlet temperature (°C)	950
Exhaust gas temperature (°C)	280
System efficiency (%)	33
Compressor isentropic efficiency (%)	75
Turbine isentropic efficiency (%)	90

Institutional Repository - Library & Information Centre - University of Thessaly
02/06/2024 00:35:58 EEST - 18.226.159.139

The model was developed in AspenPlus environment, using only built-in blocks. Performance maps were not used since the part load performance was not studied. It was calibrated in order to predict the engine behavior accurately at design point conditions.

The analysis was performed for the same environmental conditions and fuel composition. Although the selected gas turbine engine is slightly larger (200 kW electric power output) the direct comparison is not expected to affect significantly the conclusions as reduced parameters are used. The results presented in

Table 5-8 indicate that the hybrid system has almost double exergetic efficiency than a similar rated power conventional gas turbine system, while it is more environmental friendly as its CO_2 emissions are almost the half.

Table 5-8 Comparison of hybrid and conventional plants

	Hybrid SOFC/GT	Conventional GT
Exergetic efficiency (%)	61.3	34.0
CO_2 emissions (kg/kW.hr)	0.313	0.565

5.5 Conclusions

In this chapter, a simulation model for a hybrid SOFC-GT system based on existing devices is developed, using the AspenPlus process simulator.

The micro turbine is modeled and calibrated using the available manufacturer data for Capstone C30. The model incorporates typical performance maps for the compressor and turbine and is able to predict the part load performance of the engine.

The fuel cell model was developed based on available literature data for Siemens-Westinghouse tubular SOFC design. The voltage calculations were done by taking into account the fundamental phenomena taking place and fuel cell geometry.

The two independent models are incorporated into a single one and performance data for the resulting hybrid system were presented and discussed. The effect of main operating parameters on the system performance was also studied. The simulations showed that the two existing systems can be coupled safely together, achieving thus high electrical efficiency. The size of the proposed hybrid system and its efficient operation make it an attractive solution for distributed generation applications.

Moreover, an exergetic analysis of the hybrid system was performed. The results have shown that the SOFC stack and the burner are the devices with the higher exergy destruction rate. There is also, a large amount of exergy loss due to exhaust gases. A certain amount of this exergy stream may be used further through incorporated technologies.

An increase of the SOFC stack temperature has a positive impact on system exergetic efficiency, despite of the increment in exergy destruction. An increase of fuel utilization factor has an even more positive effect on the system performance; it increases the exergetic efficiency and at the same time, it reduces the exergy destruction.

Comparison of the hybrid system with a conventional GT of similar power indicated that the hybrid system is significantly more efficient in terms of second law efficiency and CO_2 emission.

Institutional Repository - Library & Information Centre - University of Thessaly
02/06/2024 00:35:58 EEST - 18.226.159.139

Institutional Repository - Library & Information Centre - University of Thessaly
02/06/2024 00:35:58 EEST - 18.226.159.139

Chapter 6
Matching consideration and performance evaluations

The present chapter aims to study the performance of the hybrid systems based on the fuel cell stack developed by Siemens-Westinghouse coupled with four different commercially available recuperated micro-turbines. The different systems considered were studied through the development of appropriate simulation models validated with available data. Full and part load performance of those systems are presented and discussed. For the part load operation two control strategies were adopted by maintaining either the SOFC stack temperature or the turbine exit temperature constant.

6.1 Introduction

Integrating a fuel cell and a gas turbine is by no means trivial and a significant system-level effort has been made to understand hybrid system integration and thermodynamics. Although there are a lot of works in the literature, most of them analyze theoretical hybrid systems. Only few papers are dealing with existing systems or systems based on actual devices.

The papers dealing with the matching of a SOFC module with a gas turbine can be classified in three categories.

In the first category are examined theoretical hybrid systems. Usually, in these works, the effect of some performance parameters on system behavior is studied. Indicatively, Tarroja et al. [86] studied the behavior of a hybrid system by changing performance parameters and also the size of system components. Uechi et al. [97] studied the effect of the design variables on a hybrid system performance and made suggestions in order to increase its efficiency.

Papers of the second category examine hybrid systems based on existing gas turbines and seek for the proper fuel cell configuration. Lundberg et al. [98] studied the appropriate size for the SOFC generator to be coupled with an actual gas turbine. Park et al. [99] based on a fixed gas turbine design studied the effect of the SOFC stack operating parameters on system behavior. Also, Song et al.[51] studied a system based on a commercially available gas turbine, specified the operating characteristics of the fuel cell stack and assessed the effectiveness of various control methods.

Finally, the works based on existing component belong to the third (and less extensive) category. Li and Weng [100] based on Siemens-Westinghouse fuel cell stack and on the Capstone C30 micro-turbine designed a hybrid system and simulated its performance for various fuels. Roberts and Brouwer [31] developed a dynamic model of an actual system and they validated it using experimental data.

Institutional Repository - Library & Information Centre - University of Thessaly
02/06/2024 00:35:58 EEST - 18.226.159.139

The present chapter aims to study the performance of the hybrid systems based on the fuel cell stack developed by Siemens-Westinghouse coupled with four different commercially available recuperated micro-turbines. There is no similar work in the related literature concerning the matching of different low rated available micro-turbines with an existing fuel cell. The effects of the different engine designs are studied through the development of appropriate simulation models validated with available data.

6.2 Gas turbine models

As mentioned previously, the present chapter deals with the study of the hybrid systems arisen from the coupling of the SOFC generator developed by Siemens-Westinghouse and commercially available micro-turbines. In the literature there are a lot of works about the coupling of the specific SOFC stack with a micro-turbine [28, 30, 31, 81, 100, 101] as well as different enhanced thermodynamic cycles [102-104]. Most of the works are not based on actual micro-turbines and adopt typical values for the performance parameters of the engine components.

Although, this approach gives realistic results, it is not fully representative when compared with an actual engine, especially in part load conditions. For this reason, the authors based on the performance data from commercially available engines, they developed reliable simulation models. Four engines were selected: C30 and C60 manufactured from Capstone Turbine Corp., the Parallon 75 kW and the T100 from Turbec. The characteristics of each engine are presented in Table 6-1.

Table 6-1 Parameters of micro-turbines at design point

Parameters	Capstone C30 [100, 105, 106]	Capstone C60 [105]	Parallon 75 [107]	Turbec T100 [108]
Rotational speed, (rpm)	96000	96000	65000	70000
Pressure ratio	3.6	4.8	3.5	4.5
Air flow rate, (kg/s)	0.31	0.48	0.75	0.79
Turbine inlet temperature, (K)	1117	1228	1148	1223
Turbine exit temperature, (K)	866	908	912	923
Exhaust gas temperature, (K)	546	578	511	543
Compressor isentropic efficiency	0.83	0.77	0.78	0.78
Turbine isentropic efficiency	0.85	0.85	0.84	0.83
Electric power, (kW)	30	60	75	100
Specific power (kW s/kg)	96.8	125	100	126.6
Electric efficiency	0.26	0.28	0.285	0.30

The developed models for each engine are based on general performance maps for the compressor and turbine components. The maps are given to the model in dimensionless form and are scaled in order to correspond to a specific engine. Performance map of the compressor is shown in Figure 6-1. The scaling of the maps is done according to the Eqs (6-1) – (6-3).

Institutional Repository - Library & Information Centre - University of Thessaly
02/06/2024 00:35:58 EEST - 18.226.159.139

$$\dot{m}_{c,map}^{scaled} = \dot{m}_{c,map}^{initial} \times \dot{m}_{c,engine}^{design} \quad (6\text{-}1)$$

$$PR_{map}^{scaled} = PR_{map}^{initial} \times \left(PR_{engine}^{design} - 1\right) + 1 \quad (6\text{-}2)$$

$$\eta_{map}^{scaled} = \eta_{map}^{initial} \times \eta_{engine}^{design} \quad (6\text{-}3)$$

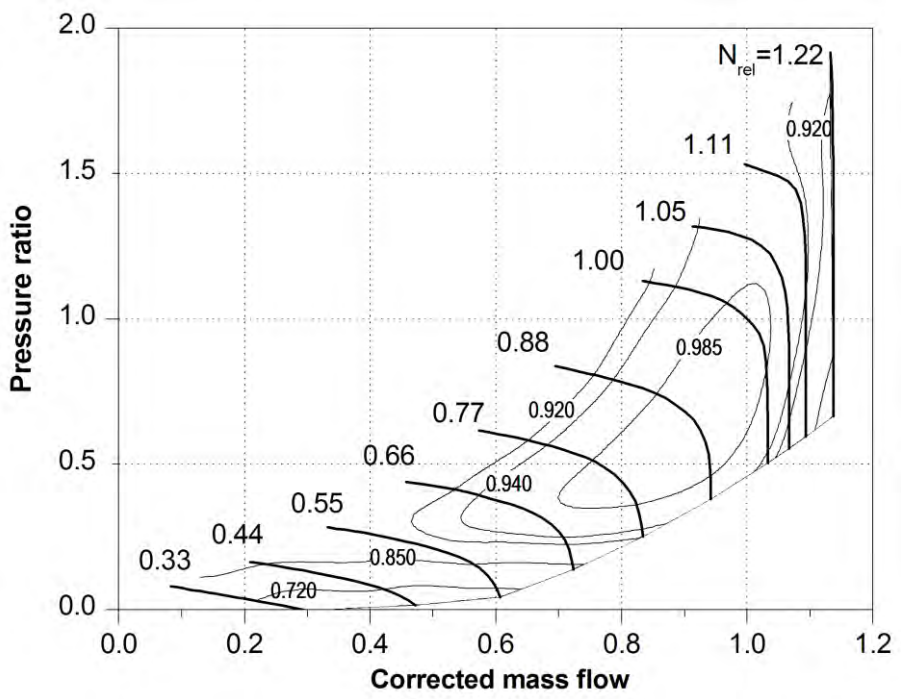

Figure 6-1 Initial compressor map

As it can be seen in Table 6-2, there is a good agreement between expected and calculated performance parameters for all engines at design point conditions.

Table 6-2 Microturbine models validation

Engine	Expected	Calculated	Error (%)
C30			
Efficiency	0.26	0.257	-1.15
Power (kW)	30	30.7	2.33
C60			
Efficiency	0.28	0.276	-1.43
Power (kW)	60	59.3	-1.17
Parallon 75			
Efficiency	0.285	0.288	1.05
Power (kW)	75	74.4	-0.80
T100			
Efficiency	0.30	0.302	0.67
Power (kW)	100	98.7	-1.30

6.3 Hybrid system model

The gas turbine and the SOFC generator model were merged into a single one by substituting the burner of the micro-turbines with the SOFC, in order to investigate the integrated hybrid systems.

Institutional Repository - Library & Information Centre - University of Thessaly
02/06/2024 00:35:58 EEST - 18.226.159.139

The hybrid system model and its assumptions have been presented in Chapter 4. The fuel supplied to the system is natural gas (CH_4 81.3%, C_2H_6 2.9%, C_3H_8 0.4%, C_4H_{10} 0.2%, N_2 14.3%, CO 0.9%)

6.3.1 Design point performance

In general there are two alternatives for the definition of the hybrid systems' design point. The first approach starts with the design point data of the existing micro-turbines and finds the resulting operating temperature of the SOFC generator, while the second approach starts with the design data of the SOFC system and predicts the operating characteristics of the micro-turbines. The present study predicted design point results are based on the first approach and are summarized in Table 6-3.

Table 6-3 Hybrid systems design point data

Parameter	C30	C60	Parallon 75	T100
Total power, (kW)	200.9	302.0	290.5	364.2
SOFC power, (kW)	164.0	235.3	214.8	259.8
GT power, (kW)	36.9	66.7	75.7	104.4
Fuel consumption, (g/s)	7.95	12.52	12.87	16.07
Air flow, (kg/s)	0.31	0.48	0.73	0.79
SOFC temperature, (K)	1256	1285	1165	1221
Afterburner outlet temperature, (K)	1402	1434	1269	1339
Exhaust gas temperature, (K)	552	583	517	549
Hybrid system global efficiency	0.66	0.63	0.59	0.59
Fuel cell efficiency	0.54	0.49	0.43	0.42

It is obvious that the total power produced increases significantly with the size of the micro turbine, as expected. On the other hand, the total efficiency decreases with the system size.

This general remark is not true when comparing C60 and Parallon 75 micro-turbines. Although the Parallon 75 is a more powerful engine than C60, the resulted hybrid system is less powerful. This can be explained by comparing the specific power values for each engine (see Table 6-1).

The reduction in the total efficiency is mainly due to the deterioration of the fuel cell stack performance because of the lower operating temperatures and the higher air mass flows. The increment in air mass flow contributes to more electric power production, and consequently to higher values of current density. The increment in current density causes a reduction in SOFC efficiency [30].

It is also evident that as part of a hybrid system, the micro-turbines produce more power compared with the power output of the stand-alone recuperated gas turbine cycles (Table 6-2). This is due to the different pressure losses caused by the SOFC generator as well as the increased turbine flow (higher fuel rates are supplied to the hybrid system in comparison to stand-alone gas turbine) [109]. The higher SOFC temperature results for the system based on C60 machine at design conditions, and is lower than the limit temperature ensuring safe operation of the device (1293.15 K) [98]. The higher afterburner outlet temperatures are also for the system based on C60 microturbine. Although the temperature values are high, they are in accordance with previous works [102, 110].

Institutional Repository - Library & Information Centre - University of Thessaly
02/06/2024 00:35:58 EEST - 18.226.159.139

The previous results are discussed analytically in the following paragraphs where the off-design performance of the hybrid systems is presented.

6.3.2 Part load performance

Part load operation in hybrid SOFC/GT systems is of major importance. Several theoretical studies [28, 30, 33, 81, 88, 111-113] and recent experimental works [114, 115] have been contacted in this subject. Campanari [28] assuming constant shaft speed, he suggested reducing air utilization factor and current density for part-load. This approach reduces the power output of the SOFC as well as the turbine inlet temperature (TIT) and consequently the power output of the GT. For variable shaft speed he suggested to reduce air flow rate and current density for maintaining constant TIT. Costamagna et al. [30] investigated the behavior of a small hybrid system using two different control strategies: constant or variable rotating speed. The results showed that the system is more efficient when its operation is controlled by the latter option. Yang et al. [85]compared three different control modes: a) only fuel flow manipulation, fuel and air mass flow manipulation by adjusting b) the speed or c) the inlet guide vanes angle. The most efficient alternative was proved again to be the one with the variable speed.

Kimijima and Kasagi [88] compared also variable and fixed shaft speed operation and concluded that variable shaft speed operation is favorable in terms of part-load performance. Chan et al. [116] proposed an external combustor for system part-load operational control. In their approach the part-load operation incorporates the inherent characteristics of a SOFC-GT hybrid system by adjusting the system power output through bypassing part of the fuel to a combustor. This enhances the upstream condition of the gas turbine and hence improves turbine performance. Though the total efficiency of the system is reduced, the operation is simpler and safe. Kaneko et al. [112] controlled the fuel cell temperature by introduction and use of a bypass valve around the recuperator. By releasing excess heat to the exhaust, the bypass valve provided the control means to avoid the self-exciting behavior of system temperature and stabilized the temperature of SOFC at 850 °C.

Stiller et al. [81] presented a multi-loop control strategy for a SOFC/GT hybrid system with the main objective being a fairly constant fuel cell temperature under all conditions. A multi-loop control strategy is also developed by Wu et al. [113] in order to ensure the system safe operation as well as long lifetime of the fuel cell. The system has four control variables, which are power, SOFC operating temperature, turbine inlet temperature and fuel utilization. The manipulated variables are current, fuel flow, air flow and bypass valve opening. Jiang et al. [111] proposed control strategies for startup and part load operation. The control objective for the part load operation regardless of load changes, as proposed, was to maintain constant fuel utilization and a fairly constant SOFC temperature within a small range by manipulating the fuel mass flow and air mass flow.

In most of the presented works part load performance is considered by manipulating the fuel flow as well as the air mass flow, through the variation of the compressor's operating conditions.

In this study during the part load operation the system follows the variation of the load by changing the rotational speed and the fuel flow rate simultaneously. Two different part load strategies were examined: in the first, the SOFC stack temperature remains constant; in the second, the turbine exit temperature remains constant. In both cases the fuel utilization factor is considered invariable.

Institutional Repository - Library & Information Centre - University of Thessaly
02/06/2024 00:35:58 EEST - 18.226.159.139

Fixed SOFC stack temperature

In Figure 6-2 is presented the part load performance of the four hybrid SOFC-GT systems which arise by coupling the Siemens-Westinghouse fuel cell generator with four different micro-turbines. It is obvious that the hybrid system with the smaller micro-turbine (Capstone C30) works more efficiently than the others, especially on high relative power outputs. The hybrid system which is based on Parallon 75 micro-turbine has the lower efficiency values. This is mainly due to the low value of this micro-turbine's specific power. It is evident also that the hybrid systems work more efficiently at part load conditions. The increment in efficiency values was expected as a rotational speed control mode was utilized [85].

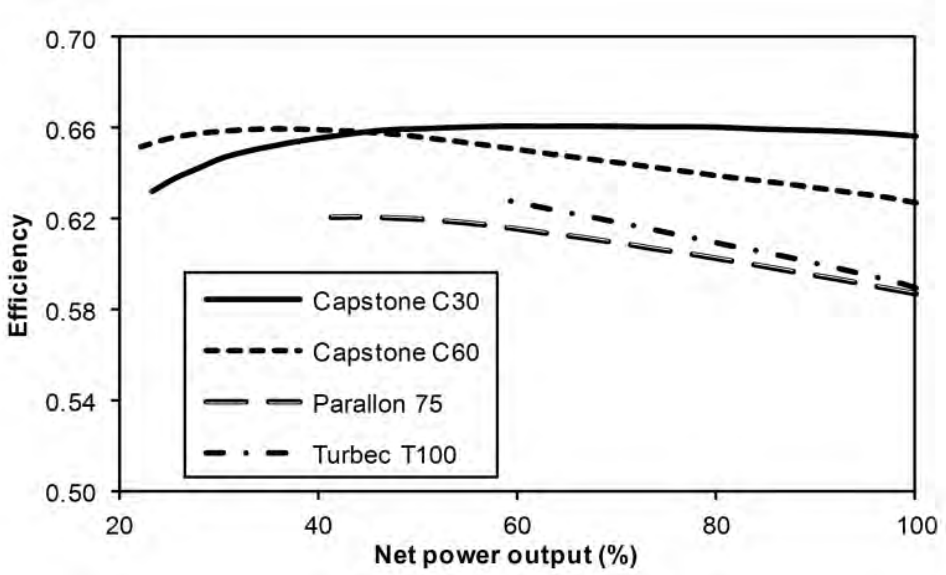

Figure 6-2 Part load performance of the hybrid systems (constant T_{SOFC})

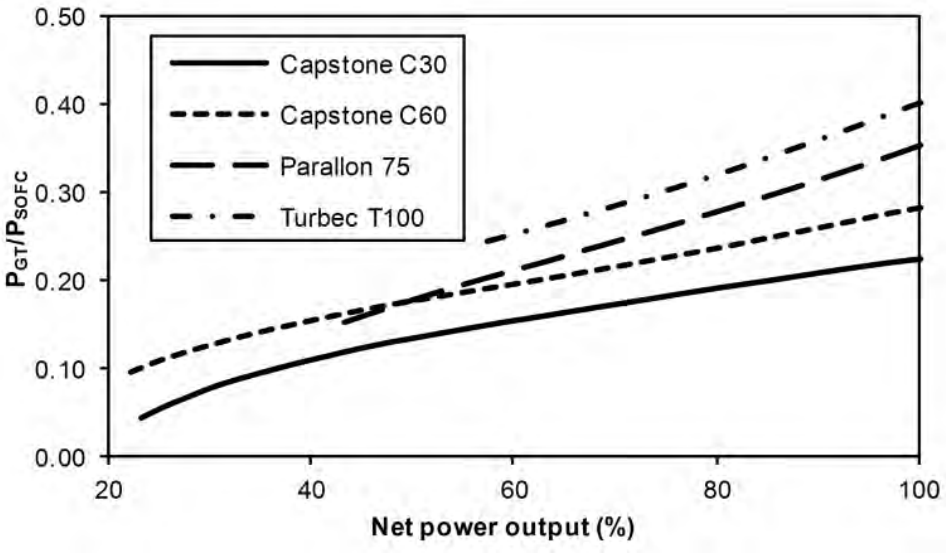

Figure 6-3 Gas turbine output to SOFC output power fractions

The smaller hybrid systems are more efficient for two reasons. Firstly, as the gas turbine size decreases, the contribution of that component to the total system output decreases, too. This fact can be seen in Figure 6-3, where the fraction of gas turbine power to the SOFC power is plotted. As

Institutional Repository - Library & Information Centre - University of Thessaly
02/06/2024 00:35:58 EEST - 18.226.159.139

fraction values increase, the system operates less efficiently since more power is produced from the less efficient component of the hybrid system. Secondly, the SOFC generator works more efficiently in the smaller systems as shown in Figure 6-4.

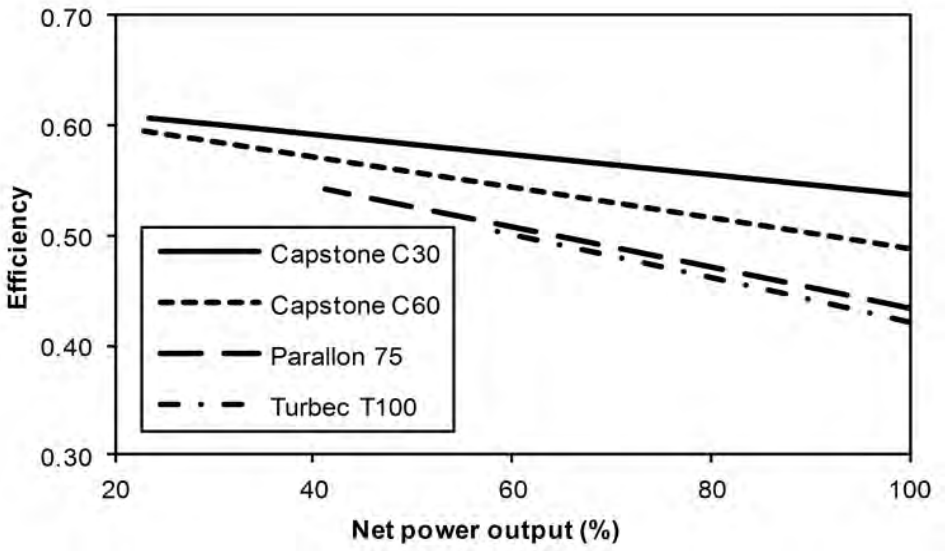

Figure 6-4 SOFC stack efficiency

SOFC polarization curves are shown in Fig. 8. It can be observed that the cell electrical characteristics for the two smaller systems (based on C30 and C60) are almost the same and better than the corresponding of the two bigger systems. The worst performance of SOFC is again for the Parallon system probably because the SOFC works with the smaller temperature in that case.

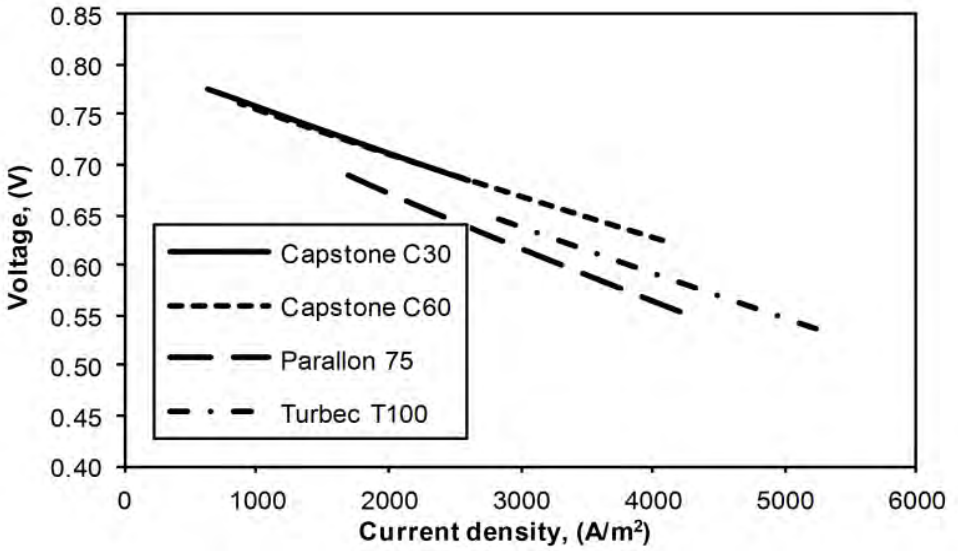

Figure 6-5 Cell voltage vs current density

At part load conditions the systems tend to operate at lower turbine inlet temperatures (Figure 6-6). This is due to the lower fuel consumption which contributes to reduction of the fuel amount reacting in the afterburner. The results are similar for the C60 and T100 engines as the design values of the turbine inlet temperatures are very close (Table 6-1).

Institutional Repository - Library & Information Centre - University of Thessaly
02/06/2024 00:35:58 EEST - 18.226.159.139

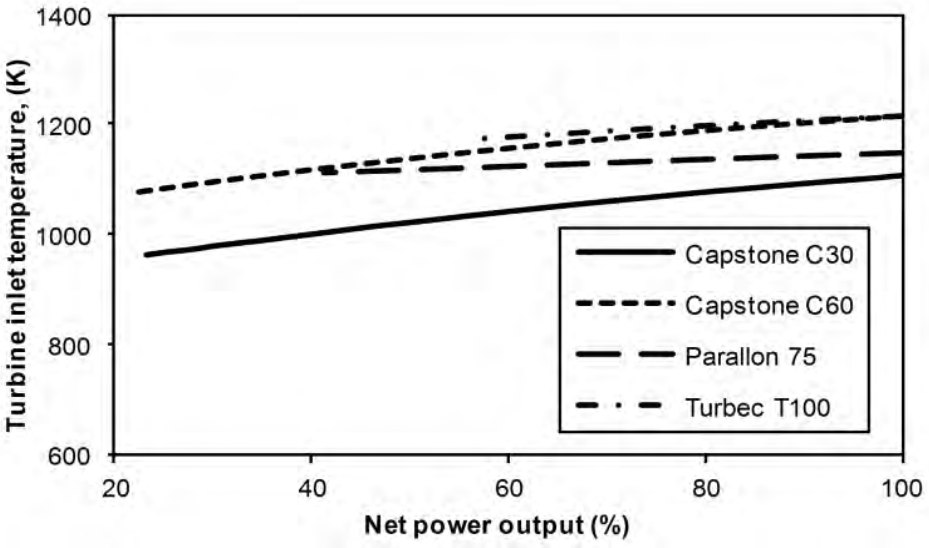

Figure 6-6 Turbine inlet temperature

The turbine exit temperature at the part load conditions is presented in Figure 6-7. The temperature increases with the total power decrement, since the turbine component operates at lower mass flow rate and pressure ratio and utilizes smaller amount of the available energy. Attention must be paid to high values since this can affect the recuperator lifetime. The turbine exit temperature increases with the micro-turbine size as expected from design point data (Table 6-1) and the turbine inlet temperature values (Figure 6-7).

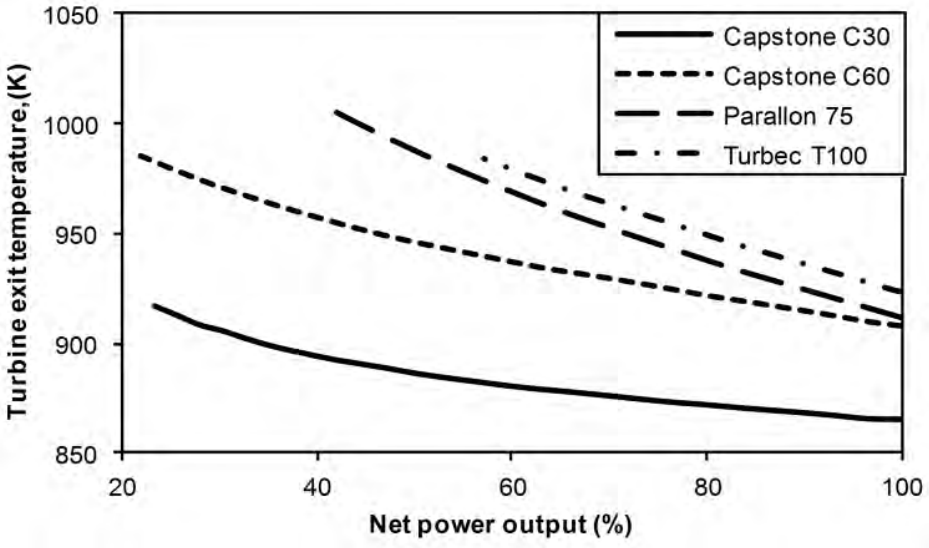

Figure 6-7 Turbine exit temperature

Figure 6-8 presents the SCR values at part load conditions for the hybrid systems. The results are in accordance with reference [81].

Institutional Repository - Library & Information Centre - University of Thessaly
02/06/2024 00:35:58 EEST - 18.226.159.139

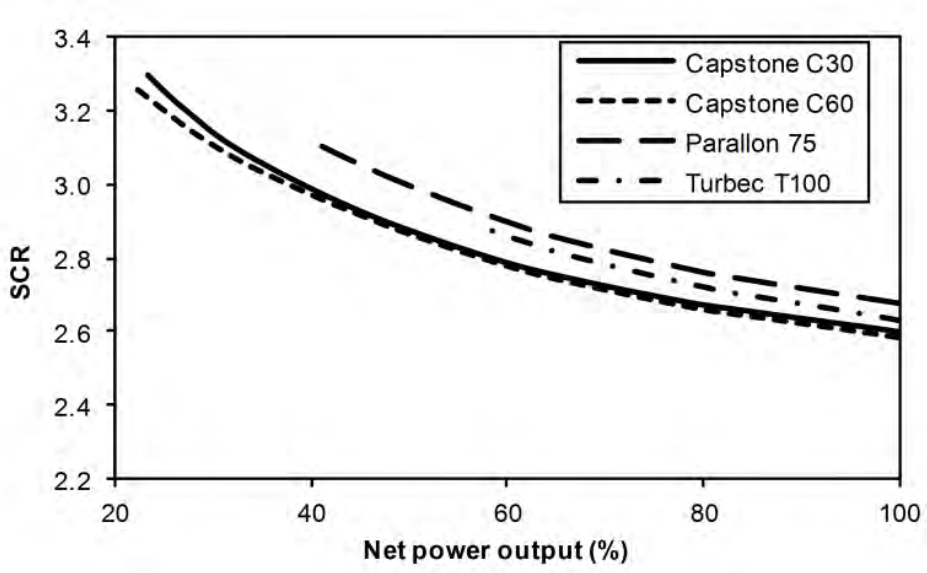

Figure 6-8 SCR variation at part load conditions

Fixed turbine exit temperature

Usually the studies of hybrid SOFC/GT systems are emphasized on fuel cell performance and utilize the appropriate control strategies in order to ensure safe and reliable operation for the system. Generally, one of the scopes of the control systems is to maintain the SOFC temperature fairly constant so as to ensure the long lifetime of the system. Except for the SOFC temperature, also the turbine inlet and exit temperatures may affect the reliability and lifetime of the system, especially the turbine and recuperator components.

In micro-turbines the turbine exit temperature is controlled by manipulating the fuel amount fed to the combustion chamber [72, 117]. When a microturbine is coupled with a fuel cell stack to create a hybrid system, the turbine exit temperature is determined from the operating conditions of the turbine and the turbine inlet temperature which is dependent with the fuel cell stack temperature. In the specific control method the turbine inlet and exit temperatures can take extremely high values since are not controlled. Although in various studies [88, 100] it is mentioned that the turbine exit temperature takes high values when the system operates at part load, nevertheless, there is no existing hybrid system with controlled turbine exit temperature.

In a hybrid system the turbine exit temperature can be controlled by two ways. The first is by changing the fuel amount in the SOFC stack. The SOFC operating temperature changes according to the fuel change. The variation of the SOFC temperature affects the fuel cell generator exhaust temperature and consequently affects the turbine exit temperature. The other one is by changing the fuel utilization factor. This parameter affects the fuel amount in the burner. In the case of a decrement in fuel utilization factor higher amount of fuel reacts in the burner and this contributes to higher turbine exit temperatures. In this work the first method was used in order to control the turbine exit temperature.

Figure 6-9 presents the expected part load performance of the studied hybrid systems in the case of keeping constant turbine exit temperature. The systems behave similarly to the previous case, where the SOFC temperature was fixed.

Institutional Repository - Library & Information Centre - University of Thessaly
02/06/2024 00:35:58 EEST - 18.226.159.139

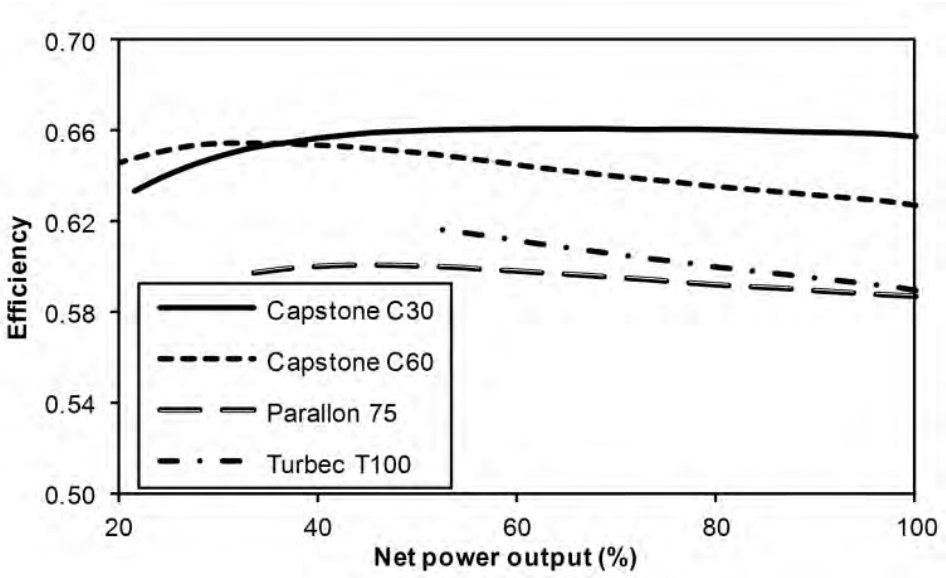

Figure 6-9 Part load performance of the hybrid systems (constant TET)

Although the SOFC temperature decreases at part load conditions (Figure 6-10) the efficiency is not affected significantly.

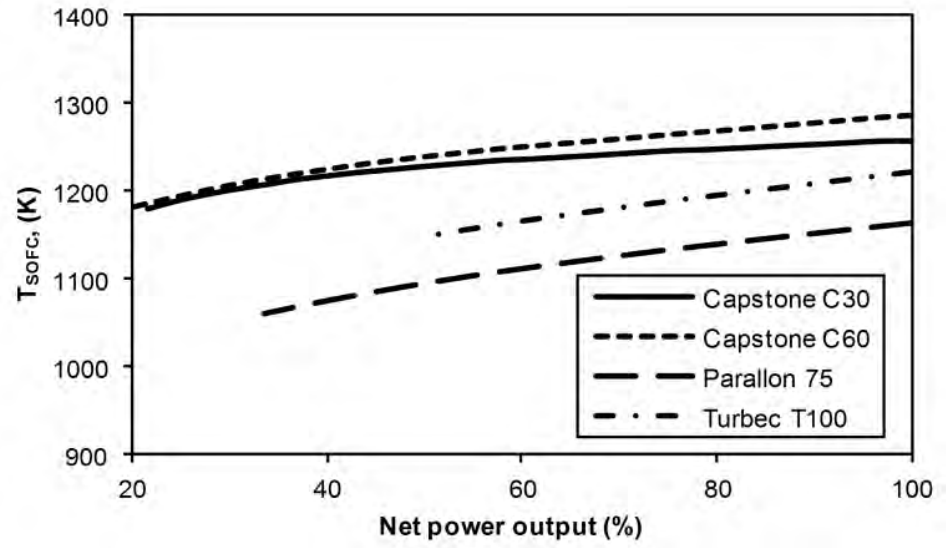

Figure 6-10 SOFC stack temperature

The higher values of SOFC stack temperature are arisen for the Capstone C60 micro-turbine (Figure 6-10). This is due to the high values of the turbine inlet temperature (Table 6-1) and the low air mass flow rate in which the system operates. However, the specific control method causes large variations of the fuel cell stack temperature, which contribute to shortening of the fuel cell lifetime.

6.4 Discussion

From the previous results it is obvious that the four engines can be combined effectively with the Siemens-Westinghouse tubular SOFC stack design. As presented in Figure 6-11, the higher efficiencies arise for the smallest micro-turbine, while the smaller size of the micro-turbine

Institutional Repository - Library & Information Centre - University of Thessaly
02/06/2024 00:35:58 EEST - 18.226.159.139

contributes to lower values of total power output, as expected . This fact is confusing when one aims at assessing which of the micro-turbines is the best choice to be coupled with the SOFC stack.

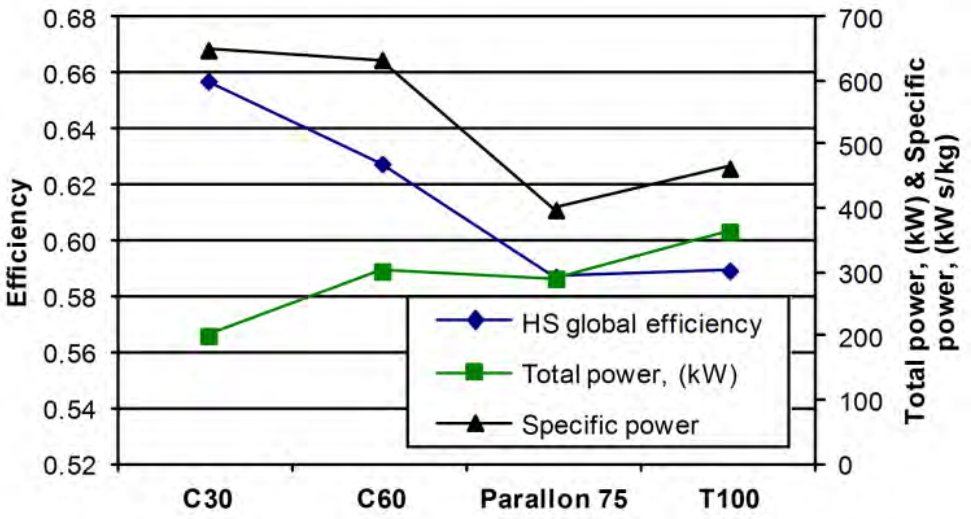

Figure 6-11 Design point data of the hybrid systems

An alternative assessment that could give a clearer picture may be based on the specific power of the systems. The specific power is the power per unit airflow which is defined as:

$$w_{spec} = \frac{P_{HS}}{\dot{m}_{air}} \tag{6-4}$$

As it can be seen in Figure 6-11 the hybrid systems based on C30 and C60 micro-turbines have the higher specific powers. The values for those systems are similar and differ significantly from the specific power of the hybrid system based on Parallon 75 and T100 micro-turbine. This fact makes those engines an attractive solution for the hybrid system which is based on the Siemens-Westinghouse SOFC stack. The high specific power output is preferred since contributes to lower airflows which requires smaller equipment for the same power output [118]. However, a compromise between the total power output and efficiency of the hybrid system must be done, since the smaller engine (C30) results in lower power output and higher efficiency whereas the larger engine (C60) results in higher power output and lower efficiency. The choice of the engine depends on the installation requirements.

An important fact that arises from the simulation of the four hybrid systems is shown in Figure 6-12. At low power demands, the same load can be provided from different hybrid systems (C30, C60) without significant loss in efficiency. This information can be useful during the choice of system configuration. The designer can select the larger engine, in order to serve peak power demands, without sacrificing the performance of the system on base load operation. The same remark (though there is an increased efficiency drop at the higher power range) applies to high power demands for the systems C60 and T100.

Institutional Repository - Library & Information Centre - University of Thessaly
02/06/2024 00:35:58 EEST - 18.226.159.139

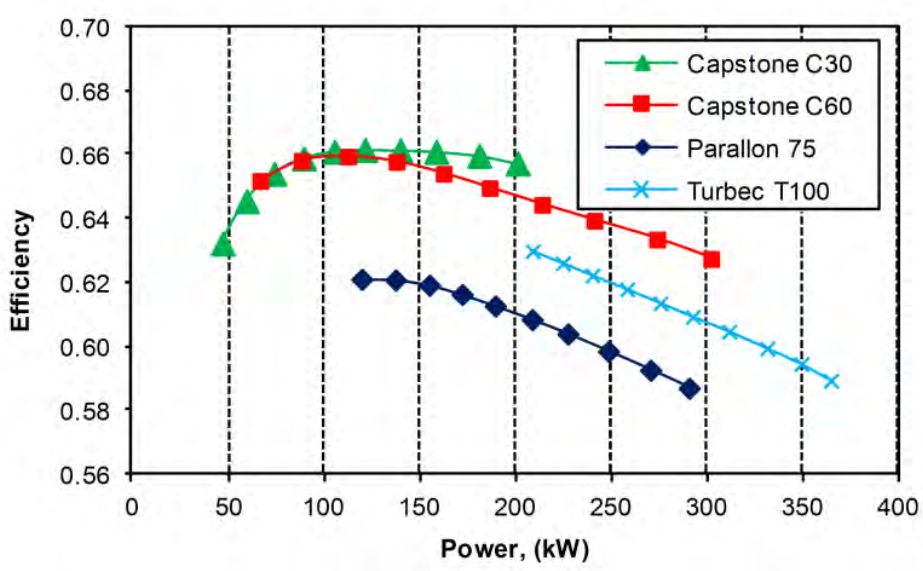

Figure 6-12 Efficiency vs power of hybrid systems

6.5 Conclusions

The coupling of SOFC generator manufactured from Siemens-Westinghouse with four commercial available micro-turbines was investigated. Separate models for the SOFC generator and micro-turbines were built and merged in order to realize the hybrid system.

Design point for each hybrid system was determined and the part load performance was studied. For the part load operation two control strategies were adopted by maintaining either the SOFC stack temperature or the turbine exit temperature constant. The performance of the hybrid systems was similar for both the control methods.

The part load results have shown large variations in SOFC stack and turbine exit temperatures. Those data must be taken into account in order to avoid system malfunctions and to ensure the long lifetime.

The smaller (among the four considered) the micro-turbine coupled with the Siemens-Westinghouse SOFC generator, the more efficient is the corresponding hybrid system.

When the power requirements are low (less than 150 kW), the designer may choose a larger micro-turbine than the required (i.e. based on C60 instead of C30), as the system operates efficiently also at higher than the base load and could satisfy peak energy demands.

Institutional Repository - Library & Information Centre - University of Thessaly
02/06/2024 00:35:58 EEST - 18.226.159.139

Chapter 7
Improving hybrid SOFC-GT systems performace through turbomachinery design

In this chapter a methodology to improve the performance of a hybrid SOFC-GT system for the whole operating range is proposed. The method suggests a way for optimizing the compressor and turbine components. It is based on the search of the compressor and turbine operating lines giving an improved system efficiency both in design and part load operation. Turbomachinery models are used to calculate the geometry that produces the desired performance maps and the corresponding operating lines. Based on the new turbomachinery design the hybrid system shows a clear efficiency advantage for the whole operating range.

7.1 Introduction

The first generation of fuel cells for stationary applications is already available in the market [119]. These fuel cell generators operate under atmospheric pressure and produce electric power less than 250 kW. SOFC-GT systems though more efficient than atmospheric SOFC generators are not commercially available yet, since they are more complex and there are reliability and availability problems [119, 120].

A lot of research has been done investigating the performance and the interaction of the main subsystems (namely the gas turbine and the SOFC generator) in a hybrid system. The works are, either theoretical [30] or based on existing devices [98]. They are dealing with the operation under steady state or transient conditions [121], the exergetic performance [76, 122-125], the utilization of alternative fuels [126-128] and the control of these systems [81]. Also, there are papers that investigate the optimal design of a SOFC-GT hybrid configuration [98, 129-131].

An important issue when designing a hybrid system is the selection of design parameters (such as pressures, temperatures) in order to achieve the optimal and efficient matching of the subsystems and to ensure the long lifetime and the safe operation. For example, Calise et al. [130] optimized a hybrid plant rated at 1.5 MW by changing many operating variables except for the geometrical dimensions of cell tubes. For the turbomachines, properly scaled typical operating maps were used. The same authors in another work [129] optimized a hybrid system based on thermoeconomic criteria without taking into account the part-load operation of the system during the optimization

Institutional Repository - Library & Information Centre - University of Thessaly
02/06/2024 00:35:58 EEST - 18.226.159.139

process. Lundberg et al. [98] in their study optimize a SOFC generator size for combination with a gas turbine by minimizing the cost of electricity produced. Sieros and Papailiou [131] studied the matching of a small gas turbine with a hybrid SOFC-GT system. The authors suggested variable geometry turbomachines in order to achieve a better match with the SOFC stack.

The good matching between the two main subsystems (SOFC stack and gas turbine generator) can offer a lot of advantages for the hybrid SOFC-GT system, such as:

- Safe operation, since all the devices work within their operating limits and they are resistant to faults.
- High efficiency, since the individual systems are designed to cooperate efficiently and ensure the best performance not only in the design point, but also in part-load conditions.
- Increased lifetime and lower maintenance costs as a result of the efficient operation and the good operating conditions ensured for all subsystems and especially for the components of the SOFC generator (fuel cell, reformer) which are most prone to degradation problems.
- Fuel savings and short payback period. The investment cost of hybrid SOFC-GT systems is high so this is a drawback for their commercialization. By designing an economical system it will be possible to compete the conventional power systems.
- Reliability and availability since the good matching of the subsystems contributes to simpler system layouts without by-pass streams or guide vanes and complicated control systems. This fact makes them less prone to faults and increase time between overhauls.

The proposed SOFC-GT systems are usually based on existing gas turbines which are modified to be able to operate with a SOFC generator. For example, Lundberg et al. [98] modified the commercial available Mercury 50 gas turbine engine, fabricated from Caterpillar/Solar Turbines, and integrated it with a SOFC generator. The final system was able to produce 12.3 MWe with a net efficiency of 59.9%. This is an economical solution as the cost for the development of new compressor and turbine components is excluded from the final product/system. The integration of the fuel cell generator and the auxiliary equipment in the flow path of the working fluid from the compressor exit to the turbine inlet can affect the operation of the turbomachines by changing their matching [132]. This fact may have a negative impact on the performance of the turbomachines, since it can change their efficiency values. Also, the rematching of the turbomachines may affect negatively the safe operation of the system, since can force the compressor to operate with smaller surge margin values. This can be dangerous, especially during transient conditions.

In the available bibliography there is a limited number of studies for the turbomachinery matching in order to improve performance at part-load conditions for a hybrid SOFC-GT system, suggesting variable geometry turbomachines and by-pass flows [131, 133]. Although, these solutions seem to give good results, they are complicated and contribute to greater investment costs and lower reliability and availability of the hybrid system.

In the present work a method is proposed in order to design the turbomachinery components aiming at an improved performance in the whole operating range, while keeping the system simple and safe. The proposed optimization method is applicable in hybrid SOFC-GT systems that incorporate either a variable speed gas turbine with a power conditioner to convert the variable frequency output of the generator to the grid frequency, or an engine that has a separate power turbine to drive the electric generator. It consists of two steps: (i) a parametric study is conducted in order to assess the operating range of the hybrid SOFC-GT system and select the desired operating

Institutional Repository - Library & Information Centre - University of Thessaly
02/06/2024 00:35:58 EEST - 18.226.159.139

line for achieving the optimum system efficiency at various operating points and (ii) based on that information, the compressor and turbine geometries are estimated using in-house turbomachinery design codes and an optimization procedure.

7.2 Hybrid SOFC-GT model

The SOFC-GT system considered in this study is shown schematically in Figure 7-1, it is based on the hybrid system developed by Siemens-Westinghouse rated at 220 kW net electric power output [44]. The system incorporates a high temperature SOFC generator integrated with a single shaft recuperated gas turbine. Because of its size, it utilizes a centrifugal compressor and a radial turbine. The air enters the system through the compressor. Thereafter, the compressed air is preheated in the recuperator and is led in the SOFC generator where it reacts electrochemically with the fuel. The hot exhaust gases from the fuel cell generator are expanded on the turbine and produces mechanical work for the compressor and electric generator. The hot gases at the exit of the turbine are used to preheat the SOFC supplied air.

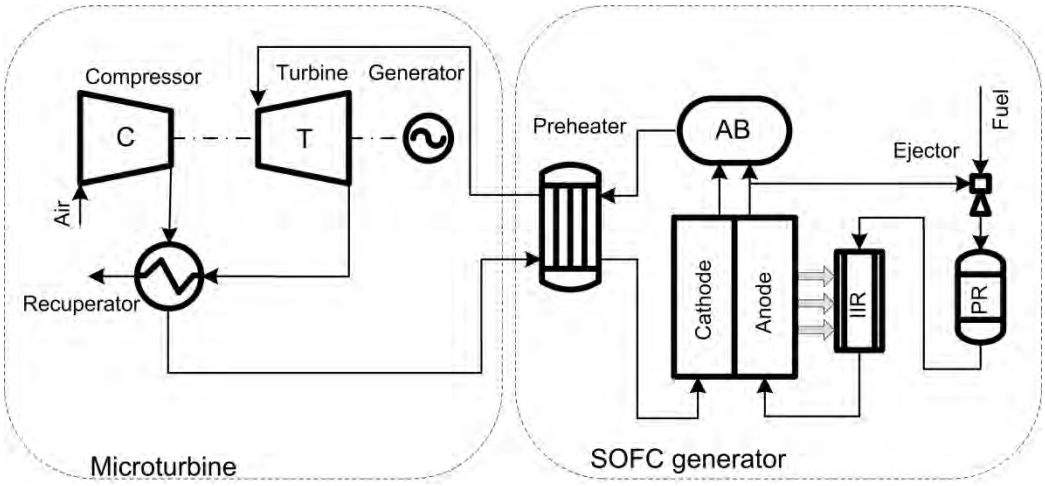

Figure 7-1 Hybrid SOFC-GT system layout (AB: Afterburner, IIR: Indirect internal reformer, PR: Pre-reformer)

The SOFC generator utilizes a tubular cell configuration. The main device of that SOFC generator is the fuel cell stack, namely an array of vertically aligned cells. Except for the cells the system contains an ejector which mixes the depleted fuel with the fresh fuel in order to supply steam for the shift and steam reforming reactions. The unreacted (and non-recycled fuel) and the air exiting the cells are burned into the burner. Next, the hot gases pass through a heat exchanger, where the fresh air is heated before entering the stack.

The system simulation is based on the methodology described in previous chapters. During the part load operation, the fuel cell stack operating temperature and the fuel utilization factor are regulated (remain constant) by changing the fuel flow rate, the SOFC current and the generator power.

For the part load operation representative performance maps from similar size turbomachines were used, which were scaled in order to correspond to the design point. The scaling process involves the derivation of scaling factors from comparison between the design point of the turbomachine and the one reference point given for the original map and then the multiplication of the original map data with the scaling factors to obtain the new map [134]. The compressor map presented in Figure 7-2,

Institutional Repository - Library & Information Centre - University of Thessaly
02/06/2024 00:35:58 EEST - 18.226.159.139

has been produced by modifying a centrifugal compressor performance map presented in reference [135]. The turbine map is taken from reference [42] and it is presented in Figure 7-3.

The design point data [44, 76] of the hybrid system are presented in Table 7-1. The values in italics represent the data originally given by the manufacturer. The model was validated against published data from reference [44]. The results are shown in Table 7-2. It is obvious that the model predicts with good accuracy the performance of the hybrid system.

Table 7-1 Hybrid system design parameters

Parameter	Value
SOFC generator	
Number of cells	*1,152*
Cell active area (m^2)	*0.0834*
Cell operating temperature (K)	1,183
Fuel utilization factor	*0.85*
Steam to carbon ratio	2.5
DC to AC inverter efficiency (%)	94
Burner thermal losses (%)	2
Gas turbine	
Compressor pressure ratio	*2.9*
Turbine pressure ratio	2.48
Air flow rate (kg/s)	*0.5897*
Recuperator pressure loss (cold/hot) (%)	3 / 7
Compressor isentropic efficiency (%)	78
Turbine isentropic efficiency (%)	82
Mechanical efficiency (%)	97
Generator efficiency (%)	97

Table 7-2 Hybrid system validation

Parameter	Reference	Model	Error (%)
Net electrical power output (kW)	220	220.7	0.30
SOFC generator – DC power (kW)	187	187.0	0.01
SOFC generator – AC power (kW)	176	175.8	-0.11
Gas turbine electrical power (kW)	47	47.8	1.80
Cell voltage (V)	0.610	0.607	-0.54
Current density (A/m^2)	3,200	3,208.5	0.26
Turbine inlet temperature (K)	1,113	1,113.2	0.01
Thermal efficiency (%)	57	58.5	2.66

Institutional Repository - Library & Information Centre - University of Thessaly
02/06/2024 00:35:58 EEST - 18.226.159.139

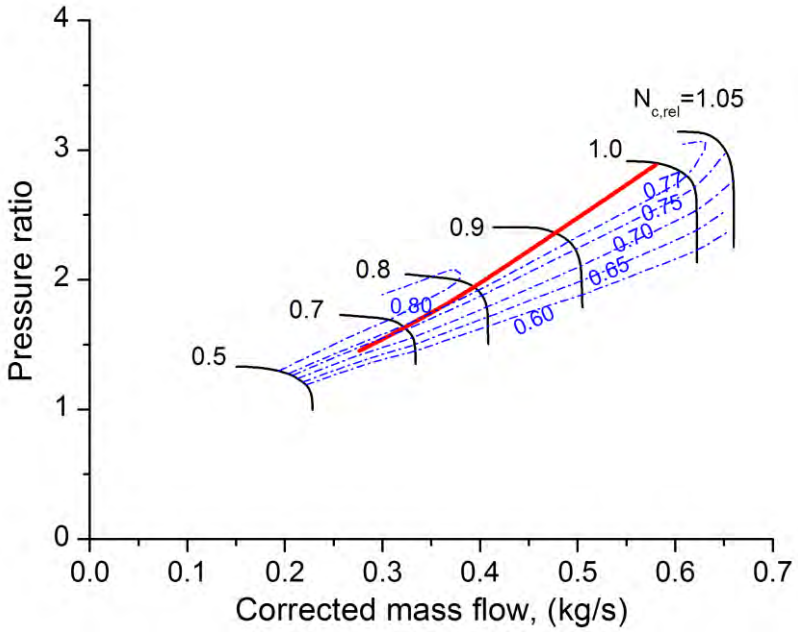

Figure 7-2 Compressor map for the reference system

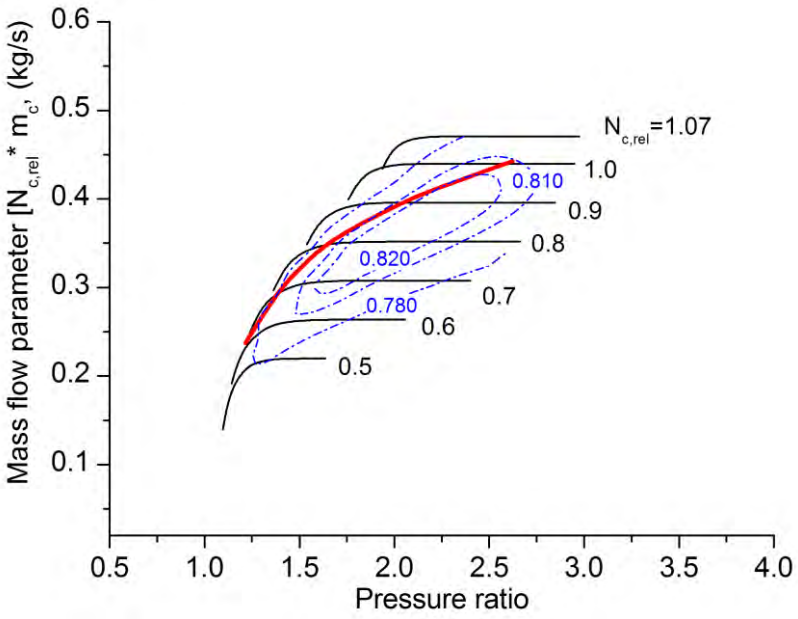

Figure 7-3 Turbine map for the reference system

Figure 7-4 presents the efficiencies of the main components of the hybrid system, namely the compressor, the turbine and the SOFC stack (Eq. (7-1)), as well the total system efficiency (Eq. (7-2)) as a function of net power output. The SOFC generator efficiency increases at part load conditions since the current density decreases and contribute to lower ohmic losses [136]. On the contrary, the total system efficiency decreases as net power output demand is below 60%. This is due to the deterioration of the turbomachinery performance.

Institutional Repository - Library & Information Centre - University of Thessaly
02/06/2024 00:35:58 EEST - 18.226.159.139

$$\eta_{SOFC} = \frac{P_{SOFC}}{\dot{m}_f LHV} \tag{7-1}$$

$$\eta_{HS} = \frac{P_{SOFC} + P_{GT} - P_{aux}}{\dot{m}_f LHV} \tag{7-2}$$

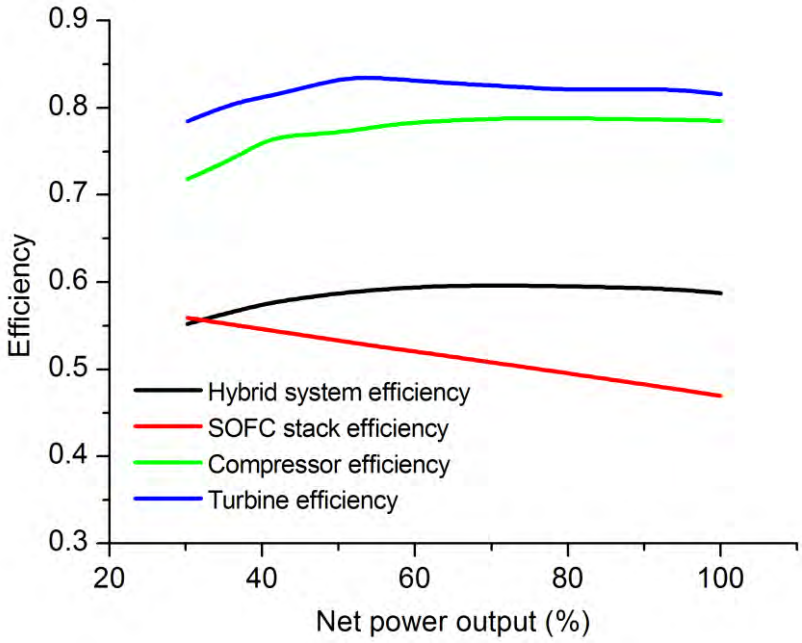

Figure 7-4 Part load performance of the reference system

Looking at the performance maps (Figure 7-2 and Figure 7-3), it is observed that the turbomachinery devices can operate with higher efficiencies even at very low rotational speeds. Nevertheless, this is not happening because of the improper matching of the compressor and turbine components at part load conditions. A reasonable question arisen thus is the following: is there any pair of turbomachinery devices capable of improving the performance of the hybrid system over the whole operating range ensuring at the same time its safe operation? To answer this question one has to seek for the appropriate turbomachineries (in terms of their characteristic performance maps) in order to obtain the theoretical maximum efficiency of the hybrid system at each operating point over the whole operating range.

7.3 Outline of the proposed method

The model described in the previous section is used for the hybrid system optimization over the whole operating range. In a hybrid system the operating line is determined by manipulating the fuel flow, the SOFC current and the power of the gas turbine. A compressor is used to determine the fuel flow and pressure of the fresh fuel. The fresh fuel pressure has no significant impact on the overall system performance, however it is important for anode gas recycling to meet the steam-to-carbon ratio values for the proper operation of the reformer [78, 137]. The SOFC current mainly affects the total power of the system. The power level of the gas turbine affects its rotational speed. The rotational speed has significant impact on the amount of the ingested air and the operating pressure of the system, since it affects the operating points of the turbomachines. The air pressure is crucial

Institutional Repository - Library & Information Centre - University of Thessaly
02/06/2024 00:35:58 EEST - 18.226.159.139

for the system performance as it could give a high efficiency advantage [138]. Consequently, the turbomachines are key elements for an efficient hybrid SOFC-GT system.

As the scope of this work is to design the compressor and turbine components that ensure an improved system performance, the ingested air mass flow and the operating pressure were selected as the decision variables. These parameters have a major impact on the geometry and the size of the turbomachines.

Thus, by using the developed model the pairs of air mass flow and pressure ratio values giving the higher system efficiency are specified. In the hybrid system, these operating parameters are determined from the air compressor, and consequently, the compressor component should be designed to operate as close as possible to the optimum pressure ratio and mass flow values (desired operating line). The turbine component should be designed to correspond to the compressor, so as to ensure the best system performance. An operating line for the turbine component is required in order to provide guidance for its design process. The operating line is estimated from the turbine operating data (e.g. pressures, temperatures, mass flows) arisen from hybrid system model when it is fed with the compressors' operating line data. The new turbomachines ensure an improved system performance. The procedure is shown schematically in Figure 7-5.

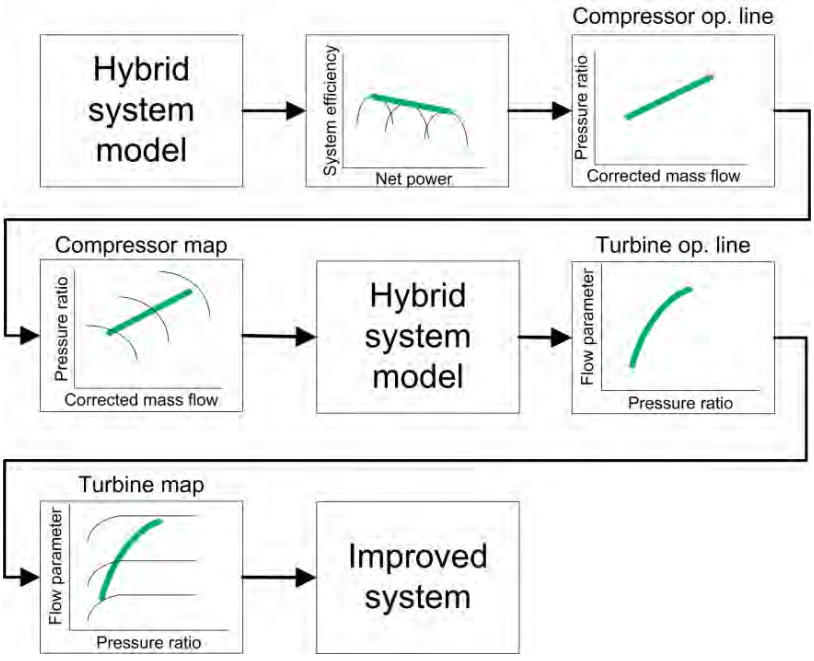

Figure 7-5 Hybrid system optimization procedure outline

7.3.1 Hybrid system theoretical best performance

In order to assess the performance of the hybrid system, a parametric study was conducted to investigate the effect of the key process variables. The parameters that mainly affect the geometry and size of the turbomachines; i.e. the mass flow and the pressure ratio, were varied over a wide range to explore the system behavior. Apart from the previous parameters, the isentropic efficiency can also affect the geometry. For this reason different values for the compressor efficiency were given to study the impact on the system performance.

Institutional Repository - Library & Information Centre - University of Thessaly
02/06/2024 00:35:58 EEST - 18.226.159.139

The results of parametric study for the whole operating range are presented in Figure 7-6. The curves have been arisen by maintaining the mass flow that enters the system as well as the compressor isentropic efficiency constant and varying the compressor pressure ratio. This is done for the design point air mass flow (the higher one) as well as for lower values in order to assess the performance at off-design conditions. It is obvious that as the mass flow decreases the system operates more efficiently. Also, the system presents a narrower operating range at lower mass flows. The peak efficiency points for the same mass flow values are connected with dotted lines. As it was expected, as the compressor efficiency increases the system works more efficiently, and the optimum operating point of the system shifts to higher power production when the mass flow remains constant. The systems' behavior was similar when varying the turbine isentropic efficiency, so the results were omitted for clarity.

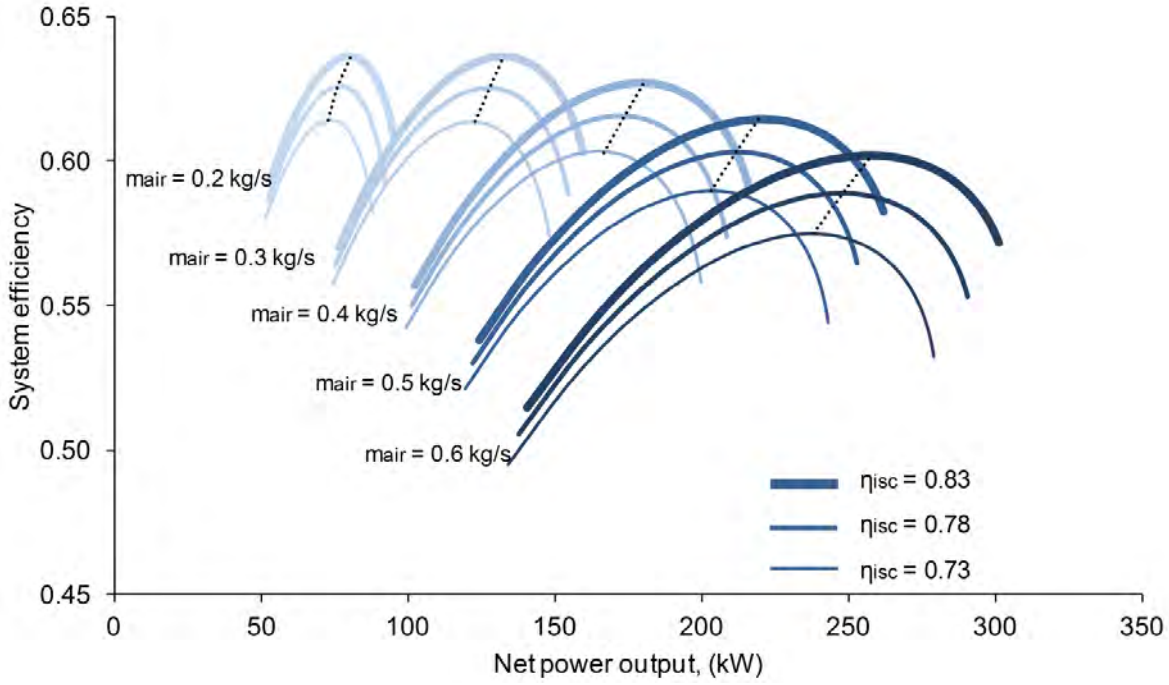

Figure 7-6 Part load performance of the hybrid system

7.4 Compressor design

Based on the results of Figure 7-6, the desired operating line for the compressor can be extracted. The points of the compressor operating line should correspond to the optimum operating points (peak points) of the system. For the sake of simplicity, the optimum operating points are selected for a single (constant) compressor isentropic efficiency value. In general, this assumption is not quite correct, since in most practical applications the compressor efficiency varies about 5 percentage points between the full load and idle conditions. However, considering the shape of the typical performance curves for a centrifugal compressor [139], it is feasible to attain a compressor which operates with an almost constant efficiency value. Consequently, the assumption of nearly a constant compressor efficiency, at the whole operating range does not impact the proposed method.

Moreover, the selected compressor efficiency values neither represent the best technology nor any attempt is made to optimize them, because the aim of this work is to propose a method to design a

Institutional Repository - Library & Information Centre - University of Thessaly
02/06/2024 00:35:58 EEST - 18.226.159.139

compressor for a hybrid SOFC-GT system that contributes to improved performance at a reasonable cost.

The operating line of the new compressor should approach the desired optimum operating line as much as possible. The procedure is described graphically in Figure 7-7. It starts with an initial compressor design in which an operating line is selected empirically. The initial design is then modified to approach the desired (optimum) operating line.

In compressors the running lines are determined by swallowing capacity of the downstream components. In this step of the optimization procedure, the swallowing capacity of the turbine is unknown, thus technically it is impossible to determine an operating line for the compressor. In order to overcome this obstacle, an operating line should be chosen. A rational choice is an operating line that approaches the peak efficiency line (in the middle of the map). This is valid for most applications since it is achieved an efficient and safe operation, because of the high surge margin levels that are obtained. Details about the optimization process are presented in section 7.4.2.

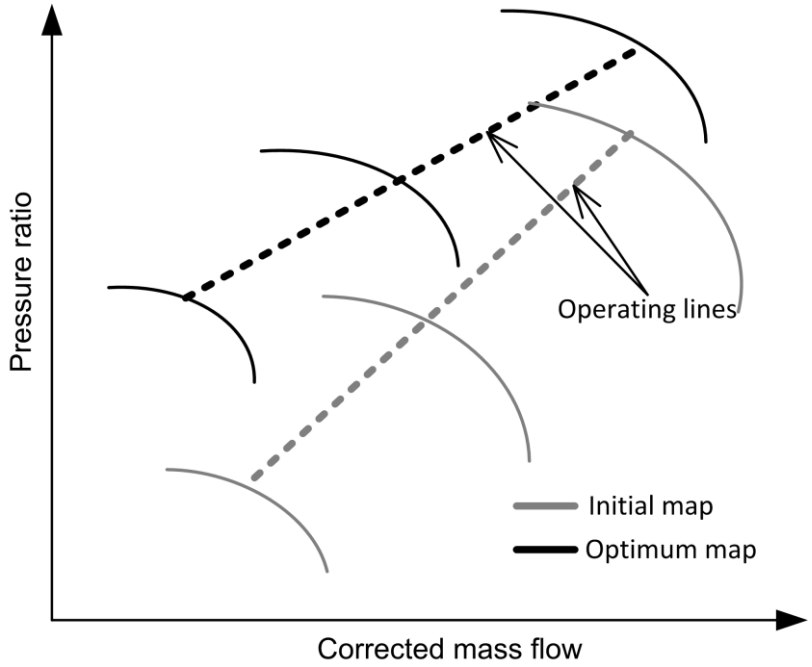

Figure 7-7 Compressor map optimization process

7.4.1 Compressor in-house model

For the compressor design, the methodology developed by Galvas [140] was adopted. This method requires the compressor overall geometry as well as the working fluid inlet conditions and physical properties. The thermodynamic properties of the working fluid are computed at five stations (Figure 7-8):

1. rotor inlet
2. rotor outlet
3. vaned diffuser leading edge
4. vaned diffuser throat
5. vaned diffuser outlet.

Institutional Repository - Library & Information Centre - University of Thessaly
02/06/2024 00:35:58 EEST - 18.226.159.139

The centrifugal compressor for this system assumed without inlet guide vanes. Also, the impeller is considered with splitter blades in order to achieve better flow condition (no slip) and higher efficiencies. The geometry parameters affecting the performance as well as the operational range are shown in Figure 7-8.

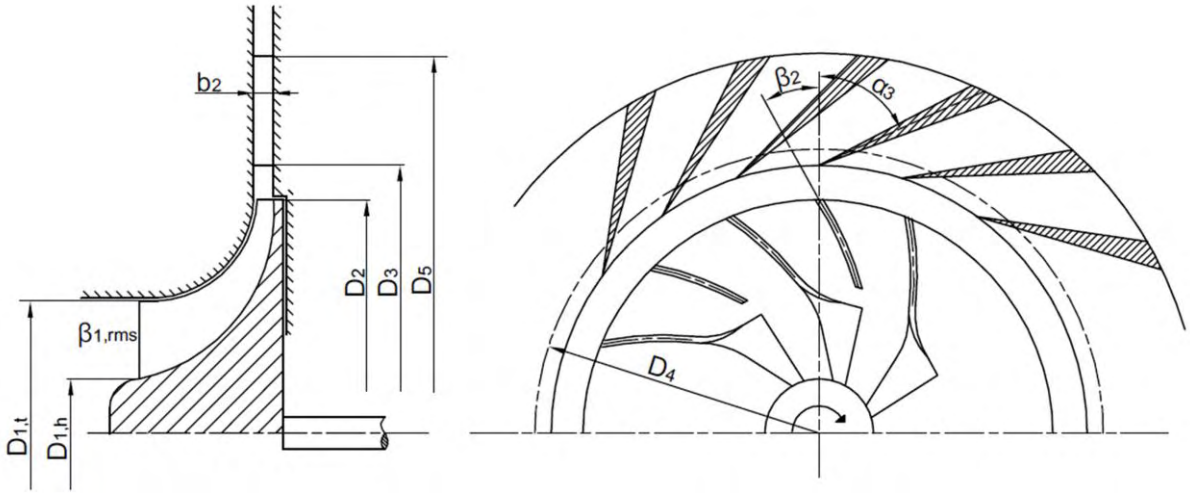

Figure 7-8 Geometric description of the compressor

The method takes into account the main loss mechanisms and predicts the behavior of a centrifugal compressor. Losses considered are: a) inducer incidence losses, b) blade loading losses, c) skin friction losses, d) disk friction losses, e) recirculation losses, f) vaneless diffuser losses and finally g) vaned diffuser losses.

The inducer incidence losses are caused from the deviation of the relative flow angle at rotor inlet from its optimum value. The optimum angle is given from the methodology developed from Stanitz [141]. The corresponding enthalpy losses due to incidence are

$$\Delta h_{inc} = 0.5\left[w_1 \sin\left(\left|\beta_1^{opt} - \beta_1\right|\right)\right]^2 \tag{7-3}$$

The optimum relative flow angle β_1^{opt} is

$$\beta_1^{opt} = \beta_1 - \varphi \tag{7-4}$$

The deviation angle φ is given from Eq. (7-5)

$$\varphi = \tan^{-1}\frac{(1-B_f)\tan\beta_1}{1+B_f\tan^2\beta_1} \tag{7-5}$$

where

$$B_f = 1 - \frac{Z_f t}{\pi\sqrt{\frac{1}{2}(D_{1,h}^2 + D_{1,t}^2)}} \tag{7-6}$$

The blade load is defined as the pressure difference between the pressure and the suction surfaces of blades. This pressure difference contributes to increment of boundary layers and the extent of leakage flows near the tip of the blade. Blade loading losses defined as:

Institutional Repository - Library & Information Centre - University of Thessaly
02/06/2024 00:35:58 EEST - 18.226.159.139

$$\Delta h_{bl} = 0.05 D_f^2 u_2^2 \tag{7-7}$$

where the diffusion coefficient is given from the following relation

$$D_f = 1 - \frac{w_2}{w_{1,t}} + \frac{0.6 C_p \left(T_{t2} - T_{t1}\right)}{\frac{(Z_f + Z_{sp})}{\pi}\left(1 - \frac{D_{1,t}}{D_2}\right) + 2\frac{D_{1,t}}{D_2}} \cdot \frac{u_3}{w_{1,t}} \tag{7-8}$$

Skin friction losses are because of the roughness of the compressor wetted areas, which raises the resistance during the passage of the working media through the compressor. The corresponding enthalpy loss is:

$$\Delta h_{sf} = 7.0 S_f \frac{L}{D_h} \bar{w}^2 \tag{7-9}$$

where the hydraulic diameter is:

$$D_h = \frac{D_2}{\frac{Z_f + Z_{sp}}{\cos\beta_2} + \frac{D_2}{b_2}} + \frac{1}{\frac{2}{D_{1,t} - D_{1,h}} + \frac{2(Z_f + Z_{sp})}{\pi(D_{1,t} + D_{1,h})}\sqrt{1 + \tan^2\beta_1\left(1 + 0.5\left(D_{1,h}/D_{1,t}\right)^2\right)}} \tag{7-10}$$

and the mean flow path length

$$L = \frac{D_2}{2}\frac{1 - \frac{D_{1,rms}}{0.3048}}{\cos\beta_2} \tag{7-11}$$

During the operation of the compressor, the rotation of the impeller backplate exerts shear forces to the fluid between the impeller and the adjacent parallel wall. The enthalpy change due to disk friction losses (or alternatively windage losses) is given from the following equation:

$$\Delta h_{df} = 0.01356 \frac{\rho_2}{\dot{m}\mathrm{Re}^{0.2}} u_2^3 D_2^2 \tag{7-12}$$

The recirculation losses represent the work performed by the backflow, which is caused from fluid portion that does not have enough energy to overcome the pressure gradient of the diffuser and returns to the impeller. The recirculation losses expressed as:

$$\Delta h_{rc} = 0.02\sqrt{\tan\alpha_2} D_f^2 u_2^2 \tag{7-13}$$

The vaneless diffuser is the space between the impeller exit and the leading edge of the vanes in vaned diffuser. The losses in that section are due to skin friction, diffusion and heat transfer phenomena. They are expressed as follows:

$$\Delta h_{vld} = C_p T_{t2}\left[\left(\frac{P_3}{P_{t3}}\right)^{\frac{\gamma-1}{\gamma}} - \left(\frac{P_3}{P_{t2}}\right)^{\frac{\gamma-1}{\gamma}}\right] \tag{7-14}$$

The vaned diffuser is characterized geometrically with the area ratio of the throat and diffuser exit. The vaned diffuser model utilizes a performance map that takes into account the Mach number, the total pressure and the blockage at throat section and estimates the pressure recovery coefficient for the specified geometric area ratio. Assuming one-dimensional flow the exit conditions are estimated and the enthalpy loss is given from the relation (7-15).

Institutional Repository - Library & Information Centre - University of Thessaly
02/06/2024 00:35:58 EEST - 18.226.159.139

$$\Delta h_{vd} = C_p T_{t2} \left[\left(\frac{P_5}{P_{t5}} \right)^{\frac{\gamma-1}{\gamma}} - \left(\frac{P_5}{P_{t4}} \right)^{\frac{\gamma-1}{\gamma}} \right] \quad (7\text{-}15)$$

The geometry parameters affecting the performance as well as the operational range are summarized in Table 7-3. These parameters do not have the same effect on the shape of the compressor characteristic curves. In order to assess the effect of each parameter on the output of the model, a sensitivity analysis was conducted by varying individual input parameters by 1%, one variable at a time, and estimating the percentage change of some key parameters.

The output of the model it is not simple technical parameters, but sets of characteristics curves. The only way to assess the effect of each one of the input parameters is to compare the resulted maps graphically. However, this is not practical since it requires so many graphs as the number of input parameters. To overcome this difficulty and get a better insight of the effect of input parameters, it was decided to study the behavior of a single operating point (i.e. the pressure ratio and efficiency variation).

Table 7-3 Sensitivity analysis of the compressor model

Parameter	Pressure ratio	Efficiency
N	3.07	-0.36
$D_{1,t}$	3.32	-0.51
$D_{1,t}/D_3$	-3.12	0.49
$D_{1,h}/D_{1,t}$	-0.15	-0.05
β_2	-0.17	0.00
D_3/D_2	-0.34	-0.23
b_2	0.19	-0.03
$\beta_{1,rms}$	0.00	0.00
A_5/A_4	0.04	0.03
t	-0.00	0.00
α_3	-0.02	-0.00
A_4	-0.05	-0.04
S_f	-0.15	-0.09
Z (full+split)	0.05	-0.02

The results are presented in Table 7-3. The values may differ if the operating point changes (e.g. at lower rotational speed). Nevertheless the conclusions are similar since the deviations have the same order of magnitude.

From the sensitivity analysis results it is clear that some geometrical characteristics did not affect significantly the compressor performance. For example, the effect of $\beta_{1,rms}$ angle was negligible. The insensitive variables, those with effect less than 0.1% (absolute value), should not be taken into account in optimization procedure, except from A_4 which is a geometric dimension that changes with the size of the compressor. On the other hand, there are parameters that affect significantly the performance map such as S_f, which is kept constant since skin friction coefficient is a technological constraint.

Institutional Repository - Library & Information Centre - University of Thessaly
02/06/2024 00:35:58 EEST - 18.226.159.139

7.4.2 Compressor optimization

The new compressor must be optimized so as the Eq. (7-16) become as small as possible.

$$OF = \sum_i w_i \left[\left(1 - \frac{PR_{i,map}}{PR_{i,desired}} \right)^2 + \left(1 - \frac{\dot{m}_{i,map}}{\dot{m}_{i,desired}} \right)^2 + \left(1 - \frac{\eta_{i,map}}{\eta_{i,desired}} \right)^2 \right] + penalty \quad (7\text{-}16)$$

Equation (7-16) represents the difference between the desired operating points for the compressor and the map operating points. The w_i are weight factors for each operating point. The penalty term is zero unless there are interpolation errors (e.g. the interpolated map point lies outside the operating region).

During the optimization process, as the independent variables vary, may arise performance maps whose mass flow or pressure ratio values are either very high or very low, as a result the optimum operating point to lie outside the map region. This situation can cause the optimization algorithm to stack on a local optimum, since the objective function (Eq. (7-16)) is non-smooth due to the penalty term. An obvious solution to that problem is a good set of initial values as a starting point in order to avoid the local minima. However, this is not practical since it requires experience and effort to choose a good set of initial values. In order to overcome this problem, the transformation of Eq. (7-17) is introduced. The transformation takes into account the fractional variation of the system parameter (mass flow or pressure ratio) from idle to full load and sets that equal to the fractional variation (from idle to full load) of the corresponding parameter in the new map. Eq. (7-17) is applied only for pressure ratio and mass flow parameter. It is not necessary to be used for the isentropic efficiency since its values vary always between 0 and 1.

$$\frac{X_{map} - X_{map}^{idle}}{X_{map}^{full\ load} - X_{map}^{idle}} = \frac{X_{desired} - X_{desired}^{idle}}{X_{desired}^{full\ load} - X_{desired}^{idle}} \quad (7\text{-}17)$$

The previous equation (Eq. (7-17)) requires the pressure ratio and the mass flow parameter at idle and full load conditions. For the hybrid system, these values can be determined during the design process based on the parametric analysis data. For the new compressor map the full load operating point (design point) is located near the peak efficiency on the design speed line, namely for N_{rel} =100%. The mass flow parameter at design point is defined as

$$\dot{m}^{full\ load} = \left(\frac{\dot{m}_{surge} + \dot{m}_{choke}}{2} \right)_{@N_{rel}=100\%} \quad (7\text{-}18)$$

whereas, the mass flow at idle conditions is defined similar to Eq. (7-18) but for N_{rel} =50%. Also, as the mass flow and speed parameter values are known, the pressure ratio and efficiency values are easy to be estimated by an interpolation process.

The foregoing method for selection of full load and idle operating points has two advantages: firstly, the speed range is constrained between the 100% and 50% of the relative rotational speed and secondly, the compressor operating line pass through the middle of the operating range, between the surge and choke flow (see the dashed line in Figure 7-7). This ensures large surge margin values and efficient operation since the efficiency values are high at that operating region

Institutional Repository - Library & Information Centre - University of Thessaly
02/06/2024 00:35:58 EEST - 18.226.159.139

The generic optimization program GenOpt [142] was used for the optimization process. The GenOpt can minimize an objective function which is calculated by external simulation software. GenOpt can be coupled to any program that utilizes text files for input and output. In the specific case, the in-house model was developed in FORTRAN programming language. All the input data were received from a text file. The FORTRAN program was executed by the GenOpt and the value of the objective function (Eq. 7-16) was written in an output file. Then, the GenOpt by taking into account the output value updates the input values. This procedure is repeated until there is no further change in the objective function value.

7.5 Turbine design

Given the compressor best operating line, the next step is to specify the turbine operating line. This is a simpler procedure than the corresponding for the compressor, since it does not require a parametric analysis for the whole system. The operating line data for the compressor, namely the pressure ratio, the mass flow and the efficiency are introduced to the model and computation of turbine performance data is performed. These data are used in order to find the turbine operating line. Attention should be paid about the varying composition of the working media at turbine inlet at different operating points which must be taken into account. The performance parameters should be expressed on a dry air basis by applying appropriate transformations to include the variable composition effects.

7.5.1 Turbine in-house model

The turbine characteristic curves are estimated based on the methodology proposed from Wasserbauer and Glassman [143]. The developed model is supplied with the working fluid data, the geometric data of the turbine as well as the design point requirements, and estimates the characteristic curves of the turbine.

The analysis is done along the mean streamline. The thermodynamic properties and the velocity triangles are estimated in three representative positions (Figure 7-9):

1. Stator exit
2. Rotor inlet
3. Rotor exit

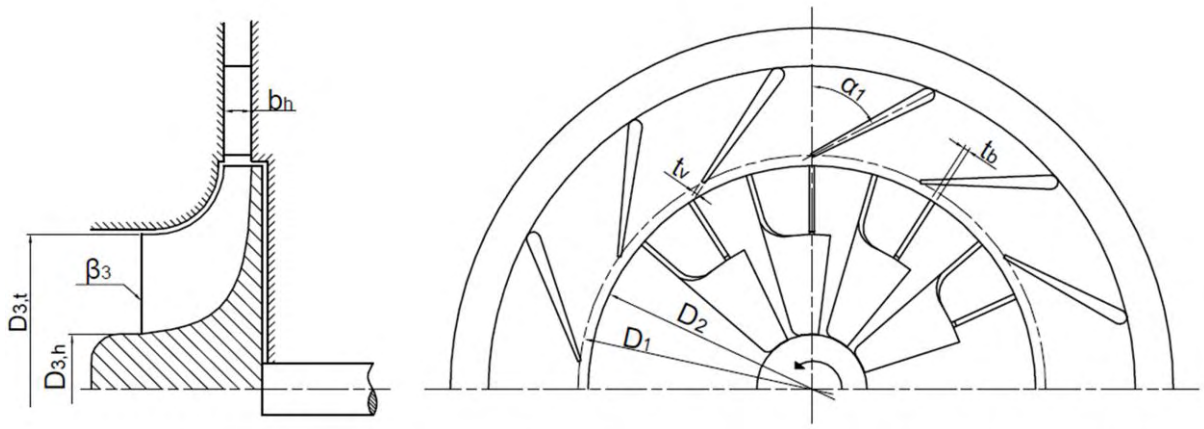

Figure 7-9 Geometric description of the turbine

Institutional Repository - Library & Information Centre - University of Thessaly
02/06/2024 00:35:58 EEST - 18.226.159.139

The model predicts the performance map by taking into account the basic loss mechanisms, namely a) stator losses, b) incidence losses and c) rotor losses.

The stator losses are due the viscous forces which contribute in kinetic energy loss of the moving media during the passage through the stator vanes. The stator losses are expressed as the ratio of the stator exit to stator inlet total pressure (Eq.7-19). The total pressure ratio remains constant during off-design operation.

$$p_{t1} / p_{t0} = \text{costant} \tag{7-19}$$

The incidence losses are due to the deviation of the incidence angle in the rotor inlet from its optimum value. The optimum flow angle is given as follows:

$$\frac{c_{u2}^{opt}}{u_2} = 1 - \frac{1.98}{Z_r} \tag{7-20}$$

$$w_{u2}^{opt} = c_{u2}^{opt} - u_2 \tag{7-21}$$

$$\varphi = \tan^{-1} \frac{w_{u2}^{opt}}{c_{r2}} \tag{7-22}$$

The incidence losses are:

$$\Delta h_{inc} = 0.5 w_2^2 \sin^n(\beta_2 - \varphi) \tag{7-23}$$

where the exponent *n* is 2 for negative incidence ($\beta_2 - \varphi$) and 3 for positive incidence.

The rotor losses are caused from the friction forces acting on the working fluid. They are assumed to be proportional to the kinetic energy of the inlet and exit relative kinetic energies (Eq.7-24).

$$\Delta h_r = \frac{w_{3,id}^2 - w_3^2}{2} = K_r \frac{w_2^2 \cos^2(\beta_2 - \varphi) + w_3^2}{2} \tag{7-24}$$

The turbine rotor is composed from full and splitter blades. The model takes into account the trailing-edge blockage at both the stator and rotor exits. The blockage is defined as the ratio of the just inside to the just outside flow area in the trailing-edge of a blade or vane row.

Table 7-4 Sensitivity analysis of the turbine model

Parameter	Mass flow parameter	Isentropic efficiency
N	-0.01	-0.07
D_2	0.04	-0.30
D_1/D_2	0.20	-0.05
$D_{3,t}$	0.83	0.24
$D_{3,h}/D_{3,t}$	-0.13	-0.08
b_h	0.75	-0.11
t_b	-0.01	0.00
t_v	-0.05	0.01
α_1	-3.41	0.62
β_3	-0.52	-0.18
Z_s	-0.05	0.01
Z_r	-0.01	-0.01

Institutional Repository - Library & Information Centre - University of Thessaly
02/06/2024 00:35:58 EEST - 18.226.159.139

p_{t1}/p_{t0}	2.21	2.24
K_r	-0.04	-0.07

In Table 7-4 are presented the input variables that specify the turbine performance maps. Beyond the geometric characteristics, the rotational speed, the stator total pressure ratio and the rotor loss coefficient must be determined. On the same table a sensitivity analysis of the input data is presented. The values have been arisen by keeping the values of pressure ratio and speed parameter constant and changing the input parameters by 1%. Then the percent deviations of interpolated values of mass flow parameter and isentropic efficiency are estimated.

Similar to the compressor, there are some input parameters that affect significantly the turbine performance and some others that have negligible effect. The less sensitive geometric variables were kept constant during the optimization process.

7.5.2 Turbine optimization process

Given the compressor best operating line which has been estimated with the previous procedure, the next step is to specify the turbine operating line. The operating line data for the compressor, namely the pressure ratio, the mass flow and the efficiency are introduced to the model and the turbine operating data are calculated. These data are used in order to determine the turbine operating line (pressure ratio, mass flow parameter).

The working media composition varies at the turbine since the fuel flow changes at different operating points. Thus, the performance parameters should be expressed on a dry air basis by applying appropriate corrections to include the variable composition effects.

$$\dot{m}_{cor} = \frac{\dot{m}\sqrt{\theta}\varepsilon}{\delta} \tag{7-25}$$

$$PR_{cor} = \left[1 - \frac{\gamma+1}{\gamma}\frac{C_p}{R}\left(\frac{\gamma}{\gamma+1}\frac{R}{C_p}\right)_{ref}\left(1 - PR^{-\frac{\gamma-1}{\gamma}}\right)\right]^{-\frac{\gamma_{ref}}{\gamma_{ref}-1}} \tag{7-26}$$

$$N_c = \frac{N}{\sqrt{\theta}} \tag{7-27}$$

where

$$\theta = \frac{\frac{\gamma}{\gamma+1}RT}{\left(\frac{\gamma}{\gamma+1}RT\right)_{ref}} \tag{7-28}$$

$$\delta = P / P_{ref} \tag{7-29}$$

$$\varepsilon = \frac{\gamma_{ref}}{\gamma}\left[\frac{\left(\frac{\gamma+1}{2}\right)^{\gamma/(\gamma-1)}}{\left(\left(\frac{\gamma+1}{2}\right)^{\gamma/(\gamma-1)}\right)_{ref}}\right] \tag{7-30}$$

Institutional Repository - Library & Information Centre - University of Thessaly
02/06/2024 00:35:58 EEST - 18.226.159.139

The isentropic efficiency variation due to changes in working media composition is not taken into account.

As the compressor operating line has been determined in Section 7.4.2, the rotational speed and the pressure ratio variation for the turbine device are known. These two parameters are adequate to determine the turbine operating point on the performance map. The final turbine component should operate with consistent mass flows values with the compressor operating line and with the desired efficiency. Therefore, Eq. (7-31) should be minimized. This process is shown graphically in Figure 7-10.

$$OF = \sum_i w_i \left[\left(1 - \frac{\dot{m}_{i,map}}{\dot{m}_{i,desired}} \right)^2 + \left(1 - \frac{\eta_{i,map}}{\eta_{i,desired}} \right)^2 \right] + penalty \tag{7-31}$$

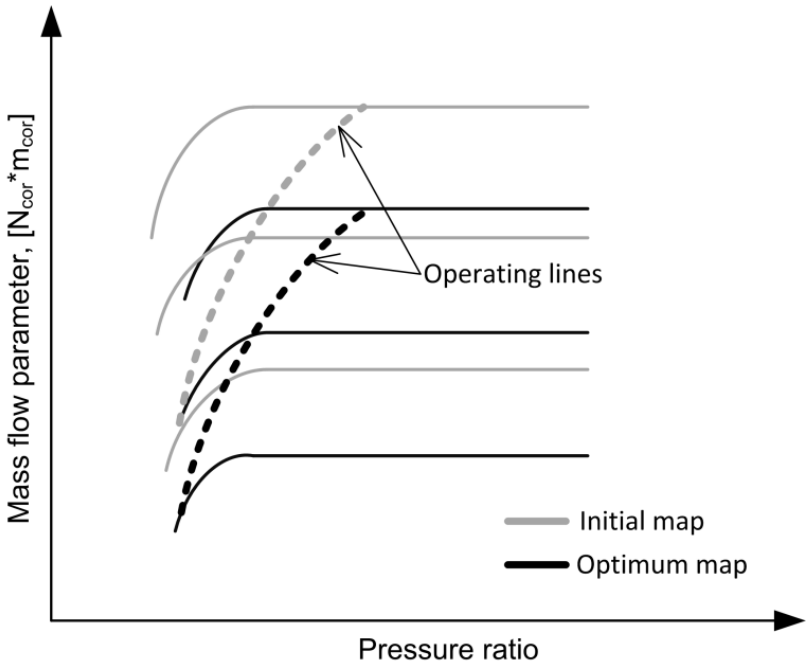

Figure 7-10 Turbine map modification process

7.6 Improved hybrid system – results

In the previous sections the parameters describing the geometry of the turbomachines were presented. For the parameters having a major effect on the performance of the turbomachines a broad variability range was chosen. For the remaining parameters, typical values were considered and were kept constant during the optimization procedure.

Table 7-5 Decision variables and constant parameters for compressor component

Variables	Unit	Range	Constant parameters	Unit	Value
N	rpm	[65000, 110000]	$\beta_{1,rms}$	°	49
$D_{1,t}$	m	[0.07, 0.013]	A_5/A_4	-	2.8
$D_{1,t}/D_3$	-	[0.5, 0.7]	t	mm	1.3
$D_{1,h}/D_{1,t}$	-	[0.4, 0.7]	α_3	°	65
β_2	°	[0, 60]	S_f	-	0.04
D_3/D_2	-	[1.05, 1.3]	$(Z_f + Z_{sp})$	-	24

Institutional Repository - Library & Information Centre - University of Thessaly
02/06/2024 00:35:58 EEST - 18.226.159.139

b_2	mm	[4, 7]	T_{in}	K	288.15
A_4	m^2	[0.0006, 0.0010]	P_{in}	kPa	101.325

Table 7-5 indicated the independent variable with their range and the fixed geometry parameters for the compressor.

In Table 7-6 are presented the input variables that specify the turbine performance maps. The less sensitive variables are kept constant during the optimization process.

Table 7-6 Decision variables and constant parameters for turbine component

Parameter	Unit	Range	Constant parameters	Unit	Value
D_2	m	[0.1, 0.17]	N_{des}	rpm	69480[a]
D_1/D_2	-	[1.02, 1.25]	t_b	mm	1.5
$D_{3,t}$	m	[0.05, 0.095]	t_v	mm	1.0
$D_{3,h}/D_{3,t}$	-	[0.2, 0.7]	Z_s	-	13
b_h	m	[0.005, 0.015]	Z_r	-	22
α_1	°	[50, 85]	p_{t1}/p_{t0}	-	0.98
β_3	°	[-70, -40]	K_r	-	0.28
			$T_{in,des}$	K	1100[a]
			$P_{in,des}$	kPa	356.0[a]

[a] These parameters are depended from the compressor device

Firstly, the optimum design for the compressor was determined, by minimizing the Eq. (7-16). Based on the new compressor operating line data, a new turbine operating line was estimated and used for its design process (minimization of Eq.(7-31)).

In Table 7-7 are summarized the design point data of the new improved system. The new system is able to produce more power (about 26 kW). This is mainly due to the increment of the pressure ratio which contributes to a higher power production from the gas turbine and the SOFC generator. Moreover, the slightly higher air mass flow contributes to higher power output but, the contribution of this parameter is negligible compared to the increment of pressure ratio. Also, the thermal efficiency at the design point shows a small improvement compared with the corresponding one of the reference system.

Table 7-7 Optimized system design point data

Parameter	Value
Net electrical power output (kW)	246.4
SOFC generator – DC power (kW)	204.5
SOFC generator – AC power (kW)	192.2
Gas turbine electrical power (kW)	57.2
Cell voltage (V)	0.596
Current density (A/m^2)	3570
Turbine inlet temperature (K)	1103
Air mass flow (kg/s)	0.594
Pressure ratio	3.7
Thermal efficiency (%)	58.7

Institutional Repository - Library & Information Centre - University of Thessaly
02/06/2024 00:35:58 EEST - 18.226.159.139

Based on the optimized turbomachines, the part-load performance of the hybrid system was estimated. The results are shown in Figure 7-11 along with the ones of the reference system. It is obvious that the new proposed system operates more efficiently (black line) than the reference system (red line). The efficiency advantage is significant in the whole operating range because of the higher operating pressures and the good matching of the turbomachinery components. The optimized system has a wider operating range (from 246 to 47 kW) compared with that of the reference system (from 218 to 64 kW). Moreover, the optimized system efficiency starts to decrease as the power drops below 100 kW, whereas in the reference system this power level is 150 kW.

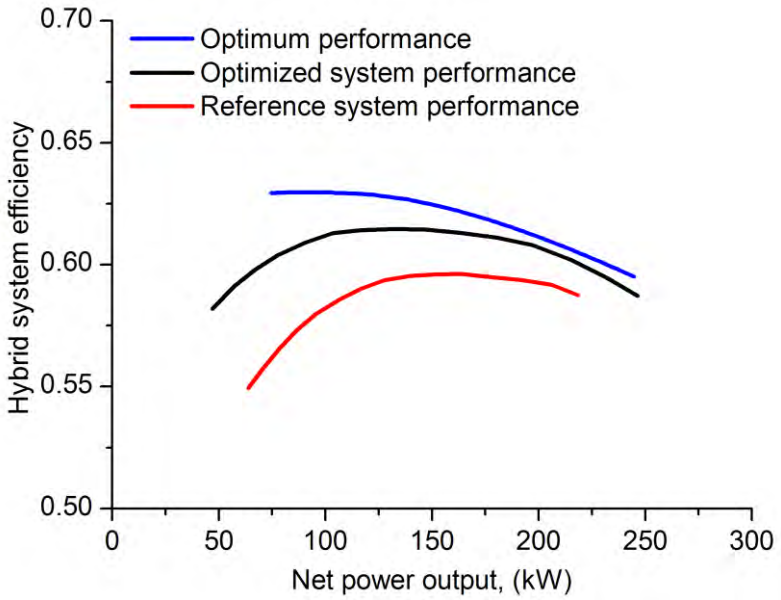

Figure 7-11 Comparison of the reference and optimum systems part load performance

The new system approaches more the optimum performance (blue line) at the high power outputs. This result was expected, since in Eqs (7-16) and (7-31), a high value for the weight factor was used in case of the design point (namely the operating point with the higher mass flow), in order to ensure the best possible system performance at the design point. Also, the new hybrid system is able to operate at lower power outputs than the optimum one. This is due to the lower operating pressures which contribute to lower power production from the hybrid system.

Figure 7-12 presents the performance map of the optimized compressor. With the red color is the operating line. The compressor device operates with a high surge margin and close to the high efficiency region.

The performance map for the optimized turbine is presented in Figure 7-13. The mass flow parameter ($N_{c,rel} \cdot \dot{m}_c$) and isentropic efficiency are shown for different values of speed parameter and pressure ratio. With the red color is the operating line of the turbine.

The efficiency advantage in the whole operating range is due to the increment of the pressure ratio values. This is shown in Figure 7-14 where the operating lines of compressor and turbine components are presented. It can be seen the optimized turbomachines cover a broader operating range. The turbine operates with lower corrected mass flow values because of the higher operating pressures according to the Eq. (7-32).

Institutional Repository - Library & Information Centre - University of Thessaly
02/06/2024 00:35:58 EEST - 18.226.159.139

$$\dot{m}_c = \frac{\dot{m}\sqrt{T_{t,in}/T_{ref}}}{p_{t,in}/p_{ref}} \tag{7-32}$$

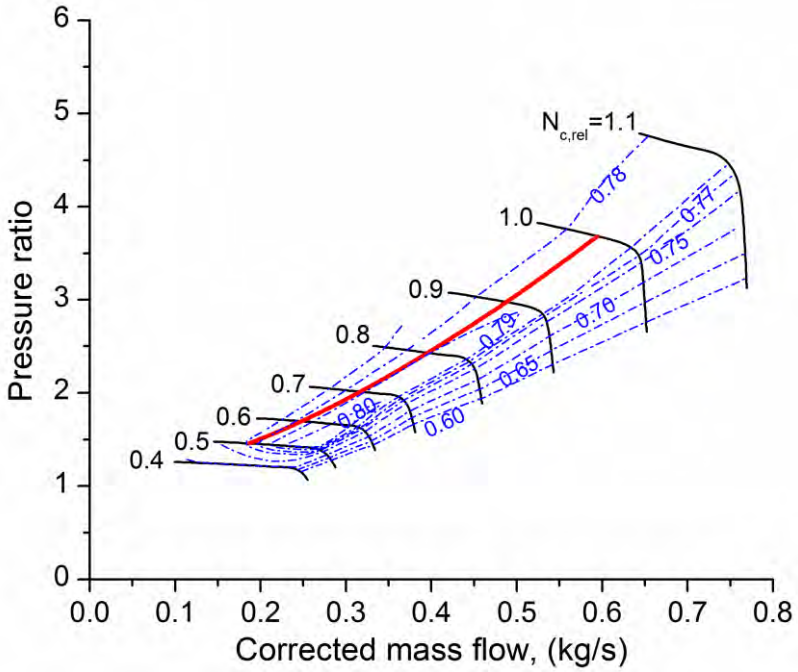

Figure 7-12 Optimized compressor map

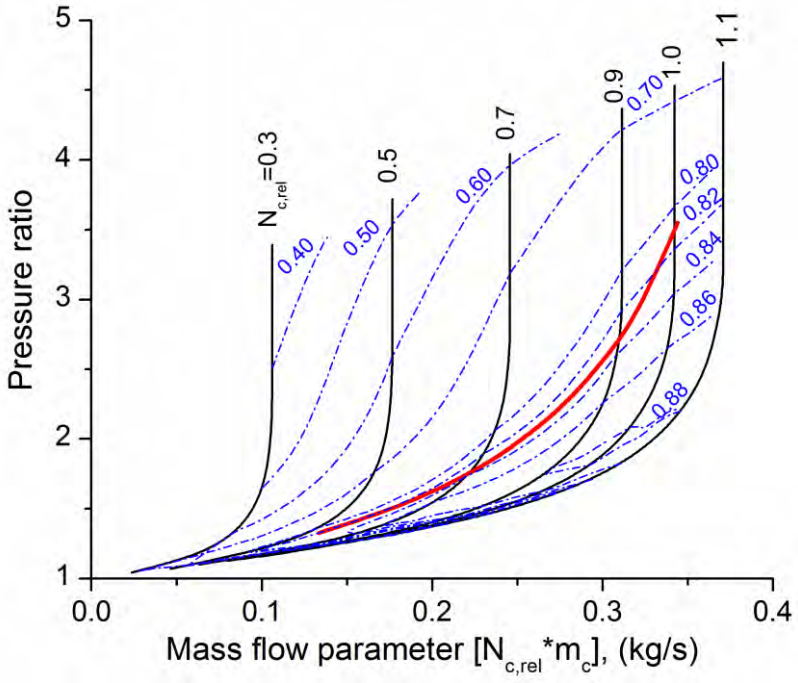

Figure 7-13 Optimized turbine map

Institutional Repository - Library & Information Centre - University of Thessaly
02/06/2024 00:35:58 EEST - 18.226.159.139

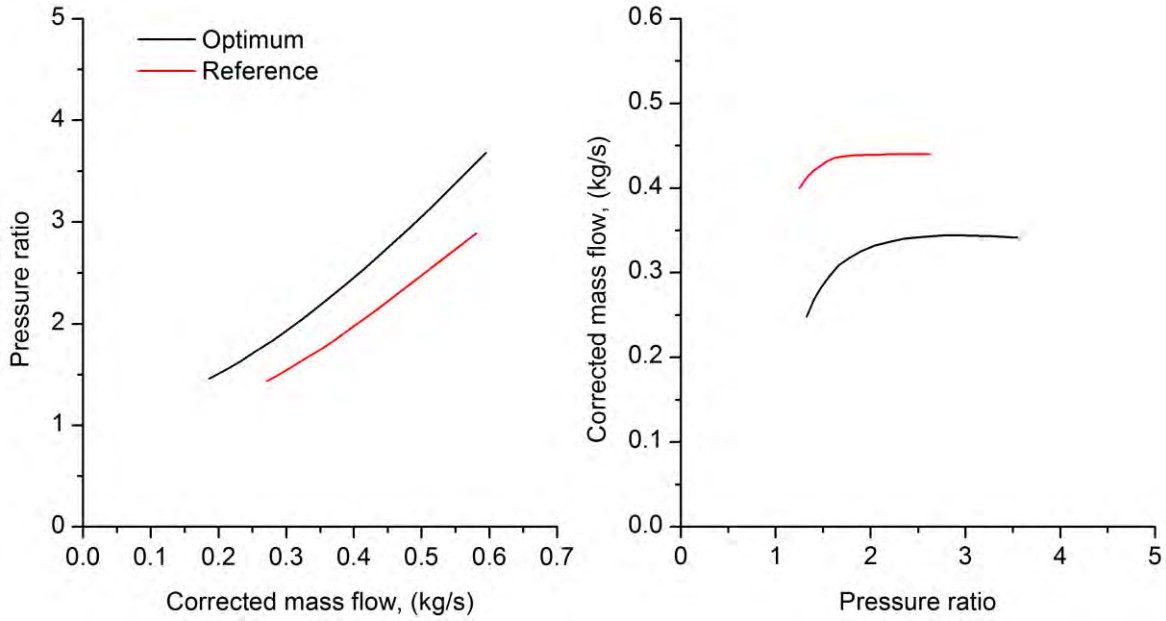

Figure 7-14 Compressor (left) and turbine (right) operating lines

The efficiencies of compressor and turbine components are illustrated in Figure 7-15. The operational efficiencies of the new components approach the target values 78% and 82% for the compressor and turbine, respectively. There is a significant improvement of the efficiency values at low power conditions, compared with the reference system.

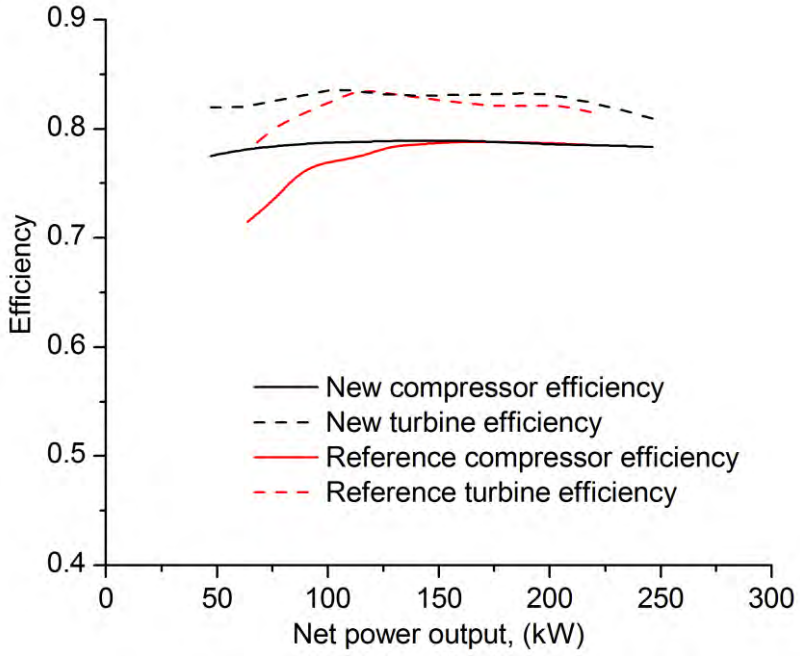

Figure 7-15 Turbomachinery efficiencies for the reference and optimized system

7.6.1 Case studies

In order to further assess the proposed method, two case studies were conducted with a smaller and a bigger system than the optimized one, presented in the previous section. The first one (HS80), is rated at ≈80% and the other (HS120) at ≈120% of the nominal power of the optimized system

Institutional Repository - Library & Information Centre - University of Thessaly
02/06/2024 00:35:58 EEST - 18.226.159.139

(HS100). The desired power outputs are achieved by changing the fuel cell area and the air mass flow and consequently the size of the turbomachines.

The SOFC generator of the reference system (HS100) consists of 1152 fuel cell. Each fuel cell has 834cm^2 effective area [44]. The cells are arranged in bundles of 24 units, which are organized in three series of eight cells. Four bundles are connected in series to form a bundle row of 96 cells. Twelve bundle rows are placed side-by-side to form the SOFC stack of the reference system. To increase or decrease the power output of the new hybrid system the number of the bundle rows should be change. The desired characteristics of the new hybrid systems are summarized in Table 7-8. Other characteristics, such as SOFC operating temperature, fuel utilization factor are kept the same.

Table 7-8 Desired characteristics of new systems

Parameter	HS80	HS120
Net power (kW)	200	300
Air mass flow (kg/s)	0.5	0.7
Bundle rows	10	14
Fuel cell area (m^2)	80.1	112.1

The same procedure used for the reference system was followed for the design of the turbomachinery devices. The optimum operating lines for the compressors were found, for constant values of $\eta_{is,c}$=0.78 and $\eta_{is,t}$=0.82. The results are presented in Figure 7-16 for the three hybrid systems. It is obvious that there are only small differences between the optimum compressor operating lines in the different hybrid systems which means that the SOFC stack size has a small effect on optimum operating pressure of the system.

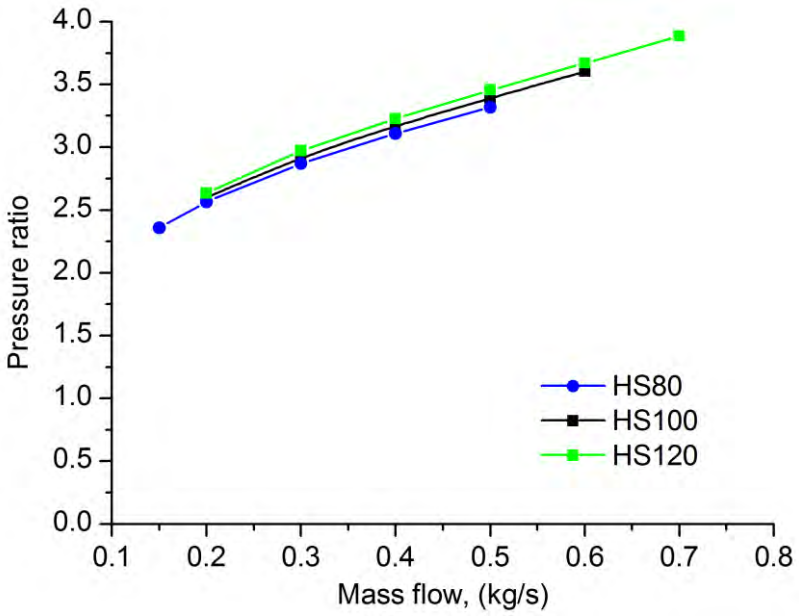

Figure 7-16 Compressor operating lines for the three systems

Institutional Repository - Library & Information Centre - University of Thessaly
02/06/2024 00:35:58 EEST - 18.226.159.139

Based on the compressors' optimum operating lines (Figure 7-16) the geometric data of the compressor and turbine components were estimated. The geometry parameters for the three systems are presented in Table 7-9.

Table 7-9 Geometric data of turbomachines

Compressor								
System	N (rpm)	$D_{1,t}$ (m)	$D_{1,t}/D_3$	$D_{1,h}/D_{1,t}$	D_3/D_2	β_2 (°)	b_2 (mm)	A_4(x10^{4}m^2)
HS80	73203	0.078	0.628	0.625	1.063	48.2	5.8	8.27
HS100	69480	0.088	0.669	0.658	1.073	47.1	6.9	9.07
HS120	67833	0.095	0.677	0.420	1.101	45.2	6.4	9.58
Turbine								
System	D_2 (m)	$D_{3,t}$ (m)	$D_{3,h}/D_{3,t}$	α_1 (°)	β_3 (°)	D_1/D_2	b_h (mm)	
HS80	0.108	0.095	0.421	60.2	-61.9	1.130	7.3	
HS100	0.122	0.093	0.245	60.3	-58.2	1.138	7.4	
HS120	0.128	0.095	0.255	66.1	-56.4	1.118	9.5	

Table 7-9 presents the compressor dimensions as the system size is changing. Rotational speed is decreasing when system size is increasing while the opposite trend is observed $D_{1,t}$, $D_{1,t}/D_3$ and A_4, something expected because the larger area requirement for the flow path as the mass flow rate is increasing. The D_3/D_2 ratio does not vary significantly with the system size. For the rest of the parameters no correlation with the system size seems to exist possibly due to insensitivity of the compressor geometry to these parameters.

Regarding the turbine dimensions (Table 7-9), it is observed again that increase of system size (and therefore greater mass flow rates) leads to greater dimensions for the inlet and outlet rotor diameters as expected. There is no evidence for any trend for the rest of the parameters.

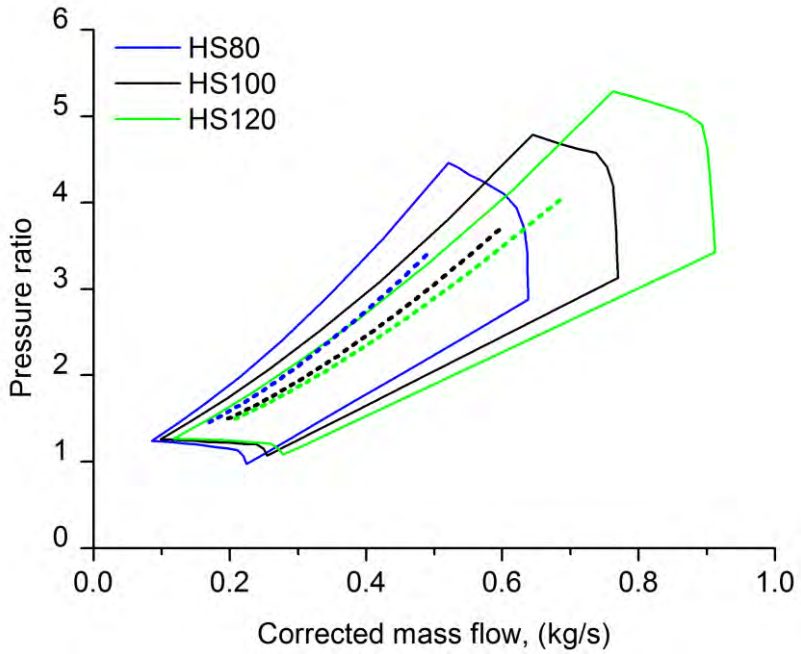

Figure 7-17 Bounds of compressor maps

Institutional Repository - Library & Information Centre - University of Thessaly
02/06/2024 00:35:58 EEST - 18.226.159.139

In Figure 7-17 are presented the bounds of the compressor maps, for clarity reasons. The operating line for each compressor is shown with a dashed line. As it was expected the compressors tend to operate with higher mass flow values as the size of the system increases. For the same mass flow rate, as the size of the hybrid system decreases the system operating pressure increases. The same behavior is shown in Figure 7-18 regarding the turbine map.

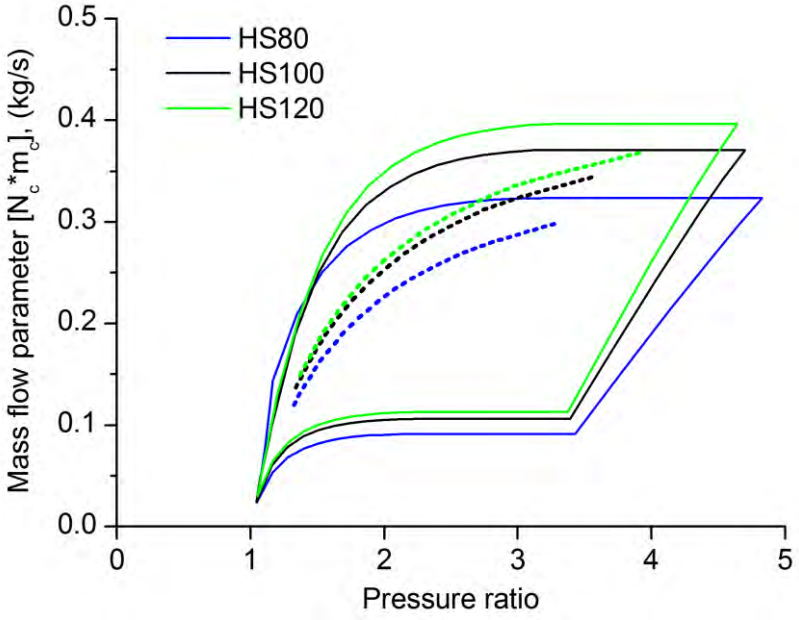

Figure 7-18 Bounds of turbine maps

7.7 Discussion

In the method presented in this chapter a significant improvement of the hybrid systems' efficiency was achieved through the design of turbomachines. Nevertheless, this method has a shortcoming, that is, the running lines of the turbomachines are not the optimum. The design process is done in two independent steps, firstly for the compressor and secondly for the turbine component. The compressor is designed to approach the optimum operating line and the turbine is designed based on the compressors' optimum running line. However, due to optimization limitations there is a slightly different matching of turbomachines when they are incorporated into the hybrid system. This shortcoming can be compensated by optimizing simultaneously the compressor and turbine components. However, this was not done because it requires a substantial computational effort.

7.8 Conclusions

In this chapter a methodology to achieve the best performance in the whole operating range of a hybrid SOFC-GT system was proposed. The results are very encouraging since a clear efficiency advantage can be achieved. The method consists of two steps. A parametric study is conducted in order to assess the operating range of the hybrid SOFC-GT system and select the desired operating line for achieving the optimum system efficiency at various operating points. Based on that information, optimum compressor and turbine geometries are estimated using in-house turbomachinery design codes and an optimization procedure. Weight factors were used during the optimization process to increase the optimality of the system in the desired operating region.

Institutional Repository - Library & Information Centre - University of Thessaly
02/06/2024 00:35:58 EEST - 18.226.159.139

Turbomachinery in house models with empirical correlations which implement an one-dimensional flow solution along the mean streamline were used to calculate the geometry that will give the desired performance maps and the corresponding operating lines. Based on the new turbomachinery design the hybrid system shows a clear efficiency advantage in the whole operating range.

The main conclusions are:

- The optimized turbomachinery components operate efficient in the whole operating range because of their better matching, especially in part-load conditions.
- From the results, it appears that not only the design variables are important for the performance of a hybrid system but also the good matching of the system components.
- The hybrid SOFC-GT system performance improved significantly. The new system was able to produce more electric power (about 12% increment) than the reference one. This was mainly due to the increment of the design pressure ratio.
- The optimized system has a wider operating range and improved performance (at low power conditions was obtained about 3% higher efficiency), since the new turbomachines (compressor-turbine) operate more efficiently due to their better matching.
- There is no considerable difference in the optimum compressor operating line as the fuel cell size changes. The optimum pressure ratios tend to greater values as the fuel cell size increases. Nevertheless, there were substantial differences between the final optimized turbomanchines not only in their geometry but also in their performance maps. The differences were mainly due to the different range of air mass flows.

Institutional Repository - Library & Information Centre - University of Thessaly
02/06/2024 00:35:58 EEST - 18.226.159.139

Institutional Repository - Library & Information Centre - University of Thessaly
02/06/2024 00:35:58 EEST - 18.226.159.139

Chapter 8

Experimental activities

In this chapter, the experience gained during the development of a small turbojet engine simulation model is presented. Data analysis procedures indicated that some measurements were not thermodynamically consistent. Model recalibration based on the use of static instead of total pressure measurements in the turbine exit has proven to be beneficial both for the prediction of the measured parameters and for producing reasonable values for the turbine efficiency. Data correction procedures were also implemented successfully in order to incorporate all the available measurements in the model.

8.1 Introduction

Microturbines are miniatures of larger gas turbine engines which are either used for thrust production or for power generation. In reality, microturbines are not simply a size reduction of larger engines. They present unique characteristics such as simple designs with single-stage compressors and turbines, high rotational speeds, usually between 50000 and 120000 rpm, low pressure ratios, and the ability to operate with a variety of fuels. They have been used by many researchers due to their ability to be operated within the confines of a laboratory.

Lichtsinder and Levy [144] used a micro-turbine to develop a real-time model for the simulation of transient performance and engine control. Davison and Birk [145] produced steady-state and transient performance models for a micro-turbine. In addition, Rahman and Whidborne [146] used experimental data from a microturbine in order to validate their numerical model for engine bleed.

The flow through a turbomachine is extremely complex [147]. It is characterized by three-dimensionality, and viscous, compressible, and turbulent phenomena. The previous considerations contribute to boundary layer development and total pressure losses. Although all gas turbines are governed by the same laws of physics, there are a number of size effects such as the value of the Reynolds number of flow along the gas path [148]. A large engine operates in a highly turbulent environment, whereas a small engine works in a much more viscous environment. Small blade heights result in increased tip clearance losses, boundary layers tend to appropriate an increasingly larger part of the flow, combustors do not scale linearly with the diameter, and their design for low pressure ratios is very different. The viscous operating environment and the loss mechanisms (such as tip clearance losses, trailing edge thickness losses, and profile losses), which are proportionally

Institutional Repository - Library & Information Centre - University of Thessaly
02/06/2024 00:35:58 EEST - 18.226.159.139

more significant in the case of small turbomachines, lead to higher total pressure losses and larger variations of the thermodynamic properties in each section of a micro-turbine.

The measurements that are mostly affected by the rough flow field in micro-turbines, are those located in the hot section. As seen in reference [149], high temperature gradients are noticed at the outlet of the combustor of a micro-turbine. The developed temperature profile is propagated through the turbine and it affects the temperature measurements in hot section areas. Apart from the temperature profile, the temperature measurements are also affected by the heat transfer mechanisms [150]. The heat transfer mechanisms contribute to deviations between the temperature of the sensor and the actual temperature of the working media. The inhomogeneous flow field also affects the pressures. The effect is more significant at the turbine exit where the loss mechanisms cause pressure losses and pressure distributions in circumferential and radial directions [151, 152].

From the above-mentioned brief review, it is obvious that high temperature and pressure variations in micro-turbines must be taken into account during experiments to avoid erroneous assessments of engine operating conditions.

The aim of this chapter is to present the experience gained during the processing of the measurements received from a small turbojet engine installed in our laboratory. In particular, it was realized during the calibration of an initial engine simulation model based on these measurements that using the model, although accurate for the reproduction of the quantities measured, leads to unrealistic values for the turbine efficiency. Therefore, it was necessary to recalibrate the simulation model after careful data analysis which indicated existing inconsistencies and suggested data correction procedures. In this chapter, the methodology adopted for the model refinement is described and the calibration results are presented.

While there are works in the literature related to the instrumentation and modeling of microturbines[145, 146, 153-157], it appears that there is no integrated approach providing a methodology for model refinement in order to match experimental data or to evaluate the reliability of the complete measurement set.

To the author’s knowledge, this is the first time an inverse approach based on adaptive performance modelling principles [158] has been applied to microturbines, and it is validated in their frame with the above-mentioned size effects.

The identified instrumentation problems, the data analysis, and correction procedures proposed as well as the model calibration methodology provide a sound framework for feature performance and diagnostic studies.

8.2 Description of experimental layout

The small gas turbine used is an Olympus HP ES, manufactured by AMT Netherlands. It is a small turbojet engine that produces a thrust of up to 230 N. The basic engine data are presented in Table 8-1. The engine has the ability to operate with different fuels, such as kerosene and paraffin oil. The micro-turbine also uses the fuel for lubrication; so, the fuel is premixed with lubrication oil. The Olympus turbine is controlled and protected from improper use by a microprocessor controller (engine control unit, ECU). ECU uses the exhaust gas temperature (EGT), the RPM, and the control box inputs as the input data.

Institutional Repository - Library & Information Centre - University of Thessaly
02/06/2024 00:35:58 EEST - 18.226.159.139

Table 8-1 Basic engine data

Engine parameter	Value
Length (mm)	384
Diameter (mm)	131
Maximum thrust (N)	230
Maximum rotational speed (rpm)	108,500
Pressure ratio	3.8:1
Mass flow (kg/s)	0.45
Fuel consumption (kg/min)	0.64
Normal EGT (K)	973
Maximum EGT (K)	1023

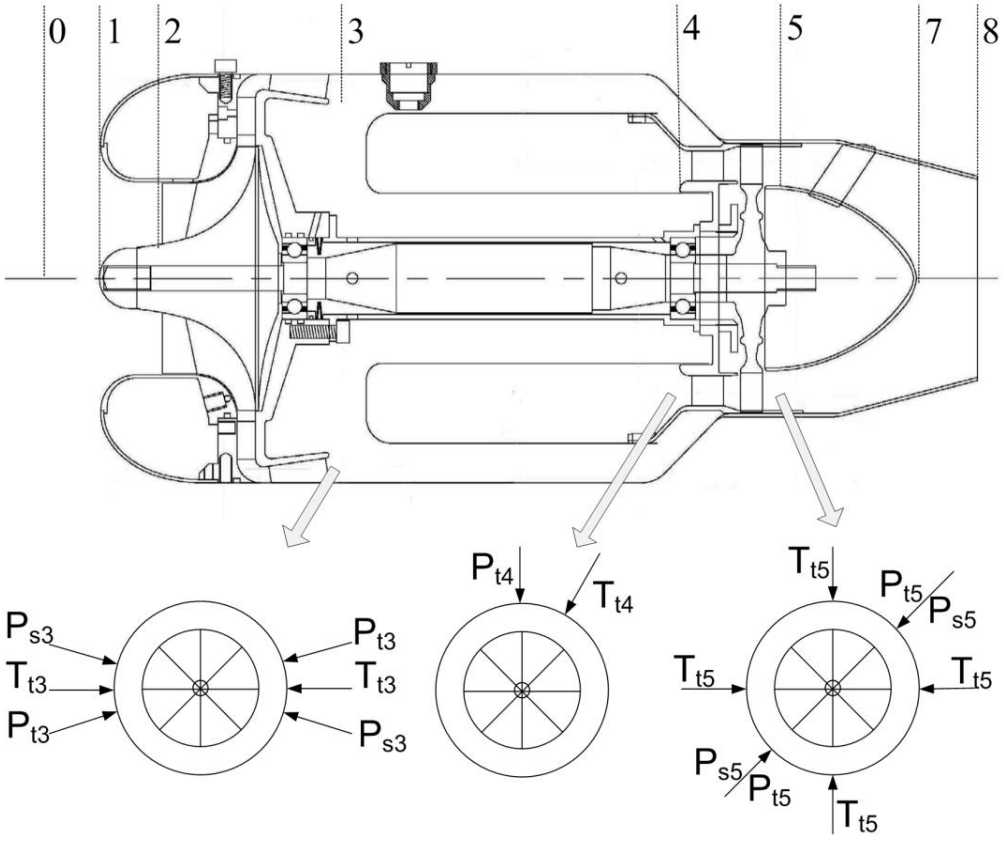

Figure 8-1 Longitudinal section through the engine, and sensor locations

The version which is used, is modified, with additional measuring probes for temperature and pressure along the gas path.

A schematic layout of the engine identifying the additional measuring points is presented in Figure 8-1. The engine is a single spool with a single-stage centrifugal compressor, a single-stage axial turbine, and a fixed geometry convergent nozzle (Figure 8-2). The combustion chamber utilizes an annular geometry. The probes (except those measuring the static pressures) are placed in the mean

Institutional Repository - Library & Information Centre - University of Thessaly
02/06/2024 00:35:58 EEST - 18.226.159.139

radius. Table 8-2 presents the measured parameters and the number of probes in each engine station.

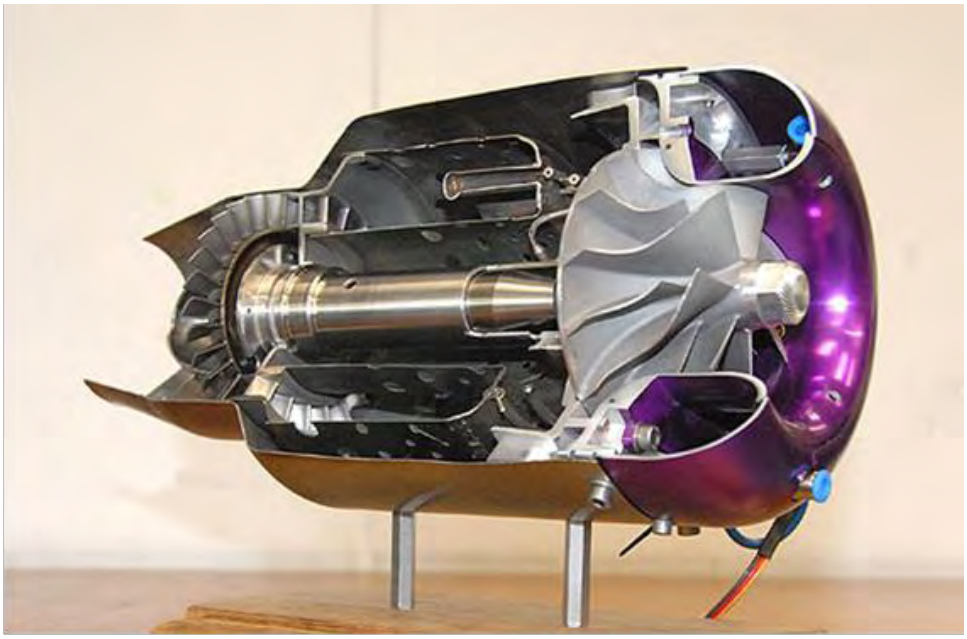

Figure 8-2 Olympus HP cutaway

Table 8-2 Measurements

Station	Description	Measured Parameters
0	Ambient conditions	Temperature Atmospheric pressure Relative humidity
1	Inlet duct	Nothing
2	Compressor inlet	Nothing
3	Compressor exhaust	2 × Total temperature 2 × Total pressure 2 × Static pressure
4	Turbine inlet	1 × Total temperature 1 × Total pressure
5	Turbine exhaust	4 × Total temperature 2 × Total pressure 2 × Static pressure
8	Nozzle exhaust	Nothing

Apart from the measurements in Table 8-2, there are two further measurements which are outputs from the ECU, the rotational speed of the engine (RPM) and the EGT. The EGT sensor is placed between stations 5 and 7, and it is used from the ECU in order to control the engine. The engine signals are transferred to a personal computer from the ECU through an RS232 interface. The

Institutional Repository - Library & Information Centre - University of Thessaly
02/06/2024 00:35:58 EEST - 18.226.159.139

resolution of the sent data strings is 8 bit. The engine speed is represented by multiples of 500 r/min, and the accuracy is about 0.5 per cent at full and 1 per cent at idle speed. In order achieve a better accuracy during transient operation of the engine, it would be necessary to bypass the ECU device. The thrust is measured with a Z-type load cell rated at about 590 N.

For the amplification of thermo-sensor signal, it was decided to build an amplifier. The amplifier uses a commercially available monolithic chip with accuracy in the range ±3°C. All the sensor signals are selected from a data acquisition card and transferred to a personal computer. The computer is equipped with in-house software developed in the laboratory which transforms the signals to engineering units and presents the data on the monitor.

Table 8-3 presents the characteristics of each type of measurement.

Table 8-3 Sensor characteristics

Station	Measurement	Accuracy	Notes
3, 4, 5	Pressure	±1% (FS)	Wika A-10
3, 4, 5	Temperature	±3 ºC	K type – 1.5 mm
	Thrust	0.046%(FS)	
5	Temperature	±5 ºC	From ECU
	RPM	± 500 rpm	From ECU

8.3 Experimental data

The data collection from micro-turbines must be conducted with accuracy, reliability, and means for the elimination of errors which affect the measurements and contribute to misleading information about the engine. When the data collection is accurate and free of errors, it is conducive to:

(a) better control and more efficient operation;

(b) better estimation of engine conditions.

The impacts of the precision, calibration, and data acquisition system are present even in the most rigorously designed test procedure. The previous factors contribute to inaccurate measurements which are susceptible to errors. There are mainly two types of error: random and systematic errors. The measurement error is the sum of these two types of error [159].

The random error appears randomly in the measurements during a test. It can be eliminated via statistical methods or using filtering methods. On the other hand, a systematic error is caused by bad calibration, poor positioning of measuring probes, environmental conditions, etc. Systematic errors can be quantified and the appropriate correction can be applied. The most frequent way to eliminate a systematic error is recalibration. However, it is a common technique to use correction factors in order to adjust the values of a measurement. When the systematic error is caused by the test conditions it is preferable to use data reconciliation in order to calculate the true values [160]. Once the erroneous measurement has been isolated, it is adjusted to produce more rational results and satisfy the governing equations.

Institutional Repository - Library & Information Centre - University of Thessaly
02/06/2024 00:35:58 EEST - 18.226.159.139

The engine was tested under steady-state operating conditions for specific operating points, from idle to higher rotating speeds. The acquired measurement sets are filtered with a median filter [161], a non-linear filter that provides the opportunity to remove gross outliers and noise from a signal while preserving features of the root signal. It uses both past and futurevalues for the prediction of the instant value. It is characterized by the parameter *l*, and length 2*l*+1, and can be represented by equation (8-0). The filtered measurement sets are averaged in order to calculate the mean value of each measured parameter

$$\hat{x}_n = median(x_{l-n}, x_{l-n+1}, \ldots x_n \ldots, x_{l+n-1}, x_{l+n}) \quad (8\text{-}0)$$

The values resulting from the previous procedure are averaged again in each section, and the final value of each parameter is obtained. Certain results from two experimental sets are presented in Figures 8-3 to 8-5.

Figure 8-3 displays the total and static pressures at the compressor exit. It is obvious that there is a small difference between the total and static pressures, since the measuring probes are placed after the diffuser, where the working media flow is decelerated. The pressures present a parabolic behaviour as expected for a centrifugal compressor [145, 146]. Also, the same occurs with the compressor exit temperature in Figure 8-3.

Figure 8-4 presents the pressure and temperature measurements at the turbine exit. As can be seen, there is a deviation between the total and static pressures because of the high velocities of the moving media at that section. EGT has a parabolic trend which is in accordance with the manufacturer's data.

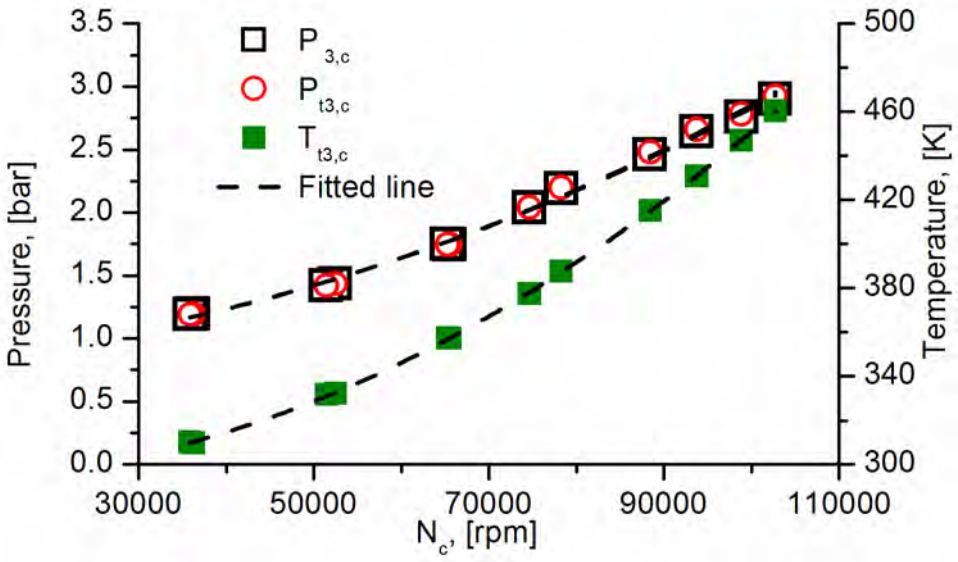

Figure 8-3 Pressures and temperature at compressor exit

Institutional Repository - Library & Information Centre - University of Thessaly
02/06/2024 00:35:58 EEST - 18.226.159.139

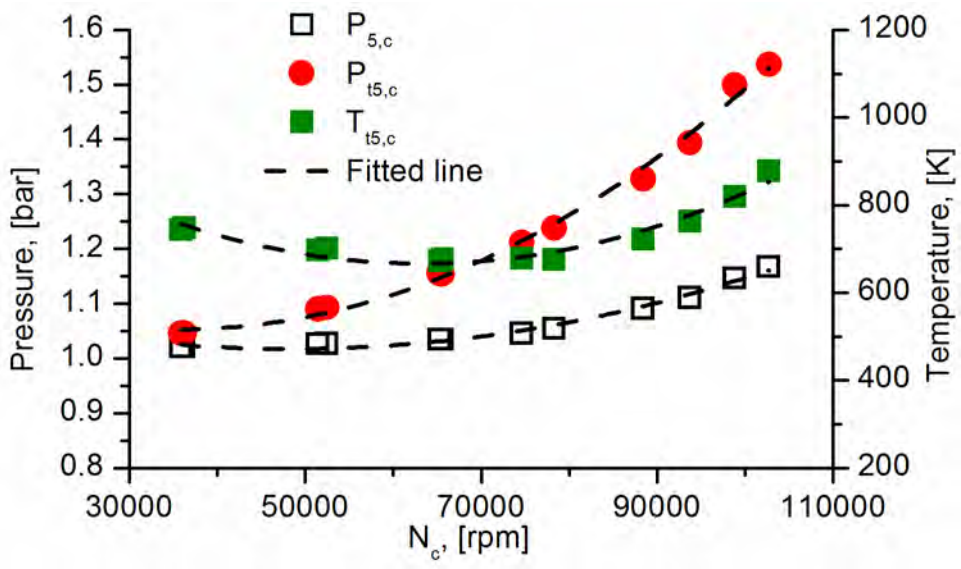

Figure 8-4 Pressures and temperature at turbine exit

The turbine inlet temperature (TIT) values (Fig. 5) deviate from their fitted line at higher rotational speeds, probably due to the heat transfer mechanisms or the variation of temperature profile at the combustor exit. The shape of the thrust measurement curve is in good agreement with the manufacturer's data as well as with similar engines [154].

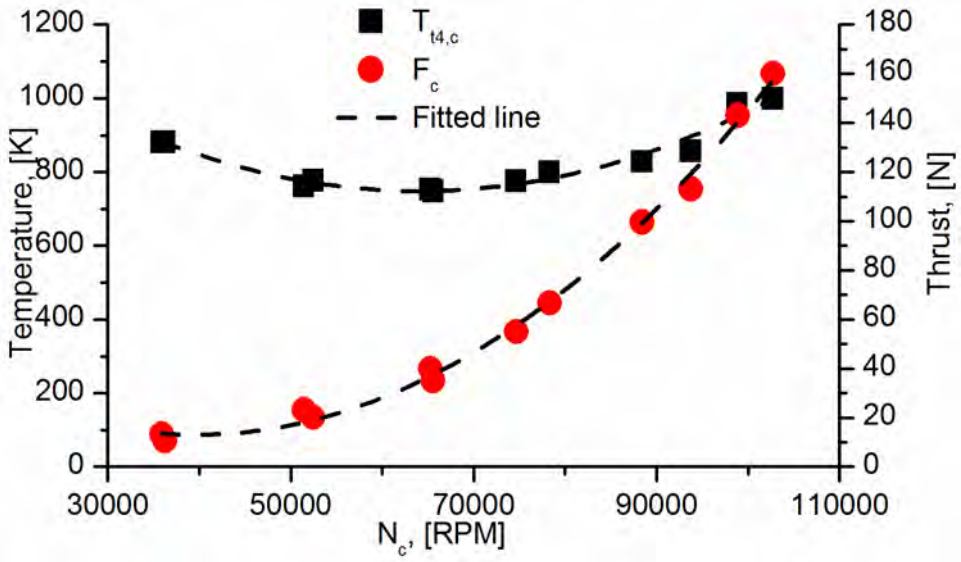

Figure 8-5 5 Turbine inlet temperature and thrust

8.4 Data analysis

The author in a previous publication presented a model for the engine under consideration [162]. The developed model was based on a modular general approach using adaptive modelling principles [158]. The small turbojet engine was divided into subsystems, e.g. compressor, combustor, etc. Each subsystem was considered as a control volume, and the appropriate governing equations were used in order to describe the operations which take place inside. Generally, each subsystem is modelled by four groups of equations:

Institutional Repository - Library & Information Centre - University of Thessaly
02/06/2024 00:35:58 EEST - 18.226.159.139

a) definition equations such as relations for isentropic efficiencies;
b) relations of characteristic parameters, for example compressor maps;
c) conservation equations;
d) compressibility equations.

The subsystems are coupled with the mechanical energy balance and the continuity equations.

Aside from the simulation of the engine's performance, the model can be supplied with measurement data collected during engine operation and calculate the unknown operating parameters of the thermodynamic cycle.

The developed model is able to predict the design and off-design performance of the engine. For the off-design simulations, performance maps are adopted, for the compressor and the turbine components, from similar engines and scaled in order to correspond to the particular engine. Apart from the performance maps, various other parameters are required in order to complete the model, such as burner and nozzle efficiencies where typical values (Table 8-4) are used from the available literature [146, 163, 164].

It should be noticed that the assumed burner pressure losses seem to be very low compared with the corresponding losses for larger engines. However, these losses are measured in our engine and found to be at that level. The assumed burner efficiency low value is in accordance with other works related to small engines [146, 165].

Table 8-4 Assumptions for simulation model

Simulation model parameters	Value
Mechanical efficiency	0.99
Burner efficiency	0.85
Burner pressure losses	0.99
Nozzle efficiency	0.94
Inlet duct pressure losses	0.99

The calibration of the model was based on the total temperatures and pressures at the compressor exit, and the total pressures and just one temperature measurement (the one with the highest value) instead of the average values of the four measurements taken at the turbine exit. The reason for that choice was the non-realistic values of the turbine efficiency that arose when the average value was considered.

The developed model helped the authors to conduct a deeper investigation of the engine behaviour, since it was possible to easily and accurately estimate various performance parameters of the engine with the available measurements.

Trying to discover why the turbine isentropic efficiency takes non-acceptable values, it was decided to investigate the heat transfer through the turbine casing. Based on reference [166], which presents a method to estimate the turbine efficiency in a turbocharger under strong heat transfer, some simple calculations were done in order to assess the amount of heat transfer.

Institutional Repository - Library & Information Centre - University of Thessaly
02/06/2024 00:35:58 EEST - 18.226.159.139

In the turbine subsystem the heat is exchanged by conduction between the metal parts of the engine, by convection between the outer casing and the ambient air, as well as by radiation from the outer casing to the surroundings.

In this specific case, the conduction phenomena are neglected since the engine has small dimensions and does not produce high temperature gradients. However, the high temperature difference between the turbine casing and the outer air flow contribute to heat losses by convection and radiation.

Assuming typical values for the velocity of ambient air around the engine casing we can calculate the Reynolds number from equation (8-0).

$$Re = \frac{VL}{\nu} \tag{8-0}$$

where *L* is a characteristic length

The flow around the engine is laminar because of the low air velocity. Assuming the casing of the turbine as a plate, the Nusselt number can be calculated from the following relationship:

$$Nu = \frac{hL}{k} = 0.664 Re^{1/2} Pr^{1/3} \tag{8-0}$$

The external heat transfer coefficient *h* arises from the equation (8-0). The heat flux by convection is

$$\dot{Q}_{conv} = Ah(T_{sur} - T_{amb}) \tag{8-0}$$

where T_{sur} is the external surface temperature of the turbine casing, which is taken equal to:

$$T_{sur} = \frac{T_{t4} + T_{t5}}{2} \tag{8-0}$$

The radiative heat flux is given by the following equation:

$$\dot{Q}_{rad} = A\varepsilon\sigma T_{sur}^4 \tag{8-0}$$

The total heat flux from the casing of the turbine is the sum of convective and radiative heat fluxes, namely:

$$\dot{Q}_{total} = \dot{Q}_{conv} + \dot{Q}_{rad} \tag{8-0}$$

The previous rough calculations indicate that the heat losses are very small compared with the power produced from the turbine (0.5-1.5%). Therefore the heat transfer cannot significantly affect the turbine's isentropic efficiency values in the specific case.

The next step was to investigate whether the measurements contained systematic errors. Starting from the compressor exit, both thermocouples indicated similar temperatures, as expected, since the compressors do not usually exhibit high temperature gradients at their exits. The same occurs with the total pressures which compared well with the total pressure at the combustor exit (and the results were in good agreement). As the engine is equipped with just one preinstalled TIT sensor, the turbine inlet temperature cannot be considered trustworthy and representative since it is strongly affected by the heat transfer effects and the rough temperature profile [149, 150]. Usually this temperature is corrected/calculated from the energy balance on the engine [156, 157]. Temperatures at the nozzle guide vanes of a microturbine are relatively low, and the radial and

Institutional Repository - Library & Information Centre - University of Thessaly
02/06/2024 00:35:58 EEST - 18.226.159.139

circumferential variation of temperature could be measured in order to derive the average temperature and the pattern factor. Of course this task would require several sensors and should also increase the flow blockage effect.

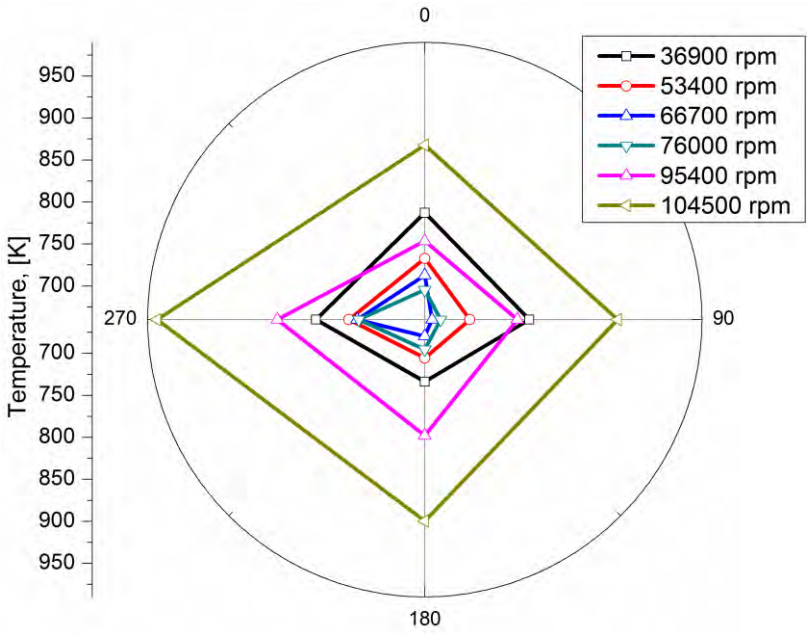

Figure 8-6 Temperature profiles at turbine exit

Although there were high variations in the measurements at the turbine exit (Figure 8-6), in the present analysis, the average value it is assumed to be representative since it is very close to the value of the EGT measurement. EGT measurements are assumed to be more reliable with respect to the radial and circumferential variations of temperature, as they are taken at a greater distance from the turbine exit. There, the flow and the profiles are smoother and therefore the sensor indication should be closer to the mean value.

For the thrust, the indicated values are considered trustworthy due to the effort made during the set-up and the calibration procedure in order to eliminate the errors as much as possible.

The static pressure at the turbine exit was not used in the initial model calibration and therefore the only questionable measurement for introducing systematic errors can be considered to be the total pressure measurements at that section.

In order to assess the quality of those measurements, some simplified calculations were made to estimate the exhaust gas mass flow using two different approaches.

In the first approach, the mass flow is calculated by eliminating the Mach number from the following equations:

$$\dot{m}_{gas} = \frac{p_{t5} A_5}{\sqrt{T_{t5}}} \sqrt{\frac{\gamma}{R}} M_5 \left(1 + \frac{\gamma - 1}{2} M_5^2\right)^{\frac{\gamma+1}{2(\gamma-1)}} \tag{8-0}$$

$$\frac{p_{t5}}{p_5} = \left(1 + \frac{\gamma - 1}{2} M_5^2\right)^{\frac{\gamma}{\gamma-1}} \tag{8-0}$$

Institutional Repository - Library & Information Centre - University of Thessaly
02/06/2024 00:35:58 EEST - 18.226.159.139

The second approach is based on the thrust measurement. The mass flow is calculated by using the following equations:

$$\frac{P_{t8}}{P_{amb}} = \left(\frac{T_{t8}}{T_8} \right)^{\frac{\gamma}{\gamma-1}} \quad (8\text{-}0)$$

$$V_8 = \sqrt{2(h_{t5} - h_8)} \quad (8\text{-}0)$$

$$F = \dot{m}_{gas} V_8 \quad (8\text{-}0)$$

where $P_{t8} = P_{t5}$ and $T_{t8} = T_{t5}$, assuming that the nozzle is adiabatic without pressure losses.

The mass flow values from the two methodologies must be the same; in the opposite case, the pressures at the turbine exit are erroneous or not representative.

Figure 8-7 clearly illustrates that the results are not in agreement and that there are large differences between the two methods. Thus, assuming that the rest of measurements are free from errors, it is reasonable to consider the total pressure measurements responsible for the discrepancy.

This problem may not be existed if there were more test points in the circumferential direction as well as in the radial direction.

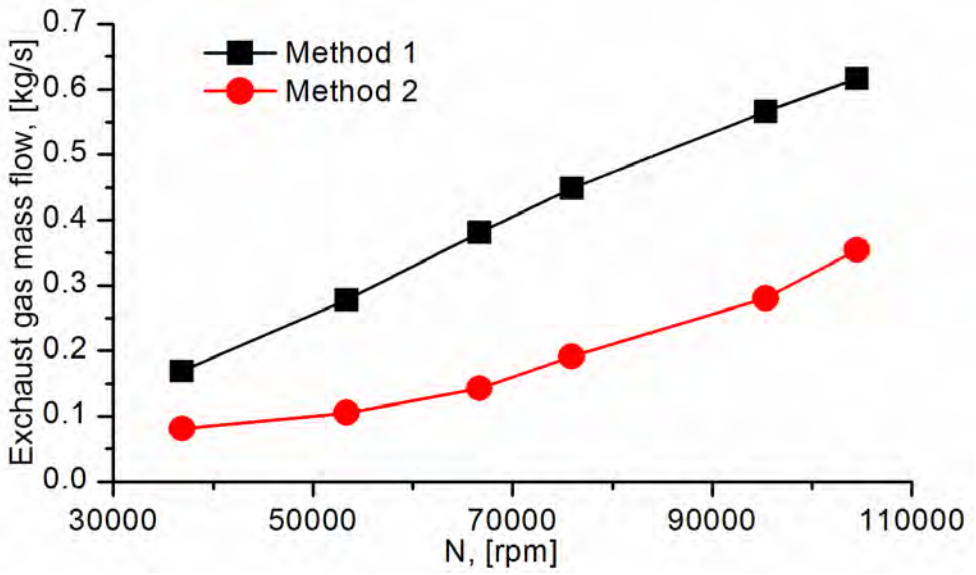

Figure 8-7 Comparison of exhaust gas mass flow resulting from simplified calculations

8.5 Model calibration and data correction

Model calibration was based on the adaptive performance modeling method [158, 162]]. In brief, the method minimizes the error between the measured and model predicted values by modifying model parameters (scaling factors of initial compressor, turbine maps, etc.). Not all the available measurements are needed in the procedure as their number is greater than the number of the calculated parameters. Therefore, in an initial calibration, a subset of the measurements including the total pressures at the turbine exit was used. Recalibration was done using static instead of total pressures at the turbine exit.

Institutional Repository - Library & Information Centre - University of Thessaly
02/06/2024 00:35:58 EEST - 18.226.159.139

Compressor and turbine final maps resulting from the calibration procedure are shown correspondingly in Figure 8-8 and Figure 8-9 . As the nozzle exhaust area is fixed, it is plausible that only a small part of the compressor and turbine maps (only for the points of each speed corresponding to the operating line) could be calibrated. Therefore, the shape of the initial maps has been adopted from existing maps of similar small engines [146].

Although this limitation has no impact on the model's ability to accurately predict the expected measured quantities, provided that the nozzle area is constant, special attention was given concerning the shape and smoothness of the adapted maps in order to be consistent with the laws of physics according to the guidelines provided in reference[135].

Another improvement of the model resulted when the burner efficiency considered being variable and described as a function of burner load adopted from reference [57].

$$\eta_b = f(BL) \tag{8-0}$$

The burner load is given from the following relation

$$BL = \frac{\dot{m}_{air}}{V_b P_{inlet}^{1.8} 10^{0.00145} (T_{inlet} - 400)}, \text{ where } V_b = \text{burner volume} \tag{8-0}$$

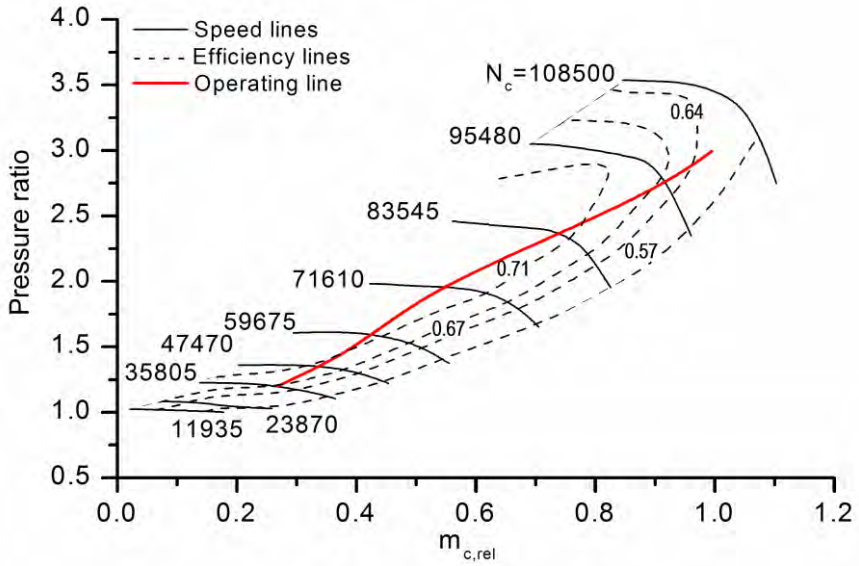

Figure 8-8 Compressor final map

Institutional Repository - Library & Information Centre - University of Thessaly
02/06/2024 00:35:58 EEST - 18.226.159.139

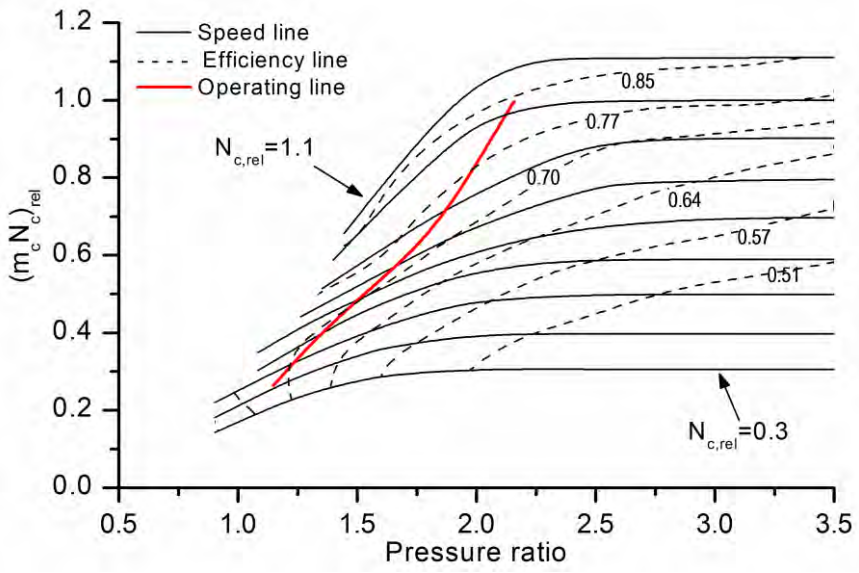

Figure 8-9 Turbine final map

Engine performance results predicted with the use of the recalibrated model are presented in Figures 8-10 to 8-12. The calculated exhaust gas mass and fuel flows (Figure 8-10) smoothly increase with the rotational speed as expected for a small turbojet engine [153, 154]. The fuel flow rate curve follows the trend of the manufacturer's data. The turbine isentropic efficiency (Figure 8-11) values are typical for that type of engine, as shown in references [145, 157, 165].

Figure 8-12 presents the measured and calculated values of the turbine inlet temperature. It is obvious that there is a large deviation between them at low rotational speeds. This is probably due to either the radiative heat transfer from hot gases to the sensor or due to the measurement of local maximum of the temperature profile [149]. In micro turbines, radiative heat transfer is pronounced at both the combustor primary zone and its exit [154, 155]. Apart from the radiation, a possible cause of high temperature indications is incomplete combustion, which implies a combustor efficiency drop particularly at low speed operation [154]. As incomplete combustion can be measured relatively easily at the engine exhaust, it is in our future plan to use a gas analyser in order to obtain a picture of the combustor efficiency variation.

Figure 8-12 also depicts the measured and calculated total pressures at the turbine exit. The measured pressures at that section are larger than the pressures which are obtained from the calculations. This probably occurs because of the non-representativeness of the measurements. The total pressure probes are placed in the mean radius where the peak value of the total pressure is located. Although in larger turbines the total pressure radial profiles are sufficiently smooth [167, 168], in small turbines they seem to exhibit a more sharp shape.

Institutional Repository - Library & Information Centre - University of Thessaly
02/06/2024 00:35:58 EEST - 18.226.159.139

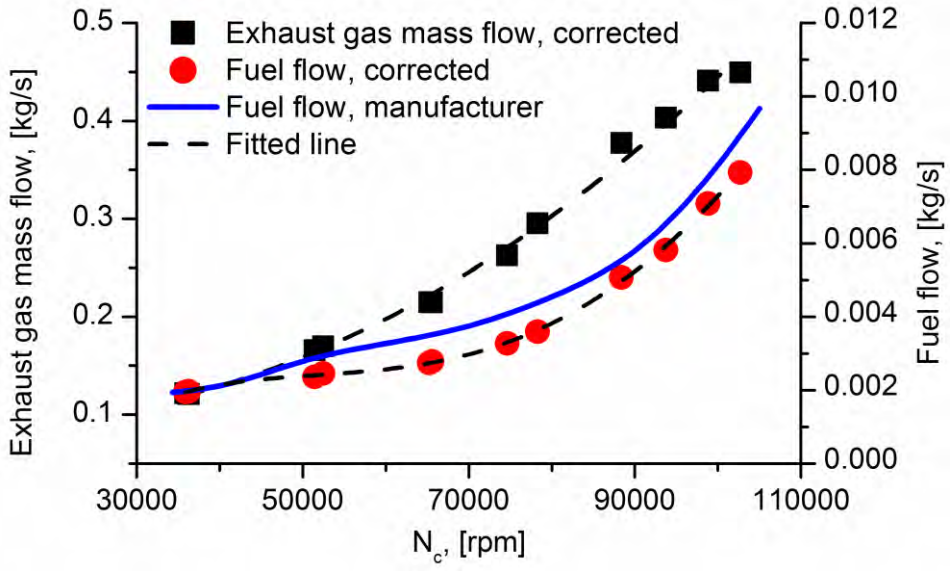

Figure 8-10 Exhaust gas mass flow and fuel flow

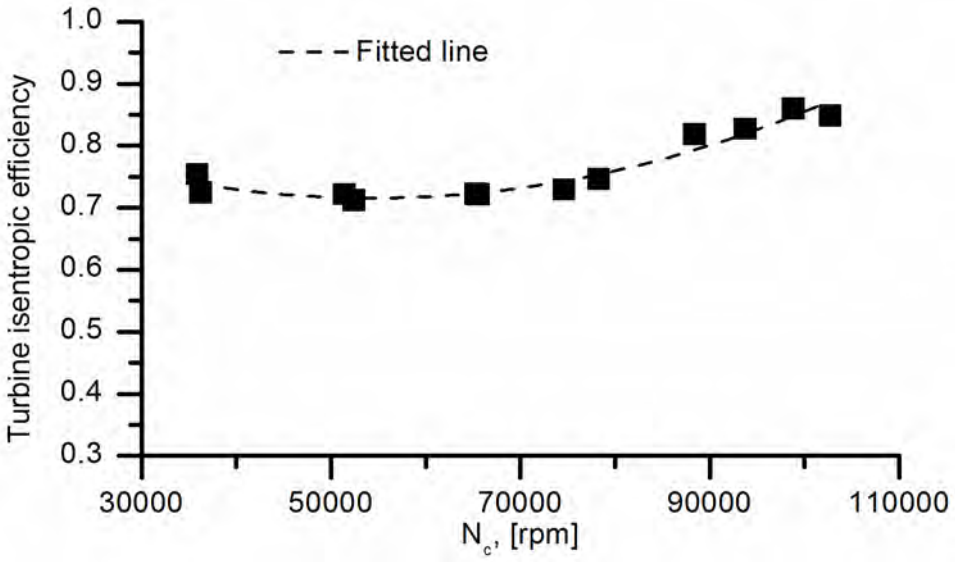

Figure 8-11 Turbine isentropic efficiency

Institutional Repository - Library & Information Centre - University of Thessaly
02/06/2024 00:35:58 EEST - 18.226.159.139

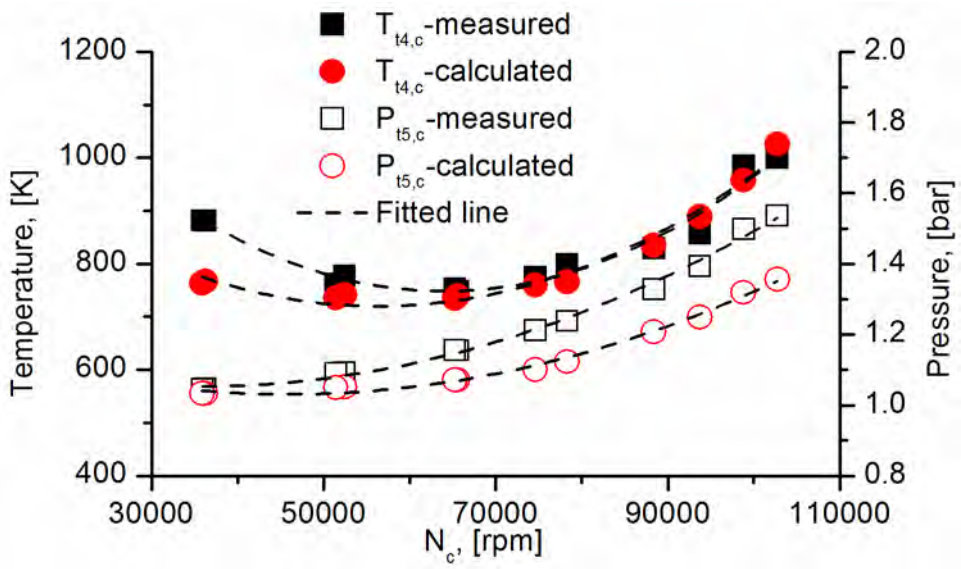

Figure 8-12 Turbine inlet temperature and total pressure at turbine exit

For the last two measurement quantities (T_{t4} and p_{t5}) it is obvious that there are systematic deviations which are repetitive. Regarding the p_{t5} the error is present over the whole range of the rotational speeds, while the error for T_{t4} is only significant at low rotational speeds. Thus, it is reasonable to introduce a correction factor for those measurements in order to correct the measured values and make them compatible with the other measurements.

The use of correction factors is widely accepted in the field of gas turbines. Jackson et al. [169] used them to relate the thrust measurements between the indoor and outdoor test beds for a micro-turbine. Also, Davison and Birk [154] used correction factors to correct the mass flow in the inlet duct of a test rig.

In order to validate the need for the introduction of correction factors, the same calculations were carried out using various other combinations of the available data. Also, the manufacturer's data for the thrust and fuel flow were taken into account for the conclusion enhancement. The cases that were examined are presented in Table 8-5. For each case, the measurements which are used and the basic calculated parameters (unknowns) are marked with different symbols.

The calculated parameters are defined as ratios of the actual (calculated) and the reference (initial) values of a performance parameter.

$$SX = \left(\frac{X_{actual}}{X_{ref}} \right) \tag{8-0}$$

where X_{actual} is the actual value

and X_{ref} is the reference value

In the case of the compressor and turbine components the reference values of manipulated parameters (pressure ratio, mass flow parameter and efficiency) are taken from the performance maps, while for other components (burner and nozzle) the reference values are the typical values assumed for the specific engine.

Institutional Repository - Library & Information Centre - University of Thessaly
02/06/2024 00:35:58 EEST - 18.226.159.139

Table 8-5 Summary of examined cases

Meas.	Case 1	Case 2	Case 3	Case 4	Case 5	Calc.
P_3	♦ ●	♦ ●	♦ ●	♦ ●	♦ ●	SP
T_{t3}	♦ ●	♦ ●	♦ ●	♦ ●	♦ ●	SE1
T_{t4}		●		●	♦	SE2
P_5	♦ ●	♦ ●	♦ ●	♦ ●	♦ ●	SW
T_{t5}	♦ ●	♦ ●	♦ ●	♦ ●	●	SE3
$F_{meas.}$	♦ ●		●	●	♦ ●	SE4
F_{man}			♦	♦		
$\dot{m}_{f,man}$		♦		♦		

(♦: used measurement, ●: estimated parameter)

Only the calculations for the correction factor of the total pressure at the turbine exit are presented. The correction factor for the turbine inlet temperature is calculated using the same procedure. The pressure error is defined as:

$$\text{Total pressure error [\%]} = 100 \times \frac{P_{t5,c}^{measured} - P_{t5,c}^{calculated}}{P_{t5,c}^{measured}} \quad (8\text{-}0)$$

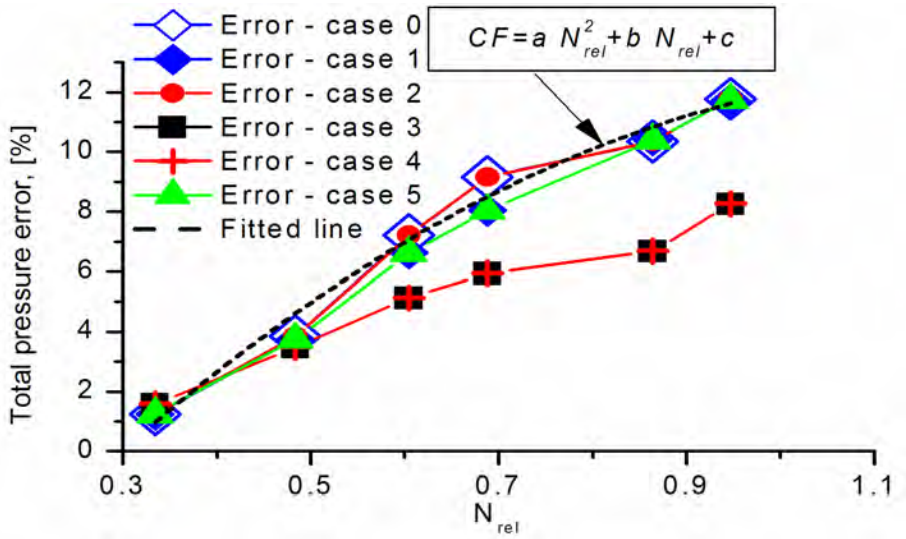

Figure 8-13 Total pressure errors for various cases

In Figure 8-13 , the total pressure errors at the turbine exit as have arisen by examining the cases described in Table 8-5 are presented: case 0 corresponds to the initial run where the measurements p_3, T_{t3}, p_5, T_{t5} (Figures 8-10 to 8-12) are used and the parameters SP, SE1, SW, SE3 are calculated. All the curves exhibit similar trends. The values for cases 3 and 4, where the manufacturer thrust values are used, are significantly smaller than the others. However, this result does not affect the conclusions, since it is expected that differences do exist between the engine installed in the laboratory and manufacturer's data for two additive reasons: small differences due to

Institutional Repository - Library & Information Centre - University of Thessaly
02/06/2024 00:35:58 EEST - 18.226.159.139

manufacturing variability and (in our case the most significant) the engine in our lab differs from the basic edition of the manufacturer as it is equipped with extended instrumentation. The extra sensors located inside the small passages affect the engine's flowfield and therefore its performance. It should be noted that the experiments were realised in almost standard ambient conditions, and data were corrected to correspond in the exact standard ambient conditions in order to be comparable with the manufacturer's data.

Obviously there is a relationship between the pressure error and the rotational speed. Therefore, a simple equation may be applied to correct the measurements in all operating points.

$$p_{t5}^{actual} = \left[1 - CF(N_{rel})\right] \times p_{t5}^{measured} \tag{8-0}$$

where the correction factor CF(N_{rel}) is a function of the (relative) rotational speed and is calculated by the interpolated curve in Figure 8-13.

The relationship between the pressure error and the rotational speed was repeatable during different experiments. The 'physics' involved most probably has the following explanation: as speed is increased the velocity and total pressure profiles are stretched due to the growing three-dimensional boundary layers. Since the sensors are in fixed locations, it is reasonable to assume that even though they have been calibrated to give the 'true' mean values for a given speed flow field, their indications deviate from the mean as the flow field is altered. The corrections applied could enhance diagnostics capabilities. Having established the baselines for the expected error as a function of the operating point through the model, any further deviation should be useful information for possible fault detection.

By introducing correction factors in the recalibrated model, it was possible to accurately reproduce all the measurements (e.g. p_5), even the non-representative ones (e.g. p_{t5}), as it can be seen in Figure 8-14.

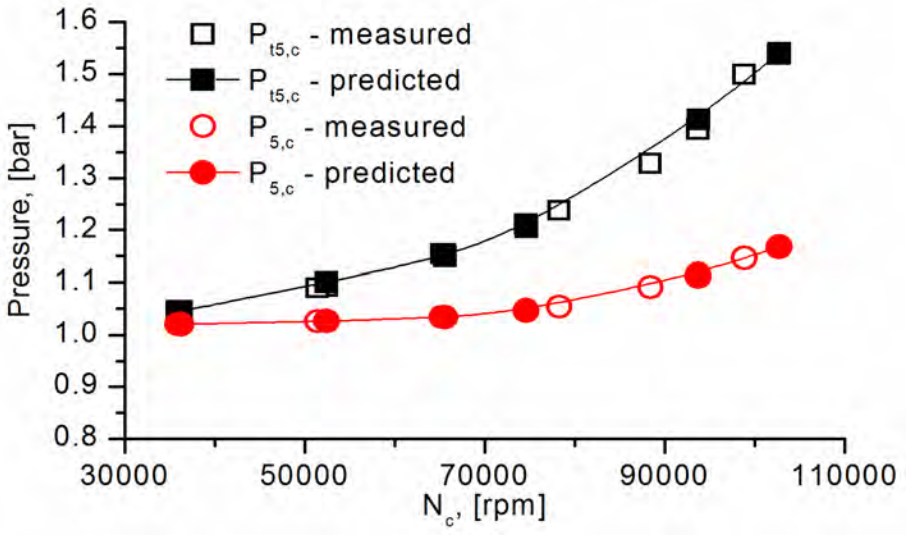

Figure 8-14 Predicted and measured pressures at turbine exit

Non-representative measurements, although they cannot be used in one-dimensional lumped volume mass, and energy balance relations, may supply extra information to various diagnostic methods (neural networks, blind parametric models, etc.) for better and safer diagnosis.

Institutional Repository - Library & Information Centre - University of Thessaly
02/06/2024 00:35:58 EEST - 18.226.159.139

8.6 Conclusions

The aim of this work was to present the problems arising and the solutions given during the development of an adaptive performance simulation model for a small turbojet engine. The experience gained can be summarised as follows:

- The use of an initial model, calibrated using total temperature and pressure measurements at compressor and turbine exits, was proven inadequate. Turbine efficiency calculations based on those measurements set were too high (in the range of 95% and above at higher speeds).
- Two possible reasons were examined for the inadequacy: heat transfer through the turbine casing which was not taken into account and the possibility of systematic errors in the measurements used.
- Simple calculations revealed that the amount of heat transfer occurring through the turbine casing is almost negligible. On the other hand, data analysis procedures indicated that two measured quantities deviate systematically from the predictions, namely the turbine inlet temperature and the turbine exit total pressures.
- Model recalibration based on the use of static instead of total pressure measurements in the turbine exit has proven adequate, both for the prediction of the measured parameters and for producing reasonable values for the turbine efficiency.
- This is a strong indication that in the case of small engines, static pressures measurements at hot sections are more reliable than the total ones. The later due to the sharper radial profile are more susceptible to systematic errors.
- Data correction procedures were finally implemented successfully in order to incorporate all the available measurements in the model, thus enhancing the model's capabilities for feature diagnostic studies.

Institutional Repository - Library & Information Centre - University of Thessaly
02/06/2024 00:35:58 EEST - 18.226.159.139

Chapter 9

Transient model

In this chapter, a transient model for the small turbojet engine described in the previous chapter is presented. The model is based on the intercomponent volume technique and takes into account the shaft dynamics, the heat transfer effects and the volume dynamics. The model is validated against experimental data and the comparison shows good agreement.

9.1 Introduction

Gas turbines operate under transient conditions during load changes, start up or shut down procedures and under abnormal conditions such as an emergency shutdown or a load rejection. During the transient operation the engine should respond quickly to load demand. The critical operating parameters such as turbine inlet temperature or surge margin should remain between certain bounds in order to ensure safe and reliable operation. Thus, a precise transient model for a gas turbine it is essential for safe system design, controller design, fault detection etc.

Several modeling methods have been proposed for the prediction of the gas turbines transient behavior. Camporeale et al. [170] developed a high fidelity aerothermal model for gas turbines in Matlab-Simulink environment. The model took into account the actual composition of the working media and the variation of specific heats with the temperature. Compressor and turbine components were considered volume-less and a volume was introduced between them in order to model the unsteady mass balance. Shaft dynamics as well as the dynamic behavior of transducers and actuators were considered in this study.

Kim et al. [171] developed a transient model for heavy duty gas turbine engines and applied on a real engine. Each component was modeled on the basis of ordinary differential equations describing the dynamics of the fluid (continuity, momentum and energy equations) flowing through the control volume. Advanced models for the compressor and turbine components were developed based on a novel stage-stacking method in order to simulate multistage axial devices with interstage bleeding and variable inlet guide vanes or variable stator vanes. Practical operations were simulated by incorporating a controller which maintained the rotational speed and either the turbine inlet or the turbine outlet temperature constant.

Martin et al. [172] presented details about a nonlinear real-time model for a civil turbofan engine and validated against dynamic performance data for a similar engine. The model accounts for the shaft dynamics, gas dynamics, heat soakage effects, actuators and transducers dynamics. A gain-scheduled controller was designed to cover the full-flight envelope. The resulted model estimations corresponded closely to a real engine.

Institutional Repository - Library & Information Centre - University of Thessaly
02/06/2024 00:35:58 EEST - 18.226.159.139

Rezvani et al. [173] created a gas turbine transient model based on feed forward neural network methodology. An aerothermal model was used to produce data points. Details of selecting proper training and verification data sets were discussed. The results of neural network showed good prediction accuracy.

9.2 Transient performance methods

There are two methods that can be adopted, in order to perform a gas turbine transient simulation [145]:

- Iterative method
- Intercomponent volume method

In the iterative method, it is assumed that the mass flow of the working media is the same at the inlet and the outlet of the control volume, flow compatibility satisfied, even if the engine operates under transient conditions.

The intercomponet volume method is more accurate compared to the previous one, because during the transient operation, the mass, the energy and the momentum imbalances are taken into account. In order to capture the gas dynamics effects, the gas turbine components are divided in two segments as shown in Figure 9-1.

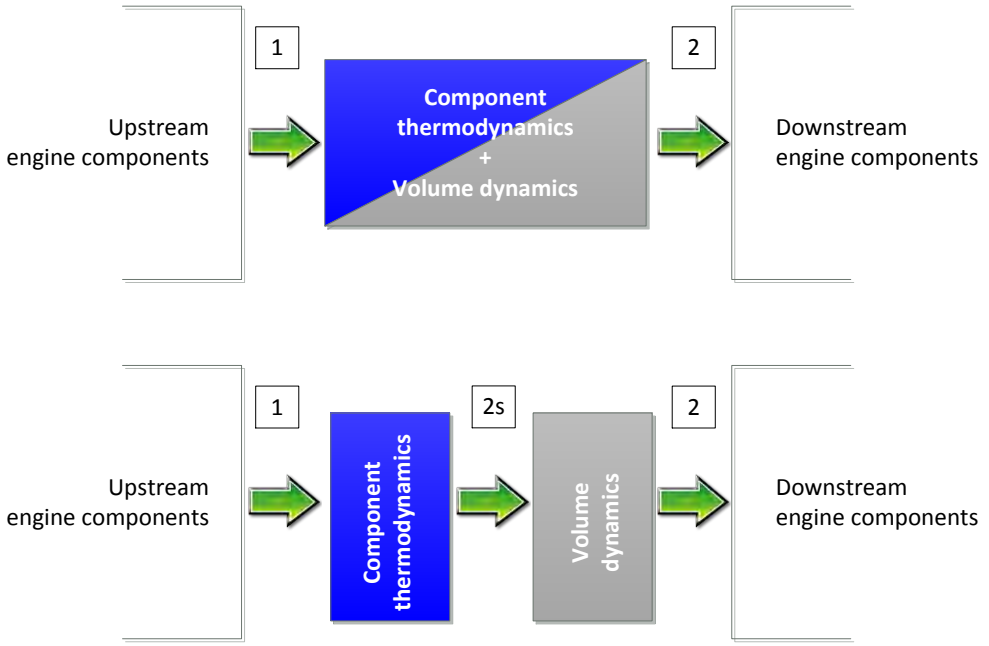

Figure 9-1 Intercomponent volume method

The first segment is the same as in steady state model. The calculations are done without taking into account the volume of the component, and thus, there is not mass storage ($\dot{m}_1 = \dot{m}_{2s}$). The thermodynamics data at the exit of this segment (2s state) are referred to as quasi steady state. In the second segment, the volume dynamic effects are calculated. In this segment is $\dot{m}_{2s} \neq \dot{m}_2$, and this difference contribute to the chance of the mass stored in the components' volume. The thermodynamic properties are calculated by using the gas dynamics equations described in section 9.3.3.

Institutional Repository - Library & Information Centre - University of Thessaly
02/06/2024 00:35:58 EEST - 18.226.159.139

9.3 Dynamic effects

Dynamic behavior of gas turbines is described by conservation laws and equations of motion. The fluid flow through the engine components is three-dimensional, and thus unsteady three-dimensional calculations are required for analyzing the transient phenomena. However, in most practical applications, it is inefficient to apply three-dimensional calculations because of their high computational cost. In an attempt to overcome this obstacle, one-dimensional equations are applied which give accurate results for integral modeling purposes [171].

The transient behavior of a gas turbine is mainly affected from:

1. Shaft dynamics
2. Heat soakage effects
3. Gas dynamics

9.3.1 Shaft dynamics

If a gas turbine operates at steady state conditions and suddenly the fuel flow increases, the turbine inlet temperature will increase causing the turbine to produce more power. This introduces an energy imbalance on the shaft, since the power produced from the turbine exceeds the required power to drive the compressor. This imbalance results in a change in the rotational speed, which is described by the following equation [57]:

$$\dot{N} = \frac{dN}{dt} = \frac{\eta_m P_t - P_c}{I_{spool} N \left(2\pi/60\right)^2} \tag{9-1}$$

A rotor inertia of I_{spool} = 0.0012 kg^2 was selected for the engine. The exact value was not available, and this value was assumed as it corresponds to a rotor with a radius of 4 cm and mass equal to 1.5 kg.

9.3.2 Heat soakage effects

Heat soakage effects account for the heat transfer between the gas passing through the engine and the body (metal parts) of the engine. This phenomenon changes both the outlet temperature and pressure of a component. The heat transfer phenomena can change the tip clearances and efficiency during transients. This is particularly important in axial flow compressors and turbines. In this work the changes in efficiencies due to the heat soakage effects were not taken into account because of the small size of the engine which do not lead to thermal expansion mismatch between the engine components. Heat soakage effects are not always included in transient models due to lack of knowledge on the heat transfer phenomena between the gas and metal parts, because it is difficult to acquire experimental data during changes of the engine operating conditions [174].

In this study the heat soakage effects are calculated based on the methodology outlined by Stamatis et al. [175]. According to this methodology the heat transfer coefficient is given from the relation (9-2)

$$h = 0.0201 \cdot C \cdot \mathrm{Re}^{0.8} \frac{k}{L} \tag{9-2}$$

where

Institutional Repository - Library & Information Centre - University of Thessaly
02/06/2024 00:35:58 EEST - 18.226.159.139

$$\mathrm{Re} = \frac{\dot{m} \cdot L}{V_{is} \cdot A} \tag{9-3}$$

According to the law of conservation of energy, the heat that is removed from the gas equals to the heat transferred to the component. This is described by the following equations:

$$(\text{Heat flow from gas to metal}) = hA_{metal}(T_{gas} - T_{metal}) \tag{9-4}$$

$$(\text{Heat flow to metal}) = C_{p,metal} m_{metal} \frac{dT_{metal}}{dt} \tag{9-5}$$

Thereby, the equation describing the heat transfer effects is:

$$\frac{dT_{metal}}{dt} = \frac{hA_{metal}}{C_{p,metal} m_{metal}}(T_{gas} - T_{metal}) \tag{9-6}$$

where

$$T_{gas} = \frac{T_{in} + T_{out}}{2} \tag{9-7}$$

In the previous analysis the metal temperature assumed uniform. The conduction through the components is very fast compared to the convection.

In case of the compressor and turbine components the temperature change affects the pressure ratio. The pressure ratio value from the performance map is modified according to equation

$$PR = TR^{x} \tag{9-8}$$

where

$$x = \frac{\ln PR_{map} / \ln TR_{map}}{1 - \dot{Q}_{Heat} / \dot{W}_{Component}} \tag{9-9}$$

9.3.3 Gas dynamics

During steady state operation of a gas turbine, the amount of gas entering into an engine component (control volume) equals the amount of gas out. But this is not valid during the transient operation, as the density in a component changes and mass either is accumulated or is rejected, resulting an imbalance of mass flow between the inlet and outlet sections.

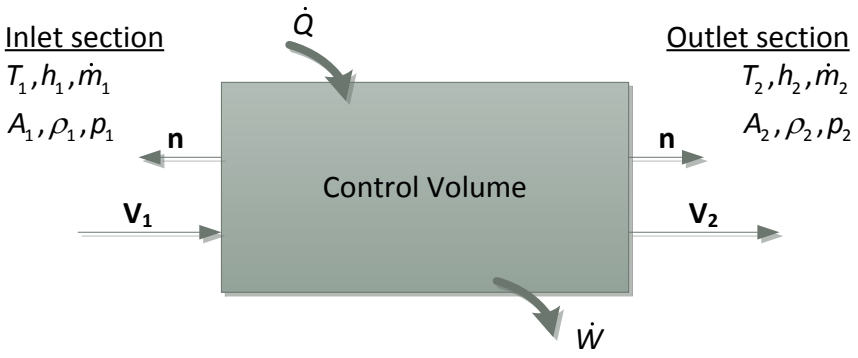

Figure 9-2 Control volume and notation used in conservation equations

Institutional Repository - Library & Information Centre - University of Thessaly
02/06/2024 00:35:58 EEST - 18.226.159.139

Gas dynamics have notable impact on gas turbine's transient operation since affect the stored mass, energy and momentum in the volumes of the engine components. Gas dynamics are modeled using the one-dimensional conservation equations of mass, energy and momentum.

For the discussion of the conservation equations, a component is represented by a control volume with inlet and outlet sections as shown in Figure 9-2.

Continuity equation

The integral form of continuity equation is [147]:

$$\int_{Vol} \frac{\partial \rho}{\partial t} dVol + \int_{A} \rho \mathbf{V} \cdot \mathbf{n} dA = 0 \tag{9-10}$$

The unsteady behavior is obtained by integrating the equation (9-10). The ordinary differential equation that describes the transient performance is

$$\frac{\partial \bar{\rho}}{\partial t} = \frac{\dot{m}_1 - \dot{m}_2}{Vol} \tag{9-11}$$

Energy equation

The conservation of energy is given by:

$$\int_{Vol} \frac{\partial (\rho e)}{\partial t} dVol + \int_{A} (\rho e \mathbf{n} \cdot \mathbf{V}) dA = \dot{Q} + \dot{W} \quad \text{where} \quad e = u + \frac{c^2}{2} \tag{9-12}$$

The mechanical power P in a control volume is the sum of the shaft power P_{Shaft} and the pressure work P_P which is needed to overcome the nominal and shear stresses at the inlet and exit of the system

$$P = P_{Shaft} + P_P \tag{9-13}$$

The pressure work is the product of the force vector and vector of displacement:

$$P_P = \int_1^2 dW_P = \int_1^2 d\left(\frac{\mathbf{F} \cdot d\mathbf{X}}{dt} \right) \tag{9-14}$$

where $\mathbf{F}$: force vector ($|\mathbf{F}| = p \cdot S$)

$d\mathbf{X}$: displacement vector

At inlet of the control volume (Section 1) the displacement and the force act towards the negative direction. Moreover, the force is the product of the pressure and the area ($p_1 \cdot A_1$). Thus,

$$d(\mathbf{F} \cdot d\mathbf{X}) = d\left[(-\mathbf{n}) \cdot (-\mathbf{n}) p A dx \right] = p dVol \tag{9-15}$$

but

$$dVol = \frac{dm}{\rho} \tag{9-16}$$

Using (9-15) and (9-16), equation (9-14) becomes:

Institutional Repository - Library & Information Centre - University of Thessaly
02/06/2024 00:35:58 EEST - 18.226.159.139

$$\dot{W}_p = \int_1^2 d\left(\frac{\dot{m}p}{\rho}\right) = \left(\frac{\dot{m}p}{\rho}\right)_2 - \left(\frac{\dot{m}p}{\rho}\right)_1 \tag{9-17}$$

Using the relation $\dot{m} = \rho AV$, the second term of equation (9-12) can be written as:

$$\int_A (\rho e \mathbf{n}\cdot\mathbf{V}) dA = \dot{m}_2 e_2 - \dot{m}_1 e_1 \tag{9-18}$$

By replacing equations (9-17) and (9-18) into equation (9-12) we get:

$$\int_{Vol} \rho\left(u + \frac{V^2}{2}\right) dVol + \dot{m}_2\left(u_2 + \frac{V_2^2}{2}\right) - \dot{m}_1\left(u_1 + \frac{V_1^2}{2}\right) = \dot{Q} + P_{Shaft} - \left(\frac{\dot{m}p}{\rho}\right)_2 + \left(\frac{\dot{m}p}{\rho}\right)_1 \tag{9-19}$$

The enthalpy and total enthalpy are:

$$h = u + \frac{p}{\rho} \quad \text{and} \quad h_t = u + \frac{p}{\rho} + \frac{V^2}{2} \tag{9-20}$$

Combining the previous equations, we take the differential equation describe the energy conservation in a control volume:

$$\frac{d(\rho h_t - p)}{dt} Vol = \dot{m}_1 h_{t1} - \dot{m}_2 h_{t2} + \dot{Q} + P_{Shaft} \tag{9-21}$$

Momentum equation

The general form of the momentum equation for a control volume is

$$\int_{Vol} \frac{d(\rho\mathbf{V})}{dt} dVol + \int_A \mathbf{n}\cdot\rho(\mathbf{VV}) dA = \int_A (-\mathbf{n}p - \mathbf{t}\tau) dA + \mathbf{G} \tag{9-22}$$

The vector G is the gravitational forces acting on the control volume. In this study the effect of gravity is considered negligible and in not included in the model equations.

The first integral of equation (9-22) can be written as

$$\int_{Vol} \frac{d(\rho\mathbf{V})}{dt} dVol = \frac{d}{dt}\left(\rho\mathbf{V}\int_{Vol} dVol\right) = Vol\frac{d}{dt}(\rho\mathbf{V}) \tag{9-23}$$

Using the continuity equation:

$$\dot{m} = \rho VA \rightarrow \rho V = \frac{\dot{m}}{A} \tag{9-24}$$

we get:

$$\frac{d}{dt}(\rho V) = \frac{1}{A}\frac{d\dot{m}}{dt} \tag{9-25}$$

Expressing the volume as a function of cross sectional are and equivalent length, we have:

$$Vol = L\cdot A \tag{9-26}$$

and, the unsteady integral of momentum becomes:

Institutional Repository - Library & Information Centre - University of Thessaly
02/06/2024 00:35:58 EEST - 18.226.159.139

$$Vol\frac{d}{dt}(\rho V)=L\frac{d\dot{m}}{dt} \tag{9-27}$$

The flux term (second integral) can be written as:

$$\int_A \mathbf{n}\cdot\rho(\mathbf{VV})dA=\rho_2V_2V_2A_2-\rho_1V_1V_1A_1=\dot{m}_2V_2-\dot{m}_1V_1 \tag{9-28}$$

The stress term (third integral) can be decomposed in two integrals, one with normal forces and an additional one with shear stress forces. The integral with normal forces is written as:

$$-\int_A \mathbf{n}pdA=p_1A_1-p_2A_2 \tag{9-29}$$

The shear stress forces term can be calculated for steady state operation from momentum balance:

$$\int_{Vol}\frac{d(\rho\mathbf{V})}{dt}dVol+\int_A \mathbf{n}\cdot\rho(\mathbf{VV})dA=-\int_A \mathbf{n}pdA-\int_A \mathbf{t}\tau dA+\cancel{\mathbf{G}} \tag{9-30}$$

$$\int_{Vol}\frac{d(\rho\mathbf{V})}{dt}dVol+\int_A \mathbf{n}\cdot\rho(\mathbf{VV})dA=-\int_A \mathbf{n}pdA+\mathbf{F}+\cancel{\mathbf{G}} \tag{9-31}$$

$$\dot{m}_2V_2-\dot{m}_1V_1=p_1A_1-p_2A_2+F \tag{9-32}$$

$$F=\dot{m}_2V_2-\dot{m}_1V_1+p_2A_2-p_1A_1 \tag{9-33}$$

Taking into account the previous analysis the momentum equation (9-22) becomes now:

$$L\frac{d\dot{m}}{dt}=\dot{m}_1V_1-\dot{m}_2V_2+p_1A_1-p_2A_2+F \tag{9-34}$$

9.3.4 Sensor dynamics

Sensor dynamics were adopted only for the temperature sensors. The response of a temperature sensor (thermocouple) to a fast temperature change in not rapid, but take some time to respond. This is because of the heat transfer effects that take place between the body of the temperature sensor and its environment. The thermocouple dynamics were modeled assumed a first order lag.

9.4 Transient model for AMT Olympus

In Figure 9-3 are presented the control volumes for the transient model of the AMT Olympus microturbine. Control volumes that take into account the gas dynamics effects were considered for the compressor, the burner and the turbine components.

Institutional Repository - Library & Information Centre - University of Thessaly
02/06/2024 00:35:58 EEST - 18.226.159.139

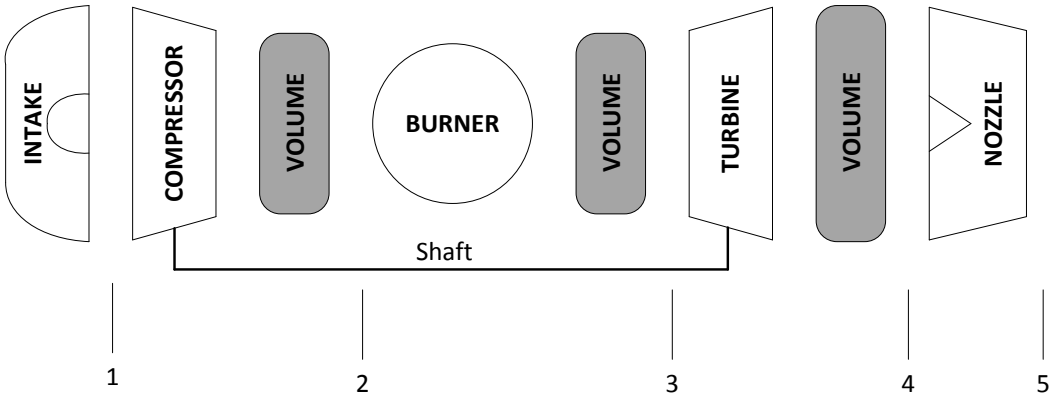

Figure 9-3 Control volumes for transient model

Representative performance maps for the compressor and turbine component from references [146, 176] were selected. The maps were modified by adopting the adaptive characteristics of the simulation model [158]. The modification process involves the use of steady state operational data from the whole operating range of the engine. The data set is given as input and the model calculates a set of modification factors which denote how the maps must change in order to be consistent with the supplied measurements. The modified maps are presented in Figure 9-4 and 9-5 in relativized form.

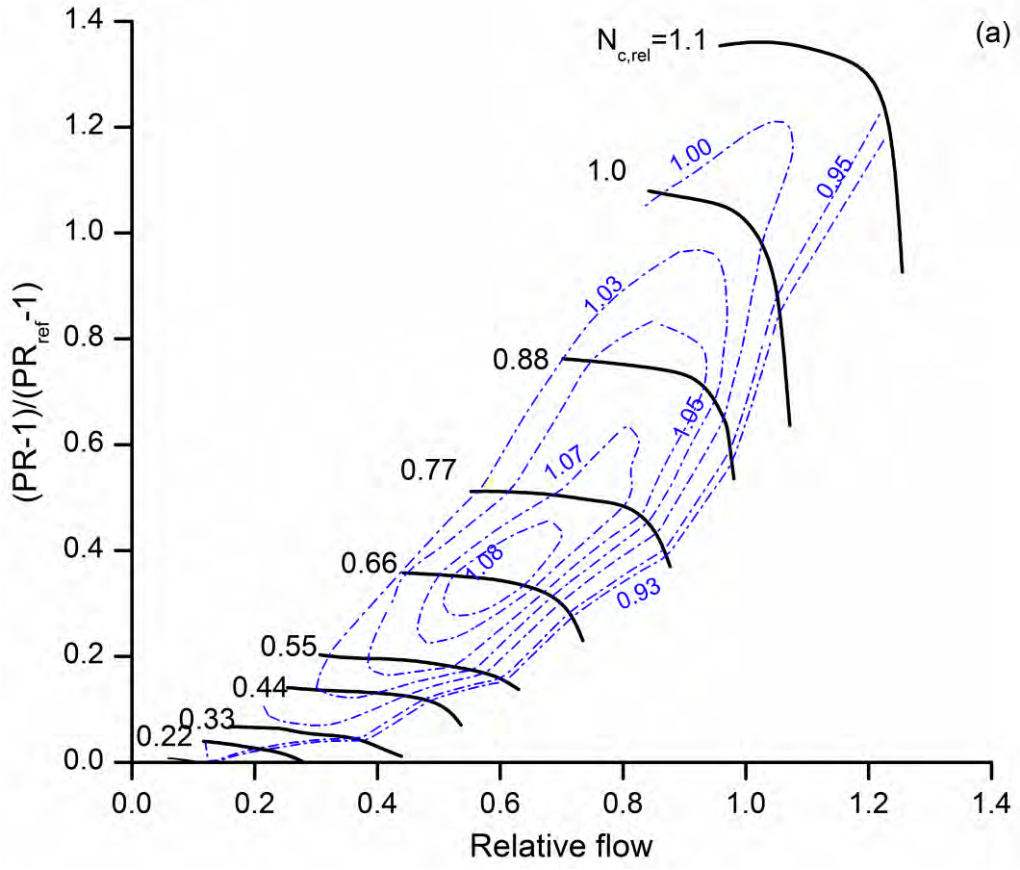

Figure 9-4 Relativized compressor map

Institutional Repository - Library & Information Centre - University of Thessaly
02/06/2024 00:35:58 EEST - 18.226.159.139

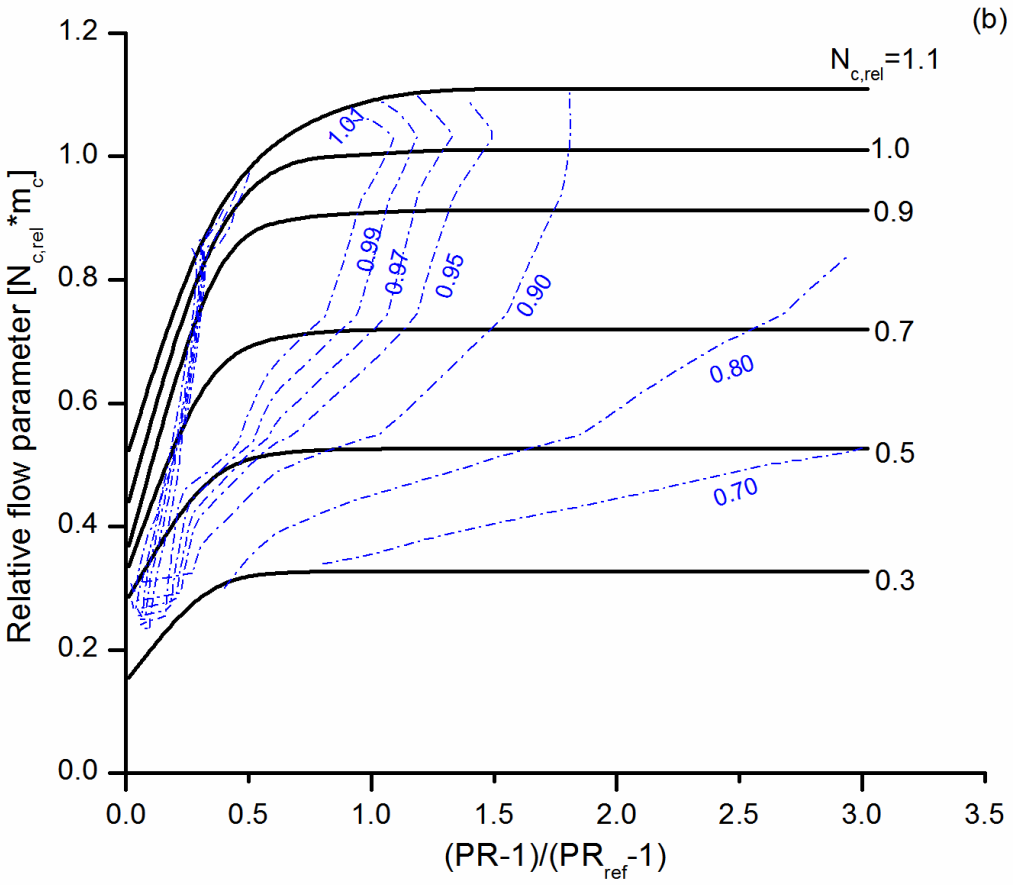

Figure 9-5 Relativized turbine map

To simulate the engine behavior under transient conditions a typical proportional, integral and derivative (PID) controller was implemented. The PID controller is extensively used in gas turbine applications, because of the robustness and simple structure [146, 177, 178]. The control scheme is shown in Figure 9-6. The engine throttle gives the operating speed required (N_{demand}). The controller input is the error signal ($e(t)$) generated between the set point and the shaft speed of the engine. Gain values for the proportional, integral and derivative were set K_P = 1.1, K_I = 0.0055 and K_D = 0.8 respectively.

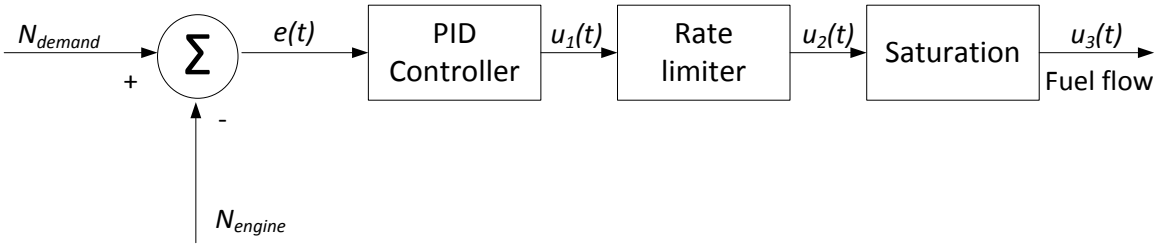

Figure 9-6 Block diagram of engine controller

A rate limiter is employed in order to prevent high temperatures and engine surge. The slew rate was set 2.8 g/s. The output of the rate limiter is given by the following function:

Institutional Repository - Library & Information Centre - University of Thessaly
02/06/2024 00:35:58 EEST - 18.226.159.139

$$u_2(t)=\begin{cases} T\cdot 2.8+u_2(t-1) & \text{if} \quad \dfrac{u_1(t)-u_2(t-1)}{T}>2.8 \\ u_1(t) & \text{if} \quad -2.8\le\dfrac{u_1(t)-u_2(t-1)}{T}\le 2.8 \\ -T\cdot 2.8+u_2(t-1) & \text{if} \quad \dfrac{u_1(t)-u_2(t-1)}{T}>2.8 \end{cases} \tag{9-35}$$

Also, fuel saturation occurs if the fuel flow exceeds a permissible upper or lower limit value. The output of the saturation block ($u_3(t)$) is calculated by:

$$u_3(t)=\begin{cases} 9.5 & \text{if} \quad u_2(t)>9.5 \\ u_2(t) & \text{if} \quad 1.7\le u_2(t)\le 9.5 \\ 1.7 & \text{if} \quad u_2(t)<1.7 \end{cases} \tag{9-36}$$

The transient model of the gas turbine consists of a set of non-linear algebraic and ordinary differential equations. The transient performance of the engine is predicted by solving this equation set numerically with the prescribed boundary and initial conditions. A time step of 10 ms is selected. At each time step, the ordinary differential equations are integrated using an implicit approach.

9.5 Model validation - Results

Experiments were carried out in order to validate the developed model. The data received during the experimental procedure were filtered with a median filter as described in section 8.2. The model is validated in the whole operating region. The model results are presented in the following sections and are compared with the experimental data.

Institutional Repository - Library & Information Centre - University of Thessaly
02/06/2024 00:35:58 EEST - 18.226.159.139

9.5.1 Acceleration from 66500 to 92000 rpm

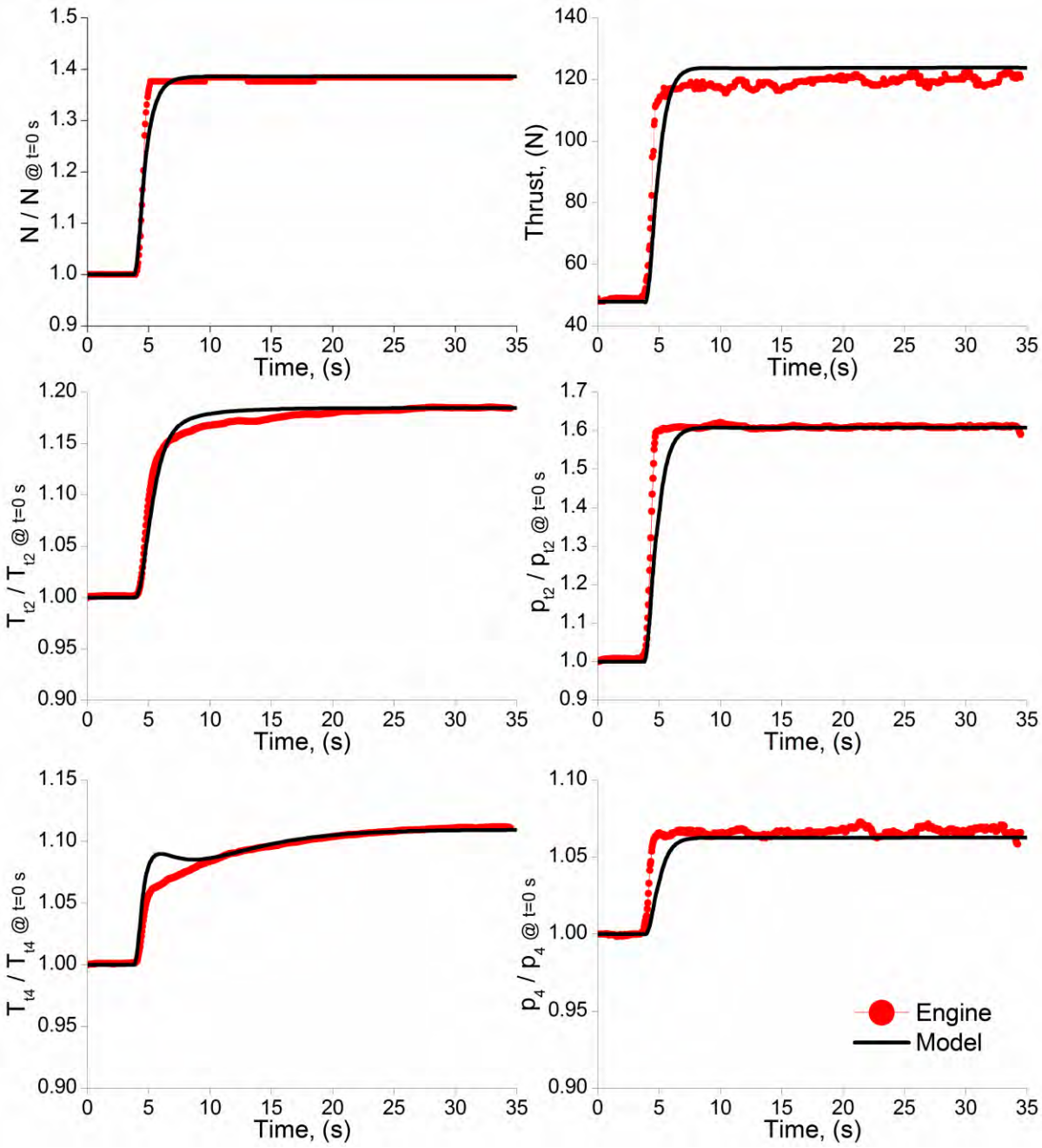

Figure 9-7 Transient response of engine to a step change from 66500 to 92000 rpm

In Figure 9-7 is presented the transient response of the engine to a step change from 66500 to 92000 rpm and compared with the model results. The model predicts very well the shaft speed and the temperature and pressure at the compressor exit. The produced thrust is slightly over estimated, contrary to the static pressure at turbine exit that is lower than the measured pressure values. The correlation of the turbine exit temperature is not as good as the other experimental data. This is probably due to the heat soakage effects that take place in the turbine component, but this point will be discussed later

Institutional Repository - Library & Information Centre - University of Thessaly
02/06/2024 00:35:58 EEST - 18.226.159.139

9.5.2 Acceleration from 80000 to 97000 rpm

Figure 9-8 presents the acceleration of the engine from 80000 to 97000 rpm. During this transition the model predicts quite well the engine behavior, the results are very close to the experimental data. The discrepancy at the turbine exit temperature is not significant compared to the previous case (see Figure 9-7).

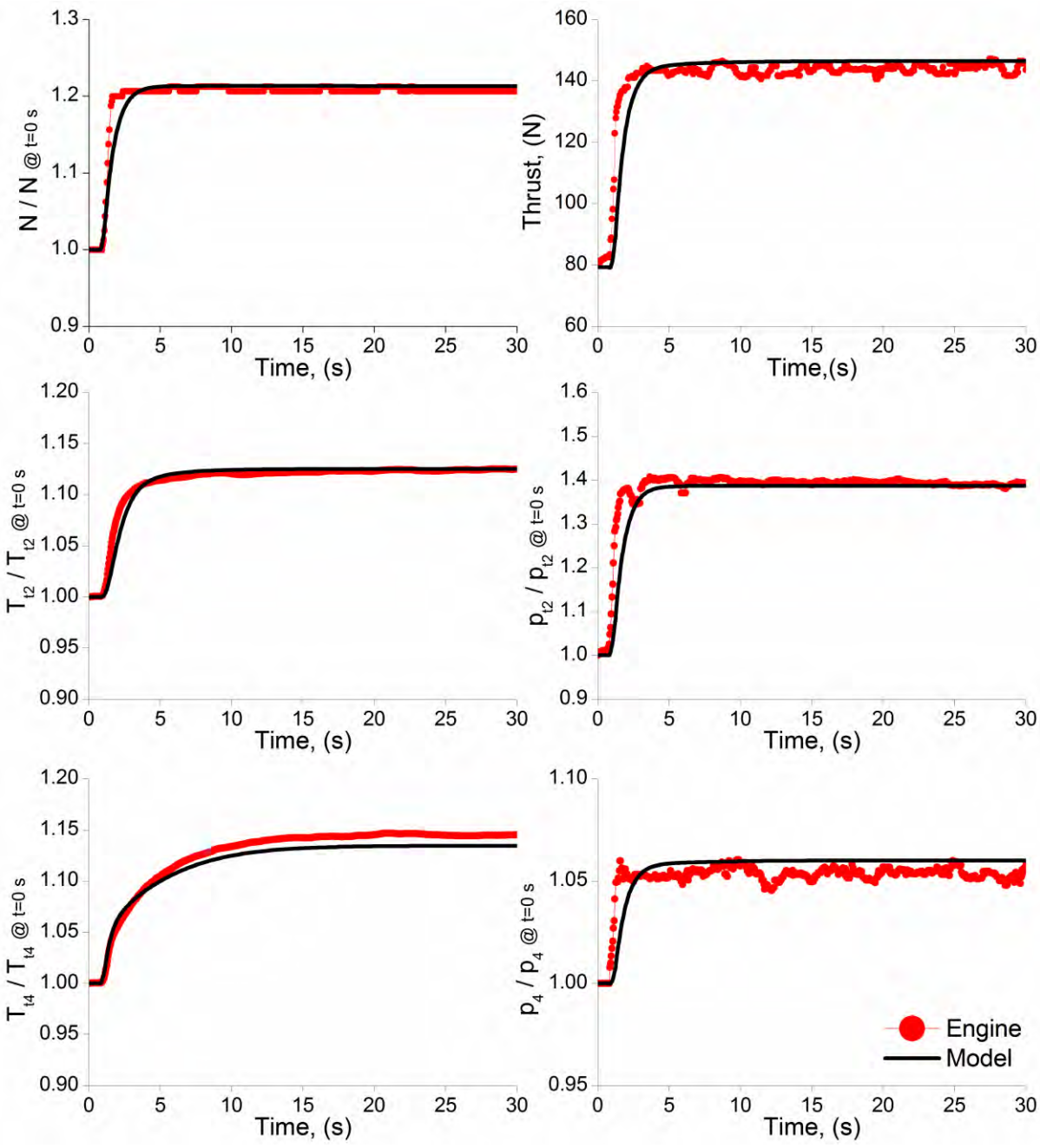

Figure 9-8 Transient response of engine to a step change from 80000 to 97000 rpm

Institutional Repository - Library & Information Centre - University of Thessaly
02/06/2024 00:35:58 EEST - 18.226.159.139

9.5.3 Deceleration from 108500 to 103500 rpm

Figure 9-9 compares the model and experimental data as the engine decelerated from 108500 to 103500 rpm, and in this case the match is very good. A remarkable fact is that pressure and trust measurements at high rotational speeds contain too much noise, which is not filtered.

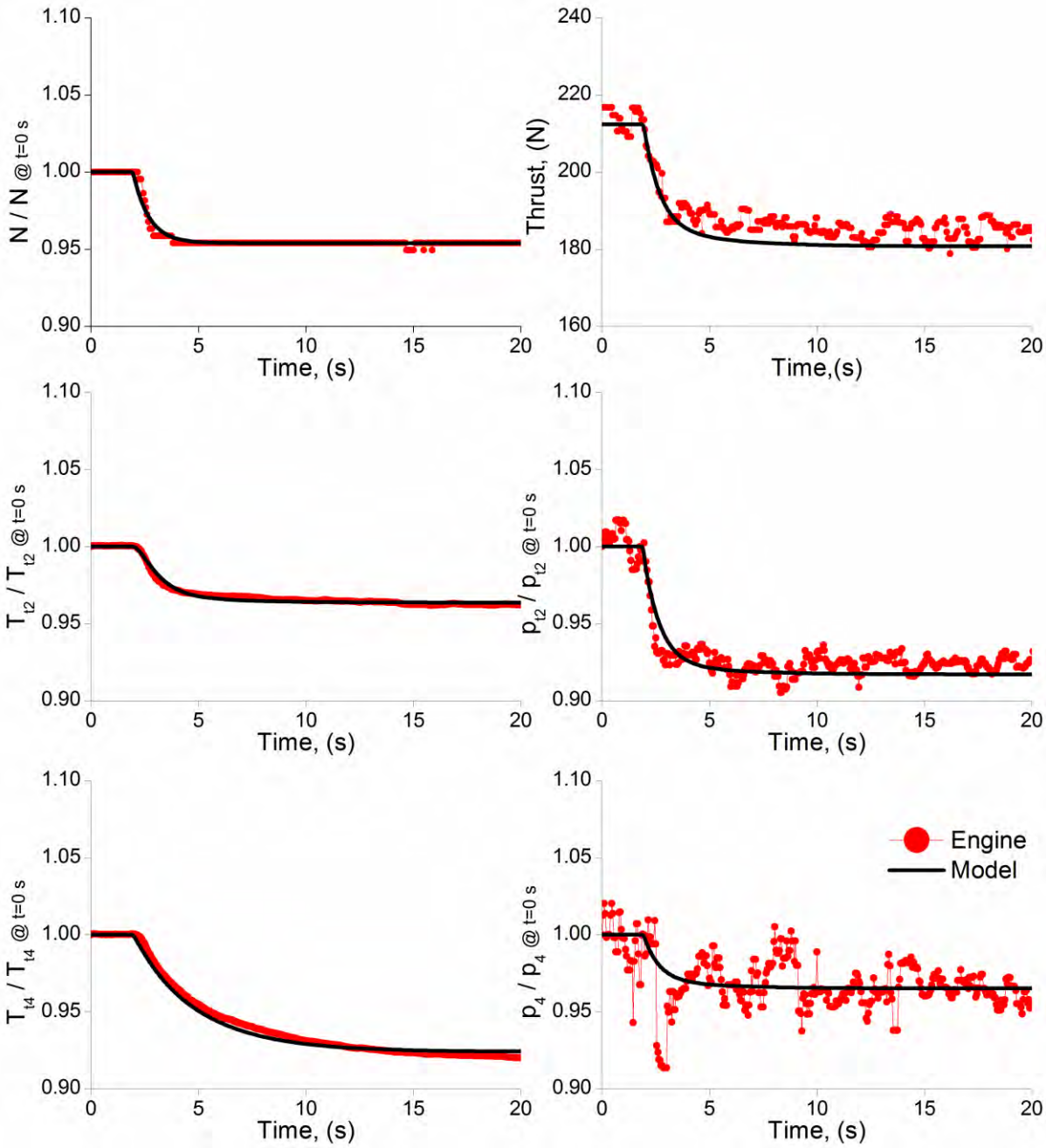

Figure 9-9 Transient response of engine to a step change from 108500 to 103500 rpm

Institutional Repository - Library & Information Centre - University of Thessaly
02/06/2024 00:35:58 EEST - 18.226.159.139

9.5.4 Deceleration from 96000 to 36500 rpm

Figure 9-10 presents the changes after a step decrease of set point from 96000 to 36500 rpm. The model responds very well, but as in the case shown in Figure 9-7, the predicted turbine exit temperature does not correlate very well with the experimental data.

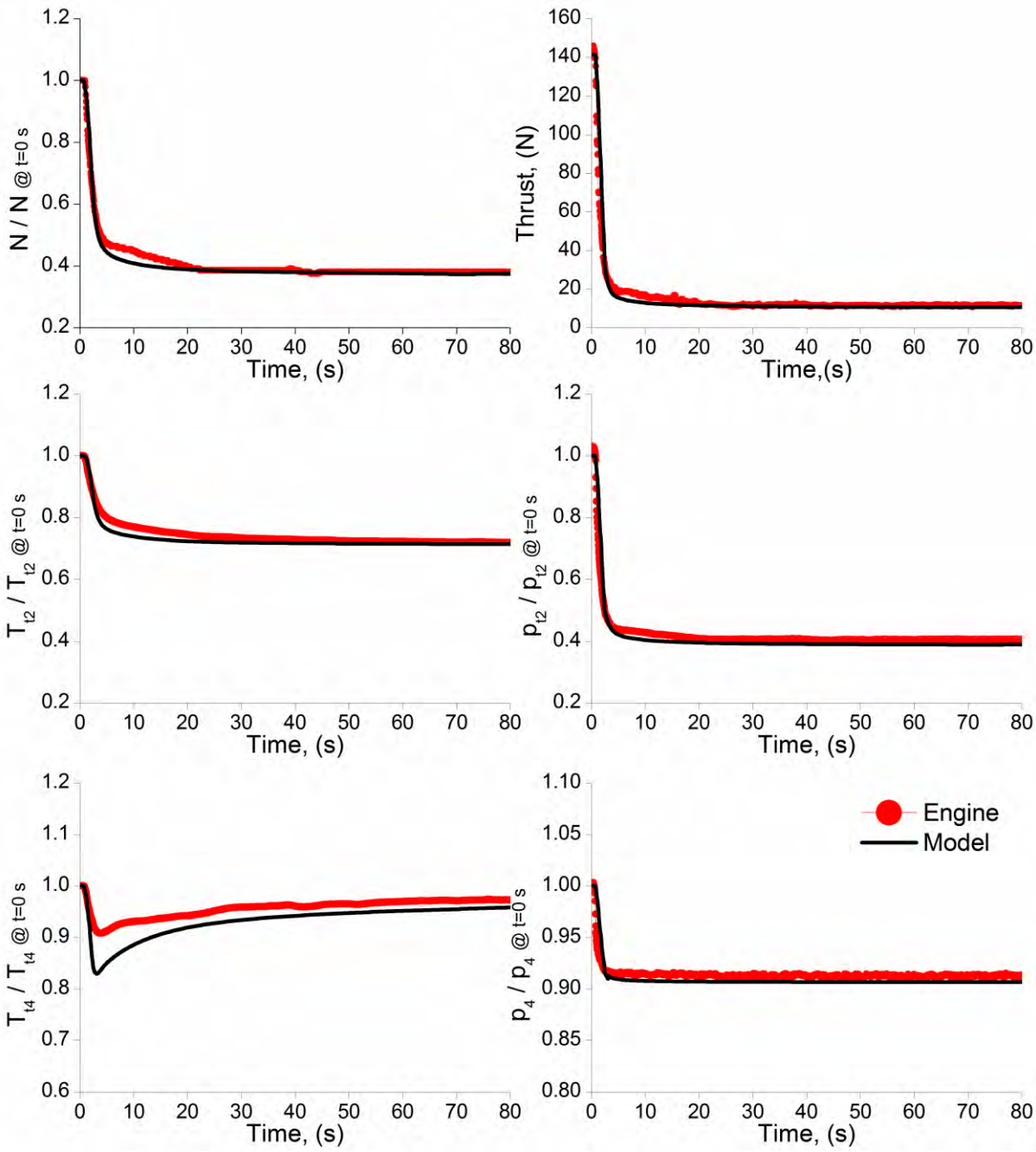

Figure 9-10 Transient response of engine to a step change from 96000 to 36500 rpm

9.6 Engine transient simulation and comparison with steady state performance data

Transient performance simulation is carried out for three different step changes using the developed model. The engine is accelerated from an initial shaft speed to maximum shaft speed. The

Institutional Repository - Library & Information Centre - University of Thessaly
02/06/2024 00:35:58 EEST - 18.226.159.139

simulation time is set to 50 s, so as to ensure that steady state conditions have been reached. The operating lines of the compressor and turbine components are presented in the following figures.

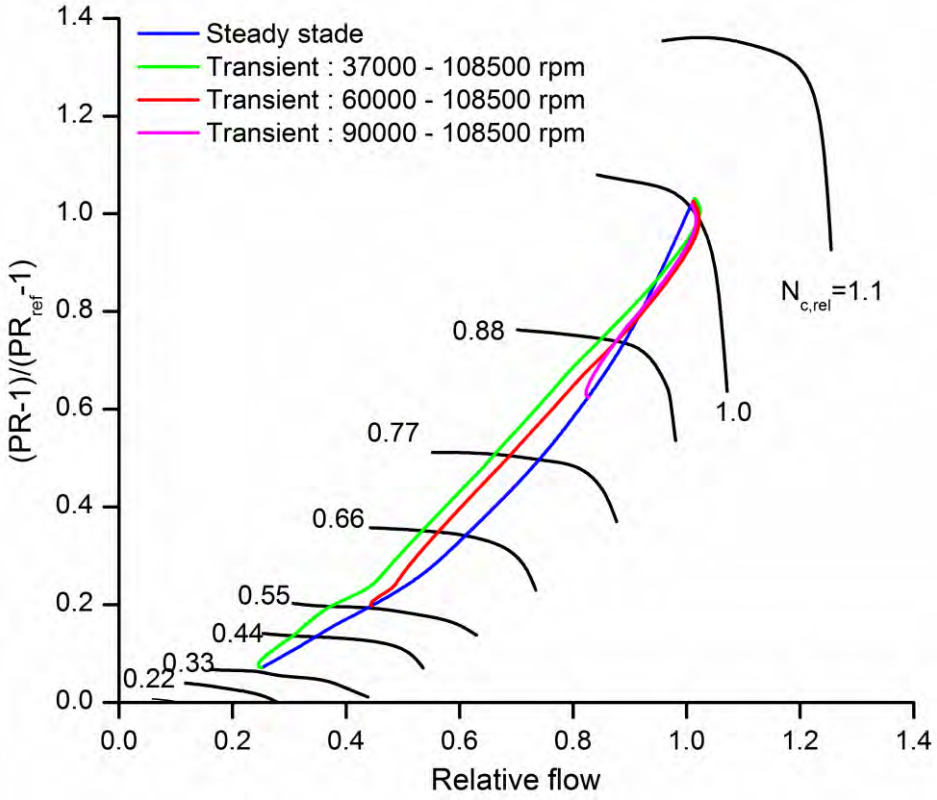

Figure 9-11 Compressor performance changes during transient operation

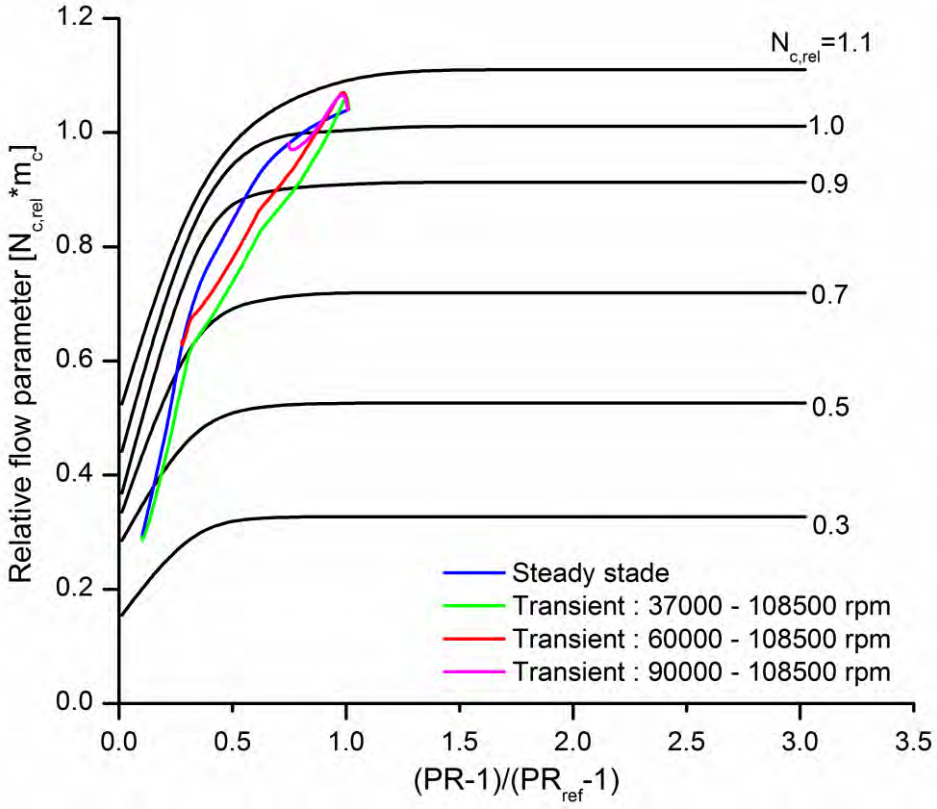

Figure 9-12 Turbine performance changes during transient operation

Institutional Repository - Library & Information Centre - University of Thessaly
02/06/2024 00:35:58 EEST - 18.226.159.139

In Figure 9-11, the compressor working lines for the three different step changes are illustrated and compared with the steady state working line. The sudden increase of the speed command causes a sudden increase of fuel flow, which moves the operating point of the compressor towards the surge. From the results it is obvious that the larger the speed increment the larger the deviation from the steady state working line. The corresponding changes in turbine working lines are shown in Figure 9-12. The increament in fuel flows moves the turbine operating point towards the choking region

9.7 Conclusions

A gas turbine simulation program was developed for the transient performance and the results were compared with experimental data from the AMT Olympus microturbine. The model takes into account the shaft dynamics, heat soakage effects, gas dynamics and sensor dynamics. In general the results are in good agreement with the experimental data. Differences were only observed for the turbine exit temperature values in some cases. This probably is due to the methodology used to calculate the heat transfer effects within the turbine component. A more detailed analysis may improve the model predictions. With the developed model the effect of amplitude of step change was studied. The results showed that as the amplitude increases the compressor tend to operate close to the surge region during the transient response.

Institutional Repository - Library & Information Centre - University of Thessaly
02/06/2024 00:35:58 EEST - 18.226.159.139

Chapter 10

Summary

This thesis investigates mainly, the applications of microturbines in hybrid SOFC-GT systems on the basis of modeling. It is the first time in the literature that is studied the matching of commercially available microturbines with an existing SOFC generator. Simulation models that represent the operation of the devices with high accuracy were developed. A novel method for the optimization of the performance of hybrid systems over the whole operating range was presented. Moreover, experimental activities were undertaken with a small turbojet engine and simulation models were developed. The experience gained from the experimental activities will be useful for further investigation of hybrid systems.

The main results can be summarized as follows:

1. A model was developed for the simulation of hybrid SOFC-GT systems performance at both design and off-design conditions. For the simulation purposes the commercially available AspenPlus process simulator was used.
2. Simulation models for four different microturbines were developed and validated against manufacturer's data.
3. Analysis of the part load performance characteristics of hybrid SOFC-GT system was performed and the effect of key performance parameters was studied. The results showed that the hybrid system operates more efficient as the power demand decreases, and that the SOFC operating temperature has significant effect on system performance.
4. Exergetic analysis was performed and shows that the SOFC stack and the burner are the devices with the higher exergy destruction rate. There is also, a large amount of exergy loss due to exhaust gases. An increase of the SOFC stack temperature has a positive impact on system exergetic efficiency, despite of the increment in exergy destruction. An increase of fuel utilization factor has an even more positive effect on the system performance; it increases the exergetic efficiency and at the same time, it reduces the exergy destruction
5. The matching of a SOFC generator design with four different recuperated microturbines was studied. Design point for each hybrid system was determined based on microturbine data and the part load performance was studied. For the part load operation two control strategies were adopted by maintaining either the SOFC stack temperature or the turbine exit temperature constant. The performance of the hybrid systems was similar for both the control methods. The results shown that, the smaller (among the four considered) the microturbine coupled with the Siemens-Westinghouse SOFC generator, the more efficient is the corresponding hybrid system.

Institutional Repository - Library & Information Centre - University of Thessaly
02/06/2024 00:35:58 EEST - 18.226.159.139

6. A methodology to achieve an improved performance in the whole operating range of a hybrid SOFC-GT system was proposed. It was based on the search of the turbomachines operating lines giving the optimum system efficiency both in design and part load operation. Turbomachinery models were used to calculate the geometry that produces the desired performance maps and the corresponding operating lines. Based on the new turbomachines the hybrid system shown a clear efficiency advantage in the whole operating range.
7. The experience gained during the development of a small turbojet engine simulation model was presented. Data analysis procedures indicated that some measurements were not thermodynamically consistent. Model recalibration based on the use of static instead of total pressure measurements in the turbine exit has proven to be beneficial both for the prediction of the measured parameters and for producing reasonable values for the turbine efficiency. Data correction procedures were also implemented successfully in order to incorporate all the available measurements in the model.
8. Moreover, the development of a transient model for a small turbojet engine was presented. The model is based on the intercomponent volume technique and takes into account the shaft dynamics, the heat transfer effects and the volume dynamics. The model has quite good agreement with the experimental data. Suggestions were done in order to increase its accuracy.

Based on the research undertaken on this study, the author suggests the following directions for future research:

- The models developed in this thesis can be used to study the performance of different designs of hybrid systems, such as configurations with separate power turbine, arrangements incorporating intercooling of reheating etc.
- The development of a transient model for hybrid SOFC-GT systems. The model by utilizing the experience gained from the present thesis, it will be a useful tool to study critical operations such as emergency shutdown or startup under different control methods.
- The transient model for the small turbojet engine can be used to research gas turbine diagnostic methods. To the author’s opinions, this is a very challenging field since the diagnostics with transient data is superior to that with steady state data.

Institutional Repository - Library & Information Centre - University of Thessaly
02/06/2024 00:35:58 EEST - 18.226.159.139

References

1. *Key World Energy Statistics*. 2012, International Energy Agency.
2. *Technology Charecterization: Microturbines*. 2008, Environmental Protection Agency.
3. EG&G Technical Services, *Fuel cell handbook*. 7th ed. 2004, Morgantown, WV: U.S. Dept. of Energy, Office of Fossil Energy, National Energy Technology Laboratory.
4. Ismail, M.S., M. Moghavvemi, and T.M.I. Mahlia, *Current utilization of microturbines as a part of a hybrid system in distributed generation technology.* Renewable and Sustainable Energy Reviews, 2013. **21**(0): p. 142-152.
5. Colombo, L.P.M., F. Armanasco, and O. Perego, *Experimentation on a cogenerative system based on a microturbine.* Applied Thermal Engineering, 2007. **27**(4): p. 705-711.
6. Gomes, E.E.B., M.A.R. do Nascimento, E.E.S. Lora, P. Pilidis, et al., *Performance evaluation and case studies of microturbines fuelled with natural gas and diesel.* Proceedings of the Institution of Mechanical Engineers, Part A: Journal of Power and Energy, 2004. **218**(8): p. 599-607.
7. Tassou, S.A., I. Chaer, N. Sugiartha, Y.T. Ge, et al., *Application of tri-generation systems to the food retail industry.* Energy Conversion and Management, 2007. **48**(11): p. 2988-2995.
8. Huicochea, A., W. Rivera, G. Gutiérrez-Urueta, J.C. Bruno, et al., *Thermodynamic analysis of a trigeneration system consisting of a micro gas turbine and a double effect absorption chiller.* Applied Thermal Engineering, 2011. **31**(16): p. 3347-3353.
9. Soares, C., *Microturbines: Applications for Distributed Energy Systems*. 2007, Butterworth-Heinemann: Burlington.
10. Krishna, C.R., *Performance of the capstone C30 microturbine on biodiesel blends*. 2007, Brookhaven National Laboratory.
11. Habib, Z., R. Parthasarathy, and S. Gollahalli, *Performance and emission characteristics of biofuel in a small-scale gas turbine engine.* Applied Energy, 2010. **87**(5): p. 1701-1709.
12. Park, J., K. Hur, S. Rhim, and H. Kang, *An analysis of CH4/N2 rich biogas production, fuel treatment process and microturbine application.* Korean Journal of Chemical Engineering, 2011. **28**(1): p. 126-132.
13. Onovwiona, H.I. and V.I. Ugursal, *Residential cogeneration systems: review of the current technology.* Renewable and Sustainable Energy Reviews, 2006. **10**(5): p. 389-431.
14. *U.S. Department of Energy*. 2013; Available from: http://www1.eere.energy.gov/hydrogenandfuelcells/fuelcells/index.html.
15. Zhang, X., S.H. Chan, G. Li, H.K. Ho, et al., *A review of integration strategies for solid oxide fuel cells.* Journal of Power Sources, 2010. **195**(3): p. 685-702.
16. Kee, R.J., H. Zhu, and D.G. Goodwin, *Solid-oxide fuel cells with hydrocarbon fuels.* Proceedings of the Combustion Institute, 2005. **30**(2): p. 2379-2404.
17. Kee, R.J., H. Zhu, A.M. Sukeshini, and G.S. Jackson, *Solid Oxide Fuel Cells: Operating Principles, Current Challenges, and the Role of Syngas.* Combustion Science and Technology, 2008. **180**(6): p. 1207-1244.
18. Winkler, W. and P. Nehter, *Thermodynamics of Fuel Cells*, in *Modeling Solid Oxide Fuel Cells*, R. Bove and S. Ubertini, Editors. 2008, Springer Netherlands. p. 13-50.
19. Larminie, J. and A. Dicks, *Fuel Cell Systems Explained*. 2003: John Wiley & Sons.
20. Park, S., J.M. Vohs, and R.J. Gorte, *Direct oxidation of hydrocarbons in a solid-oxide fuel cell.* Nature, 2000. **404**(6775): p. 265-267.

Institutional Repository - Library & Information Centre - University of Thessaly
02/06/2024 00:35:58 EEST - 18.226.159.139

21. McIntosh, S. and R.J. Gorte, *Direct Hydrocarbon Solid Oxide Fuel Cells.* Chemical Reviews, 2004. **104**(10): p. 4845-4866.
22. Kim, T., G. Liu, M. Boaro, S.I. Lee, et al., *A study of carbon formation and prevention in hydrocarbon-fueled SOFC.* Journal of Power Sources, 2006. **155**(2): p. 231-238.
23. Sasaki, K., K. Watanabe, K. Shiosaki, K. Susuki, et al., *Multi-Fuel Capability of Solid Oxide Fuel Cells.* Journal of Electroceramics, 2004. **13**(1-3): p. 669-675.
24. Ormerod, R.M., *Chapter 12 - Fuels and Fuel Processing*, in *High Temperature and Solid Oxide Fuel Cells*, S.C. Singhal and K. Kendal, Editors. 2003, Elsevier Science: Amsterdam. p. 333-361.
25. Kalantar, M. and S.M. Mousavi G, *Dynamic behavior of a stand-alone hybrid power generation system of wind turbine, microturbine, solar array and battery storage.* Applied Energy, 2010. **87**(10): p. 3051-3064.
26. Mohamed, F.A. and H.N. Koivo, *Multiobjective optimization using Mesh Adaptive Direct Search for power dispatch problem of microgrid.* International Journal of Electrical Power & Energy Systems, 2012. **42**(1): p. 728-735.
27. Verda, V. and A. Sciacovelli, *Optimal design and operation of a biogas fuelled MCFC (molten carbonate fuel cells) system integrated with an anaerobic digester.* Energy, 2012. **47**(1): p. 150-157.
28. Campanari, S., *Full Load and Part-Load Performance Prediction for Integrated SOFC and Microturbine Systems.* Journal of Engineering for Gas Turbines and Power, 2000. **122**(2): p. 239-246.
29. Lim, T.-H., R.-H. Song, D.-R. Shin, J.-I. Yang, et al., *Operating characteristics of a 5 kW class anode-supported planar SOFC stack for a fuel cell/gas turbine hybrid system.* International Journal of Hydrogen Energy, 2008. **33**(3): p. 1076-1083.
30. Costamagna, P., L. Magistri, and A.F. Massardo, *Design and part-load performance of a hybrid system based on a solid oxide fuel cell reactor and a micro gas turbine.* Journal of Power Sources, 2001. **96**(2): p. 352-368.
31. Roberts, R.A. and J. Brouwer, *Dynamic simulation of a pressurized 220 kW solid oxide fuel-cell-gas-turbine hybrid system: Modeled performance compared to measured results.* Journal of Fuel Cell Science and Technology, 2006. **3**(1): p. 18-25.
32. Fryda, L., K.D. Panopoulos, and E. Kakaras, *Integrated CHP with autothermal biomass gasification and SOFC-MGT.* Energy Conversion and Management, 2008. **49**(2): p. 281-290.
33. Chan, S.H., H.K. Ho, and Y. Tian, *Modelling of simple hybrid solid oxide fuel cell and gas turbine power plant.* Journal of Power Sources, 2002. **109**(1): p. 111-120.
34. Kimijima, S. and N. Kasagi, *Performance Evaluation of Gas Turbine-fuel Cell Hybrid Micro Generation System*, in *ASME Paper No. GT2002-30111*. 2002. p. 351-360.
35. Bang-Møller, C. and M. Rokni, *Thermodynamic performance study of biomass gasification, solid oxide fuel cell and micro gas turbine hybrid systems.* Energy Conversion and Management, 2010. **51**(11): p. 2330-2339.
36. Cocco, D. and V. Tola, *Use of alternative hydrogen energy carriers in SOFC-MGT hybrid power plants.* Energy Conversion and Management, 2009. **50**(4): p. 1040-1048.
37. Canova, A., G. Chicco, G. Genon, and P. Mancarella, *Emission characterization and evaluation of natural gas-fueled cogeneration microturbines and internal combustion engines.* Energy Conversion and Management, 2008. **49**(10): p. 2900-2909.
38. Scott, W.G., *Micro-turbine generators for distribution systems.* IEEE Industry Applications Magazine, 1998. **4**(3): p. 57-62.
39. Granovskii, M., I. Dincer, and M.A. Rosen, *Performance comparison of two combined SOFC-gas turbine systems.* Journal of Power Sources, 2007. **165**(1): p. 307-314.
40. Zabihian, F. and A. Fung, *Advanced Power Generation Technologies: Fuel Cells*, in *Paths to Sustainable Energy*, A. Ng, Editor. 2010, InTech. p. 421-458.
41. Stambouli, A.B. and E. Traversa, *Solid oxide fuel cells (SOFCs): a review of an environmentally clean and efficient source of energy.* Renewable and Sustainable Energy Reviews, 2002. **6**(5): p. 433-455.

Institutional Repository - Library & Information Centre - University of Thessaly
02/06/2024 00:35:58 EEST - 18.226.159.139

42. Stiller, C., *Design, Operation and Control Modelling of SOFC/GT Hybrid Systems.* Department of Energy and Process Engineering, 2006. **Norwegian University of Science and Technology**.
43. Huang, K. and S.C. Singhal, *Cathode-supported tubular solid oxide fuel cell technology: A critical review.* Journal of Power Sources, 2013. **237**(0): p. 84-97.
44. George, R.A., *Status of tubular SOFC field unit demonstrations.* Journal of Power Sources, 2000. **86**(1-2): p. 134-139.
45. Campanari, S. and P. Iora, *Definition and sensitivity analysis of a finite volume SOFC model for a tubular cell geometry.* Journal of Power Sources, 2004. **132**(1-2): p. 113-126.
46. Doherty, W., A. Reynolds, and D. Kennedy, *Computer simulation of a biomass gasification-solid oxide fuel cell power system using Aspen Plus.* Energy, 2010. **35**(12): p. 4545-4555.
47. Veyo, S., *Tubular SOFC Hybrid Power Systems*, in *Third Annual DOE/U.N. Hybrid Conference and Workshop* 2003.
48. Gardner, F.J., M.J. Day, N.P. Brandon, M.N. Pashley, et al., *SOFC technology development at Rolls-Royce.* Journal of Power Sources, 2000. **86**(1–2): p. 122-129.
49. Behling, N.H., *Chapter 6 - History of Solid Oxide Fuel Cells*, in *Fuel Cells*, N.H. Behling, Editor. 2013, Elsevier. p. 223-421.
50. Kazuo Tomida, M.N., S. Koga, K. Miyamoto, Y. Teramoto, and N.M. S. Yoshida, S. Suemori, T. Kabata, Y. Ando, Y. Kobayashi, *Development of the 200kW Class SOFC-MGT Combined Cycle System with Tubular Type Cell Stack*, in *Fuel Cell Seminar*. 2010.
51. Song, T.W., J.L. Sohn, T.S. Kim, and S.T. Ro, *Performance characteristics of a MW-class SOFC/GT hybrid system based on a commercially available gas turbine.* Journal of Power Sources, 2006. **158**(1): p. 361-367.
52. Mueller, F., R. Gaynor, A.E. Auld, J. Brouwer, et al., *Synergistic integration of a gas turbine and solid oxide fuel cell for improved transient capability.* Journal of Power Sources, 2008. **176**(1): p. 229-239.
53. Burbank Jr, W., D.D. Witmer, and F. Holcomb, *Model of a novel pressurized solid oxide fuel cell gas turbine hybrid engine.* Journal of Power Sources, 2009. **193**(2): p. 656-664.
54. Massardo, A.F., C.F. McDonald, and T. Korakianitis, *Microturbine/Fuel-Cell Coupling for High-Efficiency Electrical-Power Generation.* Journal of Engineering for Gas Turbines and Power, 2002. **124**(1): p. 110-116.
55. Yang, W.J., S.K. Park, T.S. Kim, J.H. Kim, et al., *Design performance analysis of pressurized solid oxide fuel cell/gas turbine hybrid systems considering temperature constraints.* Journal of Power Sources, 2006. **160**(1): p. 462-473.
56. Σταμάτης, Α., Η Διαγνωστική στις Εγκαταστάσεις Αεριοστροβίλων και η εφαρμογή της στην Προληπτική Συντήρηση, Διδακτορική διατριβή, ΕΜΠ 1990,
57. Walsh, P.P. and P. Fletcher, *Gas Turbine Performance*. 2nd ed. 2004: Blackwell Science Ltd.
58. AGARD Advisory Report No. 332, *Recommended practices for the assessment of the effects of atmospheric water ingestion on the performance and operability of gas turbine engines*. 1995: AGARD.
59. Moran, M.J. and H.N. Shapiro, *Fundamentals of engineering thermodynamics*. 2006, West Sussex, England: Wiley.
60. Çengel, Y.A., *Heat transfer : a practical approach*. 2nd ed. 2002, Boston, Mass.: McGraw-Hill.
61. Khaleel, M.A. and J.R. Selman, *Chapter 11 - Cell, Stack and System Modelling*, in *High Temperature and Solid Oxide Fuel Cells*, C.S. Subhash and K. Kevin, Editors. 2003, Elsevier Science: Amsterdam. p. 291-331.
62. Nagel, F.-P., Electricity from wood through the combination of gasification and solid oxide fuel cells. Systems analysis and Proof-of-concept, PhD thesis, ETH/PSI 2008, http://dx.doi.org/10.3929/ethz-a-005773119
63. Kupecki, J., J. Jewulski, and J. Milewski, *Multi-Level Mathematical Modeling of Solid Oxide Fuel Cells*, in *Clean Energy for Better Environment*, P.C. Aydinalp, Editor. 2012, InTech.

Institutional Repository - Library & Information Centre - University of Thessaly
02/06/2024 00:35:58 EEST - 18.226.159.139

64. Campanari, S., *Thermodynamic model and parametric analysis of a tubular SOFC module.* Journal of Power Sources, 2001. **92**(1–2): p. 26-34.
65. Zhang, W., E. Croiset, P.L. Douglas, M.W. Fowler, et al., *Simulation of a tubular solid oxide fuel cell stack using AspenPlusTM unit operation models.* Energy Conversion and Management, 2005. **46**(2): p. 181-196.
66. Akkaya, A.V., *Electrochemical model for performance analysis of a tubular SOFC.* International Journal of Energy Research, 2007. **31**(1): p. 79-98.
67. Song, T.W., J.L. Sohn, J.H. Kim, T.S. Kim, et al., *Performance analysis of a tubular solid oxide fuel cell/micro gas turbine hybrid power system based on a quasi-two dimensional model.* Journal of Power Sources, 2005. **142**(1–2): p. 30-42.
68. Zhang, X., G. Li, J. Li, and Z. Feng, *Numerical study on electric characteristics of solid oxide fuel cells.* Energy Conversion and Management, 2007. **48**(3): p. 977-989.
69. Chan, S.H. and Z.T. Xia, *Polarization effects in electrolyte/electrode-supported solid oxide fuel cells.* Journal of Applied Electrochemistry, 2002. **32**(3): p. 339-347.
70. Fuller, E.N., P.D. Schettler, and J.C. Giddings, *New Method for Prediction of Binary Gas-Phase Diffusion Coefficients.* Industrial & Engineering Chemistry, 1966. **58**(5): p. 18-27.
71. Aspentech. *Aspen Plus® user guide*. 2010; Available from: www.aspentech.com
72. Vidal, A., J. Carles Bruno, R. Best, and A. Coronas, *Performance characteristics and modelling of a micro gas turbine for their integration with thermally activated cooling technologies.* International Journal of Energy Research, 2007. **31**(2): p. 119-134.
73. Zheng, L. and E. Furimsky, *ASPEN simulation of cogeneration plants.* Energy Conversion and Management, 2003. **44**(11): p. 1845-1851.
74. Barelli, L., G. Bidini, F. Gallorini, and A. Ottaviano, *An energetic–exergetic comparison between PEMFC and SOFC-based micro-CHP systems.* International Journal of Hydrogen Energy, 2011. **36**(4): p. 3206-3214.
75. Kurzke, J., *Smooth T 8.2-Preparing Turbine Maps for Gas Turbine Performance Modeling*. 2009.
76. Akkaya, A.V., B. Sahin, and H. Huseyin Erdem, *An analysis of SOFC/GT CHP system based on exergetic performance criteria.* International Journal of Hydrogen Energy, 2008. **33**(10): p. 2566-2577.
77. Milewski, J., A. Miller, and J. Sałaciński, *Off-design analysis of SOFC hybrid system.* International Journal of Hydrogen Energy, 2007. **32**(6): p. 687-698.
78. Marsano, F., L. Magistri, and A.F. Massardo, *Ejector performance influence on a solid oxide fuel cell anodic recirculation system.* Journal of Power Sources, 2004. **129**(2): p. 216-228.
79. Zhu, Y., W. Cai, C. Wen, and Y. Li, *Fuel ejector design and simulation model for anodic recirculation SOFC system.* Journal of Power Sources, 2007. **173**(1): p. 437-449.
80. Spivey, B.J. and T.F. Edgar, *Dynamic modeling, simulation, and MIMO predictive control of a tubular solid oxide fuel cell.* Journal of Process Control, 2012.
81. Stiller, C., B. Thorud, O. Bolland, R. Kandepu, et al., *Control strategy for a solid oxide fuel cell and gas turbine hybrid system.* Journal of Power Sources, 2006. **158**(1): p. 303-315.
82. Leucht, F., W.G. Bessler, J. Kallo, K.A. Friedrich, et al., *Fuel cell system modeling for solid oxide fuel cell/gas turbine hybrid power plants, Part I: Modeling and simulation framework.* Journal of Power Sources, 2011. **196**(3): p. 1205-1215.
83. Sedghisigarchi, K. and A. Feliachi, *Impact of fuel cells on load-frequency control in power distribution systems.* Energy Conversion, IEEE Transactions on, 2006. **21**(1): p. 250-256.
84. Calı, M., M.G.L. Santarelli, and P. Leone, *Design of experiments for fitting regression models on the tubular SOFC : Screening test, response surface analysis and optimization.* International Journal of Hydrogen Energy, 2007. **32**(3): p. 343-358.
85. Yang, J.S., J.L. Sohn, and S.T. Ro, *Performance characteristics of a solid oxide fuel cell/gas turbine hybrid system with various part-load control modes.* Journal of Power Sources, 2007. **166**(1): p. 155-164.
86. Tarroja, B., F. Mueller, J. Maclay, and J. Brouwer, *Parametric Thermodynamic Analysis of a Solid Oxide Fuel Cell Gas Turbine System Design Space.* Journal of Engineering for Gas Turbines and Power, 2010. **132**(7): p. 072301-11.

Institutional Repository - Library & Information Centre - University of Thessaly
02/06/2024 00:35:58 EEST - 18.226.159.139

87. Zhu, H. and R.J. Kee, *Thermodynamics of SOFC efficiency and fuel utilization as functions of fuel mixtures and operating conditions.* Journal of Power Sources, 2006. **161**(2): p. 957-964.
88. Kimijima, S. and N. Kasagi. *Performance Evaluation of Gas Turbine-Fuel Cell Hybrid Micro Generation System*. in *Proceeidings of ASME Turbo Expo 2002*. 2002. Amsterdam, The Netherlands: Paper no. GT2002-30111.
89. Calise, F., A. Palombo, and L. Vanoli, *Design and partial load exergy analysis of hybrid SOFC–GT power plant.* Journal of Power Sources, 2006. **158**(1): p. 225-244.
90. Haseli, Y., I. Dincer, and G.F. Naterer, *Thermodynamic analysis of a combined gas turbine power system with a solid oxide fuel cell through exergy.* Thermochimica Acta, 2008. **480**(1–2): p. 1-9.
91. Chan, S.H., C.F. Low, and O.L. Ding, *Energy and exergy analysis of simple solid-oxide fuel-cell power systems.* Journal of Power Sources, 2002. **103**(2): p. 188-200.
92. Kotas, T.J., *Exergy concepts for thermal plant: First of two papers on exergy techniques in thermal plant analysis.* International Journal of Heat and Fluid Flow, 1980. **2**(3): p. 105-114.
93. Morris, D.R. and J. Szargut, *Standard chemical exergy of some elements and compounds on the planet earth.* Energy, 1986. **11**(8): p. 733-755.
94. Kotas, T.J., *Exergy criteria of performance for thermal plant: Second of two papers on exergy techniques in thermal plant analysis.* International Journal of Heat and Fluid Flow, 1980. **2**(4): p. 147-163.
95. Bakalis, D.P. and A.G. Stamatis. *Performance simulation of a hybrid micro gas turbine fuel cell system based on existing components*. in *Proceeidings of ASME Turbo Expo 2011*. 2011. Vancouver, Canada: Paper No GT2011-45834.
96. Roberts, R.A., J. Brouwer, and G.S. Samuelsen, *Fuel cell/gas turbine hybrid system control for daily load profile and ambient condition variation.* Journal of Engineering for Gas Turbines and Power, 2010. **132**(1): p. 012302.
97. Uechi, H., S. Kimijima, and N. Kasagi, *Cycle Analysis of Gas Turbine--Fuel Cell Cycle Hybrid Micro Generation System.* Journal of Engineering for Gas Turbines and Power, 2004. **126**(4): p. 755-762.
98. Lundberg, W.L., S.E. Veyo, and M.D. Moeckel, *A High-Efficiency Solid Oxide Fuel Cell Hybrid Power System Using the Mercury 50 Advanced Turbine Systems Gas Turbine.* Journal of Engineering for Gas Turbines and Power, 2003. **125**(1): p. 51-58.
99. Park, S.K., K.S. Oh, and T.S. Kim, *Analysis of the design of a pressurized SOFC hybrid system using a fixed gas turbine design.* Journal of Power Sources, 2007. **170**(1): p. 130-139.
100. Li, Y. and Y. Weng, *Performance study of a solid oxide fuel cell and gas turbine hybrid system designed for methane operating with non-designed fuels.* Journal of Power Sources, 2011. **196**(8): p. 3824-3835.
101. Veyo, S.E., L.A. Shockling, J.T. Dederer, J.E. Gillett, et al., *Tubular Solid Oxide Fuel Cell/Gas Turbine Hybrid Cycle Power Systems: Status.* Journal of Engineering for Gas Turbines and Power, 2002. **124**(4): p. 845-849.
102. Calise, F., M. Dentice d'Accadia, A. Palombo, and L. Vanoli, *Simulation and exergy analysis of a hybrid Solid Oxide Fuel Cell (SOFC)-Gas Turbine System.* Energy, 2006. **31**(15): p. 3278-3299.
103. Park, S.K., T.S. Kim, J.L. Sohn, and Y.D. Lee, *An integrated power generation system combining solid oxide fuel cell and oxy-fuel combustion for high performance and CO2 capture.* Applied Energy, 2011. **88**(4): p. 1187-1196.
104. Zhang, X., J. Li, G. Li, and Z. Feng, *Cycle analysis of an integrated solid oxide fuel cell and recuperative gas turbine with an air reheating system.* Journal of Power Sources, 2007. **164**(2): p. 752-760.
105. Akbari, P. and N. Muller. *Performance Improvement of Small Gas Turbines Through Use of Wave Rotor Topping Cycles*. in *Proceeidings of ASME Turbo Expo 2003*. 2003. Paper No. GT2003-38772.

Institutional Repository - Library & Information Centre - University of Thessaly
02/06/2024 00:35:58 EEST - 18.226.159.139

106. Vera, D., F. Jurado, K.D. Panopoulos, and P. Grammelis, *Modelling of biomass gasifier and microturbine for the olive oil industry.* International Journal of Energy Research, 2010: p. n/a-n/a.
107. Henderick, P., An assessment of biomass-powered microturbines and the potential for application in rural China, M.S. thesis, Department of Mechanical and Aerospace Engineering and Center for Energy and Environmental Studies 1999,
108. Kautz, M. and U. Hansen, *The externally-fired gas-turbine (EFGT-Cycle) for decentralized use of biomass.* Applied Energy, 2007. **84**(7-8): p. 795-805.
109. Marsano, F., L. Magistri, M. Bozzolo, and O. Tarnowski. *Influence of Fuel Composition on Solid Oxide Fuel Cell Hybrid System Layout and Performance*. in *Proceeidings of ASME Turbo Expo 2004*. 2004. Vienna, Austria: Paper No GT2004-53853.
110. Chan, S.H., H.K. Ho, and Y. Tian, *Multi-level modeling of SOFC–gas turbine hybrid system.* International Journal of Hydrogen Energy, 2003. **28**(8): p. 889-900.
111. Jiang, W., R. Fang, J. Khan, and R. Dougal, *Control strategies for start-up and part-load operation of solid oxide fuel cell/gas turbine hybrid system.* Journal of Fuel Cell Science and Technology, 2010. **7**(1): p. 0110161-0110169.
112. Kaneko, T., J. Brouwer, and G.S. Samuelsen, *Power and temperature control of fluctuating biomass gas fueled solid oxide fuel cell and micro gas turbine hybrid system.* Journal of Power Sources, 2006. **160**(1): p. 316-325.
113. Wu, X.J. and X.J. Zhu, *Multi-loop control strategy of a solid oxide fuel cell and micro gas turbine hybrid system.* Journal of Power Sources, 2011. **196**(20): p. 8444-8449.
114. Ferrari, M.L., M. Pascenti, A.N. Traverso, and A.F. Massardo, *Hybrid system test rig: Chemical composition emulation with steam injection.* Applied Energy, 2012. **97**: p. 809-815.
115. McLarty, D., Y. Kuniba, J. Brouwer, and S. Samuelsen, *Experimental and theoretical evidence for control requirements in solid oxide fuel cell gas turbine hybrid systems.* Journal of Power Sources, 2012. **209**: p. 195-203.
116. Chan, S.H., H.K. Ho, and Y. Tian, *Modelling for part-load operation of solid oxide fuel cell–gas turbine hybrid power plant.* Journal of Power Sources, 2003. **114**(2): p. 213-227.
117. Kim, T.S. and S.H. Hwang, *Part load performance analysis of recuperated gas turbines considering engine configuration and operation strategy.* Energy, 2006. **31**(2-3): p. 260-277.
118. Suther, T., A.S. Fung, M. Koksal, and F. Zabihian, *Effects of operating and design parameters on the performance of a solid oxide fuel cell–gas turbine system.* International Journal of Energy Research, 2010. **35**(7): p. 616-632.
119. Adams, T.A., J. Nease, D. Tucker, and P.I. Barton, *Energy Conversion with Solid Oxide Fuel Cell Systems: A Review of Concepts and Outlooks for the Short- and Long-Term.* Industrial & Engineering Chemistry Research, 2012. **52**(9): p. 3089-3111.
120. Åström, K., E. Fontell, and S. Virtanen, *Reliability analysis and initial requirements for FC systems and stacks.* Journal of Power Sources, 2007. **171**(1): p. 46-54.
121. Stiller, C., B. Thorud, and O. Bolland, *Safe Dynamic Operation of a Simple SOFC/GT Hybrid System.* Journal of Engineering for Gas Turbines and Power, 2006. **128**(3): p. 551-559.
122. Bakalis, D.P. and A.G. Stamatis, *Full and part load exergetic analysis of a hybrid micro gas turbine fuel cell system based on existing components.* Energy Conversion and Management, 2012. **64**: p. 213-221.
123. Duan, L., K. Huang, X. Zhang, and Y. Yang, *Comparison study on different SOFC hybrid systems with zero-CO< sub> 2</sub> emission.* Energy, 2013. **58**: p. 66-77.
124. Gandiglio, M., A. Lanzini, P. Leone, M. Santarelli, et al., *Thermoeconomic analysis of large solid oxide fuel cell plants: Atmospheric vs. pressurized performance.* Energy, 2013. **55**: p. 142-155.
125. Douvartzides, S., F. Coutelieris, and P. Tsiakaras, *Exergy analysis of a solid oxide fuel cell power plant fed by either ethanol or methane.* Journal of Power Sources, 2004. **131**(1–2): p. 224-230.

Institutional Repository - Library & Information Centre - University of Thessaly
02/06/2024 00:35:58 EEST - 18.226.159.139

126. Santin, M., A. Traverso, L. Magistri, and A. Massardo, *Thermoeconomic analysis of SOFC-GT hybrid systems fed by liquid fuels.* Energy, 2010. **35**(2): p. 1077-1083.
127. Stamatis, A., C. Vinni, D. Bakalis, F. Tzorbatzoglou, et al., *Exergy analysis of an intermediate temperature solid oxide fuel cell-gas turbine hybrid system fed with ethanol.* Energies, 2012. **5**(11): p. 4268-4287.
128. Douvartzides, S.L., F.A. Coutelieris, A.K. Demin, and P.E. Tsiakaras, *Fuel options for solid oxide fuel cells: A thermodynamic analysis.* AIChE Journal, 2003. **49**(1): p. 248-257.
129. Calise, F., M. Dentice d' Accadia, L. Vanoli, and M.R. von Spakovsky, *Single-level optimization of a hybrid SOFC–GT power plant.* Journal of Power Sources, 2006. **159**(2): p. 1169-1185.
130. Calise, F., M. Dentice d' Accadia, L. Vanoli, and M.R. von Spakovsky, *Full load synthesis/design optimization of a hybrid SOFC–GT power plant.* Energy, 2007. **32**(4): p. 446-458.
131. Sieros, G. and K.D. Papailiou, *Gas turbine components optimized for use in hybrid SOFC-GT systems*, in *Proceedings of 7th European conference on turbomachinery fluid dynamics and thermodynamics*. 2007: Athens, Greece.
132. Miller, A. and J. Milewski, *SOFC-GT hybrid system – Turbomachinery problems*, in *9th European Conference on Turbomachinery*. 2011: Istanbul, Turkey.
133. Yang, J.S., J.L. Sohn, and S.T. Ro, *Strategies to Enhance the Part-Load Performance of a SOFC/GT Hybrid System*, in *ASME TurboExpo*. 2007: Paper No. GT2007-27441.
134. Sellers, J.F. and C.J. Daniele, *DYNGEN: A program for calculating steady-state and transient performance of turbojet and turbofan engines*. NASA-TN D-7901. 1975, Washington D.C., USA.
135. Kurzke, J., *Correlations hidden in compressor maps*, in *ASME Turbo Expo 2011*. 2011.
136. Bakalis, D.P. and A.G. Stamatis, *Incorporating available micro gas turbines and fuel cell: Matching considerations and performance evaluation.* Applied Energy, 2013. **103**(0): p. 607-617.
137. Zhu, Y., Y. Li, and W. Cai, *Control oriented modeling of ejector in anode gas recirculation solid oxygen fuel cell systems.* Energy Conversion and Management, 2011. **52**(4): p. 1881-1889.
138. Singhal, S.C., *Advances in solid oxide fuel cell technology.* Solid State Ionics, 2000. **135**(1–4): p. 305-313.
139. Cohen, H., G.F.C. Rogers, and H.I.H. Saravanamuttoo, *Gas turbine theory*. 4 ed. 1996, Burnt Mill, Harlow, Essex, England: Longman Scientific.
140. Galvas, M.R., *Fortran program for predicting off-design performance of centrifugal compressors*. NASA TN D-7487. 1973, Washington D.C., USA.
141. Stanitz, J.D., *Effect of Blade-Thickness Taper on Axial-Velocity Distribution at the Leading Edge of an Entrance Rotor Blade Row With Axial Inlet, and the Influence of This Distribution on Alinement of the Rotor Blade for Zero Angle of Attack*. 1953: NACA TN-2986.
142. *GenOpt, Generic Optimisation Program, Lawrence Berkeley National Laboratory at the University of California*. January 2013]; Available from: simulationresearch.lbl.gov/GO/.
143. Wasserbauer, C.A. and A.J. Glassman, *Fortran program for predicting off-design performance of radial-inflow turbines*. NASA TN D-8063. 1975, Washington D.C., USA.
144. Lichtsinder, M. and Y. Levy, *Jet engine model for control and real-time simulations.* Journal of Engineering for Gas Turbines and Power, 2006. **128**(4): p. 745-753.
145. Davison, C.R. and A.M. Birk, *Steady state and transient modeling of a micro-turbine with comparison to operating engine*, in *Proceedings of the ASME Turbo Expo 2004*. 2004. p. 27-35.
146. Rahman, N.U. and J.F. Whidborne, *A numerical investigation into the effect of engine bleed on performance of a single-spool turbojet engine.* Proceedings of the Institution of Mechanical Engineers, Part G: Journal of Aerospace Engineering, 2008. **222**(7): p. 939-949.
147. Schobeiri, M., Turbomachinery Flow Physics and Dynamic Performance, 2005.

Institutional Repository - Library & Information Centre - University of Thessaly
02/06/2024 00:35:58 EEST - 18.226.159.139

148. Deam, R.T., E. Lemma, B. Mace, and R. Collins, *On scaling down turbines to millimeter size.* Journal of Engineering for Gas Turbines and Power, 2008. **130**(5).
149. Gonzalez, C.A., K.C. Wong, and S. Armfield, *Computational study of a micro-turbine engine combustor using large eddy simulation and Reynolds averaged turbulence models.* Anziam J, 2008. **49**: p. C407-C422.
150. Lechner, C. and M.R. Bothien, *Measurement of the inlet gas temperature of a gas turbine.* Proceedings of the ASME Turbo Expo, 2005. **1**: p. 507-515.
151. Barringer, M.D., K.A. Thole, M.D. Polanka, J.P. Clark, et al., *Migration of combustor exit profiles through high pressure turbine vanes*, in *Proceedings of the ASME Turbo Expo*. 2007. p. 1335-1346.
152. Pau, M., F. Congiu, F. Cambuli, and N. Mandas, *Numerical investigation of the flow in a two-stage axial test-turbine with open and closed cavities.* 7th European Conference on Turbomachinery Fluid Dynamics and Thermodynamics, 2007.
153. Chiang, H.W.D., C.N. Hsu, A. Lai, and R. Lin, *An investigation of steady and dynamic performance of a small turbojet engine.* American Society of Mechanical Engineers, International Gas Turbine Institute, Turbo Expo (Publication) IGTI, 2002. **1**: p. 1097-1104.
154. Davison, C.R. and A.M. Birk, *Set up and operational experience with a micro-turbine engine for research and education.* Proceedings of the ASME Turbo Expo 2004, 2004. **1**: p. 849-858.
155. Gerendas, M. and R. Pfister, *Development of a very small aero-engine.* ASME Turbo Expo 2000, 2000.
156. Mathioudakis, K. and P. Argyropoulos, *Design and Development of a Small Jet Engine Test Cell.* American Society of Mechanical Engineers, International Gas Turbine Institute, Turbo Expo (Publication) IGTI, 2003. **1**: p. 749-758.
157. Perez-Blanco, H., *Activities Around the SR-30 Minilab at PSU.* Proceedings of the 2003 American Society for Engineering Education Annual Conference and Exposition, 2003.
158. Stamatis, A., K. Mathioudakis, and K.D. Papailiou, *Adaptive simulation of gas turbine performance.* ASME J. Eng. Gas Turbines Power, 1990. **112**(2): p. 168-175.
159. Regtien, P.P.L. Measurement Science for Engineers. 2004.
160. Gülen, S.C. and R.W. Smith, *A simple mathematical approach to data reconciliation in a single-shaft combined cycle system.* Journal of Engineering for Gas Turbines and Power, 2009. **131**(2).
161. Ganguli, R., *Noise and outlier removal from jet engine health signals using weighted FIR median hybrid filters.* Mechanical Systems and Signal Processing, 2002. **16**(6): p. 967-978.
162. Bakalis, D.P. and A.G. Stamatis, *Extended instrumentation and model calibration for a small micro-turbine.* Proceedings of the ASME Turbo Expo, 2010. **1**: p. 711-719.
163. Grey Jr, R.E. and H.D. Wilstead, *Performance of conical jet nozzles in terms of flow and velocity coefficients.* NACA Report 933, 1949, 0000.
164. Müller, N. and P. Akbari, *Performance investigation of small gas turbine engines topped with wave rotors.* 39th AIAA/ASME/SAE/ASEE Joint Propulsion Conference and Exhibit, 2003: p. 1-11.
165. Pourmovahed, A., C.M. Jeruzal, and K.D. Brinker, *Development of a jet engine experiment for the energy systems laboratory.* Proceedings of IMECE'03, 2003.
166. Kefalakis, M., K. Papailiou, and S. Mavrakis, *A method for measuring turbine efficiency under strong heat transfer.* 8th European Turbomachinery Conference, 2009.
167. Bohn, E., K. Kusterer, N. Surken, and F. Kreitmeier, *Influence of endwall contouring in axial gaps on the flow field in a four-stage turbine.* ASME Turbo Expo 2000, 2000.
168. Gier, J., S. Ardey, S. Eymann, U. Reinmöller, et al., *Improving 3D flow characteristics in a multistage LP turbine by means of endwall contouring and airfoil design modification - Part 2: Numerical simulation and analysis.* American Society of Mechanical Engineers, International Gas Turbine Institute, Turbo Expo (Publication) IGTI, 2002. **5 A**: p. 261-271.

Institutional Repository - Library & Information Centre - University of Thessaly
02/06/2024 00:35:58 EEST - 18.226.159.139

169. Jackson, A.J.B., P. Laskaridis, and P. Pilidis, *A test bed for small aero gas turbines for education and for university - Industry collaboration.* Proceedings of the ASME Turbo Expo 2004, 2004. **1**: p. 901-909.
170. Camporeale, S.M., B. Fortunato, and M. Mastrovito, *A modular code for real time dynamic simulation of gas turbines in simulink.* Journal of Engineering for Gas Turbines and Power, 2006. **128**(3): p. 506-517.
171. Kim, J.H., T.W. Song, T.S. Kim, and S.T. Ro, *Model development and simulation of tansient behavoir of heavy duty gas turbines.* Journal of Engineering for Gas Turbines and Power, 2001. **123**(3): p. 589-594.
172. Martin, S., I. Wallace, and D.G. Bates, *Development and validation of a civil aircraft engine simulation model for advanced controller design.* Journal of Engineering for Gas Turbines and Power, 2008. **130**(5).
173. Rezvani, R., M. Ozcan, B. Kestner, J. Tai, et al. *A gas turbine engine model of transient operation across the flight envelope*. in *Proceedings of the ASME Turbo Expo*. 2011.
174. da Cunha Alves, M.A. and J.R. Barbosa, *A step further in gas turbine dynamic simulation.* Proceedings of the Institution of Mechanical Engineers, Part A: Journal of Power and Energy, 2003. **217**(6): p. 583-592.
175. Stamatis, A., K. Mathioudakis, J. Ruiz, and B. Curnock. *Real time engine model implementation for adaptive control & performance monitoring of large civil turbofans*. in *Proceedings of the ASME Turbo Expo*. 2001.
176. Coverse, G.L., *Extended parametric representation of compressor fans and turbines. Volume 2: Part user's manual (parametric turbine)*. NASA-CR-174646. 1984, USA.
177. Mu, J., D. Rees, and G.P. Liu, *Advanced controller design for aircraft gas turbine engines.* Control Engineering Practice, 2005. **13**(8): p. 1001-1015.
178. Watanabe, A., S.M. Ölçmen, R.P. Leland, K.W. Whitaker, et al., *Soft computing applications on a SR-30 turbojet engine.* Fuzzy Sets and Systems, 2006. **157**(22): p. 3007-3024.

Institutional Repository - Library & Information Centre - University of Thessaly
02/06/2024 00:35:58 EEST - 18.226.159.139